The Hydrodynamic Impedance of Harbour Entrances

by

Motaz Al-Mashouk

October, 1989

A thesis submitted for the degree of Doctor of Philosophy of the University of London and for the Diploma of Membership of Imperial College

Hydraulics Section
Department of Civil Engineering
Imperial College of Science, Technology and Medicine

Dedicated to my mother.

ACKNOWLEDGEMENTS

I am indebted to my supervisor, Professor Patrick Holmes, for his valuable advice and guidance throughout the course of this work.

I would like to thank Mr. Brian MacMahon for his enthusiastic interest in my research. The many discussions I have had with Drs. Kostas Anastasiou and Ping Dong have been most beneficial and enjoyable. I am very grateful to Dr. Hitchings for his patient help in developing the numerical model.

I would also like to thank Miss Parvin Djahani for her support and for help in preparing the drawings.

I am forever in the debt of my two brothers, Tarek and Motassim, for their support and continuous encouragement.

ABSTRACT

This dissertation is an investigation of the wave impedance properties of several different geometries of harbour entrance. The work is concerned with small–amplitude water waves and falls into three parts:

Firstly, an analytical theory based on the method of matched asymptotic expansions was developed to study: (a) the scattering of waves at the outlet of a semi–infinite channel, (b) the diffraction of waves by a gap in a breakwater of finite thickness and (c) the transmission of waves through a channel whose length is of the order of the wavelength. In all of these, the incident waves were assumed to be long relative to the gap width. Energy transmission coefficients have been derived and plotted for each of the above headings. For problems (b) and (c) these were found to agree with classical solutions in the limiting cases of zero breakwater thickness. In the case of (a), verification was furnished by comparison with well–known phenomena in acoustics. Generally, the results indicate that appreciable reductions in wave penetration could be achieved by such configurations.

Secondly, a numerical model based on a hybrid element method was constructed for the solution of the Helmholtz equation. The formulation entailed coupling a finite element discretisation in an interior region where the solution is sought, to an infinite element discretisation in an unbounded exterior domain. The mapped quadratic infinite element was implemented for the latter as it has been shown to be the most accurate tool for representing the outward decay of the scattered wave. The model was then used to solve diffraction problems for which analytical solutions exist and excellent agreement was found.

Thirdly, the numerical model was used to evaluate various entrance configurations comprising channels, quarter–wavelength resonators and arrangements of resonator chambers analogous to acoustic low–pass filters. Two harbour geometries have been considered, the first of which is semi–infinite while the second is a finite–size model of rectangular planform. In the case of entrance channels, the trend of behaviour was observed to agree with results from the analytical work. Resonators and filters were found to be very effective devices to protect harbours from excessive motion.

CONTENTS

NOMENCLATURE

A	wave amplitude.
A_I	incident wave amplitude.
$2a$	channel length.
$2b$	gap width.
ce_m	even Mathieu function of the first kind.
Ce_m	modified Mathieu function of the first kind.
e	base of natural logarithm.
e	end correction.
f_j	load vector.
FeY_m	modified Mathieu function of the second kind.
g	acceleration due to gravity.
h	water depth.
H_n	Hankel function of the first kind and nth order.
i	unit of imaginary numbers.
J_n	Bessel function of the first kind and nth order.
k	wave number.
k_{ij}	element in stiffness matrix.
l_{opt}	optimum length of resonator.
$\mathbf{n}$	normal vector.
N_i	shape function.
T	energy transmission coefficient.
v	test function.
(x,y)	Cartesian coordinates.
Y_n	Bessel function of the second kind and nth order.
γ	Euler constant (0.5772...)
η	surface elevation.
θ^i	angle of incidence.

NOMENCLATURE (continued)

θ	$(\theta^i - \pi)$
λ	wavelength.
(ξ,η)	local coordinates.
π	pi (3.14159...)
σ	angular frequency.
φ	reduced potential.
Φ	velocity potential.
Ω	domain in the x–y plane.
$\partial\Omega$	boundary of Ω.
r	radial distance from source except where otherwise defined.

CHAPTER ONE
Introduction

In certain favoured points on the world's coastlines, nature has provided harbours waiting only to be used, such as New York Bay, which one explorer described as "a very agreeable location" for sheltering a ship. Such inlets, bays and estuaries may require improvement by dredging and of course must be supplied with port structures, but basically they remain as nature made them and their existence accounts for many of the world's great cities. Because such natural harbours are not always at hand where port facilities are needed, engineers must create artificial harbours. The basic structure involved in the creation of these is the breakwater which performs the function of providing calm water inshore. Locations for artificial harbours are of course chosen with an eye to the existing potential of the coast; an indentation however slight is favoured. Yet it has often been found justifiable on economic or strategic grounds to construct a complete harbour on a relatively unsheltered coastline by enclosing an area with breakwaters built from the shore, with openings of minimum width for entry and exit of ships.

The cost of construction of a new harbour, or maintenance of an existing one, is often dominated by the expense of wave protection structures. The lengths of these should therefore be minimised within the limitations imposed by the wave agitation criteria, which naturally leads to the requirement of more efficient harbour entrance configurations. In fulfilling such design constraints however, an engineer is faced with a dilemma: the harbour entrance must be wide enough to allow safe access to shipping and, at the same time, small enough to limit the penetration of wave motion. The width is therefore often a compromise between the navigational requirements and the degree of protection desirable in a harbour. The navigational requirements are related to parameters such as the size of the design vessel, the density of traffic, the water depth and the height, direction and frequency of winds, waves and currents. Wave action in navigation channels and harbour basins is always undesirable both to navigation and to moored ships and the degree to which this may be considered tolerable depends upon the height and period of the waves and the hydrodynamic characteristics of the vessels. On the other hand, current action may also include such benefits as flushing of sediments and pollutants.

Accordingly, the disturbance level in the harbour must be minimised, or at least kept below an upper limit in certain specified regions, in order to maintain a reasonable level of usability. In that respect, it is virtually impossible

to prevent long–period waves from entering a harbour. The only method to minimise their effects is to shape the partially enclosed basin so that standing waves cannot form. However, shorter–period waves (those in the wind generated spectrum) may be strongly attenuated in one of the following ways: (a) restricting possibilities for input of wave energy by the proper design of the entrance, (b) energy absorption before waves reach berthing areas and (c) other special means like pneumatic breakwaters. This thesis is concerned exclusively with (a) and shall be outlined later in this chapter. The dissipation of energy in a harbour may be accomplished by promoting the breaking of waves either by constructing mild slopes along the inner boundaries or by making use of natural beaches. Pneumatic breakwaters also rely on the breaking of waves, but by opposing currents. The installation generates this current by releasing air bubbles near the bed which subsequently drag water to the surface as they rise. The flow divides at the surface, with part being directed against incoming waves. It is more effective against short–period waves where the motion is confined to the surface region. The volumes of air required to run breakwaters effective against waves of longer period are however colossal and hence no economic solution appears to be at hand.

The excitation of ships is another aspect that must be assessed in the light of our design guidelines. A ship that is assumed rigid, has motions which are usually considered to occur in the six degrees of freedom known as surge, sway, heave, roll, pitch and yaw. None of the motions occur singly; (e.g. heaving cannot take place independently of pitching because of the fore and aft assymetry of the typical hull form). The motions excited in the ship result from the wave disturbance, the hydrodynamic inertia coefficients and the ship's orientation relative to the direction of wave propagation. Excessive movements would adversely affect cargo handling for all types of ships and therefore, it is the designer's task to try, as far as possible, to eliminate the penetration of the 'harmful' incoming wave frequencies.

It is worthwhile noting that if the port basin is large enough, wave generation within it can be significant. As a consequence of reflections from boundaries, the build up of wave motion in an enclosure may be more rapid than in an equal area of open sea. The energy generated in a reasonably sized enclosed body of water should therefore be added to that entering the mouth and a conservative judgement made of the addition of these two effects. In large harbours, such locally generated wind waves may require the construction of additional internal wave protection structures for certain operations.

1.1 Outline of the thesis

The work commences in chapter two by reviewing the main analytical theories that have been developed for solving diffraction problems in hydrodynamics. Such methods have been widely used by engineers in the design of harbours and accordingly, a large section of the U.S. Shore Protection Manual(1984), often referred to as "the bible of the coastal engineer", is dedicated to their results. However, as these are mostly based on analytical formulations, it is our intention here to put forward and qualify any shortcomings or limitations that might have been imposed by the analyses.

In chapter three, we undertake an analytical investigation into the transmission of water waves through channels under the assumption, $\lambda > 2b$, where λ is the incident wavelength and 2b is the harbour gap width. The method of matched asymptotic expansions is utilised to solve what amounts to singular perturbation problems in which there are typically two disparate length scales such as the gap width and the wavelength or the boundary layer thickness and the chord in the flow over an aerofoil. In this context, the method is based on the premise that in the immediate vicinity of the gap, the wave motion resembles streaming flow while far away, the aperture appears as a wave source. Consequently, near–field and far–field solutions are independently sought and then matched in the intermediate regions to determine unknown constants. The first problem studied is the scattering of waves at the outlet of a semi–infinite channel. In this respect two geometries have been looked at, the first being a flanged channel and the second an unflanged one. Our aim here is to effectively demonstrate the process of reflection at an open end which has many practical applications. The next two problems tackled are respectively the diffraction of waves by a gap in a breakwater of finite thickness and the transmission of waves through a channel whose length is of the same order as the wavelength. It is hoped that this study would then provide a comprehensive account of the behaviour of entrance channels in the limiting case where the wavelength is long relative to 2b.

To extend the coverage of the work, a numerical model is developed in chapter four to solve the Helmholtz equation. A hybrid form of the finite element method is utilised for this purpose which entails coupling a finite element discretisation in an interior region to infinite elements in an exterior one. The latter simulate the decay of the outward scattered wave so as to satisfy the radiation condition at infinity. The implementation is on a general–purpose finite element package, FINEL, which is extensively modified for our requirements. In order to verify the model, a few simple problems are then tackled.

With a powerful tool now at our disposal, we proceed in chapter five to study the impedance properties of several harbour entrance configurations. Among these are channels, quarter–wavelength resonators and filter arrangements. Only semi–infinite harbour geometries are considerd here to avoid the complexity of internal reflections. Throughout, emphasis is placed on the physical explanation of important phenomena. Our intention here is to provide the practicing engineer with sufficient data so that the design of efficient entrances can be rationalised.

In chapter six, the resonance characteristics of a finite–size harbour are examined to make our work more applicable to real problems. We focus on two entrance configurations of a channel and a resonator with the aim of minimising the adverse effects that occur as a result of resonance.

The conclusions arrived at in all the previous chapters are then summarised in chapter seven. Recommendations for the future extension of the work are also given.

1.2 Assumptions and formulations

The following assumptions are made in the development of our diffraction theories:

(1) Water is an ideal fluid, i.e., inviscid and incompressible.

(2) Waves are of small amplitude and can be described by linear wave theory.

(3) Flow is irrotational and conforms to a potential function which satisfies the Laplace equation.

(4) The water depth is uniform.

A summary of the equations governing the fluid motion is given here. A more detailed account may be found in Wehausen and Laitone(1960). Under the above assumptions, the velocity field may be expressed in terms of a potential function $\Phi(x,y,z,t)$ by $\mathbf{q} = -\nabla\Phi$, where (x,y,z) are Cartesian coordinates with z measured vertically upwards, $z=0$ coinciding with the undisturbed free surface. It is assumed that Φ is periodic in time, with an imposed angular frequency σ. Further, since all solid boundaries are supposed vertical and the undisturbed fluid depth h is constant, both the vertical and time dependence of the fluid motion can be anticipated and subsequent calculations simplified by setting:

$$\Phi = \mathrm{Re}\left[\frac{g}{i\sigma} \frac{\cosh k(z+h)}{\cosh kh} \varphi(x,y)\, e^{-i\sigma t} \right]$$

The wavenumber k is given by the dispersion relation

$$\sigma^2 = gk \tanh (kh)$$

The vertical displacement of the free surface from its equilibrium position is:

$$\eta(x,y,t) = \mathrm{Re} \left[\varphi(x,y)\, e^{-i\sigma t} \right]$$

where $\varphi(x,y)$ is a reduced potential satisfying the Helmholtz equation:

$$(\nabla^2 + k^2)\, \varphi = 0$$

at all points (x,y) corresponding to the fluid domain.

CHAPTER TWO
A review of classical diffraction theories

2.1 Survey

The diffraction of linear monochromatic water waves by breakwaters has been the subject of numerous theoretical and experimental investigations. The phenomenon is analogous to the diffraction of light, sound and electromagnetic waves, and theories for breakwater diffraction have, in the most, been adapted from the theory of these phenomena. In general, two diffraction problems are encountered: (a) The bending of waves around the end of a semi–infinite impermeable breakwater; and (b) their passage through a gap in a harbour wall. As well as providing a brief literature review of work in this field, we shall, in this chapter, describe in detail the main theories that have been developed for the solution of (a) and (b) and which have gained acceptance in engineering practice. The last section is dedicated to an area which has not been previously explored in the context of water waves. The interference effects in a harbour are examined in relation to the distinction between Fresnel and Fraunhofer diffraction, and the existence of amplitude maxima and minima along the centre line from the gap is investigated.

The rigorous mathematical approach to diffraction was initiated by Sommerfeld(1896) who derived a solution for light waves interrupted by a semi–infinite screen. The screen was assumed to be lying in a plane parallel to that of the polarised light. The acoustic equivalent of this problem was later taken up by Lamb(1932), who utilised a system of parabolic coordinates to solve the governing Helmholtz equation. This accomodated the application of the boundary conditions and the resulting solution is generally recognised to be one of the strong points of his well known book, 'Hydrodynamics'. After proving that a correspondence existed between the propagation of water and light waves, Penney and Price(1944,1952) devoted their efforts to this same problem. They utilised Sommerfeld's solution to model the diffraction of water waves by semi–infinite breakwaters and presented results that were directly applicable to the design of harbours. Putnam and Arthur(1948) later undertook experimental tests which verified this theoretical solution. Penney and Price also presented a solution for the diffraction by a gap, which was based on the superposition of the solutions for two semi–infinite breakwaters. This gave a reasonable representation of the wave field, providing the width of the opening was large enough (greater than about two wavelengths). An experimental verification was carried out by Blue and

Johnson(1949), who found that the superposition approximation was accurate for gap widths as small as 1.4 wavelengths.

A totally independent approach to the aperture problem was formulated by Lacombe(1952). He derived a method which was based on a generalisation of Huyghens' principle, under certain restrictive assumptions. An alternative theory was also developed by Morse and Rubenstein(1938) in studying the diffraction of sound and electromagnetic waves by ribbons and slits. They utlilised an elliptic system of coordinates to solve the Helmholtz equation, which resulted in an exact solution, expressed in terms of the Mathieu functions, that was valid for any gap width. It was not practical, however, to apply this analysis to gap widths greater than about one wavelength as the convergence of the series for the Mathieu functions becomes quite slow. The solution was later adopted and modified by Carr and Stelzriede(1952) for the case of water waves. They presented theoretical and experimental results, pertaining to the energy distribution in a harbour, whose agreement was reasonably close. It should be noted that this exact solution could just as well be applied to the diffraction of waves by a detached breakwater, where the boundary conditions in the problem are similarly accomodated. The length of the breakwater, however, comes under the same restriction as the width of the harbour gap, for finite computations.

When the aperture is small in relation to the wavelength (less than about 0.2 wavelengths), the asymptotic solution developed by Rayleigh(1897), and later by Lamb(1932), may be used. This is based on the premise that the streamlines of the motion of the water waves through the gap are like those of the flow of a liquid through the same aperture. The analysis procedure therefore comprised dividing the solution domain into near–field and far–field flows. Solutions to each of these problems were obtained separately and then matched to determine unknown constants. A diffraction coefficient was then derived which was a function of the radial distance from the centre of the opening.

More recently, Memos(1980) presented a useful work in which he reviewed all of the above diffraction theories from an engineering application aspect. He also discussed the range of validity of each of them with regard to the gap width, and plotted curves to illustrate this point. One criticism that arises with regards to these graphs, however, is that the validity of Lamb's(1932) solution is taken as extending to a maximum gap width of about 0.8 wavelengths. This is obviously erroneous as the asymptotic theory on which the analysis is based, would no longer be valid under such circumstances. Memos(1980) also proposed a formulation for the case when the two breakwater arms, forming the gap, are inclined to one another. To this end, he combined two independent solutions, as was done by Penney and Price(1952), which imposed some limitations

on the applicability of the results.

Sobey and Johnson(1986) returned to the analytical solution of Morse and Rubenstein(1938) to investigate the diffraction of water waves by narrow gaps. They concentrated on the wave field near the gap where available details are generally approximate and most sparse. In their work, diffraction diagrams are presented for several combinations of gap widths and angles of incidence, and comparisons are made with the superposition approximation. Results are also presented for island breakwater configurations.

The use of analytical results in breakwater design is made convenient when summarised in a diagram with curves of equal values of diffraction coefficients in a coordinate system for which the origin is at the tip of a single breakwater or at the centre of an aperture. (The diffraction coefficient in this instance is defined as the ratio of diffracted wave height to the incident wave height). A comprehensive selection of such maps, covering many gap width to wavelength ratios, is given in the Shore Protection Manual(1984).

2.2 Semi–infinite breakwater

As with all linear diffraction problems in hydrodynamics, the governing differential equation is that due to Helmholtz:

$$\nabla^2\varphi + k^2\varphi = 0 \qquad (2.1)$$

In order to solve this, subject to the boundary conditions in the problem, a transformation from cartesian to parabolic coordinates, given by,

$$k(x + iy) = (\xi + i\eta)^2 \qquad (2.2)$$

must be made. Figure 2.1 shows contours of equal ξ and η in relation to the x and y axes as well as the semi–infinite breakwater which is taken to be occupying the positive x–axis (η=0).

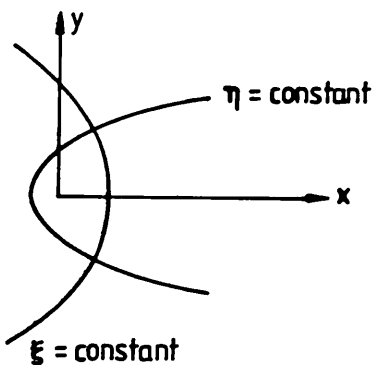

Figure 2.1 Definition sketch

As the primary waves are represented by,

$$\varphi = e^{iky} \tag{2.3}$$

two solutions of the following form are sought:

$$\varphi = \begin{cases} F(x,y)\ e^{iky} & (2.4a) \\ G(x,y)\ e^{-iky} & (2.4b) \end{cases}$$

These correspond to the diffracted fields of the plane incident and plane reflected waves which are linearly superimposed to obtain the general solution. Substituting each of these expressions in turn in the governing equation, and transforming coordinates to the (ξ,η) reference frame, the following two equations for F and G ensue:

$$\frac{\partial^2 F}{\partial \xi^2} + \frac{\partial^2 F}{\partial \eta^2} + 4i\left[\eta\frac{\partial F}{\partial \xi} + \xi\frac{\partial F}{\partial \eta}\right] = 0 \tag{2.5a}$$

$$\frac{\partial^2 G}{\partial \xi^2} + \frac{\partial^2 G}{\partial \eta^2} - 4i\left[\eta\frac{\partial G}{\partial \xi} + \xi\frac{\partial G}{\partial \eta}\right] = 0 \tag{2.5b}$$

which are satisfied by,

$$F(\xi,\eta) = f(s), \qquad s = (\xi+\eta) \tag{2.6}$$

$$G(\xi,\eta) = g(s), \qquad s = (\xi-\eta) \tag{2.7}$$

and yield,

$$F(\xi,\eta) = A + B\int_0^{\xi+\eta} e^{-is^2}\,ds \tag{2.8a}$$

$$G(\xi,\eta) = C + D\int_0^{\xi-\eta} e^{-is^2}\,ds \tag{2.8b}$$

A,B,C and D being unknown constants to be determined by imposing the following boundary conditions:

(1) When x is large and negative, while y=0, (ξ=0, η=∞), φ must reduce to expression (2.3).

(2) When y=0 and x$\geq$0, (η=0), $\partial\varphi/\partial y = 0$.

Thus, the final solution becomes,

$$\varphi = \frac{e^{i\pi/4}}{\sqrt{\pi}}\left[\, e^{iky}\int_{-\infty}^{\xi+\eta} e^{-is^2}ds + e^{-iky}\int_{-\infty}^{\xi-\eta} e^{-is^2}ds \,\right] \tag{2.9}$$

where,

$$\xi+\eta = \pm\sqrt{k(r+y)} \qquad (2.10)$$

$$\xi-\eta = \pm\sqrt{k(r-y)} \qquad (2.11)$$

The signs of $(\xi+\eta)$ and $(\xi-\eta)$ are given according to figure 2.2.

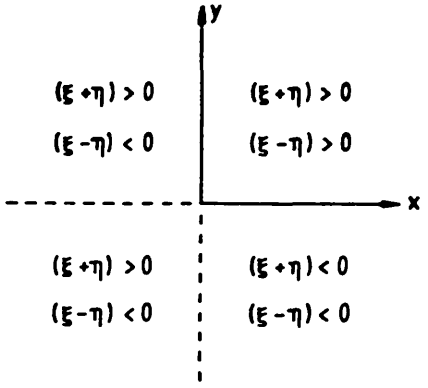

Figure 2.2 Signs of the integration limits

The Fresnel integrals in expression (2.9) may be evaluated from widely available tables on this topic, such as those in Abramowitz and Stegun(1965). Alternatively, the Cornu spiral could be calibrated so that the magnitudes of vectors drawn on it would correspond directly to these integrals.

2.3 Superposition approximation for the gap problem

This method of solution adopted by Penney and Price(1952) assumes that the phenomenon at the gap can be divided into two independent processes: the diffraction of the waves by (a) the left–hand and (b) the right–hand breakwater. The solution for the resultant wave in the aperture case is therefore the sum of the fields in two single breakwater problems. Obviously the boundary conditions at the solid walls are not satisfied, because the method does not take into account the interaction effect between the two structures. The induced error, however, decreases with increasing gap width.

The solution derived afore for the semi–infinite breakwater may be restated here in the notation used by Penney and Price(1952) as,

$$\varphi(x,y) = e^{iky}\, f(\sigma) + e^{-iky}\, f(\sigma') \qquad (2.12)$$

$$f(\sigma) = \frac{1}{2}(1+i) \int_{-\infty}^{\sigma} \exp\left(-\frac{\pi}{2} i u^2\right) du$$

$$\sigma = \sqrt{\frac{4(r+y)}{\lambda}}\,, \qquad \sigma' = \sqrt{\frac{4(r-y)}{\lambda}}$$

where the signs of σ and σ' are given by figure 2.2.

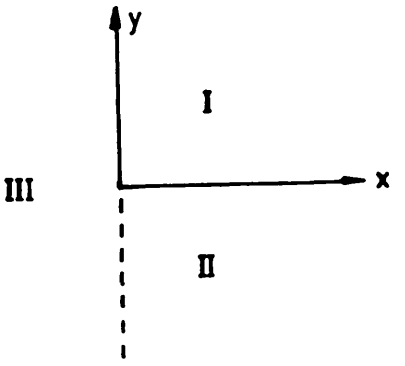

Figure 2.3 Definition sketch

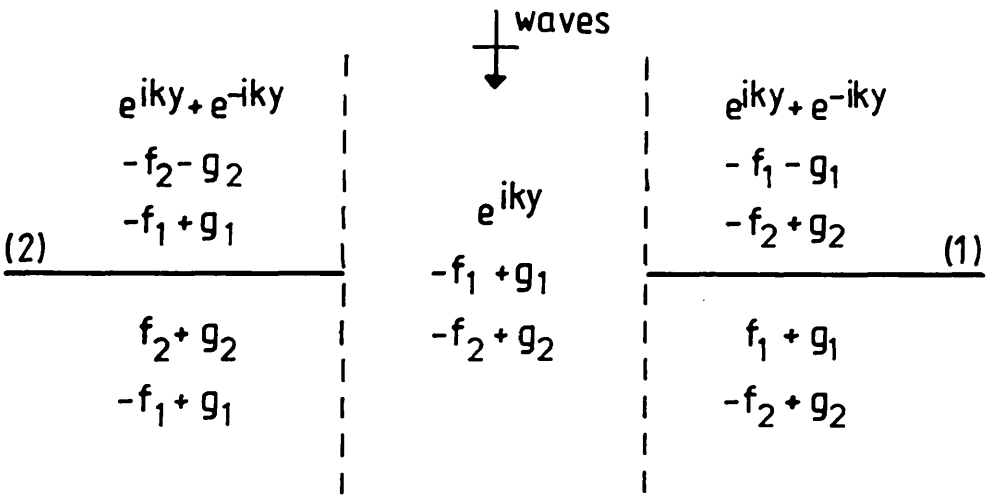

Figure 2.4 Wave field in the gap problem

The relation,

$$f(\sigma) + f(-\sigma) = 1 \qquad (2.13)$$

which can be easily verified, makes possible a decomposition of the wave field of equation (2.12), according to the position of the point (x,y). Hence, after making use of this relation and defining the following quantities:

$$f_1 = e^{iky}\, f(-\sigma)$$

$$g_1 = e^{-iky}\, f(-\sigma')$$

the wave field in each of the regions shown in figure 2.3 becomes:

I: $\qquad \varphi = e^{iky} + e^{-iky} - f_1 - g_1$

II: $\varphi = f_1 + g_1$

III: $\varphi = e^{iky} - f_1 + g_1$

For the case of a gap formed by a pair of semi-infinite breakwaters, we may superpose two such solutions to obtain the scheme of values for $\varphi(x,y)$ shown in figure 2.4. It should be noted that the subscripts, 1 and 2, refer to the two arms. The distances, r_1 and r_2, needed for evaluating σ and σ', are measured from the ends of barriers 1 and 2 respectively.

2.4 Lacombe's method

Lacombe(1952) presented a practical approximate solution for evaluating the amplitude of a swell diffracted at any incidence by a gap in a harbour wall. He applied Green's theorem to a closed contour, l, formed by the portion X'A of the breakwater, the gap AB, the portion BX and then a line to infinity represented schematically in figure 2.5.

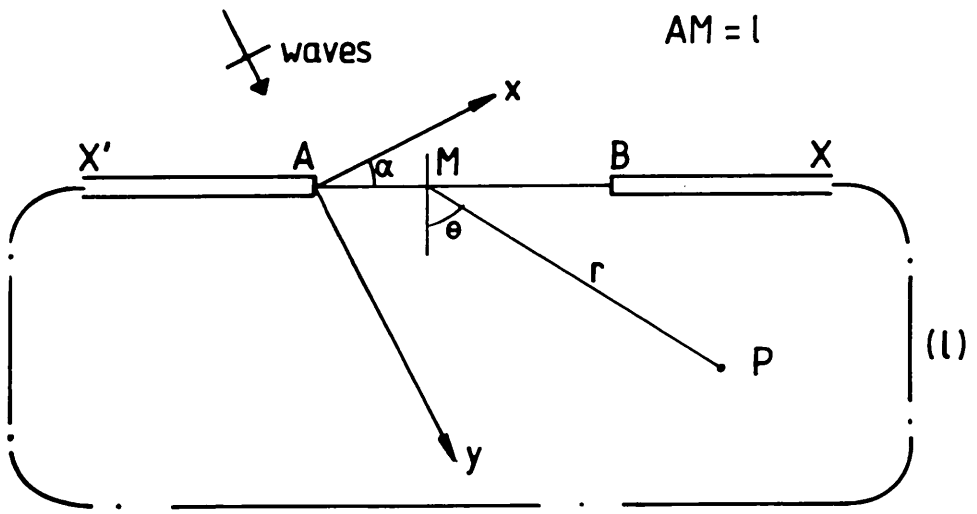

figure 2.5 Definition sketch

The following assumptions were made:

(1) The functions φ and $\partial\varphi/\partial n$ equal zero along the inner faces of the breakwaters.

(2) Between A and B, φ has the value that it would have had in the absence of the breakwaters.

(3) Green's theorem can be applied despite the discontinuities in φ and $\partial\varphi/\partial n$ along the contour.

It may be easily seen that the first of the above assumptions does not allow for the effect of the relative position of the two branches of the breakwater. Thus any geometry of the problem leads to the same result provided the width of the opening is kept constant.

Applying Green's theorem to the present situation we get,

$$4i\varphi_p = \int_l \left[\varphi \frac{\partial H_0}{\partial n} - H_0 \frac{\partial \varphi}{\partial n} \right] dl \qquad (2.14)$$

where H_0 is the Hankel function of the first kind and zeroth order. Equation (2.14) may be interpreted in the following way: The reduced potential at a point, p, enclosed within the contour l is due to the distribution of wave sources, $H_0(kr)$, and wave doublets, $\partial H_0(kr)/\partial n$, on that boundary. $\partial\varphi/\partial n$ and φ represent the densities of the sources and doublets respectively on l.

Using the asymptotic expansion of the Hankel function for large arguments, the following expression for the potential is finally derived:

$$\varphi_p = \int_{AB} \frac{k}{4\pi} (\lambda/r)^{\frac{1}{2}} (\cos\theta+\cos\alpha) \exp(-i(kl\sin\alpha+kr-\pi/4)) dl \qquad (2.15)$$

Another restriction that has been imposed is that r=r(l) is greater than 2 or 3 wavelengths.

2.5 Exact solution

Although this solution is generally credited to Morse and Rubenstein(1938), the basis of their method is largely due to Schwarzschild(1902). The procedure involves the following transformation to elliptic coordinates,

$$(x + iy) = b \cosh(\xi + i\eta) \qquad (2.16)$$

so as to facilitate the application of the boundary conditions.

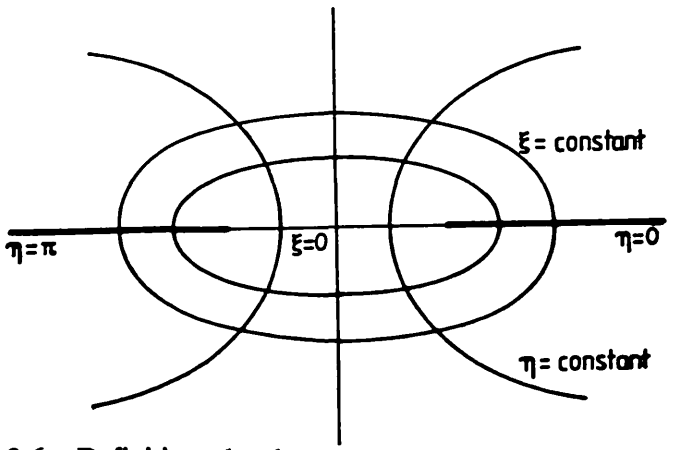

Figure 2.6 Definition sketch

Figure 2.6 shows contours of equal ξ and η where it is important to note that the two breakwater arms are represented by $\eta=0$ and $\eta=\pi$, and the gap by $\xi=0$. b, here, is the half–width of the aperture.

The governing Helmholtz equation then becomes,

$$\frac{\partial^2\varphi}{\partial\xi^2} + \frac{\partial^2\varphi}{\partial\eta^2} + 2k_0^2\,(\cosh 2\xi - \cos 2\eta)\,\varphi = 0 \qquad (2.17)$$

where,

$$k_0 = \frac{kb}{2}$$

Separation of variables in the usual manner,

$$\varphi(\xi,\eta) = F(\xi)\,G(\eta)$$

results in the following two ordinary differential equations for F and G,

$$\frac{d^2F}{d\eta^2} + (a - 2k_0^2\cos 2\eta)\,F = 0 \qquad (2.18)$$

$$\frac{d^2G}{d\xi^2} - (a - 2k_0^2\cosh 2\xi)\,G = 0 \qquad (2.19)$$

where a is the separation constant. Equations (2.18) and (2.19) are respectively called the Mathieu and Modified Mathieu equations. Their solutions, expressed in terms of infinite series of Mathieu functions, are quite standard and may be found in such works as McLachlan(1947).

After imposing the boundary conditions in the problem, which are simply:

(1) $\partial\varphi/\partial y = 0$, at the two breakwaters ($\eta=0$ and $\eta=\pi$).

(2) Continuity of potential across the gap, i.e. φ due to the plane incident, plane reflected and scattered waves on the seaward side, should be equal to φ due to the scattered wave inside the harbour.

The final result for the scattered potential inside the harbour becomes:

$$\varphi = \sum_{n=0}^{\infty}\left[\frac{2}{P_{2n}}\cos\gamma_{2n}\exp(-i\gamma_{2n})\,Me_{2n}(\xi)\,ce_{2n}(\eta)\,ce_{2n}(\theta) + \frac{2i}{P_{2n+1}}\cos\gamma_{2n+1}\exp(-i\gamma_{2n+1})\,Me_{2n+1}(\xi)\,ce_{2n+1}(\eta)\,ce_{2n+1}(\theta)\right] \qquad (2.20)$$

where,

$$\gamma_m = \operatorname{arcotan}\frac{Fe_m'(0)}{Ce_m(0)}$$

and,

$$Me_m = Ce_m + iFeY_m$$

ce_m are even periodic Mathieu functions of the first kind, while Ce_m and FeY_m are modified Mathieu functions of the first and second kinds, respectively. p_m are known constants that are related to the potential of the incident wave.
The complexity of equation (2.20) suggests the use of its asymptotic form at points where the radius of curvature of the wave crest in plan is greater than about three wavelengths. This was done by Carr and Stelzriede(1952) in deriving an 'intensity factor' which gave an indication of the energy transmission into a harbour.

2.6 Interference effects inside a harbour

The existence of amplitude maxima and minima on the centre line through an aperture is well–known in optics but has received little attention in the case of water waves. It may however present a navigational hazard to ships and as such, needs to be closely studied. With this purpose in mind, the superposition approximation of Penney and Price has been utilised to derive the variation of amplitude along the centre line of a semi–infinite harbour at each of the following two gap widths:

$2b/\lambda = 2.0$ and 4.0.

With the narrower opening (figure 2.8), we notice that the variation is quite gradual which implies that such effects would not be of any practical consequence to vessels, especially the larger ones. With the wider gap (figure 2.9) however, the variation is more severe as the numbers of maxima and minima increase. This suggests that vessels might then experience manoeuvring difficulties when entering the harbour. In both cases, the amplitude eventually decays monotonically to zero. In attempting to provide a brief physical interpretation of this behaviour, we may resort to Fresnel's theory of half–period zones (Longhurst(1973)). For points at large distances from the entrance inside the harbour, there is no phase opposition between the contributions from the secondary wave sources in the gap. Closer to the entrance, on the centreline, there is a succession of maxima and minima corresponding to odd and even numbers of Fresnel wave source strips in anti phase on the entrance. These half–period strips increase with the width of the gap which results in interference patterns with more maxima and minima of amplitude for the wider openings as has been demonstrated by the results. In the case of a spectrum of different frequencies, the amplitude variations would be the

square root of those in regular waves as the superposition is by intensities (amplitude squared) in the random case.

Out of theoretical interest, the distinction between Fresnel and Fraunhofer diffraction patterns is now briefly examined. The two types of diffraction can only be differentiated when considering the variation of amplitude along various sections perpendicular to the centre line of a harbour and accordingly, two have been chosen which are 0.2λ and 1.3λ away from a gap whose width is 2.0λ. These two sections would respectively characterise the effects of Fresnel or near–field diffraction and Fraunhofer or far–field diffraction. The corresponding plots shown in figure 2.7 illustrate clearly that the far–field pattern is governed by a linear variation of the phase of contributions from elements across the aperture as is observed in the optical analogy.

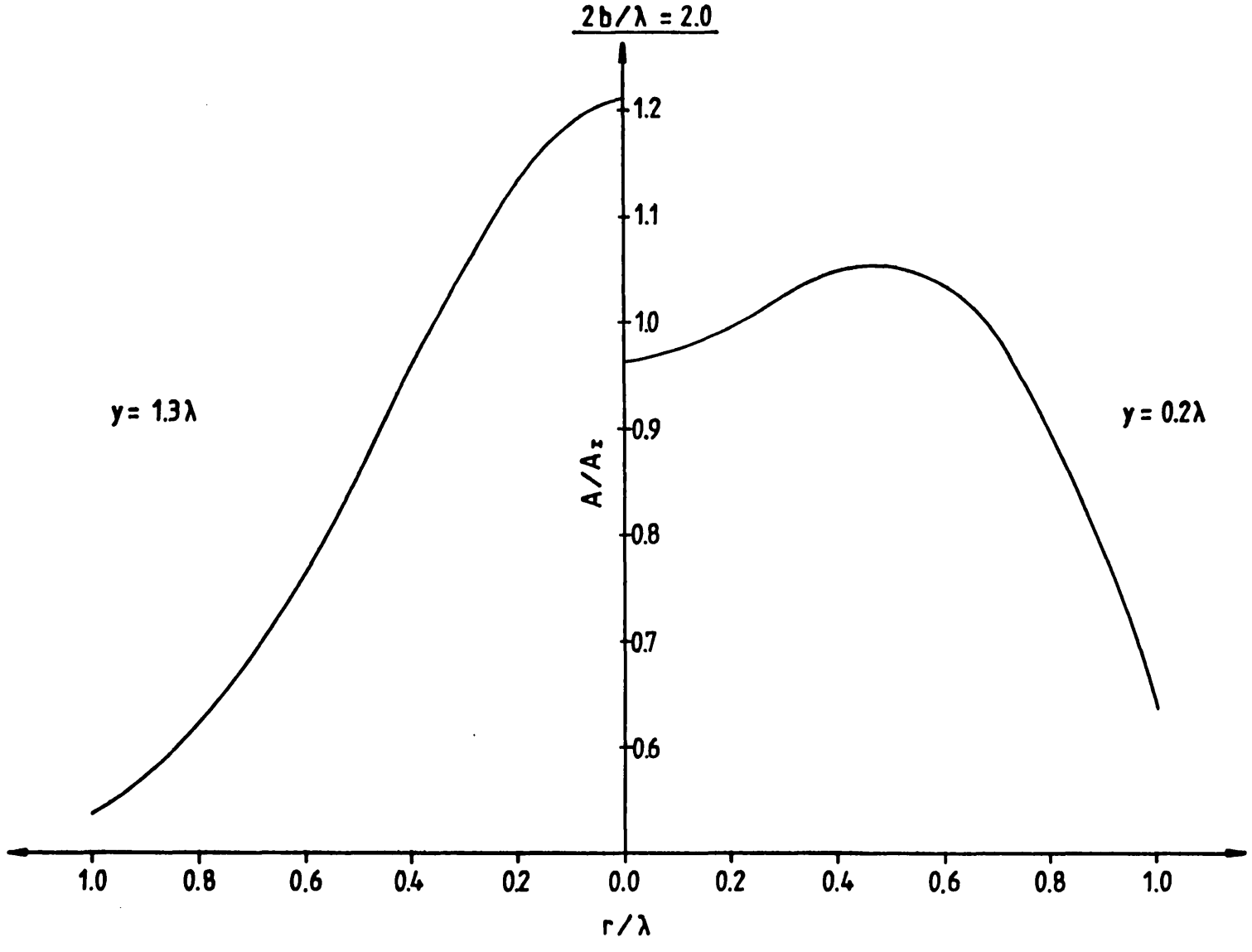

Figure 2.7 Variation of amplitude along two sections perpendicular to the centreline

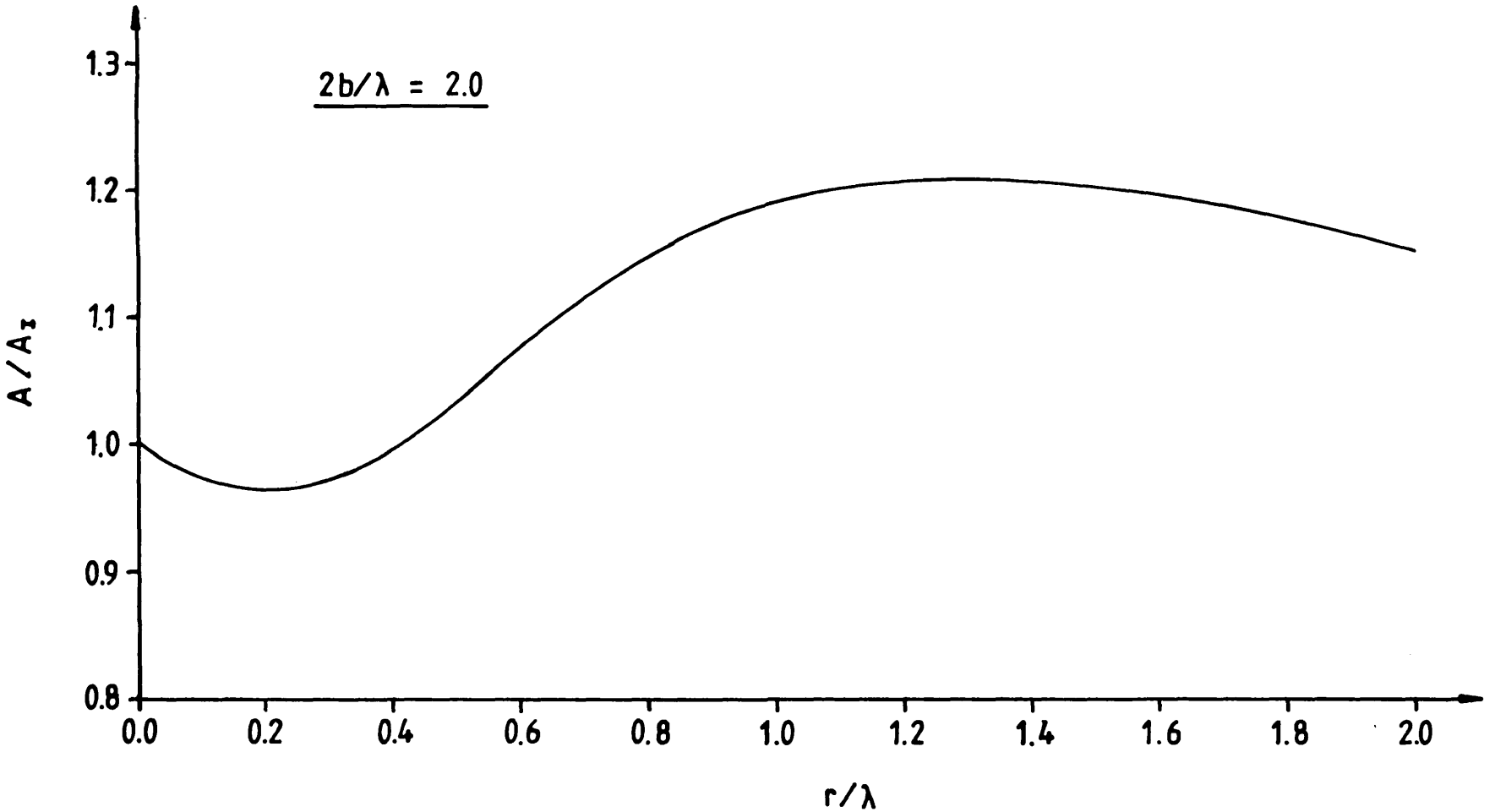

Figure 2.8 Variation of amplitude along the centreline

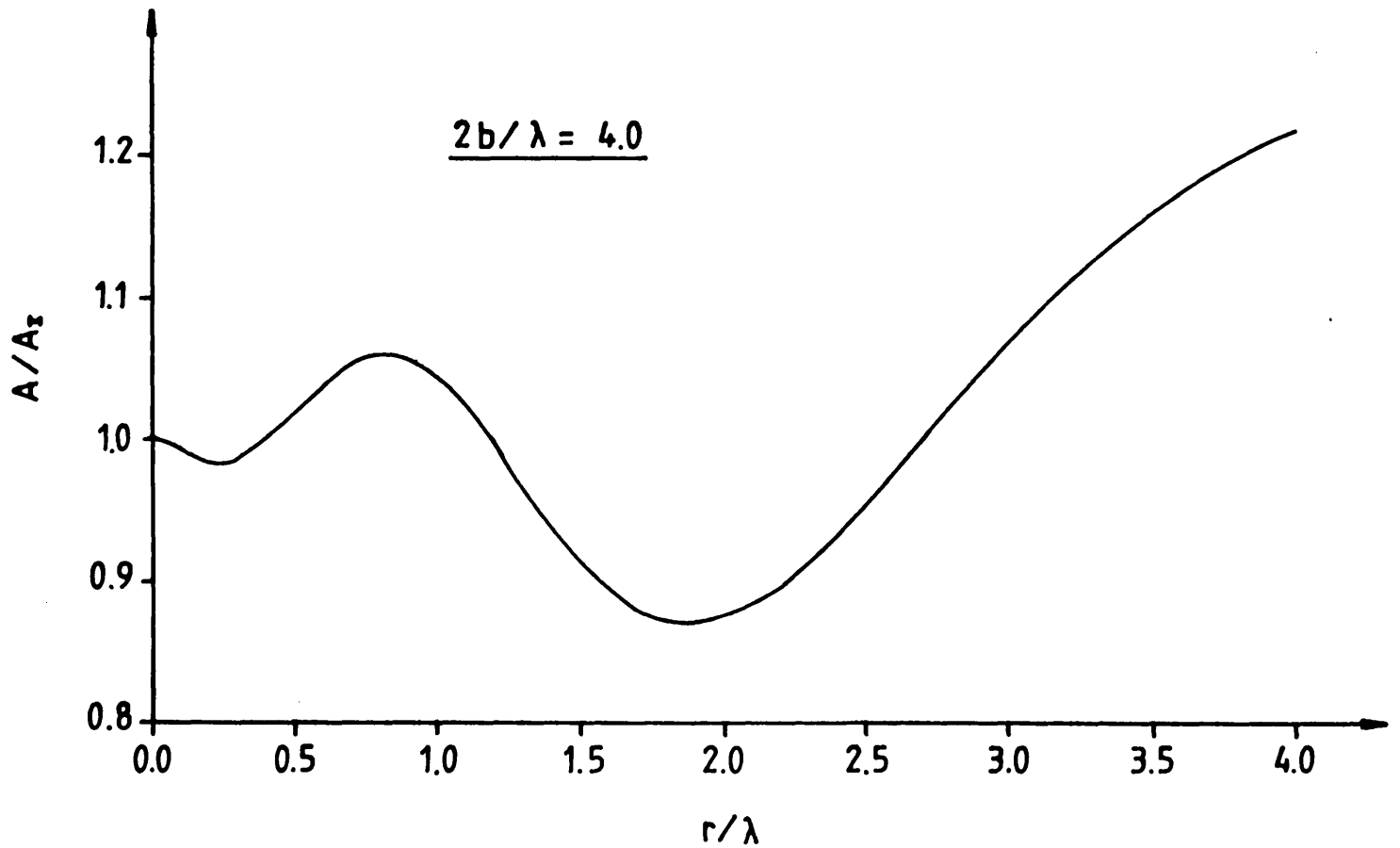

Figure 2.9 Variation of amplitude along the centreline

CHAPTER THREE

An analytical study of the transmission of waves through channels

3.1 Scope of the work

It has long been noted by competent observers (e.g. Bruun(1973)) that significant reductions in wave transmission take place when channels are provided for navigational purposes at harbour entrances. Four different configurations for such channels are considered in this chapter with the aim of investigating analytically their impedance properties. The first two problems studied (figures 3.1a and 3.1b) are concerned with the propagation of small amplitude water waves along a semi–infinite channel, and their consequent scattering at the mouth into an unconfined basin. In this respect, two geometries have been considered: one when the channel is provided with an infinite flange at its outlet and the other when it is unflanged. In both cases the separation of the channel walls, 2b, is taken to be small in relation to the wavelength. The next problem examined is the diffraction of waves by an opening in a breakwater of finite thickness (figure 3.1c). Here, both the gap width, 2b, and the thickness of the arms, 2a, are assumed small relative to the wavelength. The last problem considered is perhaps the most interesting from a practical point of view and concerns the transmission of waves through a long channel (figure 3.1d). No maximum restrictions are imposed on the length of the channel but its width, 2b, is again assumed small relative to the wavelength.

Viewed as perturbation problems for $\epsilon \to 0$ (ϵ=kb, k being the wavenumber), all of the above involve two disparate length scales, b, and k^{-1}, so displaying the hallmark of singular perturbation problems. Accordingly, we anticipate the need for two complementary solutions, termed the inner and outer, appropriate to the length scales b and k^{-1} respectively. The method of matched asymptotic expansions is particularly suitable for two–dimensional diffraction problems and as such, shall be used in this context. The basic idea underlying the method is the representation of the solution by more than one expansion, each of which is valid in part of the domain, and neighbouring expansions overlap so that they can be matched. The method involves loss of boundary conditions as an outer expansion cannot be expected to satisfy conditions that are imposed in the inner region; conversely, the inner will not in general satisfy distant conditions. The possibility of matching, which is the crucial feature of the method, rests on the existence of an overlap domain where both the inner and outer expansions are valid. The presence of this realm of joint applicability

implies that the inner expansion of the outer solution should, to appropriate orders, agree with the outer expansion of the inner solution. This general matching principle can be given various specific formulations.

3.2 Previous work

The method of matched asymptotic expansions has been widely used in the general problem of wave transmission through apertures. Rayleigh(1897) pioneered the technique when studying the diffraction of plane sound waves by a small gap in a thin barrier. He used the idea that, in the neighbourhood of the aperture, the flow is purely local without far–field influence apart from the over–all scale of velocities. The field equation then changes in the inner region from the wave equation to Laplace's equation. This inner solution then matches an outer solution which looks just like an acoustic source situated at the position of the infinitesimal aperture. Although he did not use the formal language or apparatus of 'matched asymptotic expansions', Rayleigh was already thinking in such terms last century. The same problem was later taken up by Lamb(1932) who derived an energy transmission coefficient (to be defined later) and found that as the gap width is made smaller, the proportion of energy that penetrates through increases significantly. This has obvious implications for the design of entrances to harbours that are subjected to the action of long waves. An alternative configuration of a gap formed by two inclined barriers was analysed by Memos(1980) using similar theory. In the limiting case of the two barriers being aligned, his solution reduces to that of Lamb. A more general geometry where the gap was not confined to being in–line with one of the barriers was studied by Smallman(1986). Liu(1975) developed an asymptotic theory to investigate the interaction of water waves with two parallel breakwaters as a first step towards studying the harbour inlet problem. A transmission coefficient was derived which was found to be insensitive to the incident wave angle and the separation between the barriers. There has also been a considerable amount of work devoted to the equivalent case of the submerged horizontal aperture. The initial advance by Tuck(1971) in this field, in which he examined the transmission of waves through a narrow horizontal slit in a thin vertical wall was extended to include the effects of a small finite thickness of the barrier by Guiney et al(1972). Later, Liu and Wu(1986) looked at the case where the thickness of the barrier was of the same order as the wavelength.

Although the perturbation parameter has to be small in all of the above problems, there is no clearly defined limit at which the asymptotic theory fails. A comparison was therefore made for the purpose of guidance, between

Rayleigh's(1897) solution and that obtained by Morse and Rubenstein(1938), which is exact for all gap widths. The latter solves the Helmholtz equation in elliptic coordinates, resulting in an energy transmission coefficient that is expressed as a series of Mathieu functions. A similar coefficient was determined for the former solution by Lamb(1932), and the variation of these with the dimensionless gap width is plotted in figure 3.2. The exact solution is presented for an angle of incidence of 90° i.e. normal incidence. Lamb's solution, on the other hand, is independent of the angle of incidence as the matching theory utilised is of a low order. From this graph it is apparent that the asymptotic theory must not be extended beyond a gap width of 0.2 wavelengths for this particular case. This result throws some light on the limit for other configurations.

A comprehensive account of the mathematical theory of matched asymptotic expansions is found in the work of Van Dyke(1964) where a simplified but effective matching principle is proposed. This has been slightly modified by Fraenkel(1969) where the necessity of grouping together logarithmic with algebraic terms is implied. Applications to a wide variety of problems in fluid mechanics, especially in the field of viscous flow, are also presented by Van Dyke(1964). A similar exposition is given by Nayfeh(1981) who discusses the method in relation to boundary layer problems.

3.3 Scattering at the outlet of a semi–infinite channel

As mentioned before, two cases corresponding to the channel being flanged and unflanged at its end shall be treated here. In both cases, the analysis procedure involves seeking outer and inner solutions at length scales of $O(k^{-1})$ and O(b) respectively, which are consequently matched to determine unknown constants.

3.3.1 Flanged channel : mathematical analysis

Outer solution

Two outer regions, located far away from the origin, in the basin and the channel, emerge when viewing this problem at the larger length scale. In the 'basin outer region' the channel walls are effectively collapsed and therefore the flow there appears to be due to a simple oscillatory source placed at the channel mouth. The potential of a source of unit strength, situated at the origin and emitting waves in an unconfined two–dimensional plane is given by:

$$\varphi = \frac{i}{4} H_0(kr) \qquad (3.1)$$

where $H_0(kr)$ is the Hankel function of the first kind and zeroth order. In the present context, the source is required to radiate in a restricted region given by the upper half of the x–y plane, whence we have to multiply φ by a factor of 2. A further factor is introduced when bringing the unknown strength of the source, taken as Q, into the formulation. In the 'channel outer region' the propagation is one–dimensional and accordingly, the flow may be represented by the superposition of a plane incident wave of unit amplitude and a plane reflected wave of as yet unknown amplitude, $|R|$. Thus, the complete specification of the outer solutions is given as:

$$\varphi = \begin{cases} e^{ikx} + Re^{-ikx} & : \text{channel} \qquad (3.2a) \\ \frac{Qi}{2} H_0(kr) & : \text{basin} \qquad (3.2b) \end{cases}$$

The inner expansions of (3.2a) and (3.2b) may now be obtained by taking the limits as $kx \to 0$ and $kr \to 0$. Making use of the following asymptotic expansions,

$$e^{ikx} \approx 1 + ikx \ , \ \text{as } kx \to 0 \qquad (3.3)$$

$$H_0(kr) \approx 1 + \frac{2i}{\pi} \left(\log \frac{kr}{2} + \gamma\right) \ , \ \text{as } kr \to 0 \qquad (3.4)$$

where, $\gamma = 0.5772$, is the Euler constant, the inner expansions of the outer solutions become:

$$\varphi \approx \begin{cases} (1+R) + (1-R)ikx & : \text{channel} \qquad (3.5a) \\ \frac{Qi}{2} \left[1 + \frac{2i}{\pi} \left(\log \frac{k}{2} + \gamma\right) + \frac{2i}{\pi} \log r \right] & : \text{basin} \qquad (3.5b) \end{cases}$$

Inner solution

It is required here to examine the flow in the neighbourhood of the channel outlet at the smaller length scale. Under this condition, the governing Helmholtz equation reduces to Laplace's equation and consequently the flow may be approximated to a streaming motion. The problem therefore becomes one of solving a conformal transformation of the Schwarz–Christoffel type. With reference to figure 3.3, the z–plane is mapped to the upper half of the ζ–plane by the following transformation:

$$z = \frac{2b}{\pi}\left[-i(\zeta^2-1)^{1/2} + \log\left[\frac{\zeta}{(\zeta^2-1)^{1/2} + i} \right] \right] \qquad (3.6)$$

which is given by Newman et al(1984) in their work on the added mass and damping of rectangular bodies close to the free surface, where similar geometries were encountered. Under this transformation, a simple streaming source placed at the origin of the ζ–plane would give the required flow in the z–plane. The inner solution then takes the form,

$$\varphi = m \log |\zeta| + n \qquad (3.7)$$

where m and n are unknown constants. The outer expansions of the inner solution are obtained by approaching the vicinities of the two outer regions. Looking at the conformal map of figure 3.3, this is seen to be achieved by taking the limits as $|\zeta| \to 0$ where the channel outer region is approached and $|\zeta| \to \infty$ where the basin outer region is approached. Now, from equation (3.6) we can derive the following approximations,

$$\text{as } |\zeta| \to 0, \qquad z \to \frac{2b}{\pi}\left[1 + \log \frac{\zeta}{2i} \right], \qquad |\zeta| \to \frac{2}{e} e^{\pi x/2b}$$

and,

$$\text{as } |\zeta| \to \infty, \qquad z \to -\frac{2b}{\pi} i\zeta, \qquad |\zeta| \to \frac{\pi r}{2b}$$

which upon substitution in equation (3.7), the outer expansions of the inner solution become:

$$\varphi \approx \begin{cases} \dfrac{m\pi}{2b} x + m \log \dfrac{2}{e} + n & : \text{channel} \qquad (3.8a) \\ m \log r + m \log \dfrac{\pi}{2b} + n & : \text{basin} \qquad (3.8b) \end{cases}$$

Matching

The matching principle first used by Rayleigh(1897) and later formalised by Van Dyke(1964) states that the inner expansions of the outer solution shall be equivalent to the outer expansions of the inner solution. In using this principle, equations (3.5a) and (3.5b) are equated to equations (3.8a) and (3.8b) respectively. Coefficients of x as well as of log r are grouped together and separated from the constant terms. This results in four simultaneous equations for the four unknown constants in our problem:

$$1 + R = m \log \frac{2}{e} + n \tag{3.9}$$

$$(1 - R)\ ik = \frac{m\pi}{2b} \tag{3.10}$$

$$\frac{Qi}{2} \left[1 + \frac{2i}{\pi} \left[\log \frac{k}{2} + \gamma \right] \right] = m \log \frac{\pi}{2b} + n \tag{3.11}$$

$$-\frac{Q}{\pi} = m \tag{3.12}$$

After some algebraic manipulation, the above equations yield for Q and R,

$$Q = \frac{2}{\left[\frac{1}{\pi} \log \frac{\pi e}{2kb} - \frac{\gamma}{\pi} + \frac{i}{2} \left[1 + \frac{1}{kb} \right] \right]} \tag{3.13}$$

$$R = 1 - \frac{i}{kb \left[\frac{1}{\pi} \log \frac{\pi e}{2kb} - \frac{\gamma}{\pi} + \frac{i}{2} \left[1 + \frac{1}{kb} \right] \right]} \tag{3.14}$$

Q being the quantity of interest as far as the transmission into the harbour is concerned while R gives an indication of the amplitude of the wave that is reflected at the open end. Following Lamb's(1932) lead, an energy transmission coefficient, T, may now be defined as the ratio of the energy flux of the scattered waves, in the harbour, to that of the primary waves in the channel. As the energy flux across a specific section of the wavefront is the product of the length of this section and the square of the wave amplitude there, T becomes,

$$T = \frac{\pi r}{2b} |\varphi|^2 \tag{3.15}$$

where r is the radius of a semi–circle centered on the origin, and extending into the harbour, and $|\varphi|$ is the constant amplitude along its circumference. The distance, r, has to be large in relation to the wavelength so that the circular wavefronts may be approximated to plane ones, thus validating our definition of the energy flux. Substituting for φ (the potential in the basin outer region), from equation (3.2b), we obtain,

$$T = \frac{\pi r}{2b} \left| \frac{Qi}{2} H_0(kr) \right|^2$$

which may be simplified further by making use of the following asymptotic

expansion:

$$H_0(kr) \approx \sqrt{\left[\frac{2}{\pi kr}\right]}\, e^{-i(kr+\pi/4)} \quad , \text{ as } kr \to \infty \qquad (3.16)$$

Substituting this in turn, we get the final expression for the energy transmission coefficient as:

$$T = \frac{1}{kb\left[\left[\frac{1}{\pi}\log\frac{\pi e}{2kb} - \frac{\gamma}{\pi}\right]^2 + \frac{1}{4}\left[1 + \frac{1}{kb}\right]^2\right]} \qquad (3.17)$$

This result has been checked by ensuring it satisfies the following energy conservation relationship:

$$T + |R|^2 = 1$$

3.3.2 Unflanged channel : mathematical analysis

Outer solution

The steps involved here are as in the previous case, where we look at the solution far away from the origin. Indeed, the mathematical formulation is identical except for one minor difference. As the channel is unflanged, the flow in the basin outer region appears to be due to an oscillatory source situated at the channel mouth and emitting waves in the whole x–y plane as opposed to a confined part of it. Thus, the outer solutions are given by:

$$\varphi = \begin{cases} e^{ikx} + Re^{-ikx} & : \text{channel} \qquad (3.18a) \\ \frac{Qi}{4} H_0(kr) & : \text{basin} \qquad (3.18b) \end{cases}$$

Taking the limits as $kx \to 0$ and $kr \to 0$, and making use of the asymptotic expansions (3.3) and (3.4), the inner expansions of the outer solutions become:

$$\varphi \approx \begin{cases} (1+R) + (1-R)ikx & : \text{channel} \qquad (3.19a) \\ \frac{Qi}{4}\left[1 + \frac{2i}{\pi}\left[\log\frac{kr}{2} + \gamma\right]\right] & : \text{basin} \qquad (3.19b) \end{cases}$$

Inner solution

Again, it is required to examine the streaming flow situation at the mouth of the channel in a manner analogous to that used by Newman(1974) and Liu(1975). We have for the conformal transformation,

$$z = \frac{b}{\pi}\left[\exp(-m(\varphi + i\psi) + n) - m(\varphi + i\psi) + n + 1\right] \qquad (3.20)$$

where $z = x + iy$, as before, and ψ is the stream function. The outer approximation of (3.20) is obtained by taking the limits as $(m\varphi - n) \gg 1$, where the channel outer region is approached, and $(m\varphi - n) \ll 1$, where the basin outer region is approached. Thus we get,

$$\varphi \approx \begin{cases} -\frac{\pi x}{bm} + \frac{(1+n)}{m} & : \text{channel} \qquad (3.21a) \\ -\frac{1}{m}\log(\frac{\pi r}{b}) + \frac{n}{m} & : \text{basin} \qquad (3.21b) \end{cases}$$

Matching

Equations (3.19a) and (3.19b) are to be matched with equations (3.21a) and (3.21b). Four simultaneous equations ensue,

$$(1 + R) = \frac{1 + n}{m} \qquad (3.22)$$

$$(1 - R)ik = -\frac{\pi}{bm} \qquad (3.23)$$

$$\frac{Qi}{4}\left[1 + \frac{2i}{\pi}\left(\log\frac{k}{2} + \gamma\right)\right] = -\frac{1}{m}\log\frac{\pi}{b} + \frac{n}{m} \qquad (3.24)$$

$$\frac{Q}{2\pi} = \frac{1}{m} \qquad (3.25)$$

from which we get the following results:

$$Q = \frac{2\pi}{\left[\frac{1}{2}\left[1 - \gamma + \log\frac{2\pi}{kb}\right] + \frac{i\pi}{4kb}(2 + kb)\right]} \qquad (3.26)$$

$$R = 1 - \frac{i\pi}{kb\left[\frac{1}{2}\left[1 - \gamma + \log\frac{2\pi}{kb}\right] + \frac{i\pi}{4kb}(2 + kb)\right]} \qquad (3.27)$$

The energy transmission coefficient is defined as,

$$T = \frac{2\pi r}{2b}|\varphi|^2$$

where r is now the radius of a circle (as opposed to a semi–circle), centred on the origin. Substituting for φ from equation (3.18b) and making use of the asymptotic expansion, given by (3.16), for $H_0(kr)$ as $kr \to \infty$, T becomes:

$$T = \frac{\pi^2}{\left[\frac{\pi^2}{8kb}(2 + kb)^2 + \frac{kb}{2}\left[1 - \gamma + \log\frac{2\pi}{kb}\right]^2\right]} \qquad (3.28)$$

This again has been checked in the energy conservation relationship.

3.3.3 Results

The variation of the above–derived energy transmission coefficients with the dimensionless separation of the channel walls has been plotted in figure 3.4 to illustrate the physical ideas behind the mathematics. In keeping with our approximate guideline on the limit of the asymptotic theory, the range for $2b/\lambda$ has been taken as extending from 0.0 to a maximum value of 0.2. An interesting feature that is immediately apparent from this graph is the noticeably higher energy penetration into the harbour when the channel is flanged as compared to when it is unflanged. To give a numerical example, when $2b/\lambda = 0.10$, the difference between the transmission coefficients, corresponding to the two different cases, is about 55%. In attempting to explain this finding, we shall have recourse to an acoustical analogy. Morse and Ingard(1968) studied the radiation of sound waves from a plane circular piston, of radius a, set in a plane baffle of infinite extent. This resembled the radiation from a cone loudspeaker which made the problem of practical interest. Their investigations in that respect revealed the following:

"Long–wavelength sound spreads out uniformly in all directions from the piston, with an intensity four times that due to a simple source of strength $\pi a^2 u_0$. If the wall were not present and the piston were the open end of a pipe, this end would act like a simple source of strength $\pi a^2 u_0$ for long wavelengths, so that

the wall, or baffle plate, produces a fourfold increase in intensity. The sound reflected from the baffle reinforces the sound radiated outward, thereby doubling the amplitude of the wave, and thus quadrupling the intensity, which depends on the square of the amplitude. Of course, to have the baffle give this considerable increase in amplitude, it must be considerably larger than the wavelength of the sound radiated, so that it will act as though it were infinite in extent."

This is consistent with our result which may now be seen to have a bearing on the design of harbour entrances. According to this finding, entrance channels should protrude into harbours in the manner illustrated by figure 3.5 if the energy transmission is to be minimised. This configuration corresponds to the channel being flanged at its inlet and unflanged at the outlet, which would also promote radiation damping when the harbour is in resonance, thus leading to a reduction in wave agitation. This is because as far as the radiation damping is concerned, the roles of the inlet and outlet of the channel are reversed as energy 'leaks' out of the harbour thereby reducing amplitudes. The optimum geometry of figure 3.5 is, however, based on a crude deduction, as the above derivation is valid only for semi–infinite channels, which do not exist in reality. Furthermore, this study is incomplete in the sense that we focused only on the outlet problem. A complementary study of the inlet for both flanged and unflanged channels, as carried out by Liu(1975) for the latter case, is desirable in order to extend our conclusions regarding such configurations. Nevertheless, the preceding analysis is useful at a preliminary design stage.

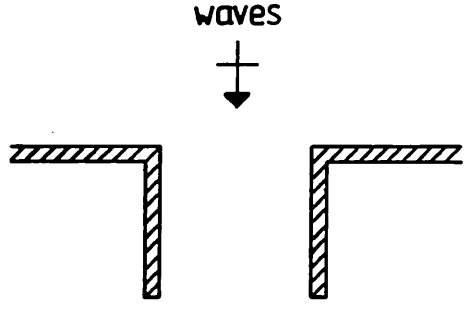

Figure 3.5 Optimum geometry for entrance channels

A second feature emerging from the graph, that is quite striking, is the low energy penetration into the harbour for small values of $2b/\lambda$ (typically, less than about 0.10). The energy transmission coefficients for both channels are seen to diminish to zero as the separation between the walls is made infinitesimal, which suggests a high amount of reflection at the open ends. This

again is consistent with theories in acoustics, where for example, in calculating the specific acoustic impedance at an open end of a tube, Morse(1948) deduced the following:

"At low frequencies the resistive term is quite small, so that very little energy is lost from the open end. Open tubes having cross–sectional perimeter much smaller than the sound wavelength are therefore nearly as good hoarders of energy as are closed tubes, for only a small percentage of the stored energy can be radiated away in any cycle."

The resistive term mentioned above is a purely frictional reaction. In the hydrodynamic case, the process of reflection at an open end can play a major role in the propagation of tides through channels. For example, the geometry of the inlet of the Mediterranean basin (from the straits of Gibraltar to the coast of France) resembles a slowly diverging channel with many sudden widenings in section at which significant backward reflections could occur. The cumulative effect could contribute to the low tidal amplitudes found in that basin. As noted by Defant(1960), the Meditterranean is relatively deep and therefore, the reduction of the tide by comparison with the Atlantic could not solely be a consequence of dissipative forces.

3.4 Diffraction by a gap in a thick breakwater

The diffraction of water waves by a gap in a breakwater of finite thickness is examined here under the assumptions, $kb<1$ and $ka<1$ (where a and b are as defined in figure 3.1c). In the limit $2a\to 0$, the problem reduces to that treated by Rayleigh(1897) and Lamb(1932). As with the previous problem, the method of matched asymptotic expansions is employed in the ensuing analysis.

3.4.1 Mathematical analysis

Outer solution

We seek in the outer problem expressions for the reduced potential of the flow far away from the gap, on both sides of the breakwater. Under these conditions, the gap appears infinitesimal and may therefore be replaced by a pair of simple oscillatory sources, each of which radiates in a confined half–plane. If Q_1 and Q_2 are the strengths of these sources on the seaward and leeward sides of the breakwater respectively, and assuming normally incident plane waves, we have for the outer flow field:

$$\varphi = \begin{cases} e^{ikx} + e^{-ikx} + \dfrac{Q_1 i}{2} H_0(kr) & : \text{seaward side} \qquad (3.29a) \\ \dfrac{Q_2 i}{2} H_0(kr) & : \text{leeward side} \qquad (3.29b) \end{cases}$$

Making use of the asymptotic expansions given by (3.3) and (3.4) for e^{ikx} as $kx \to 0$, and $H_0(kr)$ as $kr \to 0$, we obtain the inner approximations of the outer solutions as:

$$\varphi \approx \begin{cases} 2 + \dfrac{Q_1 i}{2} \left[1 + \dfrac{2i}{\pi} \left(\log \dfrac{kr}{2} + \gamma\right)\right] & : \text{seaward side} \qquad (3.30a) \\ \dfrac{Q_2 i}{2} \left[1 + \dfrac{2i}{\pi} \left(\log \dfrac{kr}{2} + \gamma\right)\right] & : \text{leeward side} \qquad (3.30b) \end{cases}$$

Inner solution

The flow in the neighbourhood of the gap is approximated to a streaming motion when the predominant length scale is of the order of the gap width, and hence it is required here to solve a conformal transformation of the Schwarz–Christoffel type. With reference to figure 3.6, the z–plane is mapped to the upper half of the ζ–plane by the following transformation:

$$\frac{dz}{d\zeta} = i\alpha \frac{(\zeta^2 - s^2)^{1/2} (\zeta^2 - 1)^{1/2}}{\zeta^2} \qquad (3.31)$$

where,

$$\alpha = - \frac{b}{2E(s) - s'^2 K(s)} \qquad (3.32)$$

$$s'^2 = 1 - s^2 \qquad (3.33)$$

and s is a root of:

$$\frac{a}{b} = \frac{K(s')s'^2 - 2K(s') + 2E(s')}{2(K(s)s'^2 - 2E(s))} \qquad (3.34)$$

The functions K(s) and E(s) are complete elliptic integrals of the first and second kinds respectively. Equations (3.31) to (3.34) were first derived by Davy(1944) in relation to a problem concerning the magnetic field between two rectangular electrodes, and have since been included in the dictionary of conformal representations by Kober(1957). A simple streaming source situated at the origin of the ζ–plane would give the required flow in the z–plane. The inner solution is

then given by,

$$\varphi = m \log |\zeta| + n \tag{3.35}$$

where m and n are unknown constants relating to the strength of the source. The outer expansions of (3.35) are obtained by letting $|\zeta| \to 0$, where we approach the vicinity of D (the seaward side outer region), and $|\zeta| \to \infty$, where we come close to A (the leeward side outer region). Now, from equation (3.31), we can deduce the following,

$$\text{as } |\zeta| \to 0, \qquad z \to \frac{i\alpha s}{\zeta}, \qquad |\zeta| \to \frac{\alpha s}{r}$$

and,

$$\text{as } |\zeta| \to \infty, \qquad z \to i\alpha\zeta, \qquad |\zeta| \to \frac{r}{\alpha}$$

which upon substitution in equation (3.35) we obtain the outer expansions of the inner solution:

$$\varphi \approx \begin{cases} m \log \dfrac{\alpha s}{r} + n & : \text{seaward side} \qquad (3.36a) \\ m \log \dfrac{r}{\alpha} + n & : \text{leeward side} \qquad (3.36b) \end{cases}$$

Matching

In utilising the matching principle as before, we equate expressions (3.30a) and (3.30b) with (3.36a) and (3.36b) respectively. This yields four simultaneous equations for the four unknown constants.

$$2 + \frac{Q_1 i}{2} - \frac{Q_1}{\pi}\left(\log \frac{k}{2} + \gamma\right) = m \log \alpha s + n \tag{3.37}$$

$$\frac{Q_1}{\pi} = m \tag{3.38}$$

$$\frac{Q_2 i}{2} - \frac{Q_2}{\pi}\left(\log \frac{k}{2} + \gamma\right) = -m \log \alpha + n \tag{3.39}$$

$$-\frac{Q_2}{\pi} = m \tag{3.40}$$

On solving these equations, we get for the source strengths,

$$Q_1 = -Q_2 = -2/\left[i - \frac{1}{\pi}\left(\log\frac{\alpha^2k^2s}{4} + 2\gamma\right)\right] \qquad (3.41)$$

and therefore, the potential far into the lee is given by (3.29b) as:

$$\varphi = i\,H_0(kr)/\left[i - \frac{1}{\pi}\left(\log\frac{\alpha^2k^2s}{4} + 2\gamma\right)\right] \qquad (3.42)$$

An energy transmission coefficient may now be defined in a slightly different fashion, as the ratio of the energy flux of the scattered waves inside the harbour, to that of a section of the primary waves equal in length to the width of the gap. This serves as a comparison between the actual energy transmitted and what would be predicted by geometrical optics at normal incidence, and is given by,

$$T = \frac{\pi r}{2b}\,|\varphi|^2 \qquad (3.43)$$

where, as before, r is the radius of a semi–circle centred on the origin and protruding into the harbour, and φ is derived from expression (3.42) by taking the limit as $kr\to\infty$. Making use of the asymptotic expansion (3.16) for $H_0(kr)$ as $kr\to\infty$, and after some algebraic manipulation, T becomes:

$$T = \pi^2/kb\left[\pi^2 + \left(\log\frac{\alpha^2k^2s}{4} + 2\gamma\right)^2\right] \qquad (3.44)$$

3.4.2 Results

A useful check on our theory was carried out by letting the thickness of the breakwater diminish to zero to see whether the above expression for T reduced to that derived by Lamb(1932) for the equivalent problem of a small gap in a zero–thickness barrier. Lamb's result is given as:

$$T_0 = \pi^2/kb\left[\pi^2 + 4\left(\log\frac{kb}{4} + \gamma\right)^2\right] \qquad (3.45)$$

This indeed was found to be the case as when $2a\to 0$, $s\to 1$ and $\alpha\to b/2$, and therefore $T\to T_0$. The procedure for calculating T involved initially plotting a graph of a/b against s, and then, knowing the particular value of s corresponding to a certain required a/b ratio, α was evaluated and hence T. The elliptic integrals which are part of the formulation were computed using the relevant

subroutines from the NAG library.

In figure 3.7, the variation of T/T_0 with the dimensionless gap width is plotted for three values of breakwater thickness to gap width ratios corresponding to, a/b = 0.3, 0.5 and 1.0. This, in effect, is a measure of the added impedance of the harbour gap due to the finite thickness of the breakwater. From this graph, we may immediately deduce that there is a considerable advantage to be gained, in terms of decreasing the wave penetration into a harbour, by incorporating what amounts to short entrance channels in the overall design of harbours. As an example, consider the case when the gap width and breakwater thickness are equal, i.e. a/b = 1. From the appropriate curve of figure 3.7, we see that there is about a 60% reduction in the energy transmission as compared with the case when the breakwater is of infinitesimal thickness. This reduction is seen to be constant over a range of gap widths extending from $2b/\lambda$ = 0.05 to 0.20. Similarly, for the two other cases plotted (a/b = 0.3 and 0.5), there is a lower but nevertheless noticeable reduction.

The usual approach followed in explaining the physical mechanisms involved in the above impedance process centres around the idea of a finite mass or constriction at the entrance which, in being excited by incoming waves communicates the vibrations to the interior of the harbour. The fluid in the constriction has a total mass of $\rho S l_e$, where S is the cross–sectional area and l_e is the effective length of the channel. An effective length is used because it turns out that some fluid beyond the ends of the constriction moves along with the fluid in the constriction, and this must be included to obtain the effective mass. If $\lambda \gg l_e$, as it is in the present context, the fluid in the constriction moves as a unit with an acceleration dependent upon the difference in elevation across the two ends. An additional effort is required to accelerate this mass if the length of the channel is increased and hence the energy transmission is further impaired.

An alternative explanation, which is thought to be original, is now given by having recourse to an electrical analogy. A gap in a breakwater may be seen to be equivalent to an electrical inductance as far as its impedance properties are concerned. In the circuit of figure 3.8, a magnetic field is induced in the coil, producing a back electro–motive force (e.m.f.) that opposes the flow of current. One way of increasing the inductance of this coil, and hence the impedance of the circuit, may be achieved by increasing its length. In the hydrodynamic case, the backward scattered wave is responsible for the impedance of the gap. The introduction of an entrance channel to a harbour provides not one but two ends at which reflection occurs. The result is an increase in the total impedance, as has been demonstrated in the preceding analysis. Lengthening this channel is equivalent therefore to augmenting the dimensions of the coil. In

both cases the impedance process is non–dissipative. The wave scattering approach adopted here, is, in the opinion of this author, better suited to dealing with this type of problem than the 'plug of fluid' idea which misses the phenomenon of reflection at the end of the channel where it debouches into the harbour.

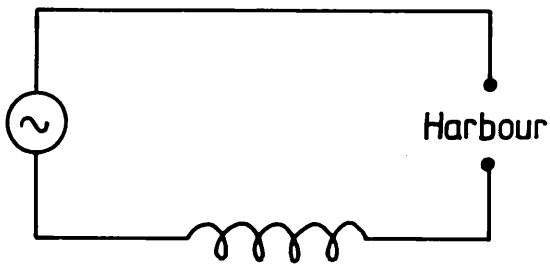

Figure 3.8 Electrical analogy to the problem

3.5 Transmission through a long channel

The transmission of small amplitude water waves through a channel, flanged at both ends, of length, 2a, and width, 2b, is examined under the assumptions, $kb \ll 1$, and $ka = O(1)$. At the larger length scale, k^{-1}, three outer regions emerge, located far away from the channel ends on the seaward and harbour sides, as well as in the middle of the channel. At the smaller length scale, b, two inner regions emerge, located within the vicinities of the channel ends. Inner and outer solutions are sought in the usual way for these near–field and far–field problems and their expansions are subsequently matched in overlap domains in accordance with the schematic illustration of figure 3.9.

3.5.1 Mathematical analysis

Outer solution

In the 'sea' and 'harbour' outer regions, the scattered waves emanating from the channel ends appear as due to simple oscillatory sources placed at the origins of the x–y and x'–y' axes (defined in figure 3.1d). The associated flow fields are thus given accordingly, with plane incident and reflected waves superimposed on the seaward side. In the 'channel' outer region, the flow field comprises two plane waves travelling in opposite directions. If Q_1 and Q_2 are the strengths of the two sources, radiating in the sea and harbour outer regions

respectively, and if $|A|$ and $|B|$ are the amplitudes of the two waves in the channel outer region, we have for the outer solutions,

$$\varphi(\text{sea}) = e^{ikx} + e^{-ikx} + \frac{Q_1 i}{2} H_0(kr) \tag{3.46a}$$

$$\varphi(\text{harbour}) = \frac{Q_2 i}{2} H_0(kr') \tag{3.46b}$$

$$\varphi(\text{channel}) = Ae^{ikx} + Be^{-ikx} \tag{3.46c}$$

where $r'=\sqrt{(x'^2 + y'^2)}$. In deriving the inner expansions of these equations, we have to take the limits as the two inner regions are approached. For the sea outer solution, we let $kx\to 0$ and $kr\to 0$, so that the inner region at the seaward end is approached, while for the harbour outer solution, we let $kr'\to 0$, so that the harbour end inner region is approached. Two inner expansions are needed for the channel outer solution as we have to approach the two inner regions at either end of the channel, and hence we first let $kx\to 0$ and then $kx'\to 0$. Making use of the usual asymptotic small argument expansions for e^{ikx} and $H_0(kr)$ and utilising the following relation,

$$x = -(x' + 2a) \tag{3.47}$$

the inner expansions of the outer solutions become:

$$\varphi(\text{sea}) \approx 2 + \frac{Q_1 i}{2}\left[1 + \frac{2i}{\pi}\left(\log\frac{kr}{2} + \gamma\right)\right] \tag{3.48a}$$

$$\varphi(\text{harbour}) \approx \frac{Q_2 i}{2}\left[1 + \frac{2i}{\pi}\left(\log\frac{kr'}{2} + \gamma\right)\right] \tag{3.48b}$$

$$\varphi(\text{channel} : \to\text{sea}) \approx A + B + ik(A-B)x \tag{3.48c}$$

$$\varphi(\text{channel} : \to\text{harbour}) \approx Ae^{-2ika} + Be^{2ika} + (Ae^{2ika} - Be^{-2ika})ikx' \tag{3.48d}$$

Equations (3.48c) and (3.48d) correspond to the seaward end and harbour end inner expansions respectively.

Inner solution

As the wavelength is much greater than the channel width, the flow in each of the inner regions is approximated to streaming motion at the mouth of a

flanged semi–infinite channel. The problem, which is now seen to be the same as the first one tackled, on the scattering of waves at the outlet of a similar channel, becomes one of solving a conformal transformation of the Schwarz–Christoffel type. This is given by equation (3.6) as,

$$z = \frac{2b}{\pi}\left[-i(\zeta^2-1)^{1/2} + \log\left[\frac{\zeta}{(\zeta^2-1)^{1/2} + i} \right] \right]$$

where, z=x+iy, for the 'seaward end' inner region, and z=x'+iy' for the 'harbour end' inner region.

Two streaming sources, each situated in turn at the origin of the ζ–plane, would give the required flow in the z–plane. The inner solutions are thus obtained as,

$$\varphi(\text{sea}) = m_1 \log|\zeta| + n_1 \qquad (3.49)$$

$$\varphi(\text{harbour}) = m_2 \log|\zeta| + n_2 \qquad (3.50)$$

where m_1, n_1, m_2, n_2 are unknown complex constants, relating to the strengths of the sources. Equations (3.49) and (3.50) have two outer expansions associated with them, that are derived by letting $|\zeta|$ approach zero and infinity. From the map of figure 3.10, this is seen to be equivalent to approaching the vicinities of C and A respectively. After taking these limits, the outer expansions of the inner solutions become:

$$\varphi(\text{sea}) \approx \begin{cases} m_1 \log\frac{2}{e} + n_1 + \frac{m_1\pi}{2b}x & : \text{channel} \qquad (3.51a) \\ m_1 \log\frac{\pi r}{2b} & : \text{sea} \qquad (3.51b) \end{cases}$$

$$\varphi(\text{harbour}) \approx \begin{cases} m_2 \log - + n_2 + \frac{m_2\pi}{2b}x' & : \text{channel} \qquad (3.52a) \\ m_2 \log\frac{\pi r'}{2b} + n_2 & : \text{harbour} \qquad (3.52b) \end{cases}$$

Matching

The matching process used here is a complicated one as there are three outer and two inner solutions. The overlap domains defined in figure 3.9 provide a useful guide, however, and in following them we see that equations (3.48a), (3.48b), (3.48c) and (3.48d) have to be matched with equations (3.51a), (3.51b), (3.52a) and (3.52b) respectively. This results in eight simultaneous equations for the eight unknown constants in our problem:

$$2 + \frac{Q_1 i}{2}\left[1 + \frac{2i}{\pi}\left(\log\frac{k}{2} + \gamma\right)\right] = m_1 \log\frac{\pi}{2b} + n_1 \qquad (3.53)$$

$$\frac{Q_1}{\pi} = -m_1 \qquad (3.54)$$

$$A\, e^{-2ika} + B\, e^{2ika} = m_2 \log\frac{2}{e} + n_2 \qquad (3.55)$$

$$A\, e^{-2ika} - B\, e^{2ika} = \frac{i\pi m_2}{2kb} \qquad (3.56)$$

$$A + B = m_1 \log\frac{2}{e} + n_1 \qquad (3.57)$$

$$A - B = -\frac{i\pi m_1}{2kb} \qquad (3.58)$$

$$\frac{Q_2 i}{2}\left[1 + \frac{2i}{\pi}\left(\log\frac{k}{2} + \gamma\right)\right] = m_2 \log\frac{\pi}{2b} + n_2 \qquad (3.59)$$

$$\frac{Q_2}{\pi} = -m_2 \qquad (3.60)$$

After lengthy algebraic manipulation, these yield for the unknown wave amplitudes, A and B, in the channel and the strength of the source radiating into the harbour outer region, Q_2,

$$A = \frac{i\pi\,(\alpha - i\beta)\, e^{4ika}}{kb(\alpha^2+\beta^2)}\left[\log\frac{2kb}{\pi e} + \gamma - \frac{i\pi}{2}\left(1 - \frac{1}{kb}\right)\right] \qquad (3.61)$$

$$B = \frac{i\pi\,(\alpha - i\beta)}{kb(\alpha^2+\beta^2)}\left[\log\frac{2kb}{\pi e} + \gamma - \frac{i\pi}{2}\left(1 + \frac{1}{kb}\right)\right] \qquad (3.62)$$

$$Q_2 = -\frac{2i\pi^2\,(\alpha - i\beta)\, e^{2ika}}{kb(\alpha^2+\beta^2)} \qquad (3.63)$$

where α and β are given by:

$$\alpha = (\log \frac{2kb}{\pi e} + \gamma)^2 \ (\cos 4ka - 1)$$

$$+ \pi \ (\log \frac{2kb}{\pi e} + \gamma) \ (1 - \frac{1}{kb}) \ \sin 4ka \qquad (3.64)$$

$$- \frac{\pi^2}{4} \ (1 - \frac{1}{kb})^2 \cos 4ka + \frac{\pi^2}{4} \ (1 + \frac{1}{kb})^2$$

$$\beta = (\log \frac{2kb}{\pi e} + \gamma)^2 \ \sin 4ka$$

$$- \pi \ (\log \frac{2kb}{\pi e} + \gamma) \ (1 - \frac{1}{kb}) \ \cos 4ka \qquad (3.65)$$

$$- \frac{\pi^2}{4} \ (1 - \frac{1}{kb})^2 \ \sin 4ka + \pi \ (\log \frac{2kb}{\pi e} + \gamma) \ (1 + \frac{1}{kb})$$

3.5.2 Results

An energy transmission coefficient may now be defined in the usual way, as,

$$T = \frac{\pi r'}{2b} \ |\varphi|^2 \qquad (3.66)$$

where $|\varphi|$ is the uniform far–field amplitude of the waves inside the harbour along a semi–circle of radius, r' (r'$\gg\lambda$), centred on the x'–y' origin. Substituting for φ from equation (3.46b) and making use of the asymptotic expansion, (3.16) for $H_0(kr)$ as $kr\to\infty$, T becomes,

$$T = \frac{\pi^4}{(kb)^3 \ (\alpha^2+\beta^2)} \qquad (3.67)$$

where α and β are as given by equations (3.64) and (3.65) above.
When the channel length is equal to an integral number of half–wavelengths, i.e. $2a = n\lambda/2$, n=0,1,2,3,..., equation (3.67) reduces to,

$$T' = \pi^2/kb\left[\pi^2 + 4 \ (\log \frac{2kb}{\pi e} + \gamma)^2\right] \qquad (3.68)$$

which bears a great resemblance to T_0, the equivalent expression derived by Lamb(1932) for the transmission of long waves through a gap in a thin barrier. A comparison between the two expressions for T' and T_0 in fact reveals that

they are in total agreement except for a minor difference in the argument of the 'log' term, which is $2kb/\pi e$ (=0.23kb) for T', and kb/4 (=0.25kb) for T_0. Considering the complexity of analysis undertaken in the present work, this is seen to be an extraordinary result which substantiates, to some extent, our theory. The reason for T' and T_0 being so similar is because under the condition, $2a = n\lambda/2$, n=0,1,2,..., the change in phase of a wave travelling from one end of the channel to the other, and back again, is such that the problem becomes exactly equivalent to the case when the channel length is zero, as far as the energy transmission into the harbour is concerned.

The variation of T/T_0 with the dimensionless channel length, $2a/\lambda$, is plotted in figure 3.10 to assess the relative wave impedance afforded by the channel. Four curves are plotted corresponding to four different channel widths, given by, $2b/\lambda$= 0.05, 0.10, 0.15 and 0.20. The amplitudes of the waves in the channel, $|A|$ and $|B|$, are similarly plotted in figures 3.11 and 3.12. These graphs repeat periodically at every half–wavelength increment in 2a, and therefore, a representative range for $2a/\lambda$, extending from 1.0 to 1.5, is covered.

The periodic dependence of T on $2a/\lambda$ is an interesting finding from the point of view of optimising channel lengths in the design of harbour entrances. One would at first wrongly suspect that if the channel length was increased indefinitely, the transmission into the harbour would eventually decrease to zero. However, since we have introduced an extra degree of freedom into the system, by allowing one–dimensional waves to exist in the channel, resonance, which is a repetitive process, now plays a major role as is clearly demonstrated by the graphs of figures 3.10, 3.11 and 3.12. This finding is confirmed by analagous problems in acoustics, where for example, in studying the propagation of sound waves in horns, Morse(1948) found that the power radiated out from the mouth was periodically dependent on the length.

The impedance properties of a long channel at the entrance to a semi–infinite harbour may now be assessed in the light of our results. As the physics of this problem is governed by whether or not resonance occurs in the channel, we have to consider its 'performance' over a range of incoming wavelengths. Generally, the occurrence of resonance leads not only to higher wave amplitudes in the channel, but also to higher energy transmission into the harbour due to the added radiation damping from both ends. From the graphs plotted, we notice that the severity of this resonance is rapidly diminished as the width of the channel is increased. As an example, for the case of the widest channel considered ($2b/\lambda$=0.20), the resonance peak is quite flat and the ratio T/T_0 does not deviate by much from unity. Hence, there is no advantage to be gained by utilising such a channel over a simple gap in a thin breakwater, from the point

of view of minimising the wave agitation in a harbour. For the case of the narrowest channel considered ($2b/\lambda=0.05$), on the other hand, the resonance peak is quite sharp and the ratio T/T_0 varies from a maximum value of 4.0 to a minimum one of less than 0.5. This channel may therefore be used to impede the penetration of waves into the harbour over a wide range of wavelengths, at the expense, however, of severe amplification at resonance. For this same case, we see that the amplitude of the wave in the channel increases considerably at resonance so that $|B|$ becomes four times the incident wave amplitude. Needless to say, this may pose a hazard to navigation.

In attempting to provide a physical explanation for the above processes, we may once again resort to an electrical analogy. Whereas with the previous problem, the short entrance channel was seen to be equivalent to an electrical inductance, the behaviour of the long channel in the present case bears a remarkable similarity to an L–C circuit. That is, it is equivalent to an inductance and capacitance connected in series, as shown by figure 3.13. The nett effect of such a circuit is to impede the flow of alternating current for a wide range of frequencies, while amplifying it considerably when the resonance criterion is satisfied. The storage of electrical charge in the capacitor is equivalent to the accumulation of fluid in the channel. Hence, in the hydrodynamic case, a combination of backward scattering and mass build–up leads to the reduced transmission of waves. On a purely theoretical plane, one could envisage a channel of variable length and width so that regardless of the wavelength, the harbour could always be 'tuned' to reflect the incoming waves back to the sea.

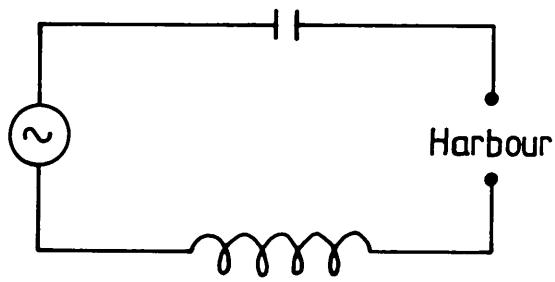

figure 3.13 Electrical analogy to the problem

An interesting point that emerges from our graphs is that the values of $2a/\lambda$ at which resonance occurs in the channels differ slightly from those predicted by the simple theory of harmonics. This is attributable to the effects of the end corrections. A transition takes place in a small region near the channel

ends from plane waves within the channel, to diverging cylindrical waves outside. The total effective length of the channel then becomes,

$$l_e = 2a + 2e$$

where e is the correction at each end. The relationship between e and the width of the channel may be derived by differentiating equation (3.67) with respect to the channel length and equating the resulting expression to zero. This is a condition of stationarity of the function T, which would then correspond to resonance. From the graph of figure 3.10, e is seen to decrease as the width of the channel is reduced. This agrees qualitatively with Rayleigh's(1894) work on resonance in open–ended circular pipes, where the end correction was found to be proportional to the radius of the pipe.

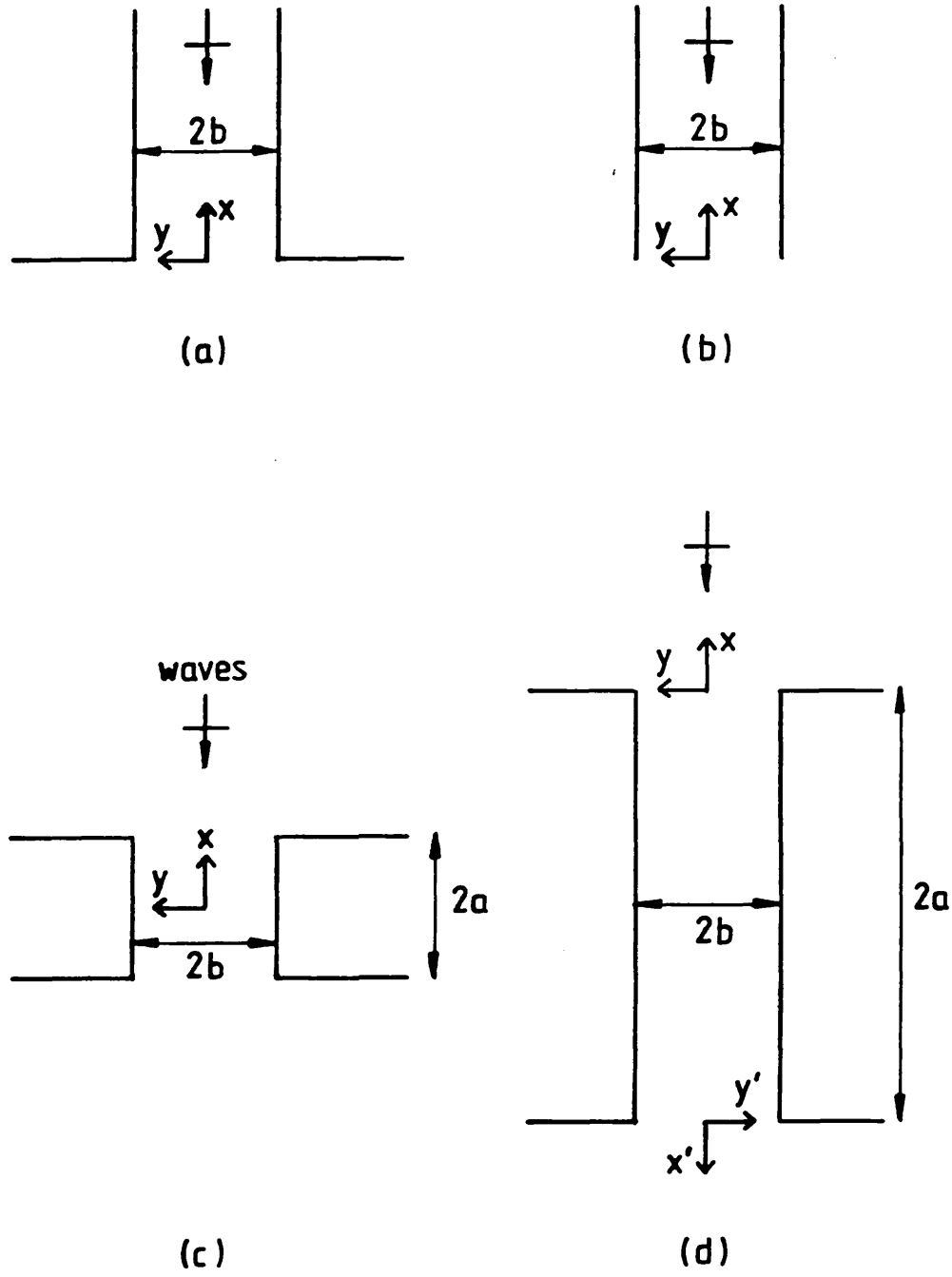

Figure 3.1 Geometries of the problems tackled

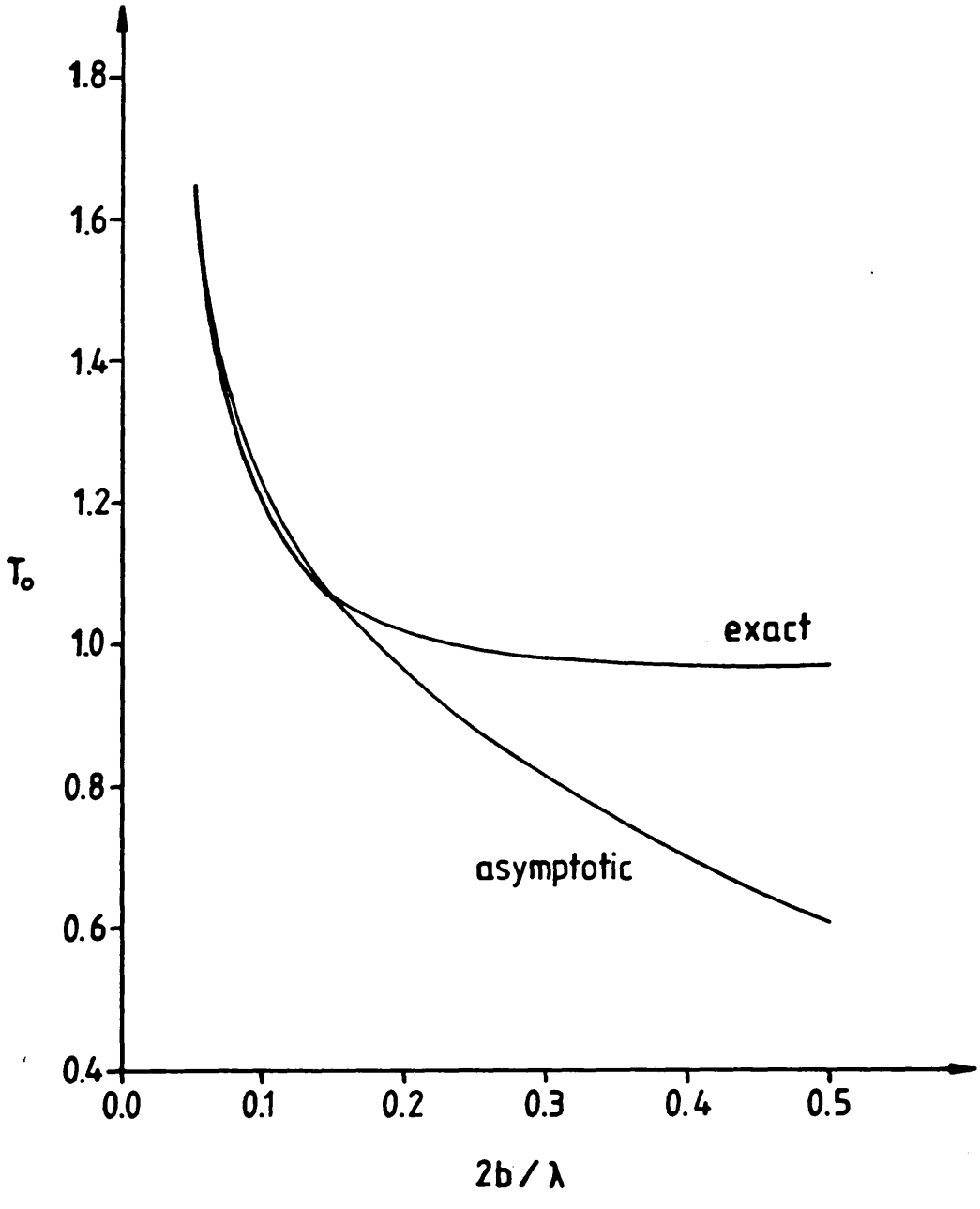

Figure 3.2 Comparison between exact and asymptotic solutions

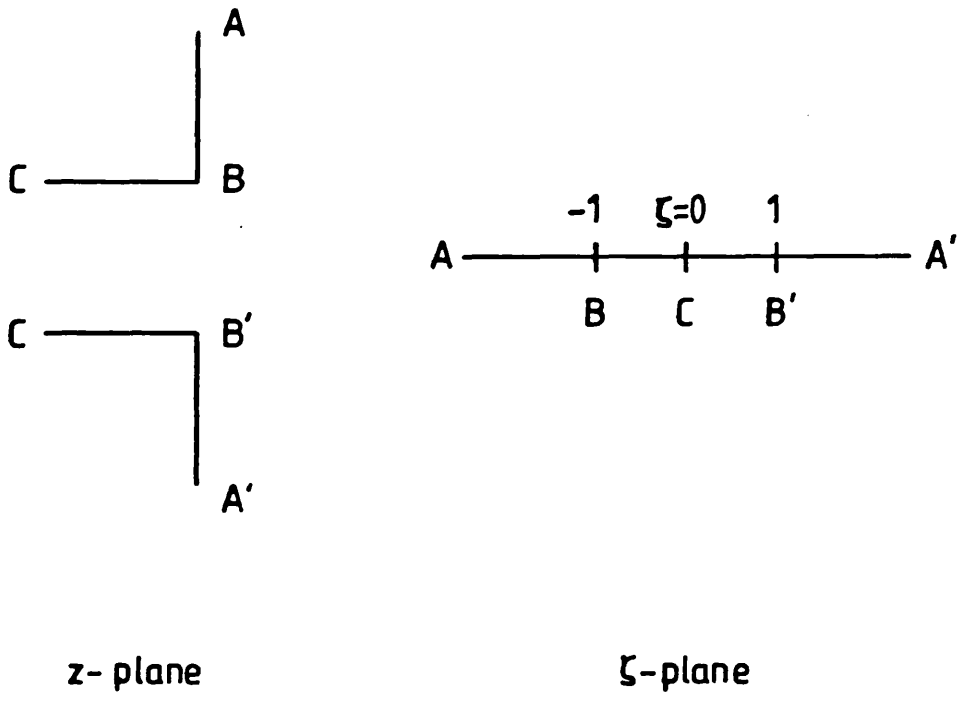

Figure 3.3 Conformal transformation for flanged channel

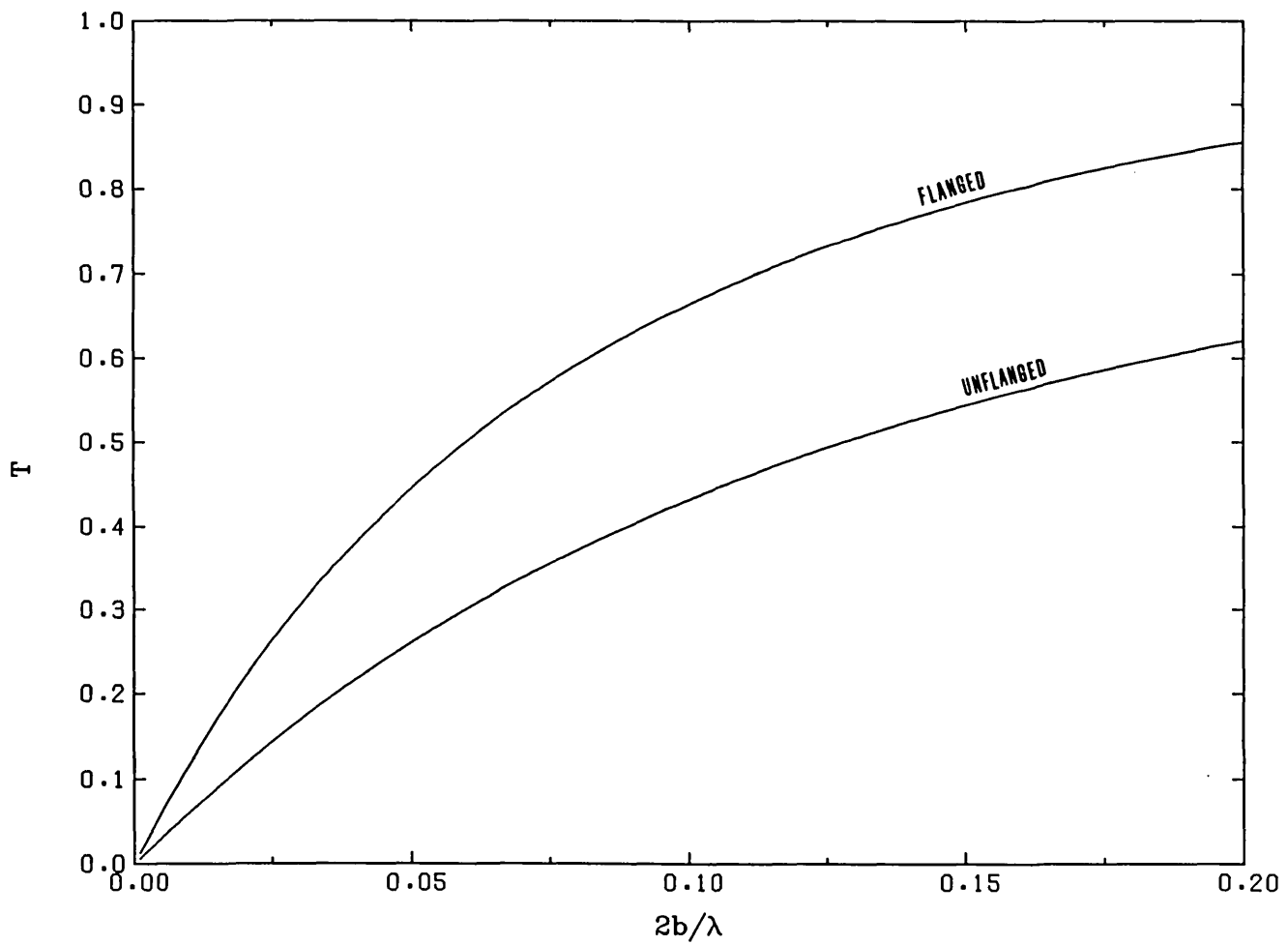

Fig. 3.4 VARIATION OF THE ENERGY TRANSMISSION COEFFICIENTS

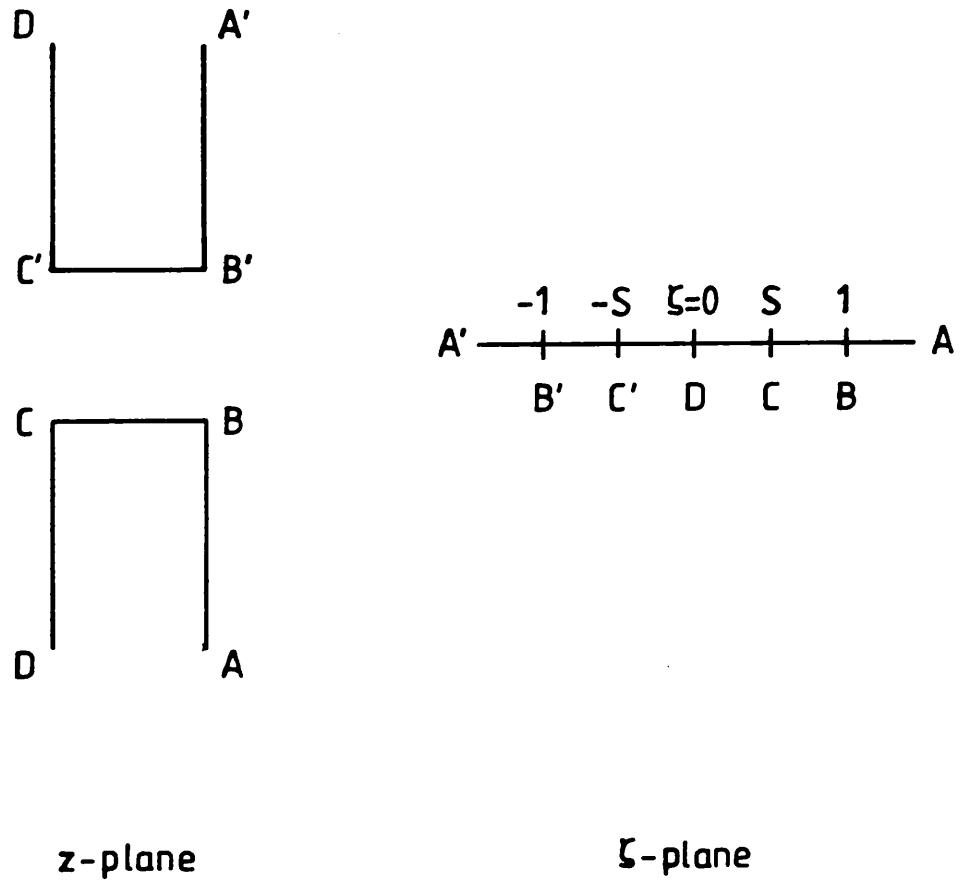

Figure 3.6 Conformal transformation for breakwater gap

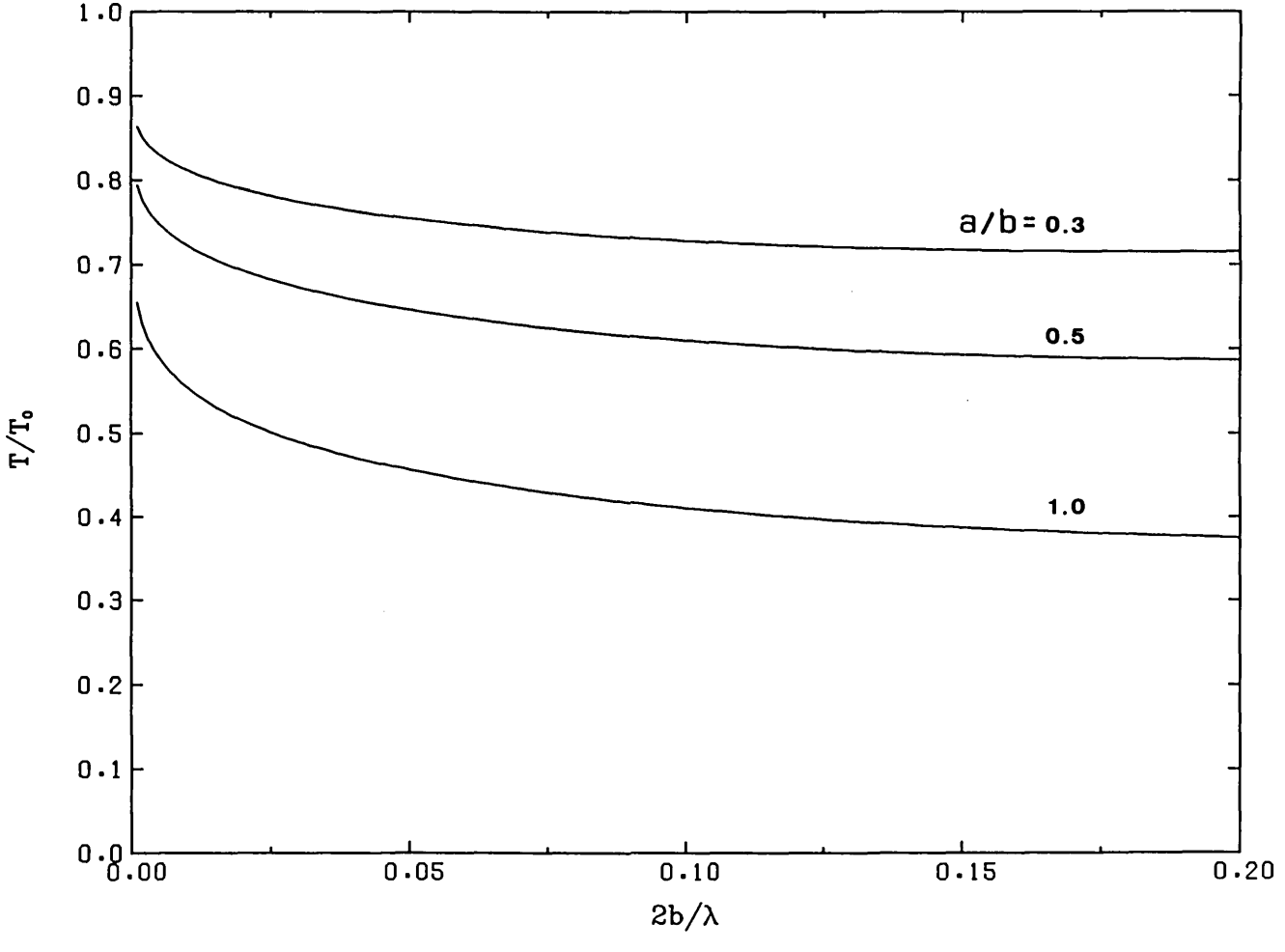

Fig. 3.7 VARIATION OF THE RATIO OF ENERGY TRANSMISSION COEFFICIENTS

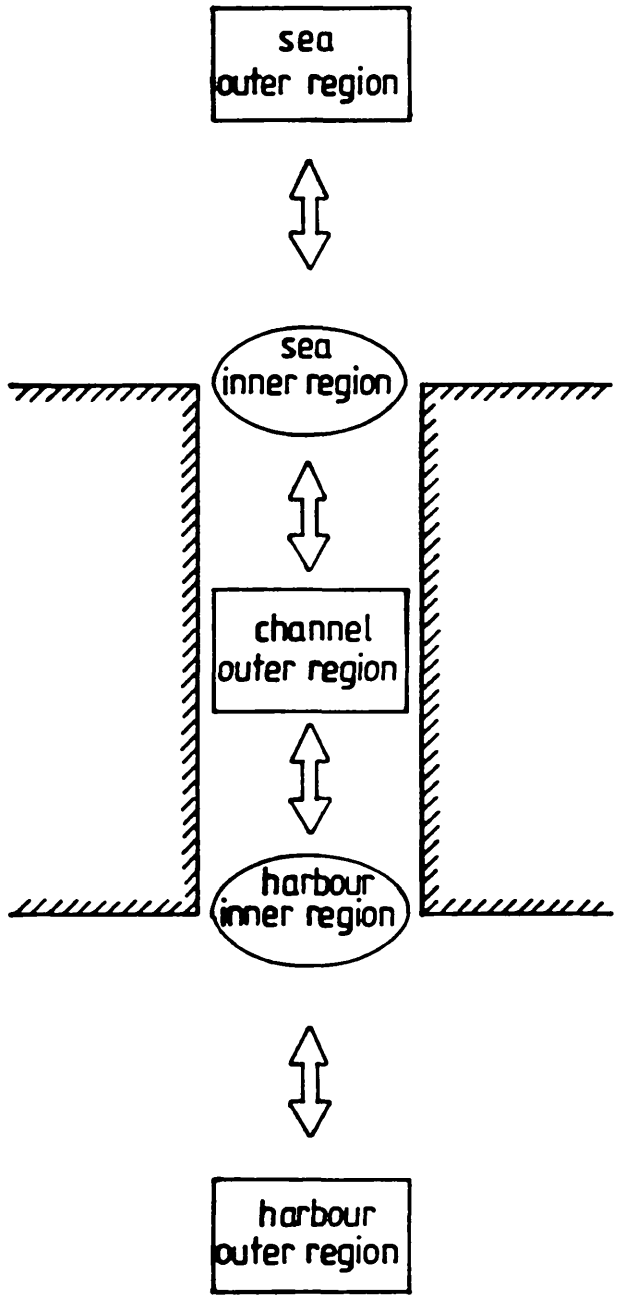

Figure 3.9 Illustrative sketch of matching procedure for long channel problem

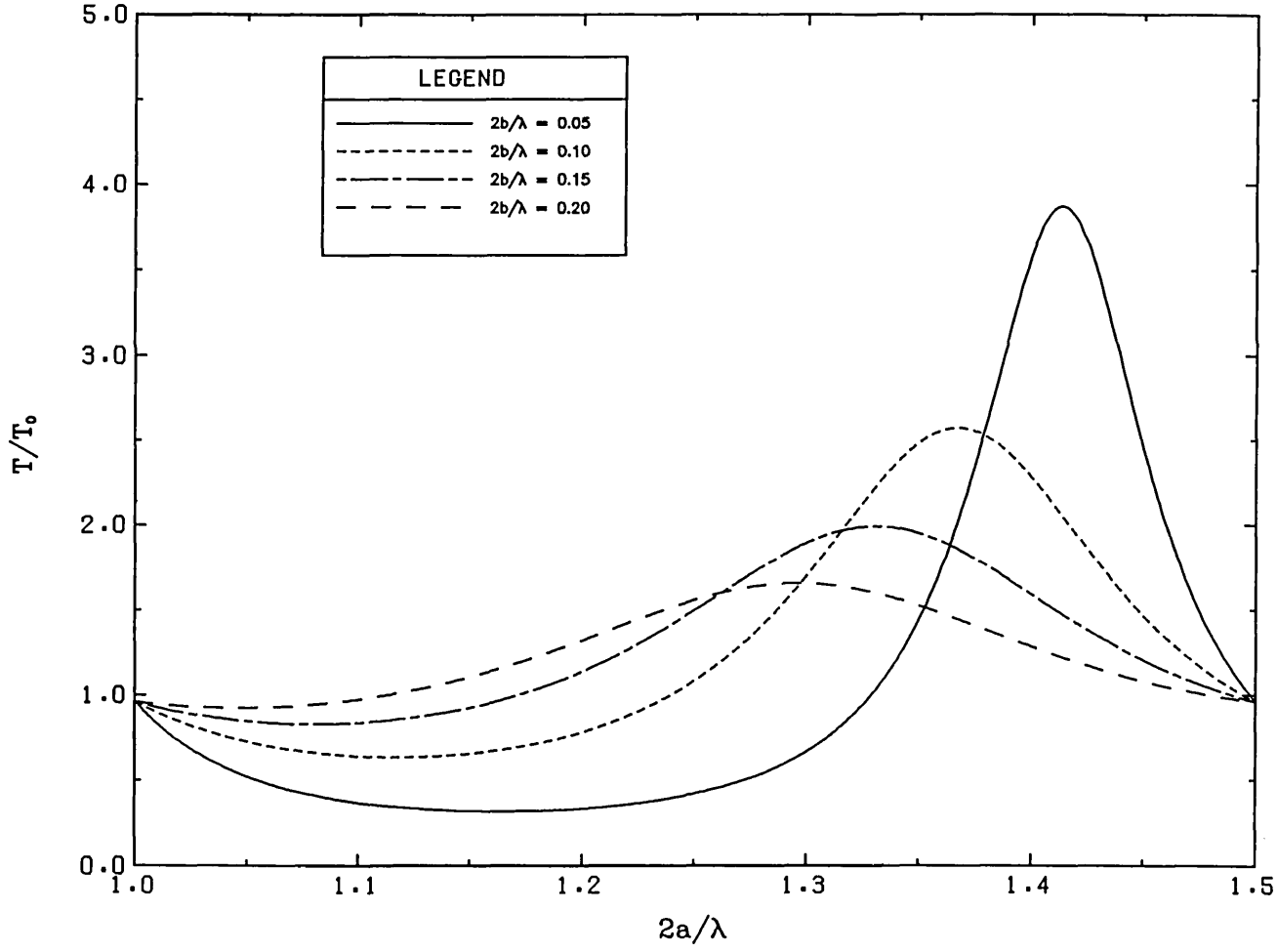

Fig. 3.10 VARIATION OF THE RATIO OF ENERGY TRANSMISSION COEFFICIENTS

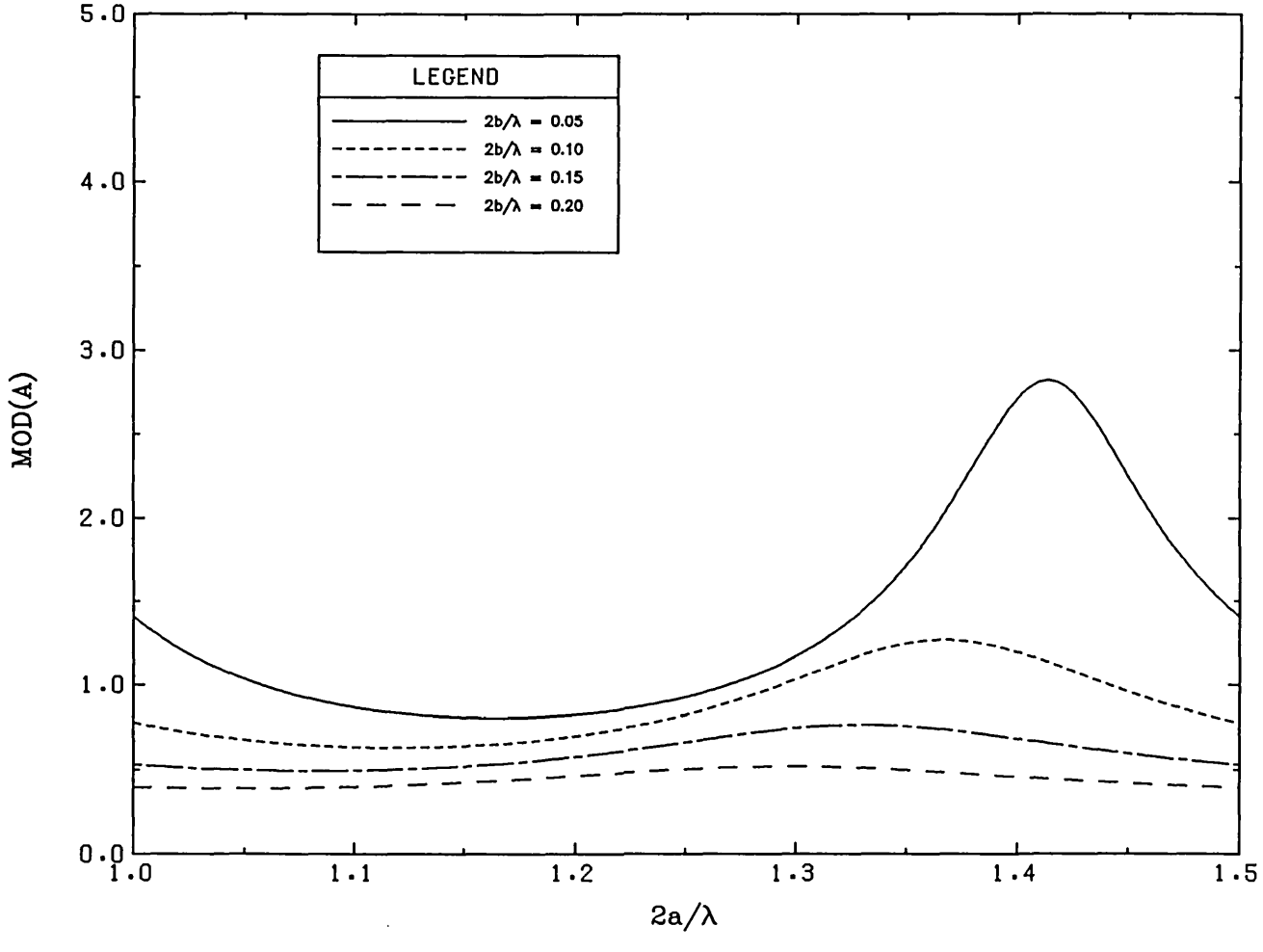

Fig. 3.11 VARIATION OF THE WAVE AMPLITUDE IN THE CHANNEL

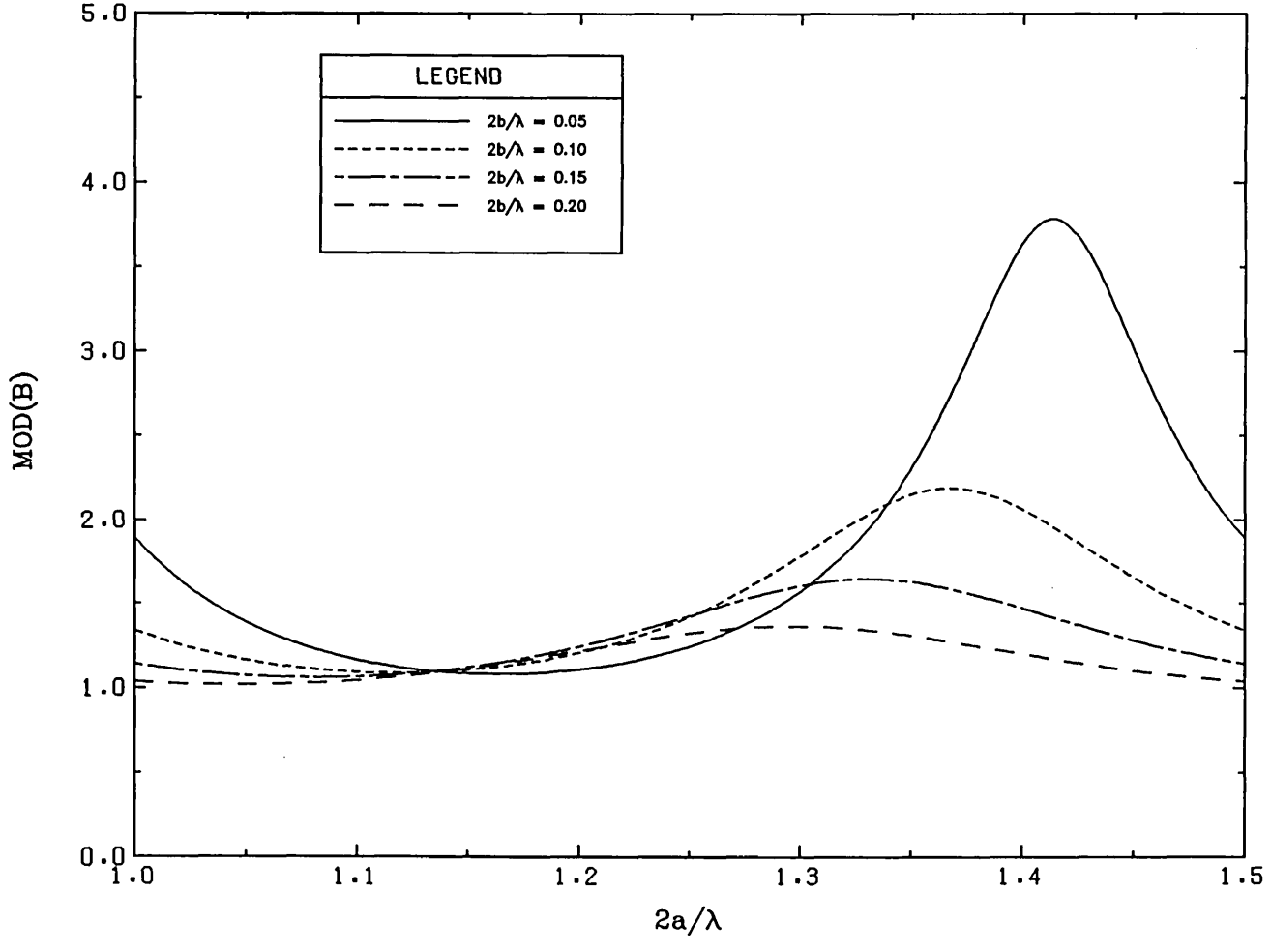

Fig. 3.12 VARIATION OF THE WAVE AMPLITUDE IN THE CHANNEL

CHAPTER FOUR
The numerical model

4.1 An overview

The field of numerical modelling in fluid mechanics has witnessed a tremendous growth over the past fifteen years which, in large measure, has been allied to the growth of large computational systems. Solutions may now be realised to a wide variety of problems that had previously been deemed insoluble because of the limitations of existing mathematics. As computational systems continue to undergo significant transformations every four or five years, fuelled by a rapidly expanding technology and market, more sophisticated numerical models will become available. Increased emphasis on algorithm development will provide an improvement in software standards that may compensate for difficulties in augmenting hardware perfomance.

In the diffraction of linear water waves, we are concerned with the solution of the following boundary value problem:

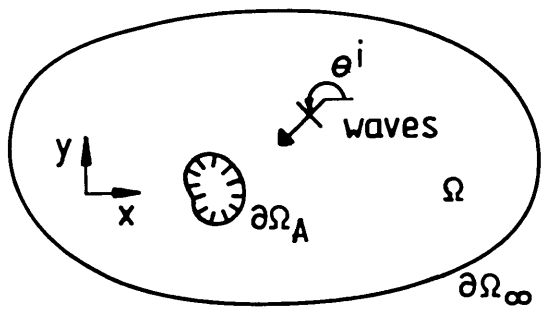

Figure 4.1 Definition sketch

$$(\nabla^2 + k^2)\,\varphi = 0 \quad , \text{ in } \Omega \tag{4.1a}$$

$$\frac{\partial \varphi}{\partial n} = 0 \quad , \text{ at } \partial\Omega_A \tag{4.1b}$$

$$\lim_{kr\to\infty} \sqrt{kr}\left[\frac{\partial}{\partial r} + ik\right]\varphi^s = 0 \quad , \text{ at } \partial\Omega_\infty \tag{4.1c}$$

The governing equation, (4.1a), is the familiar Helmholtz formulation to be satisfied by the reduced potential, φ, in the solution domain, Ω. The first of the two conditions, (4.1b), requires the normal velocity to be zero at the solid boundary, $\partial\Omega_A$, thus implying total reflection of the wave. The second, (4.1c), is

the Sommerfeld radiation condition which is imposed on the scattered wave potential, $\varphi^s = \varphi - \varphi^i$, φ^i being the known potential of the incident plane wave, and is applied at the infinite boundary, $\partial\Omega_\infty$. This latter condition simply states that φ^s and its first derivative, with respect to the distance away from the scattering body, shall decay to zero at infinity in a $1/\sqrt{r}$ fashion.

Three essentially different numerical schemes exist for solving the above equations: the method of boundary integral equations, the finite difference procedure and the finite element technique. Each has advantages and disadvantages that must be assessed before making a choice. A comprehensive survey of these methods is provided by the work of Mei(1978).

The method of boundary integral equations, with a long history that lies in potential theory (Kellog(1929), Lamb(1932)), has been the most popular approach for tackling diffraction problems in both two and three dimensions (Hwang and Tuck(1970), Lee(1971), Gilbert and Brampton(1985), Gerber(1986), Liu and Wu(1988)). It is based on a rigorous mathematical background whose essence is the representation of the potential at a point in a domain by distributions of single and double sources along its boundaries viz. Green's theorem. Analytical solutions to integral equations exist for a few simple scattering shapes only. For more complex ones, the scattering surface is discretized so as to replace the integral equation by a finite but large system of algebraic equations for the average strengths of the sources over the surface elements. Although, in this formulation, the radiation condition is automatically satisfied, the associated singular functions make the method cumbersome to handle.

The finite difference method is an alternative approach that has gained great momentum in the solution of combined refraction–diffraction problems. Its simplicity and computational cost–effectiveness, especially in terms of matrix storage requirements, has made it popular among engineers. The major shortfall of the method, however, lies in its lack of flexibility, unless elaborate modifications are made, in handling irregular grids. Thus, for coastal engineering applications, it is more suited for the modelling of open coastlines, where the geometry is relatively simple, rather than harbour studies.

Lastly, we consider the finite element method which has been the subject of considerable research effort over the last three decades, and has evolved into a powerful tool for the solution of problems in engineering and science. Its true strength was revealed in its development by structural engineers using the early digital computers available in the 1950s, but, its first application in fluid mechanics to linear potential flow problems did not come until the late 1960s. The finite element method is an attractive choice for solving partial differential equations because of its great flexibility in the mesh generation.

Elements may be concentrated in areas where rapid changes are taking place, thus allowing wide variations of scale in the solution domain. This flexibility also leads to an accurate representation of irregular boundaries. Furthermore, for our particular problem, inhomogeneities such as variations in depth are easily dealt with. For these reasons, the method was chosen as the basis for the numerical model.

4.2 Previous work

The application of finite elements to the diffraction of water waves presents special difficulties as a consequence of the unbounded nature of such problems. Waves scattered by solid bodies have to be allowed to propagate to boundaries that are deemed to represent infinite conditions. As the computational domain cannot be infinite in extent, various hybrid element formulations have emerged for dealing with this requirement. These invariably involve the coupling of a finite element discretization in an interior region (the region of interest) to one of four methods, summarised below, that satisfy the infinite conditions in an exterior region. An interesting discussion and comparison of these techniques is provided by Zienkiewicz et al(1978).

(1) Boundary 'dampers' based on the radiation boundary condition being imposed on a finite boundary, $\partial\Omega_c$.

$$\frac{\partial\varphi^s}{\partial n} + ik\,\varphi^s = 0 \quad , \text{ at } \partial\Omega_c$$

This method has the merits of conceptual and computational simplicity but has the disadvantage that the domain which must be idealized using finite elements may be extensive.

(2) Boundary integrals based on source distributions and Green's identity. Berkhoff(1972,1975,1976) adopted this approach for solving the mild slope equation for various refraction–diffraction problems. The variational formulation he used, however, destroyed the symmetry of equations thereby leading to excessive computational time and storage requirements.

(3) Boundary solutions based on the Hankel function series solution for the scattered wave potential that is given by :

$$\varphi^s = \sum_{n=0}^{\infty} H_n(kr)\,(\,\alpha_n \cos n\theta + \beta_n \sin n\theta\,)$$

α_n and β_n are constant coefficients which become part of the unknowns in the algebraic system of equations. The infinite series is truncated at a term, n=s,

decided upon by numerical experiments, for finite computation. s generally depends on the wavelength and is gradually increased until the outcome is insensitive to it. Chen and Mei(1974) developed this method for solving the linear shallow water wave equation to study the oscillations in an offshore harbour. Houston(1978), using a similar formulation, studied the interaction of tsunamis with the Hawaiian islands and later, Houston(1981), generalized the model to intermediate depth theory i.e. for solving the mild slope equation. The model was further used by Tsay and Liu(1983) and Behrendt(1985).

(4) Infinite elements, based on the idea of simply extending the domain of a finite element so that it is unbounded. The first such element, introduced by Bettess(1977), was based on exponential decay shape functions and was successfully applied to solve a variety of refraction and diffraction problems by Bettess and Zienkiewicz(1977). Pos(1983,1985), using the same formulation in the exterior region, studied the diffraction of waves by breakwaters and channels. A drawback with using this particular infinite element, however, is that there exists a parameter, specified in the shape functions, that controls the severity of the decay and is to some extent arbitrary. More recently, another type of infinite element was introduced by Zienkiewicz et al(1983), the so called mapped infinite element which can model a 1/r type decay by virtue of a special mapping function. The $1/\sqrt{r}$ type decay, characteristic of the scattered wave, can also be modelled by a minor modification in the shape functions, thus leading to an accurate physical representation. It is not surprising therefore that, for wave problems, this was shown to be the most accurate approach to date by Zienkiewicz et al(1985). Yet another addition to the infinite element family has emerged recently by way of an acoustic application. This is the wave envelope element devised by Astley(1983). It is similar in all respects to the previous infinite elements except that instead of the usual Galerkin approximation for the weight function, the complex conjugate of the shape function is used, resulting in the elimination of the wave periodicity term that is built into the equations. An important advantage is therefore gained in that standard integration techniques can be used. Furthermore, as discussed by Bettess(1987), this element could indicate the way towards solving the short wave problem as the formulation is independent of the wavelength. However, the price to be paid is that the corresponding stiffness matrix becomes unsymmetrical. Nevertheless, the wave envelope element warrants further investigation. In the present work, the mapped infinite element is implemented.

4.3 Mathematical formulation

We shall omit here a description of the mathematical theory of finite

elements as this is well covered in a number of standard textbooks on the subject (e.g. Zienkiewicz(1978), and Becker, Carey, and Oden(1981)). Instead, we shall confine ourselves to the variational formulation of equations (4.1) and the construction of the finite element approximation.

The weak formulation, obtained by employing the method of weighted residuals, may be written as,

$$\int_{\Omega} v\ (\nabla^2\varphi + k^2\varphi)\ d\Omega = 0 \qquad (4.2)$$

where $v = v(x,y)$ is a suitable weight function and $d\Omega = dx\ dy$. The use of Gauss' divergance theorem on equation (4.2) leads to a lower order of derivatives thus weakening the smoothness requirements on the solution and gives,

$$\int_{\Omega} (\nabla v \nabla\varphi - k^2 v\varphi)\ d\Omega = \int_{\partial\Omega_A} v \frac{\partial\varphi}{\partial n}\ ds + \int_{\partial\Omega_\infty} v \frac{\partial\varphi}{\partial n}\ ds \qquad (4.3)$$

The natural boundary condition, (4.1b), is satisfied simply by putting the first term of the right hand side of the above equation equal to zero. The total domain, Ω, is now divided into an interior region, Ω_1, and an exterior region, Ω_2. In Ω_2, the total wave field, φ, is replaced by the sum of the incident wave field, φ^i, and the scattered wave field, φ^s, to facilitate the application of the infinite elements.

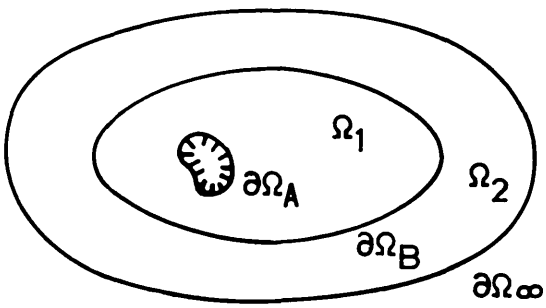

Figure 4.2 Definition sketch

Thus, equation (4.3) becomes,

$$\int_{\Omega_1} (\nabla v \nabla\varphi - k^2 v\varphi)\ d\Omega + \int_{\Omega_2} (\nabla v \nabla\varphi^s - k^2 v\varphi^s)\ d\Omega$$

$$+ \int_{\Omega_2} (\nabla v \nabla\varphi^i - k^2 v\varphi^i)\ d\Omega = \int_{\partial\Omega_\infty} v \frac{\partial\varphi^i}{\partial n}\ ds \qquad (4.4)$$

where,

$$\varphi^i = e^{ik(x\cos\theta^i + y\sin\theta^i)} \tag{4.5}$$

Now as,

$$\nabla v \nabla \varphi^i - k^2 v \varphi^i = \frac{\partial}{\partial x}\left[v \frac{\partial \varphi^i}{\partial x}\right] + \frac{\partial}{\partial y}\left[v \frac{\partial \varphi^i}{\partial y}\right] - v\,(\nabla^2 \varphi^i + k^2 \varphi^i)$$

and since, $(\nabla^2 + k^2)\,\varphi^i = 0$, we may use Green's theorem to obtain,

$$\int_{\Omega_2} \left[\frac{\partial}{\partial x}\left[v \frac{\partial \varphi^i}{\partial x}\right] + \frac{\partial}{\partial y}\left[v \frac{\partial \varphi^i}{\partial y}\right]\right] d\Omega = \int_{\partial\Omega_B} v \frac{\partial \varphi^i}{\partial n} ds + \int_{\partial\Omega_\infty} v \frac{\partial \varphi^i}{\partial n} ds$$

which may be substituted back into equation (4.4) to yield the final variational statement:

$$\int_{\Omega_1} (\nabla v \nabla \varphi - k^2 v \varphi)\, d\Omega + \int_{\Omega_2} (\nabla v \nabla \varphi^s - k^2 v \varphi^s)\, d\Omega$$

$$= -\int_{\partial\Omega_B} v \frac{\partial \varphi^i}{\partial n} ds \tag{4.6}$$

A piecewise Galerkin approximation is utilised in the following manner,

$$\varphi^e(x,y) = \sum_{i=1}^{n} \varphi_i^e N_i^e(x,y) \;,\; v^e(x,y) = N_j^e(x,y) \tag{4.7}$$

where N_i are prescribed shape functions of polynomial form, φ_i are the nodal variables and n is the number of nodes in an element. In this work, a quadratic approximation for N_i has been used. The superscript, e, denotes variation over a typical element. The finite element discretization of the interior region, Ω_1, is now easily derived, with reference to equations (4.6) and (4.7), and may be written as,

$$\sum_{i=1}^{n} k_{ij}^e \varphi_i \;,\; j = 1,\ldots,n$$

$$k_{ij}^e = \int (\nabla N_i^e \nabla N_j^e - k^2 N_i^e N_j^e)\, d\Omega \tag{4.8}$$

$[\, k_{ij} \,]$ being the element stiffness matrix which is assembled into the global matrix by standard techniques. Similarly, the discretization of the load vector becomes,

$$f_j = - \int_{\partial\Omega_B} N_j^e \frac{\partial \varphi^i}{\partial n} ds \qquad (4.9)$$

(Note that φ^i, the incident wave potential, should not be confused with the nodal variable for the total potential, φ_i). All of the above calculations are carried out on a standard reference element in the local coordinate system, (ξ,η). The associated transformation is the usual one, given by,

$$x = \sum_{i=1}^{n} x_i \, N_i(\xi,\eta) \quad , \quad y = \sum_{i=1}^{n} y_i \, N_i(\xi,\eta) \qquad (4.10)$$

where (x_i,y_i) are the global coordinates of the nodes in the element.

4.4 Infinite elements

4.4.1 Theory

A detailed theoretical description of the mapped infinite element is presented in this section. The one–dimensional element is considered first to better illustrate the derivations involved, which are then extended to the two–dimensional counterpart.

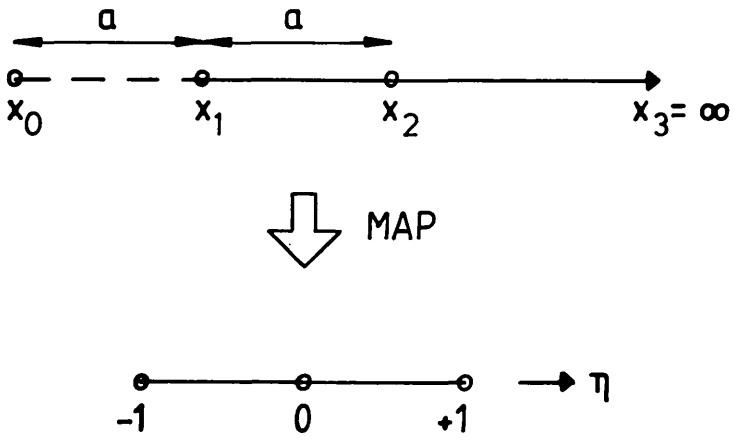

Figure 4.3 1–D infinite element mapping

The element in figure 4.3 extends from point x_1 through x_2 to x_3, which is at infinity. It is to be mapped onto the finite domain $-1 < \eta < 1$. A suitable mapping expression is:

$$x = \tilde{N}_0(\eta)x_0 + \tilde{N}_2(\eta)x_2 \qquad (4.11)$$

where,

$$\tilde{N}_0(\eta) = \frac{-\eta}{1-\eta} \quad , \quad \tilde{N}_2(\eta) = 1 + \frac{\eta}{1-\eta} \tag{4.12}$$

At

$$\eta = 1, \qquad x = \frac{\eta}{1-\eta}(x_2 - x_0) + x_2 = x_3 = \infty$$

$$\eta = 0, \qquad x = x_2$$

$$\eta = -1, \qquad x = (x_0 + x_2)/2 = x_1$$

The last point, $\eta = -1$, is to correspond to the point x_1, so that the coordinate of this point is now defined to be midway between x_0 and x_2. Given this relationship, the mapping can be written in terms of any pair of quantities from the set: $\{x_0, x_1, x_2, a\}$ (where $a = x_2 - x_1 = x_1 - x_0$). For example it can be written as:

$$x = (2x_1 - x_2)\tilde{N}_0 + x_2\tilde{N}_2$$

Having established a mapping between the infinite and finite domains, the next step is to see into what form polynomials in the finite, η domain are transformed in the unbounded x plane. Consider a polynomial, P,

$$P = \alpha_0 + \alpha_1\eta + \alpha_2\eta^2 + \alpha_3\eta^3 \tag{4.13}$$

which is typical of those used in finite element methods. The η to x mapping already obtained is:

$$x = \frac{\eta}{1-\eta} 2a$$

and its inverse is:

$$\eta = 1 - \frac{2a}{(x - x_0)} = 1 - \frac{2a}{r} = 1 - \frac{A}{r} \tag{4.14}$$

where $r = x - x_0$. On substitution into the general polynomial, P, a new polynomial in inverse powers of r is obtained:

$$P = \beta_0 + \frac{\beta_1}{r} + \frac{\beta_2}{r^2} + \frac{\beta_3}{r^3} + \ldots \tag{4.15}$$

where β_i can be determined from the α's and a. If the polynomial is required to decay to zero at infinity, as in the present work, then $\beta_0 = 0$. The point x_0,

not defined until now, is seen to be the pole of the expansion of P.

The extension to two dimensions is straightforward, if the above mapping is used in the η direction, and standard Lagrange functions used in the ξ direction. The complete mapping in two dimensions would be:

$$
\begin{aligned}
x = {} & N_1(\xi)\,[(2x_1 - x_4)\tilde{N}_0 + x_4\tilde{N}_2] + \\
& N_2(\xi)\,[(2x_2 - x_5)\tilde{N}_0 + x_5\tilde{N}_2] + \\
& N_3(\xi)\,[(2x_3 - x_6)\tilde{N}_0 + x_6\tilde{N}_2] \\
y = {} & N_1(\xi)\,[(2y_1 - y_4)\tilde{N}_0 + y_4\tilde{N}_2] + \\
& N_2(\xi)\,[(2y_2 - y_5)\tilde{N}_0 + y_5\tilde{N}_2] + \\
& N_2(\xi)\,[(2y_3 - y_6)\tilde{N}_0 + y_6\tilde{N}_2]
\end{aligned}
\qquad (4.16)
$$

where,

$$N_1(\xi) = \xi(\xi-1)/2, \qquad N_2(\xi) = 1-\xi^2, \qquad N_3(\xi) = \xi(\xi+1)/2$$

and the node numbers are as defined in figure 4.4.

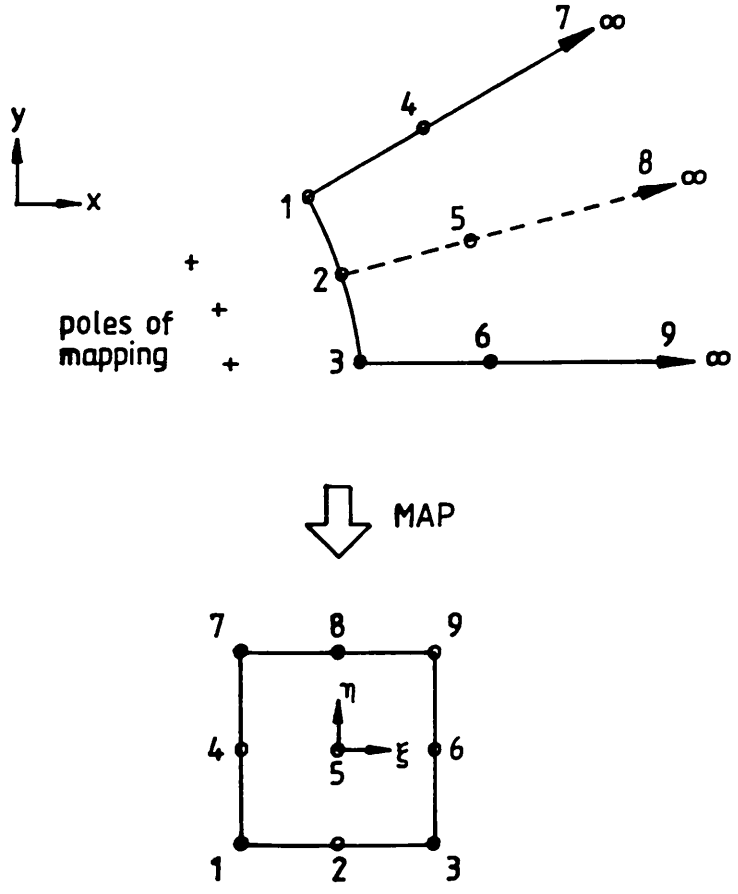

Figure 4.4 2–D infinite element mapping

4.4.2 Introducing the wave component

The potential of the scattered wave in the exterior region behaves like $H_0(kr)$ which is the simplest solution to the Helmholtz equation. For large kr, the zeroth–order Hankel function oscillates roughly like cos(kr) + i sin(kr) while decaying in magnitude as $r^{-1/2}$. As it stands, the element can model a decay of the form, 1/r, $1/r^2$, etc., generated by the mapping (4.16). However, in order to model the proper $r^{-1/2}$ type decay and the periodicity of the wave, the shape function has to be multiplied by the periodic component, exp(ikr), and the term, $r^{1/2}$, so that it becomes:

$$N(\xi,\eta) = M(\xi,\eta)\ r^{1/2}\ \exp(ikr) \qquad (4.17)$$

$M(\xi,\eta)$ being the original shape function and r is given from the inverse mapping relationship (4.14):

$$r = \frac{A}{(1-\eta)} \qquad (4.18)$$

Substituting for r from (4.18), (4.17) becomes:

$$N(\xi,\eta) = M(\xi,\eta)\ \left[\frac{A}{1-\eta}\right]^{-1/2} \exp\left[\frac{ikA}{1-\eta}\right]$$

Although the absolute value of $N(\xi,\eta)$ is unity at $\eta = -1$ (the boundary with standard finite elements), the phase of $N(\xi,\eta)$ may not be zero. If the shape functions are to be continuous between finite and the new infinite elements, the phase must be made zero. At $\eta = -1$, the value of $N(\xi,\eta)$ is:

$$N(\xi,-1) = M(\xi,-1)\ \left[\frac{A}{2}\right]^{-1/2} \exp\left[\frac{ikA}{2}\right]$$

To ensure continuity, a further factor is introduced so that the final expression for the shape function becomes:

$$N(\xi,\eta) = C\ M(\xi,\eta)\ \left[\frac{A}{1-\eta}\right]^{-1/2} \exp\left[\frac{ikA}{1-\eta}\right]$$
$$C = \left[\frac{2}{A}\right]^{1/2} \exp\left[-\frac{ikA}{2}\right] \qquad (4.19)$$

4.4.3 Integration procedure

In the 'worst' case, an integral of the following form will have to be evaluated:

$$\int_{-1}^{+1} \frac{1}{(1-\eta)^2} P(\eta) \exp\left[\frac{2ikA}{1-\eta}\right] d\eta \qquad (4.20)$$

where $P(\eta)$ is a polynomial of η, the term $P(\eta)\,(1-\eta)^{-1/2}$ includes all the effects of the shape functions and the exponential term deals with the periodic behaviour. It is therefore necessary to integrate terms of the form:

$$\int_{-1}^{+1} \frac{s^n}{(1-s)^2} \exp\left[\frac{iB}{1-s}\right] ds$$

Letting $u = B/(1-s)$, this becomes:

$$\int_{B/2}^{\infty} \frac{1}{B}\left[1 - \frac{B}{u}\right]^n \exp(iu)\, du \qquad (4.21)$$

Integrating (4.21) by parts gives,

$$\sum_{k=0}^{n} \frac{n!\,(-1)^k\,B^{k-1}}{(n-k)!\,k!}\,Tr(k,B/2) \qquad (4.22)$$

where,

$$Tr(k,B/2) = \int_{B/2}^{\infty} u^{-k} \exp(iu)\, du$$

$$(k = 0) \quad = i \exp(iB/2)$$

$$(k = 1) \quad = \int_{B/2}^{\infty} \frac{\exp(iu)}{u}\, du$$

$$(k > 1) \quad = \frac{\exp(iB/2)}{(k-1)!} \sum_{j=1}^{k-1} \frac{i^{k-j-1}\,(j-1)!}{(B/2)^j} + \frac{i^{k-1}}{(k-1)!} \int_{B/2}^{\infty} \frac{\exp(iu)}{u}\, du$$

The integral of the second term in the above equation is evaluated as a function in the NAG subroutine library. The procedure for deriving the resulting integration or Gaussian point abscissae and weights as given by Zienkiewicz et al(1985) is summarised below.

(1) Choose n integration point abscissae, which are quite arbitrary, s_i, i=1, to n, where n is generally one greater than the highest power of s appearing in the polynomial.

(2) Form the matrix **X**,

$$\mathbf{X} = \begin{bmatrix} 1 & s_1 & s_1^2 & \dots & s_1^{n-1} \\ 1 & s_2 & s_2^2 & \dots & s_2^{n-1} \\ \vdots & & & & \vdots \\ 1 & s_n & s_n^2 & \dots & s_n^{n-1} \end{bmatrix}$$

and since,

$$y = \sum_{i=1}^{n} \alpha_i \, s^{i-1}$$

where α_i are the unknown polynomial coefficients, it is clear that,

$$\alpha = \mathbf{X}^{-1} \, y$$

where y is the vector of values at the Gaussian points. Setting y = 1,0,0,...,0,1,1,...,...,...,0,0,1 corresponds to finding the polynomials which are equal to unity at each integration point in turn, and zero at the others. The terms in each column of $\mathbf{X}^{-1}$ then give the polynomial coefficients for each integration point in turn.

(3) For each Gaussian abscissae j, and for each term in the column of $\mathbf{X}^{-1}$, i, the weight is found from:

$$W_j = \sum_{i=1}^{n} \int_{-1}^{+1} X^{-1}_{ij} \frac{s^{i-1}}{(1-s)^2} \exp\left[\frac{2ikA}{1-s}\right] ds \qquad (4.23)$$

The integral is carried out using equation (4.22).

(4) The following equation is used in the computation of expression (4.20):

$$\int_{-1}^{+1} \frac{1}{(1-s)^2} \Sigma \, a_m s^{m-1} \exp\left[\frac{2ikA}{1-s}\right] ds = \sum_j \sum_k W_j \, a_k s_j^{k-1}$$

The set of abscissae and weights, s_j, W_j, for j=1 to n are calculated at the beginning of each run of the infinite element program, and are sufficient to carry out the integrations in the infinite direction over the element domain. The above–mentioned work of Zienkiewicz et al(1985) contains listings of the subroutines required to carry out the calculation procedure, (1) – (4).

4.5 Implementation in FINEL

FINEL is an engineering analysis computer program utilising the finite

element method to solve field problems. The program was initially conceived and written by Dennis Hitchings, in the Department of Aeronautics, Imperial College, London, and is currently installed on a CDC Cyber 960 mainframe computer. Although FINEL is primarily geared as a structural analysis package, it has a flexible base on which to develop new ideas and as such, was chosen for the present implementation.

The next section summarises some of the information given by Chatterton(1983) in the FINEL user and programmer manuals.

4.5.1 Structure of FINEL

FINEL is a highly structured program, the basis of which follows directly the steps involved in the finite element method itself. One of the reasons for the success of the F.E. method for computer implementation is that it can be broken down into a set of discrete, almost unrelated, steps such as mesh definition, assembly, solution and so on. This feature is used within FINEL to define a modular structure for the program. Each module defines a discrete aspect of the F.E. method. The program has a central executive section whose main purpose is to control the sequence in which the modules are executed, and hence to control the analysis that FINEL carries out. No modules communicate directly with each other, they all pass through the executive. The modular structure is then carried down to one lower level within FINEL by the definition of a series of FINEL libraries. Again the idea of these libraries stems naturally from the finite element method itself. Within the F.E. analysis a continuum is divided into discrete regions, or elements. These elements can take different forms depending upon the actual problem being solved. Within FINEL the various types of elements available are gathered together within the FINEL element library. Similarly, the loadings that can be applied to the continuum vary according to the problem being solved. These loading types are then contained within the FINEL load library. There are also a variety of other libraries within FINEL, but all of these have a similar structure and serve a similar purpose.

Any large arrays generated by a module are not returned to the FINEL executive. Instead, in order for them to be communicated to other modules they have to be written to the FINEL data base. This is a random access mass storage file which allows the programmer free access to any data which has been generated by a run of FINEL. The FINEL data base is organised as a two level system containing thirty files, each of which consists of five hundred pages, where a page can be of any length. Each is organised such that any page of any file can be read from or written to directly. To simplify

communication within FINEL, some files are dedicated to storing particular sets of data whilst other files are free for the programmer to use as he desires.

A FINEL analysis is conducted by calling a sequence of modules in turn. A typical run consists of the following execution flow:

1. GRID – mesh generation
2. ASMB – matrix formation
3. BNCN – boundary conditions
4. CHOL – matrix factorisation
5. LOAD – loading specification
6. SLVE – equation solution

The program starts in the FINEL executive. Control is then passed to the GRID module which generates the mesh. After mesh generation, control is passed back to the executive, which then passes control back to the next module, in this case ASMB. The execution continues in this way, with control being passed between the executive and the modules alternately, until the job is completed.

4.5.2 Module entries

A major problem encountered in the implementation was that FINEL did not accommodate the manipulation of complex numbers. The consequent alteration of the program (which is about 30,000 lines long) for this purpose, consisted of not only redefining all the relevant variables as being complex but also, more importantly, restructuring the way in which arrays are transferred from and onto the data base. The data base interface routine was changed so that upon the specification of a certain code number, two, instead of one, real numbers could be read and written at a time. This meant that complex numbers could be manipulated without explicitly declaring them as complex which was a great advantage as the handling of real arrays, generated for example in the GRID module, would not be affected in any way. Having done this, it was decided to keep the changes in the assembly module, ASMB, to a minimum as the associated coding is quite extensive. A strategy was therefore devised whereby the calculation of the single complex coefficient array entailed the seperate calculation and storage of two real matrices comprising the components of the complex array. A user–written module, OWN1, was then employed to retrieve these matrices and form, by simple addition, the complex matrix, which was stored in turn onto the data base by making use of the modified interface routine.

The next step was the factorisation of the complex matrix in the CHOL module. Within FINEL, the standard form of matrix factorisation for

symmetric matrices is the Cholesky method, which involves decomposing the coefficient matrix **A** as follows:

$$\mathbf{A} = \mathbf{L}\mathbf{L}'$$

where **L** is a lower triangular matrix and $\mathbf{L}'$ is its transpose. Again, here, the coding was changed so that the data base was accessed in accordance with the new criterion. Furthermore, apart from changing the algebra to handle complex numbers, the modifications mostly involved switching off the many flags that test whether the matrix is positive–definite or singular, rules which do not apply in the present context. Similar changes to the next two modules, LOAD and SLVE, completed this part of the implementation. The sequence of modules is then given schematically by figure 4.5.

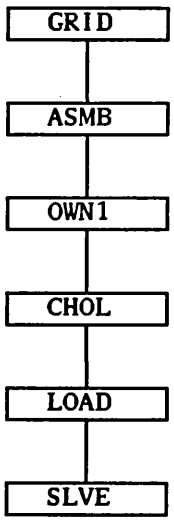

Figure 4.5 Sequence of execution of the modules

4.5.3 Library entries

Within this part of the work, user–written entries were added to three of the FINEL libraries: the element library, the load library and the region library. The highly flexible structure of FINEL and the provision of the many guidelines for its modification (Chatterton(1983)) greatly facilitated the linking of these new entries to the main body of the program. A brief description of the implementation is given below.

In the FINEL element library, three entries were added comprising the isoparametric forms of the six–noded triangle and eight–noded quadrilateral elements as well as the mapped infinite element, discussed previously. The first two elements were already available for the solution of mainly stress and strain problems but were completely re–written so as not only to set up the coefficient matrix corresponding to the Helmholtz equation but also to conform to the new

scheme of handling complex numbers. The mapped infinite element was implemented as a six–noded element as the three nodes at infinity do not come into play in the formulation.

The first of the two entries added to the FINEL load library is the load vector given by expression (4.9) which is simply the 'right hand side' of the above–derived variational statement, (4.6). This is imposed on the nodes at the boundary between finite and infinite elements at a local level and then assembled in the usual way to obtain the global vector. The second load entry was implemented to facilitate the change in nodal variable, from total potential φ to scattered potential φ^S, at the finite–infinite element interface. Theoretically, this change was effected in the manner illustrated by the following simple example:

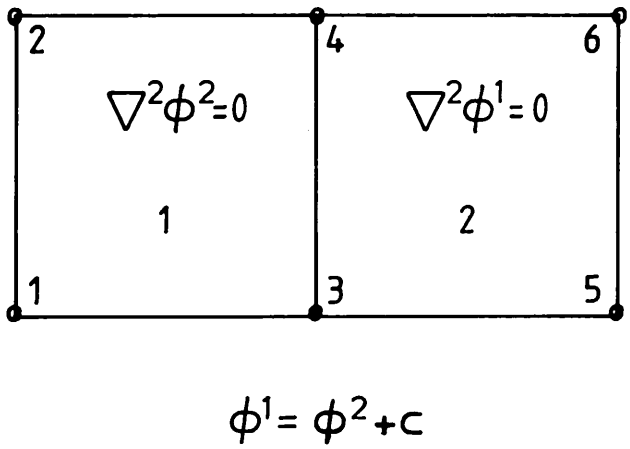

Figure 4.6 Definition sketch

The load vector resulting from the change in nodal variable across the boundary, $\partial\Omega_B$, is then given by the product of the following two matrices:

$$\begin{bmatrix} 0 & 0 & 0 & 0 & 0 & 0 \\ 0 & 0 & 0 & 0 & 0 & 0 \\ 0 & 0 & x & x & x & x \\ 0 & 0 & x & x & x & x \\ 0 & 0 & x & x & x & x \\ 0 & 0 & x & x & x & x \end{bmatrix} \begin{bmatrix} 0 \\ 0 \\ c \\ c \\ 0 \\ 0 \end{bmatrix}$$

where the x's mark the entries in the global stiffness matrix due to element number 2. The solution vector then gives, simultaneously, φ^2 at nodes 1 and 2 and φ^1 at nodes 3,4,5 and 6. A similar approach was followed in the real problem whereby the element stiffness matrices were calculated and multiplied by a vector of the incident wave potential, φ^i, at the finite–infinite element boundary

to yield an extra correcting term for the overall load vector.

The single entry added to the FINEL region library is a quadrilateral with circular edges. It was implemented to allow the mapped infinite element to be used in a plane polar form for the discretization of the exterior region. Although the coding was based primarily on a similar entry in the library for the generation of one–dimensional circular elements, suitable modifications had to be made for coping with the extra dimension. A major disadvantage with the mesh generating facilities within FINEL is the lack of provision for the automatic generation of triangular elements. It was felt that the writing and installation of subroutines to achieve this goal would have been too much of a deviation from the main lines of this work. Therefore, to get round this, the node and element numbers had to be manually specified for all of the triangular elements, a method that proved to be very cumbersome when dealing with large grids.

4.6 Verification

As is common with all numerical models, the verification is an essential concluding stage in the process of development. Simple problems for which analytical solutions exist, provide a useful means by which these models could be tested and if the results turn out to be favourable, confidence is gained in their use for tackling hitherto untried problems. In the present context, three problems were solved: The diffraction of water waves by a circular cylinder, the resonant response of a fully open rectangular harbour and the diffraction of water waves by a gap in an infinite breakwater of zero thickness. In all of these, the plane waves were assumed to be normally incident so that, due to symmetry, only half of the solution domain was discretized. A minimum resolution of about four elements per wavelength, which works out at nine nodes in both the x and y directions, was maintained for reasonable accuracy. This is the standard resolution for not only finite element work but also finite differences as demonstrated by Dong and Al–Mashouk(1989). When dealing with relatively short waves this constraint has to be relaxed for obvious reasons.

4.6.1 Circular cylinder

The analytical solution to this problem was first obtained by Havelock(1940) for the case of plane sound waves impinging on obstacles of various cross–sections and later extended to water waves by MacCamy and Fuchs(1952). It is given by:

$$\varphi = J_0(kr) - \frac{J_0'(ka)}{H_0^{(2)}{}'(ka)} H_0^{(2)}(kr)$$

$$+ \quad 2 \sum_{m=1}^{\infty} i^m \left(J_m(kr) - \frac{J_m'(ka)}{H_m^{(2)}{}'(ka)} H_m^{(2)}(kr)\right) \cos m\theta$$

Where $H_m^{(2)}(kr)$ is the Hankel function of the second kind and equals $J_m(kr) - iY_m(kr)$. Figure 4.8 shows a comparison between this solution and that obtained by our numerical model. It may be seen that the two are in excellent agreement.

4.6.2 Fully open harbour

The resonant response of a fully open rectangular harbour, whose geometry is shown in figure 4.7b, was first tackled by Unluata and Mei(1973) using the method of matched asymptotic expansions. In figure 4.9 the amplification factor at the centre of the backwall is plotted, over a range of wavelengths, to compare the results from both the analytical solution and the numerical model. Again, the two are in excellent agreement except near the shorter wavelengths where the theory of matched asymptotic expansions fails.

4.6.3 Gap in an infinite breakwater

This problem has concerned coastal engineers for many years prior to the introduction of computer models and accordingly, many analytical theories have been developed for its solution. For our purpose, we have chosen the solutions presented by Sobey and Johnson(1986), based on the Mathieu functions, as these are the most accurate. In their work, these authors also present some results from the superposition approximation of Penney and Price(1952). Figures 4.10 and 4.11 show a comparison of the profiles in the lee of the breakwater for a variety of gap widths corresponding to both the analytical and numerical models. Comparisons of two–dimensional contour plots are also shown in figures 4.12 and 4.13. The agreement is good except near the gap where the singularities at the tips of the breakwater, associated with the infinite velocities at the core of the irrotational vortices, force a localised error. This singularity has been simulated numerically by Bettess, Liang and Bettess(1984) using a technique which was originated in the field of elasticity by Henshell and Shaw(1975). Their method was to deliberately move the mid–side node of the eight–noded isoparametric element to the quarter point, which induces a singularity at the

closest corner, as the Jacobian matrix is no longer invertible at that point. This singularity is of the form:

$$\nabla\varphi \approx r^{-1/2}$$

which is of precisely the kind needed at the tips of the breakwater. It should be noted that although this device enables the numerical technique to simulate the singularity found in the analytical solution, this singularity does not occur in the real flow where the high velocity gradients produce viscous forces that lead to separation and the formation of vortices.

Although this approach proved to be a successful one, as demonstrated by the work of Bettess, Liang and Bettess(1984) on the diffraction of water waves by semi–infinite breakwaters, it was decided not to follow it in the present work. This is because the increase in accuracy obtained, which is highly localised to the immediate vicinities of the tips of the breakwater, is not so great as to warrant such a modification.

In all of the above problems, the convergence of the numerical scheme was verified by varying the number of finite elements used in the discretisations and ensuring that the solutions remain unaltered. This of course is subject to the minimum resolution criterion discussed previously.

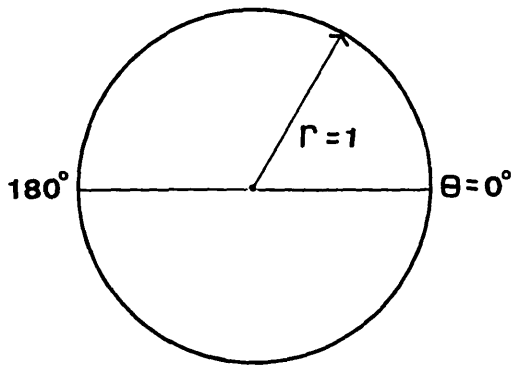

(a)

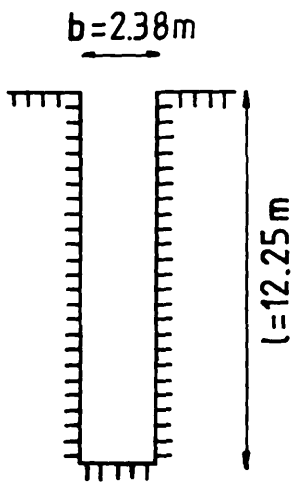

(b)

Figure 4.7 Cylinder and harbour geometries

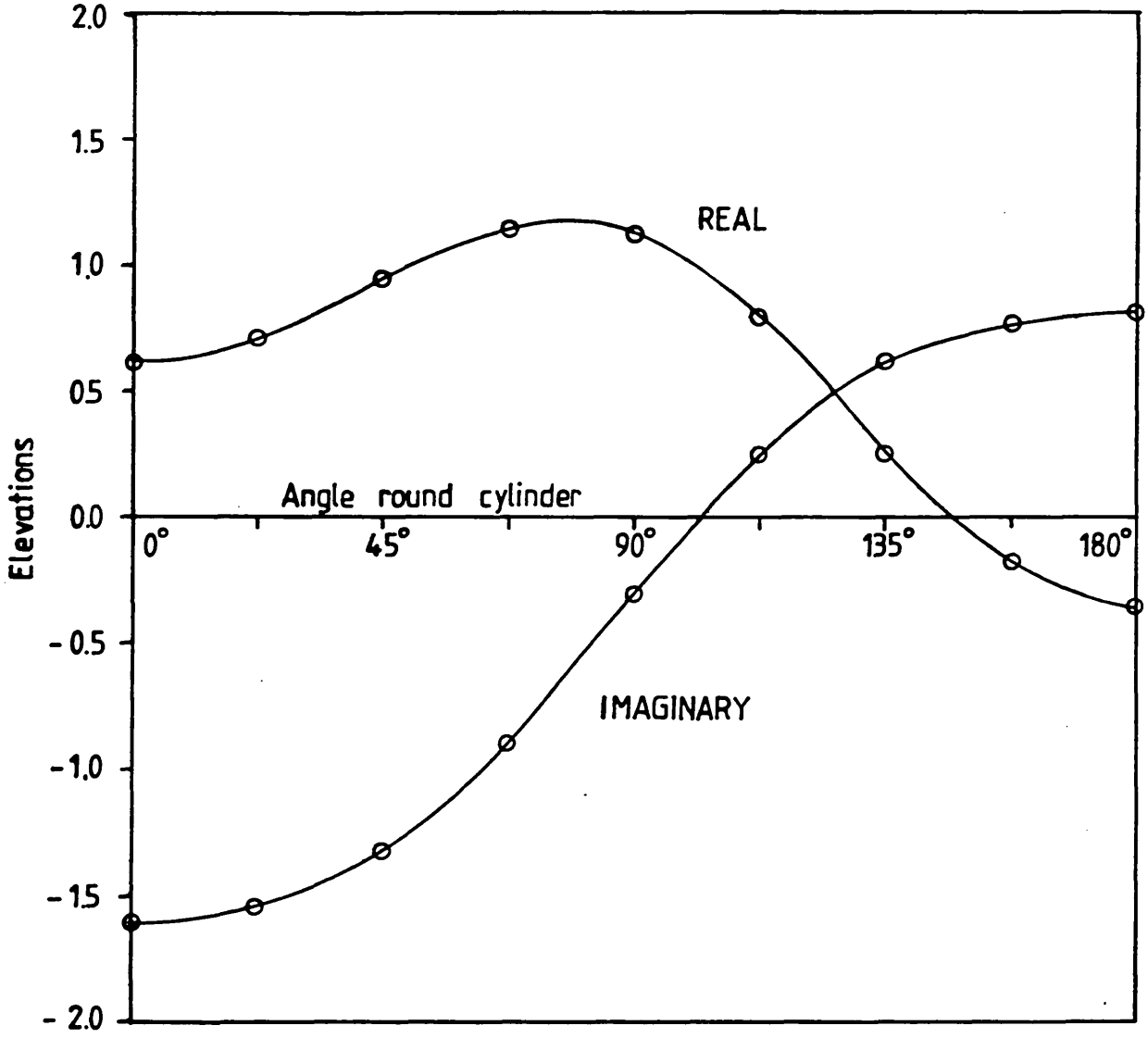

Figure 4.8 Wave diffraction by a circular cylinder
r = 1.0 , k = 1.0

Solid line : analytical solution

Circles : numerical model

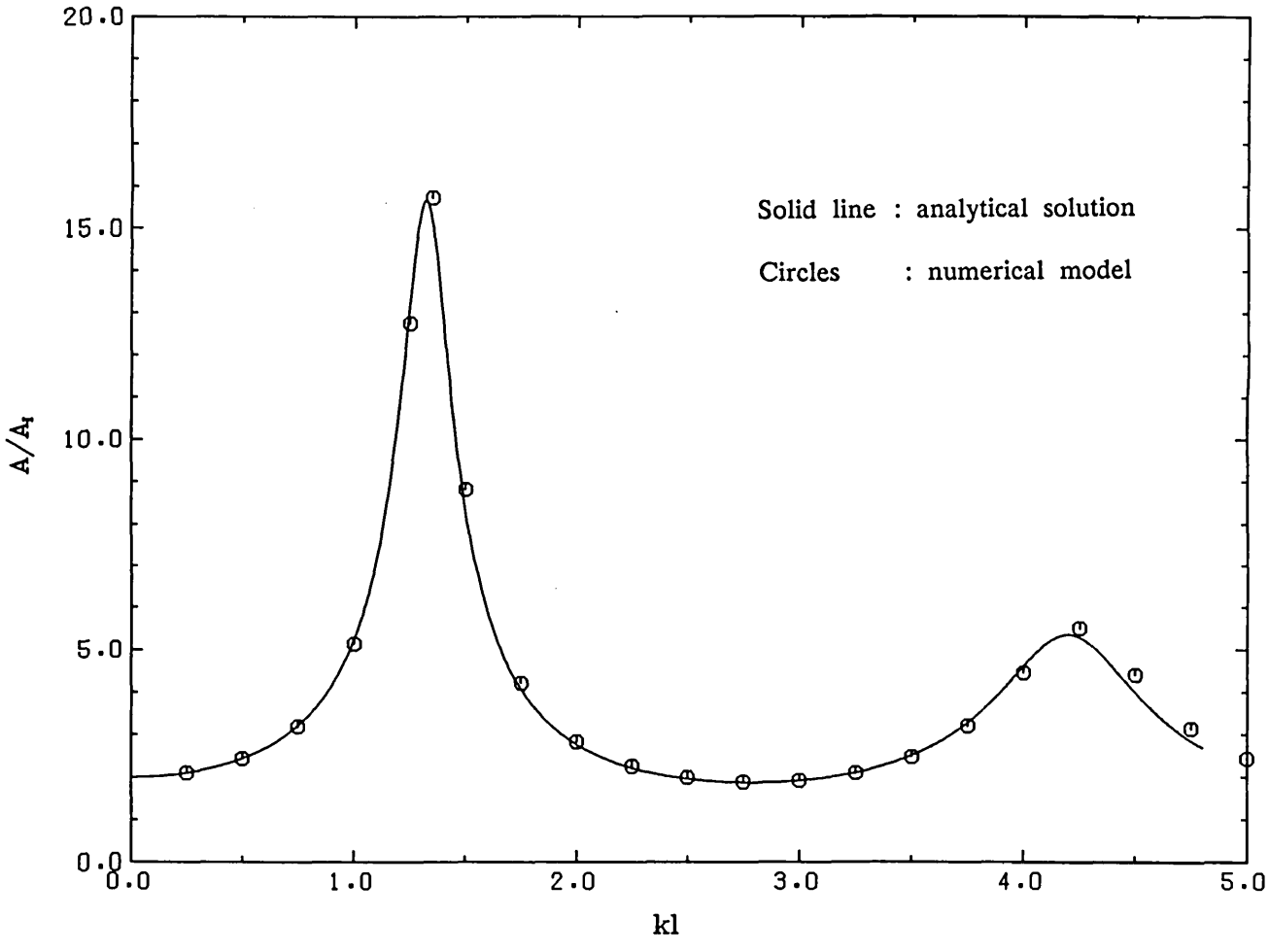

Fig. 4.9 RESPONSE CURVE OF FULLY OPEN HARBOUR

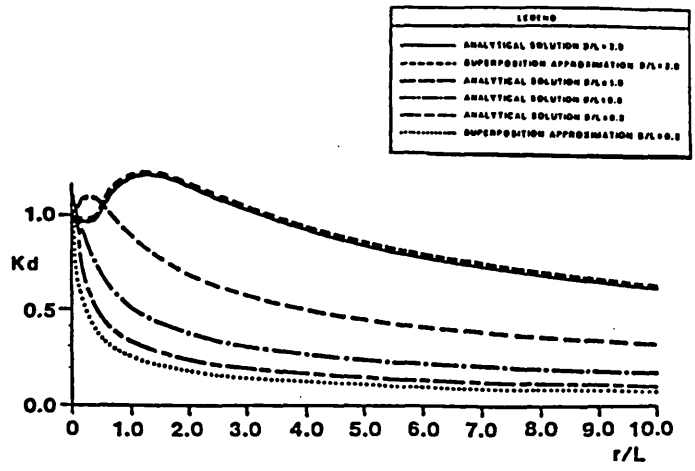

(a) Analytical model

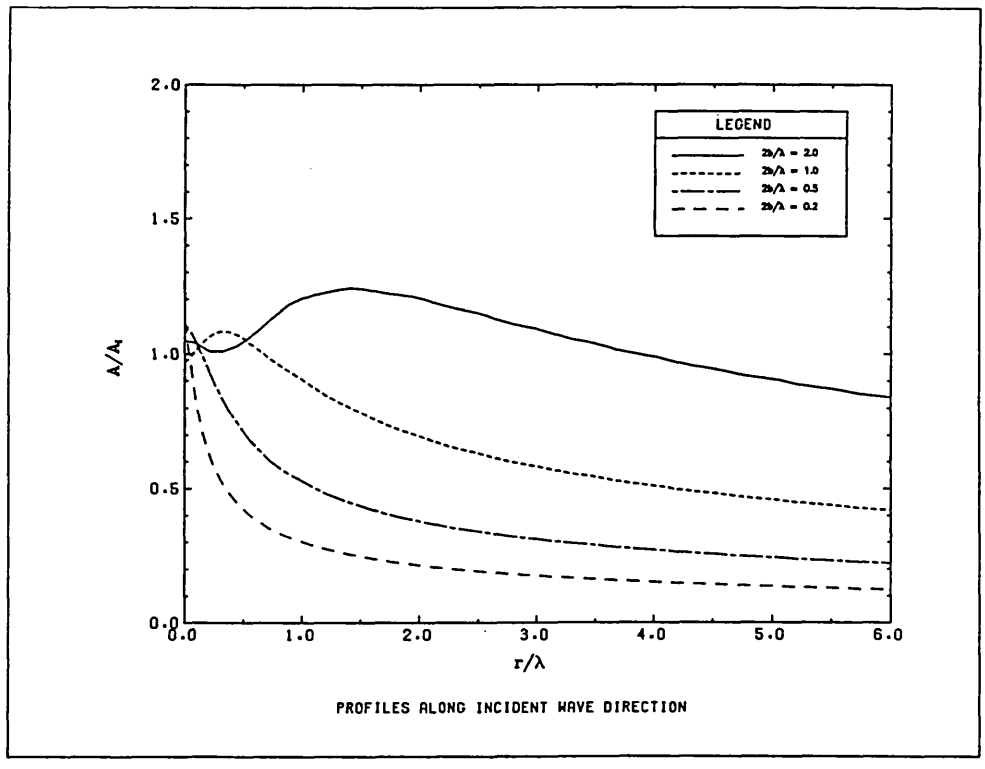

(b) Numerical model

Gap in an infinite breakwater.

Figure 4.10 Amplitude profiles

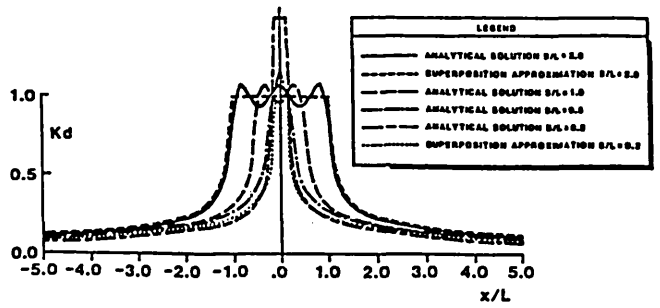

(a) Analytical model

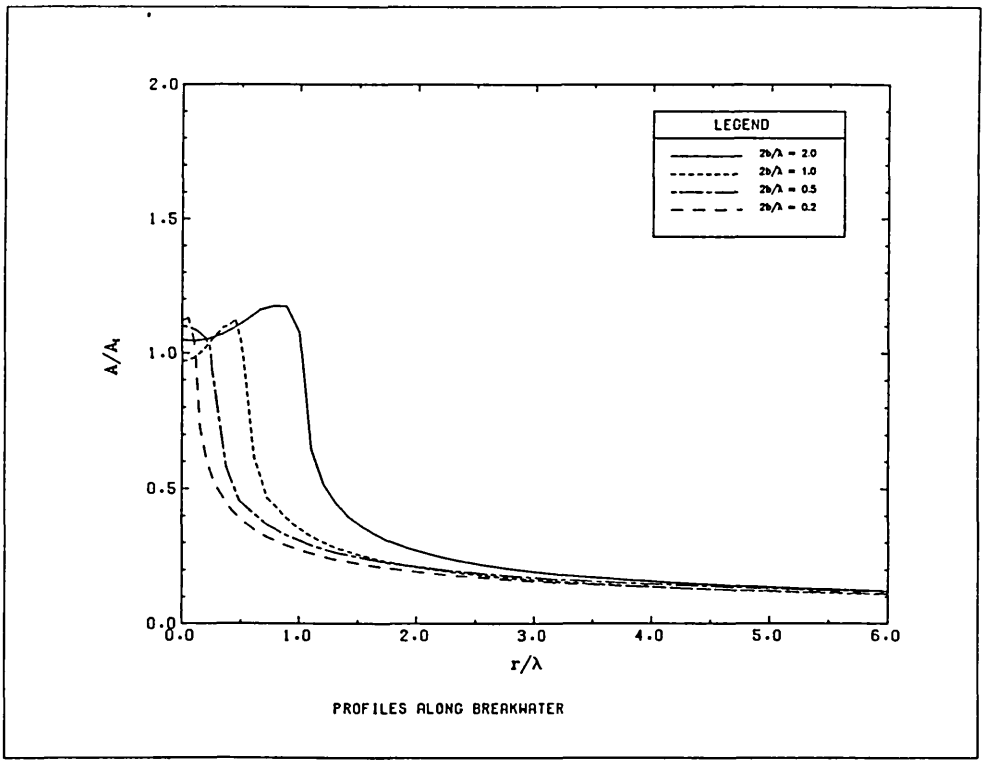

(b) Numerical model

Figure 4.11 Amplitude profiles

analytical

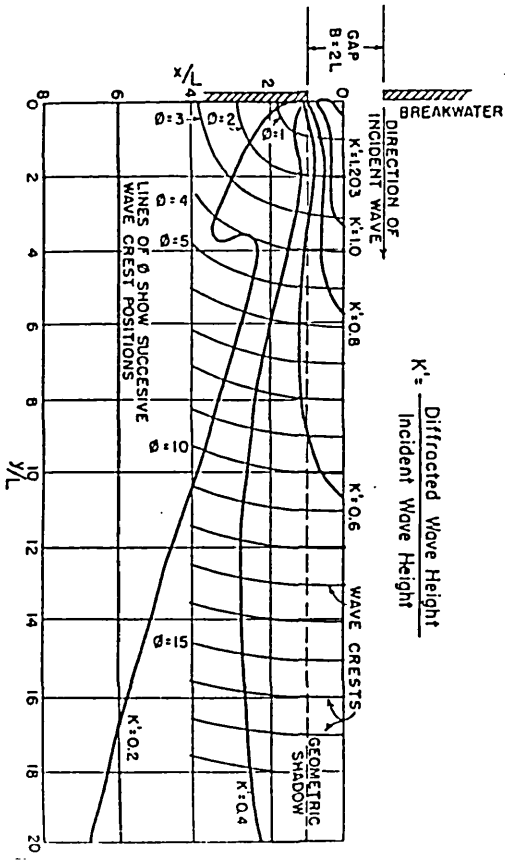

numerical

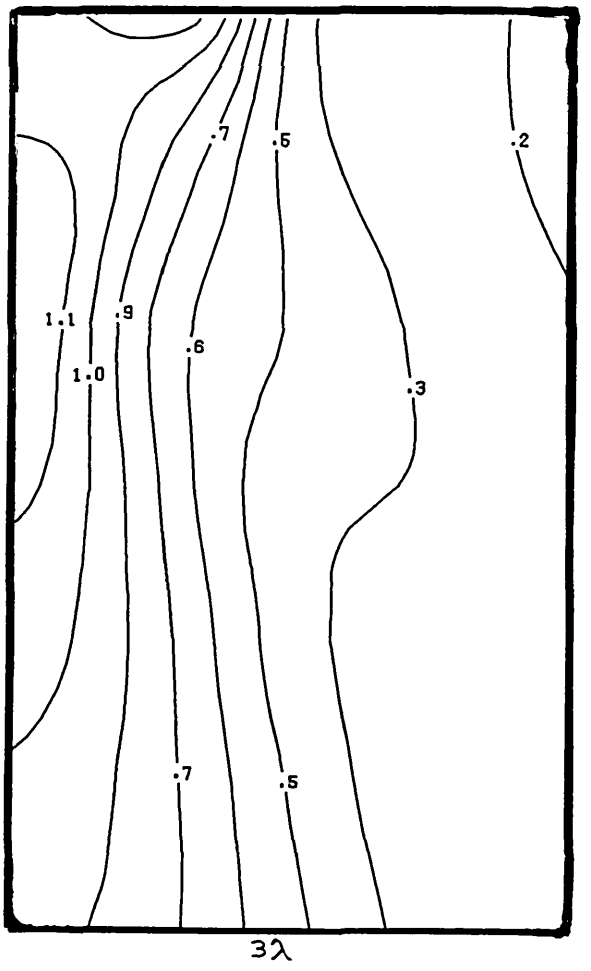

Figure 4.12 Amplitude contours
(gap width = 2 wavelengths)

analytical

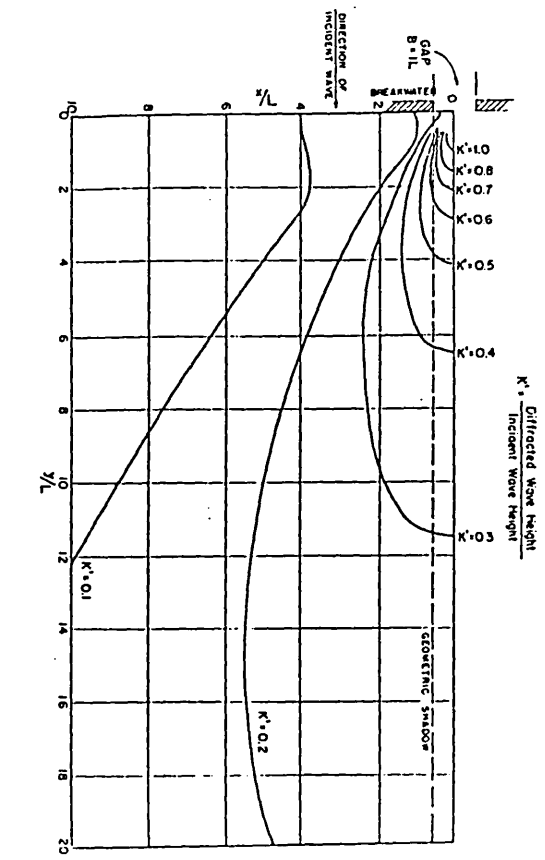

numerical

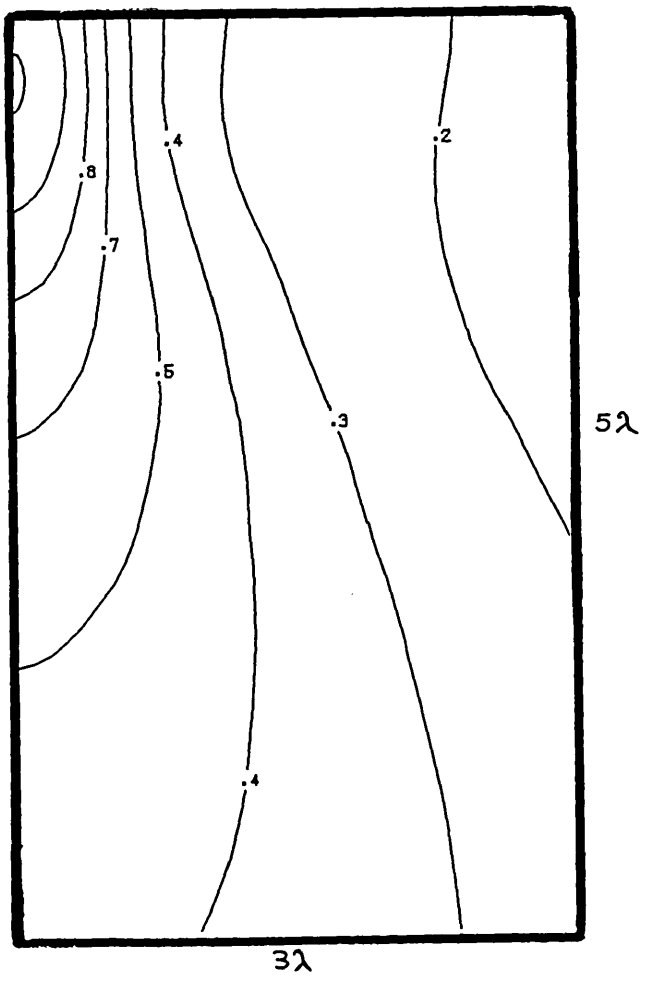

Figure 4.13 Amplitude contours
(gap width = 1 wavelength)

CHAPTER FIVE
A study of harbour entrances

The minimisation of energy transmission into a harbour is a matter of paramount importance to a coastal engineer and accordingly much effort has been spent on investigating ways of achieving this goal. A common approach is to place the outer protective breakwaters in an optimum directional layout in relation to the predominant direction of the incident waves. However, unless the entrance to the harbour is suitably designed, by incorporating appropriate resonators for example, energy will inevitably leak in leading to disturbances to shipping activities and in extreme cases to the breaking of mooring lines. It is our aim here to investigate the impedance properties of various harbour entrance configurations, comprising channels, resonators, and filter arrangements, using the numerical model developed in the previous chapter. Specifically, a semi–infinite harbour geometry, i.e. one that is unbounded by a coast, has been examined. This was chosen so that the effectiveness or otherwise of the various entrance configurations could be investigated without the added complication of internal reflections that arise when dealing with finite–size models. Where appropriate, ideas on filtering techniques have been adopted from other branches of physics involving wave motion, such as acoustics and electricity, where analysis procedures and theories are generally more advanced than those in hydrodynamics.

5.1 Previous work

Research into the effects of channels at entrances to semi–infinite harbours was presented and discussed in Chapter 3 within the confines of analytical modelling. A more general exposition extending to alternative harbour geometries as well as the application of numerical modelling techniques is given here as a prelude to further work on this topic.

The effort in this field was initiated by Roy(1962) who developed a simplified theory for tackling resonance problems and supported his results by performing some basic experiments. Using a more refined model, Carrier, Shaw and Miyata(1971) studied the resonance characteristics of several narrow–mouthed rectangular basins connected to the open sea by short channels. An asymptotic theory was developed which was applicable as long as the width of the channel, and therefore, the harbour entrance was small compared to the incident wavelength and to the characteristic dimensions of the harbour basin. Their analysis procedure, much like that of the method of matched asymptotic

expansions, involved dividing the solution domain into three regions comprising the open sea, the entrance channel and the basin. The wave field in each of these regions was then separately derived and by utilising the requirements of continuity for both pressure and velocity across the interfaces, unknown constants were determined. Of particular interest, the wave field in the basin was derived by assuming it to be completely closed so that the eigenvalues of the normal modes of oscillation formed the basis for its solution. The final results indicated that at resonant frequencies the amplification was augmented as the length of the channel was increased while at non–resonant frequencies the channel served to diminish the response in the basin. This anomaly was termed the channel paradox in analogy with the harbour paradox put forward by Miles and Munk(1961). Furthermore, the critical wavenumbers at which resonance occured were found to decrease with increasing channel length. Similar investigations by Unluata and Mei(1973), who concentrated more on developing a working analytical model rather than the explicit study of entrance channels, yielded similar conclusions. These findings shall be elaborated on later, in relation to our results.

More recently, Pos(1983,1985) attempted to model numerically the propagation of water waves along a semi–infinite channel and their consequent scattering at the mouth into a semi–infinite basin as shown in figure 5.1. He employed a finite element model for this purpose similar to the one developed in the present work except that an exponential type decay infinite element was used for discretizing the exterior region. Unfortunately, it is the opinion of this author that Pos made a serious theoretical mistake in modelling the scattered wave inside the channel by the use of the infinite element as this assumes that the wave decays to zero at infinity in the manner specified by Sommerfeld(1896). The physics of the problem, however, dictates that the wave field inside the channel shall be composed of a plane incident wave and another wave reflected at the open end which is necessarily plane as the walls of the channel are parallel and consequently no spreading can occur. This plane reflected wave does not fulfill the Sommerfeld radiation condition as it does not die out at infinity. Instead, it has a constant amplitude governed purely by the width of the channel which if small, could be determined by the theory of matched asymptotic expansions as presented previously. If this is not the case on the other hand, an alternative analytical approach such as the Wiener–Hopf technique (Noble(1958)) is needed. Therefore, the theoretical results pertaining to this work cannot be used to draw any sensible conclusions and furthermore, this problem is not amenable to solution by finite elements given the geometric constraints. Pos also modelled the same configuration experimentally, partly to corroborate the numerical results, and focused on the second order diffraction effects where he concluded that these add

to the energy transmission predicted by linear theory.

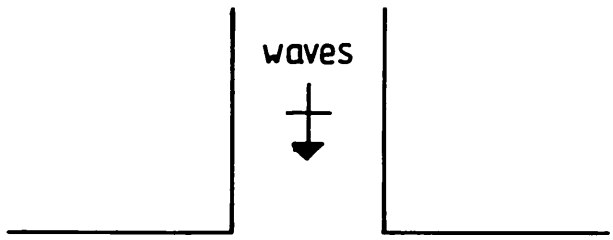

Figure 5.1 Geometry modelled by Pos(1983,1985)

An alternative design for harbour entrances may be realized in the light of the resonator whose behaviour was first investigated by Valembois(1953). His work involved the experimental and theoretical modelling of wave propagation in a channel in which resonators were placed along the path of the wave. He deduced that the resonator acts as a reflective structure, without obstructing passages, for a certain range of wave periods encompassing its natural frequency. He also recommended that the length of the resonator be $\lambda/4$, where λ is the wavelength of the incoming wave, for optimum perfomance. However, in following this recommendation, no regard is paid to the end effects which can play a major role in determining the efficiency of the resonator with respect to its length as demonstrated by later work.

A more thorough investigation was undertaken by James(1968,1970,1971) who studied, again experimentally and theoretically, a variety of resonator arrangements in channels. Proper account was taken of the end effects which were found to depend on both the widths of the resonator and channel. Tests on batteries of three resonators indicated that a wider frequency band of the incident ocean wave spectrum would be reflected if the distance between the resonators is sufficiently large.

The work of both of the above researchers was confined to channels that were narrow in relation to the wavelength so that a simplified one–dimensional propagation theory could be used. Although this was useful for demonstration purposes, the real problem of a semi–infinite ocean and a harbour on either side of the resonator was not solved until the work of Kubo, Aoki and Segura(1985) who developed a numerical model based on the method of boundary integral equations, for calculating the wave height distribution around a pair of breakwaters with arbitrary shape of the edge. Results were presented pertaining to

the effects of resonators equipped in these breakwaters, on the wave penetration into a semi–infinite harbour. Only narrow resonators were examined for a variety of entrance gap widths where it was found that these were more effective for smaller gaps. Comparisons with experiments did not however fully verify the theoretical results for a reason supposed to be due to energy dissipation at the resonator mouth. A purely numerical difficulty was experienced with their model in that the solution was sensitive to the number of segments used in discretizing the domain. Another approach to the design of harbour entrances has been proposed recently by Liu(1987). In deriving a one–dimensional wave equation for water wave propagation in a long channel with corrugated boundaries, he found that under a certain condition, when the wavenumber of the boundary undulations is twice that of the incident wavenumber, significant wave reflections could occur. This was the Bragg reflection condition which was first defined in connection with the diffraction of X–rays by a crystal lattice. Liu stated that because the amplitude of the bank undulations is small compared to the incident wavelength, this approach would be an attractive alternative to the conventional quarter–wavelength harbour resonator. For the particular configuration he studied, this amplitude was 0.1λ, and the length of the undulation region, L, was 15 times the mean channel width. A maximum reflection coefficient of 0.762 was obtained, which by all standards is quite impressive. However, with realistic channel widths, varying from 0.5λ to 2.0λ, L would have to be between 7.5λ and 30.0λ to achieve similar results, as otherwise the efficiency would be dramatically reduced. Clearly, this renders the method impractical as enormous works would have to be carried out in constructing such channels.

5.2 Harbour entrances

Several harbour entrance geometries are herein examined in order to establish a comprehensive outlook on the problem in hand. Amongst the configurations studied are long parallel–walled channels, narrow and wide resonators and filters consisting of several resonator 'cells'. In all these cases, the analysis has been undertaken at each of four gap widths, which were thought to cover an adequate range. In their dimensionless forms these are given by:

$2b/\lambda$ = 0.5, 1.0, 1.5, and 2.0.

As well as providing detailed results for the case of normal incidence of the incoming waves ($\theta^i = 270^\circ$), an outline of results is also given for two further angles. These are,

$\theta^i = 210^\circ, 240^\circ$

which correspond to angles of 30° and 60° respectively, from the direction of

propagation to the positive x–axis. In practice, the refraction process tends to bend the waves so that they approach the coastline normally, to an extent which is dependent on the wavelength and the variation in the sea–bed contours.

Restrictions imposed by the insufficient memory capacity of the computer, as allocated to individual users, limited the extent of discretization of the domain to approximately six wavelengths inside the harbour and two wavelengths outside. The finite elements employed had mostly plane polar forms with the outer rings on each side of the breakwater being made up of the infinite elements to model the outward decay of the scattered waves. A minimum resolution of about four elements per wavelength was maintained except near the gap where this figure was increased to cope with the rapid variations in the solution. For problems involving normal incidence, only half the domain was discretised as advantage could be taken of symmetry. Typical meshes used for normal and oblique incidence are shown in figures 5.2a and 5.2b respectively.

Results for the ratio of diffracted to incident wave height (A/A_i) are presented for all the cases treated, in two different formats. Two–dimensional contours are plotted for the harbour region using the graphics package, UNIRAS, which has the advantage of colour representation. This makes the displays easy to visualise, enabling one immediately to identify areas of low or high energy intensities, which is essential in the design process. The variation of the amplitude profiles along two critical sections inside the harbour are also plotted. The first is along the incident wave direction, or the centre line from the gap in the cases of normal incidence. This is important to a harbour engineer for assessing not only wave penetration but also navigational hazards as this is usually the path followed by ships in entering the port. The second section is along the inner face of the breakwater. Particularly when smaller boats, which are more susceptible to excitation, are docked there it becomes important to know the wave conditions.

5.2.1 Channels

The impedance properties of two channels of different lengths have been investigated at each of the four gap widths mentioned previously. The diffracted wave fields inside the harbour for these cases are compared with those for a simple gap in a breakwater of infinitesimal thickness (i.e. no channel at the entrance). The configurations studied correspond to the following three lengths:

$2a/\lambda$ = 0.0, 1.0 and 2.0.

Before analysing the general pattern of results obtained, it is worthwhile reiterating some of the physical insights gained thus far from our previous work, which have some bearing on the present problems.

In the analytical investigations of chapter 3, we examined the energy transmission through a long channel whose width, $2b/\lambda$, was assumed small in relation to the wavelength. It was found that when $2b/\lambda$ was typically less than 0.1, significant reflections occured at the open ends which served to diminish the amplitudes in the harbour. However this situation was reversed when the length of the channel was made approximately equal to an integral number of half wavelengths, as then an effectively one–dimensional resonant standing wave was set up, which amplified the response in the basin due to the added radiation damping of the oscillation from the inner end. As $2b/\lambda$ was increased to the maximum value of 0.2, the energy transmission coefficient, T, was found to vary little from that for an equivalent opening in a zero–thickness barrier, T_0. This was the case however long the channel was made, because of the greatly reduced reflections at the two ends. Thus, for a channel whose length is comparable to the wavelength, we may deduce that when the separation between its walls is relatively small ($2b/\lambda \leqslant 0.2$), the energy transmission charateristics are largely dominated by the processes of reflection at an open end. Although the asymptotic theory leading to this conclusion is not valid over the gap widths considered in the present work, it will nevertheless throw light on some of the physical principles.

In considering the results obtained from the present investigation, let us first examine the case of the smallest gap width, corresponding to $2b/\lambda = 0.5$. We would anticipate by the above reasoning and sensible extrapolation, that there would not be any noticeable differences in the amplitudes inside the harbour for either of the two channels as compared with the case of the simple aperture. This indeed is found to be the case as the plots* corresponding to the three lengths, $2a/\lambda = 0.0$, 1.0 and 2.0 are almost identical. Thus, from an 'added impedance' point of view, we have so far seen that it would not be beneficial to incorporate channels in the design of harbours unless their widths are relatively small. It was decided at this stage to increase $2a/\lambda$ from 0.0 to 2.0 in steps of 0.2 to check whether any unusual phenomena, which we might have missed by our coarse increment of 1.0, occured. However, none were detected so the results pertaining to these intermediate lengths are not included in the presentations.

The results corresponding to the three other gap widths, $2b/\lambda = 1.0$, 1.5 and 2.0+ show a distinct departure from the above trend of behaviour. We notice that the amplitudes along the centre line become more pronounced as the length of the channel is increased while those along the breakwater are diminished. This is in contrast to the previous case where the effects of the channels were practically undetectable as far as the energy transmission into the harbour was concerned. This may be explained in the following manner: as the

* Fig. 5.11a-c

\+ Fig. 5.12a – Fig. 5.14c

waves become shorter relative to the opening, there is practically no reflected wave. The incident wave radiates out from the open end with little subsequent spreading, as though the channel was still guiding it. The wave, as it emerges into the open, does not realise that it has left the channel and so sees no need as it were for sending back a reflected wave. The channel therefore exaggerates the beaming effect for the shorter waves, which makes the energy propagate in a predominantly forward direction and leads to the observed amplification of intensities along the centre line. The amplitudes outside the region of the beam are consequently reduced as little radiates from its envelope. Clearly, spreading must inevitably occur after a few wavelengths, and this is seen in the results. The practical implications of this beaming of short waves by channels and the consequent redistribution of energy inside a harbour are twofold. Firstly, the concentration of energy along the centreline from the mouth may pose a threat to ships traversing that route. However, as seen from the relevant graphs, the variations of amplitude along this path are generally quite gradual and in that sense, larger ships will be able to ride such 'bumps' without any adverse effects. Secondly, the low amplitudes outside the envelope of the beam provide an area of relative calm, especially along the inner face of the breakwater. This could then be utilised to provide shelter for smaller vessels whose motions are usually easily excited by waves of short period.

An interesting analogy may be drawn here between the physics of our problem and those ideas encountered in the development of early radar systems, which to some extent substantiate our findings. When a radar transmitter scans the sky, its radio signal can be compared to the light beam of a searchlight. Obviously if a radar beam is too wide, it will not locate objects very precisely and therefore much development work was aimed at narrowing it. Investigators concluded that the most logical approach to achieve this was to employ high transmitter frequencies such as those in the microwave range. This is then equivalent to using short waves which, as shown by our results, would propagate more as beams.

Wave conditions inside the channels are just as important to consider from the point of view of navigational hazards and therefore results are presented for the variation of amplitude along the axes of these, for all the cases studied. At the smallest gap width, $2b/\lambda = 0.5$, we notice a distinct, periodically repetitive pattern which suggests the existence of a longitudinal standing wave. The amplitudes involved are however small because, as mentioned previously, there are no significant reflections at the open ends. As the separation between the channel walls is increased, the pattern becomes confused and physical interpretation is difficult as phase interactions with transverse standing waves create a complex

wave field. It may nevertheless be said that the variation of amplitudes for the two cases, $2b/\lambda = 1.0$ and 2.0 are more severe than those for $2b/\lambda = 0.5$ and 1.5. This is because in the latter cases, a nodal line of elevation would exist all along the middle of the channel by virtue of the particular modes of oscillation that would exist, while in the two former cases, an antinodal line would be present.

Although the transverse standing wave, which is set up whenever the gap width is equal to an integral number of half–wavelengths, plays no role in either impeding or promoting the propagation of waves down the channel, it may perhaps present a problem to navigation. The large horizontal velocities associated with nodes of standing waves would cause the drifting of vessels. This obviously has to be counteracted, which makes for difficult manoeuvring. As this effect is more pronounced for longer waves, it would be inadvisable to make channels so wide as to permit long period transverse oscillations to exist. Furthermore, it would be helpful to make channels as deep as possible in order to limit the movements at such nodes. This is because the ratio of maximum horizontal to vertical particle displacements in a standing wave, obtained from standard linear theory, is coth(kh), where h is the mean water depth, which increases dramatically as kh approaches zero.

The results pertaining to the oblique incidence of the waves* reveal a complex behaviour which follows, to a limited extent, the same trends observed with normal incidence. Under such conditions, the modes of propagation of the water waves in the channels would be analagous to those of sound waves in waveguides where the combination of transverse standing waves and advancing waves usually leads to extremely intricate mathematical formulations. We may, however, deduce the following: at the larger gap widths, as the channels are introduced, conditions become generally better along the inner face of the breakwater that lies in the direction of the incidence and worse along the other. Thus, the situation whereby the energy inside the harbour propagates mostly in the direction of the incident waves, as in the case of the zero–thickness breakwater, is reversed. Also, as the length of the channel is increased to 2.0λ, the radiation out from the mouth is seen to become more symmetrical, as one would expect. At the smallest gap width considered, we notice that, as in the case of normal incidence, the channel has little effect.

5.2.2 Resonators

The four resonator geometries shown in figures 5.3a–d have been investigated. These are numbered from 1 to 4 and range in classification from

* Fig. 5·32 - Fig. 5·39

narrow to wide resonators, according to the dimensions of their widths compared with the wavelength. Resonators 1 and 2 are grouped together as they fall under the 'narrow' category, while resonators 3 and 4 come under the 'wide' category. The particular geometry of resonator 4 was chosen to determine the consequences of the longitudinal oscillations, which can occur as its width is 0.5λ, on the overall perfomance. The effects of all of these on the penetration of waves into a harbour are assessed in relation to the case when they are not present, i.e. the problem of diffraction by an equivalent opening in a breakwater of vanishing thickness. Before discussing the many results obtained, we shall provide an account of the physical mechanisms that lead to the impedance properties of such resonators. In doing so, several important concepts concerning the general scattering of waves shall be presented and related in an effort to provide a coherent theoretical account. In that respect, Morse and Ingard(1968) put forward the following explanation for such processes:

"When a wave encounters an obstacle, some of it is deflected from its original course. It is usual to define the difference between the actual wave and the undisturbed one, which would be present if the obstacle was not there as the *scattered* wave. When a plane wave, for instance, strikes a body in its path, in addition to the undisturbed plane wave there is a scattered wave, spreading out from the obstacle in all directions, distorting and interfering with the plane wave. If the obstacle is very large compared with the wavelength, half of this scattered wave spreads out more or less uniformly in all directions from the scatterer, and the other half is concentrated behind the obstacle in such a manner as to interfere destructively with the unchanged plane wave behind the obstacle, creating a sharp–edged 'shadow' there. This is the case of geometrical optics; in this case the half of the scattered wave spreading out uniformly is called the *reflected* wave, and the half responsible for the shadow is called the *interfering* wave. If the obstacle is very small compared with the wavelength, all the scattered wave is propagated out in all directions, and there exists no sharp–edged shadow. In the intermediate cases, where the obstacle is about the same size as the wavelength, a variety of curious interference phenomena can occur."

Although they do not specifically state this, it is clear that the above effects discussed by the two authors, are those of near–field behaviour. Far away from the scattering body, the influences of both the interfering and reflected waves will be gradually diminished as a shadow behind a relatively large obstacle will become progressively blurred. Also, the two waves which are to some extent directional in the near–field, i.e. higher intensities in certain, rather than other directions, lose their circumferential variation in the far–field. Therefore, the definition of the reflected wave as that which is spread out uniformly from a

body is misleading. This might be the case in the far–field, but in that instance, one should not distinguish between components of the scattered wave, as it then appears as a single uniformly outgoing circular wave, regardless of the relative dimensions of the body. In the long wavelength limit, the interfering and reflected waves are rapidly attenuated so that the behaviour is more or less uniform in both the near and far fields.

The interfering and incident waves, which propagate roughly in the same direction, must be 180° out of phase so as to cancel one another and produce, for example, the calm behind a relatively large cylinder in a water wave environment. The reflected wave, on the other hand, must be in phase with the incident wave in order to give rise to the approximate standing wave pattern just in front of the cylinder. In attempting to explain the physical factors that result in such effects, Lamb(1932) considered the origin of the scattered wave field to have two separate causes:

(1) The 'impenetrability' of the obstacle. Were the body not there, the space it filled would be occupied by water moving up and down, generating outgoing waves on Huyghens' principle. The effect of its presence is to cancel out this radiation which may be visualised (in the first approximation) as the superposition on the incident wave of a radiation equal and opposite (in phase) to that which the heaving water volume would have produced in its absence.

(2) The 'immovability' of the obstacle. Again, were there no body present, the fluid in the space would be moving backwards and forwards. The second component of the scattered wave may be visualised, as the pattern generated by the oscillation of the solid, in antiphase to the unobstructed incident motion.

In the special case of small kb where b is the cylinder radius, the first effect is that of a simple wave source and the second, that of a wave doublet. "It might appear, at first sight, that the former of these disturbing influences would be much less important than the second, but in its effect at a distance it becomes comparable, owing to the greater attenuation by a lateral motion of the waves proceeding from a double source." (Lamb(1925)). When the horizontal dimensions of the obstacle are equivalent to, or larger than the wavelength, the boundary must be represented by distributions of single and double sources in accordance with Green's theorem.

In relating the two components of the scattered field, discussed by Morse and Ingard, to the above causes, we may say that the reflected wave is that part of the doublet type radiation that propagates in a direction opposite to that of the incident wave (backward direction), while the interfering wave is that part which propagates mainly in the forward direction. As waves generated in this fashion have to eventually bend and meet, this would explain the diminution of

the effects of the two waves in the far–field. Also, as the velocity potential suffers a change in phase of 180° across a doublet, the interfering wave must consequently be out of phase by a similar amount with the reflected wave, which would explain its cancellation of the incident wave. The source type radiation, associated with the impenetrability of an obstacle, gives rise to an independent uniform scattered wave which would be dominant in the far–field, in the short–wavelength limit and in both the near and far–fields in the long–wavelength limit, as the doublet is less efficient than the simple source for radiating at low frequencies.

To illustrate the above principles, and for ease of visualisation, consider the example of the scattering of waves by an infinitely long plane wall. In this case, the source effect is absent as the thickness of the wall does not enter into the problem and hence it can be treated as if it were infinitesimally thin and so the only motion is due to a distribution of doublets. These would therefore radiate two equal waves which travel in opposite directions and superimpose on the incident wave field. In front of the wall, the reflected wave reinforces the incident as the two are in phase, while behind the wall, the interfering wave annuls it. This is illustrated schematically in figure 5.4. At first, the foregoing arguments may appear to unnecessarily complicate the simple plane reflection process. However, when dealing with more complex scattering systems, such as harbour resonators, the concept of an interfering wave becomes more physical and the behaviour must be analysed in that manner in order to maintain a grasp on the interpretation.

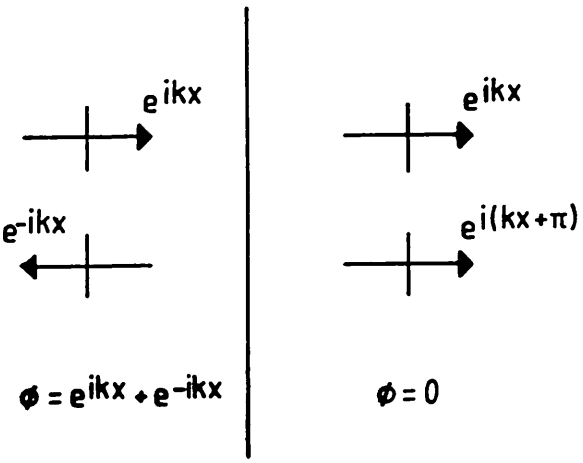

Figure 5.4 Scattering at a plane wall

The impedance characteristics of quarter–wavelength resonators at entrances to semi–infinite harbours are now examined with reference to the above principles. When such configurations are subjected to the action of linear water waves, the total wave field may be decomposed into two constituents, the first of

which is the diffracted wave field, or that which would be present in the absence of the resonators. The second is the radiated wave field, otherwise known as the radiation damping, which arises from the action of the resonators alone. This decomposition is useful because a correspondence may now be seen between that part of the radiated wave which penetrates the harbour and the interfering wave, and also between that part which is returned seawards and the reflected wave. As the reflected and interfering waves are respectively in and out of phase with the incident wave, this situation would then lead to the observed diminished amplitudes inside the harbour and the increased amplitudes outside. It is, however as yet, not clear how these changes in phase come about, as we do not have here the doublet effect associated with a solid obstacle. Instead, the resonator itself creates the phase difference by virtue of the 'extra distance' which has to be travelled by a wave in entering the harbour. The interfering wave is known to be that part of the incident wave that enters the resonator, and on being amplified, propagates into the harbour. As the effective length of these resonators is $\lambda/4$, this wave would have consequently suffered a path lag of $\lambda/2$ as compared with those waves that enter the harbour directly. This is then equivalent to a phase difference of 180°. The same phase loss in the reflected wave is recovered as it retraces its path back out to sea. Therefore, whereas in the case of the obstacle, the doublet property gave rise to the phase differences, it is the phase differences that simulate a doublet type radiation in this case.

Having established a clear physical picture of the scattering process, we are now in a position to examine our results. The geometries corresponding to the four resonators investigated in this work were fixed except for their lengths which had to be determined subject to the condition of maximum induced amplification. This was obviously a necessary step as the efficiency of the resonators in impeding the energy of incoming waves is highly dependent on resonance occuring inside them. Therefore, the first stage in the analysis involved plotting curves for the variation of amplitude with resonator lengths for points at the centres of the backwalls (where antinodes would exist). The optimum lengths were then those that corresponded to the peaks of these curves. Examples for resonators 1 and 2 are shown in figures 5.5a–b, for each of the four gap widths considered. A table summarising the optimum lengths for each combination of resonator and gap width is also given (Table 5.1). The discrepancy that arises between the effective and optimum lengths ($\lambda/4 - l_{opt}$) is due to the end correction which plays a major role because of the imperfect reflections at an open end. A physical discussion of these effects is provided in chapter 3.

In looking at the results corresponding to the smallest gap width,* $2b/\lambda=0.5$, it is immediately apparent that the resonators possess an impedance

* Fig. 5.15 a-c, Fig. 5.19 a-c

quality that is quite remarkable, as with the wider ones (resonators 3 and 4), an almost 100% reduction in energy transmission is achieved. For the narrower resonators (1 and 2), this figure is approximately 60%, which still implies considerable improvements in wave conditions inside the harbour. Resonator 1, being the narrowest, tended to augment the amplitudes in the immediate vicinity of the gap due to the severe resonance (associated with narrow channels) that is set up, which results in high–intensity radiation damping 'leaking' into and contaminating the harbour region. As the gap width is increased to $2b/\lambda=1.0$, we observe a departure from this trend of behaviour as areas of higher amplitudes emerge in the immediate lees of the breakwaters. This is especially apparent with the narrower resonators as then, an approximate doubling in the amplitudes occurs along the breakwaters (as compared with the case when the resonators are not present). Along the centre line, however, the amplitudes are reduced by as much as 65%. Although for this case, resonators 3 and 4 are not as efficient at impeding the wave penetration, they are nevertheless more desirable to incorporate in the design of harbour entrances as they do not lead to augmented amplitudes either behind the breakwaters or near the gap as do resonators 1 and 2. Increasing the gap width further results in a progressive growth of the areas of higher amplitudes (or energy lobes) behind the breakwaters which in turn lead to reduced resonator efficiencies. Furthermore, in the case of $2b/\lambda=1.5$, we notice severe amplifications near the gap when the narrower resonators are employed which affect the surrounding areas to such an extent that even along the centre line, the full sheltering benefit of the resonators is gained only when ships are at least one wavelength into the harbour. When $2b/\lambda=2.0$, the energy lobes become quite significant in size and consequently the use of narrow resonators has then to be questioned.

We have so far established that when the gap width is of the order of the wavelength, typically between 0.5λ and 1.0λ, there is a considerable advantage to be gained by employing quarter–wavelength resonators. The perfomances of the wider ones were generally seen to be more acceptable as these did not lead to excessive amplifications near the entrance. As the gap width is increased to beyond 1.0λ, however, there is a penalty to be paid in using narrow resonators as the reduced amplitudes in the centre of the harbour are counteracted by higher amplitudes behind the breakwaters. This would inevitably prevent any loading and unloading activities that might otherwise take place there.

In attempting to provide physical explanations for the above findings, we have to refer once more to our concepts in relation to the scattering process. We mentioned earlier that the total wave field inside the harbour was the superposition of the diffracted and interfering waves which are 180° out of phase.

As the intensities of these are not necessarily equal, their phase interactions will not lead to complete mutual cancellations in all places. At points where the intensity of the interfering wave far exceeds that of the diffracted wave, such as near the mouths of the resonators, high amplitudes would ensue. This would then explain the excessive amplifications near the entrance of the harbour. In order to explain the existence of the energy lobes behind the breakwaters, however, we have to explore this physical approach further. The actions of the resonators in generating the interfering and reflected waves, which are acknowledged to be in antiphase, is equivalent to the radiation from two doublets placed at the extremities of the gap. Now, a doublet is equivalent to two simple and equal wave sources, which are a small distance apart but are pulsating 180° out of phase with each other. Although there would be no resultant mass flow across a spherical surface surrounding the dipole, there would be a resultant momentum flux. This would be similar to a force acting on the medium and can only be provided by the reaction from a solid surface. Thus, in the case of the narrow resonators where the present analogy is more appropriate, the radiation from the two doublets may be considered to arise from the vibrations of two small plates that are located in similar positions. When the gap width, $2b/\lambda$, is small, these would effectively act as one, with the result that the radiation would spread out uniformly, as shown by the rough sketch of figure 5.6a. As $2b/\lambda$ is increased, the two resonators would tend to function independently and consequently, the waves radiated by the two plates, would be concentrated near the edges of the entrance, as shown by figure 5.6b. These would then penetrate into the sheltered regions behind the breakwaters, where the intensity of the diffracted wave is low, and give rise to the increased amplitudes there.

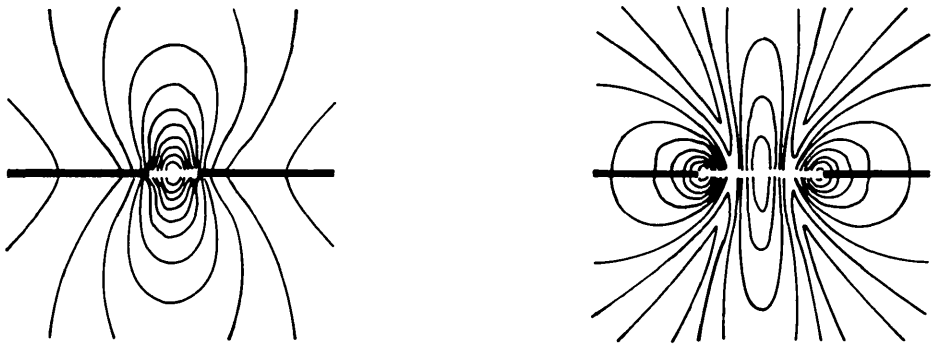

Figure 5.6 Radiation patterns from oscillating plates

In the case of the wider resonators, the interfering wave would not be of a high intensity as the associated resonance will not be marked because of poor

reflection at the open end. This implies that the wave would be attenuated rapidly inside the harbour, thus making such resonators generally not as efficient as the narrower ones: a deduction which has been confirmed by our results. The reason for resonators 3 and 4 being more effective than their narrow counterparts for the smallest gap width considered is because the 'amount' of radiation damping is then larger and the intensity of the diffracted wave, which has to be annulled, is not as high.

Let us now turn our attention to the cases of oblique incidence. The results* seem to display similar trends as before in that the narrower resonators are again seen to lead to worse conditions near the entrance and in the lees of the breakwaters, especially with the wider gaps. Two interesting points emerge however, which shall be looked at briefly. The first concerns the perfomance of resonator 4 which has been found to be the most efficient over all the gap widths considered, in contradiction with previous results. It is thought that the adverse longitudinal oscillations which would exist by virtue of the particular geometry of this resonator, would not have as strong an influence when the incoming waves are incident obliquely and therefore, a much improved efficiency is obtained. The second point arises in connection with the increased amplitudes that are observed in that part of the harbour which would otherwise be sheltered due to the angled incidence. As the two resonators at the entrance are disproportionately excited by the incident wave, it follows that the action of one resonator would surpass that of the other, to an extent that is dependent on the actual angle of incidence. Clearly, this asymmetry in the behaviour would be maximised in the limiting case of grazing incidence. With the smaller gaps, all four resonators are seen to be very effective.

5.2.3 Filters

When a series of resonators or of apertures are arranged as side branches to an acoustical conduit, the arrangements constitute acoustical filters, the former tending to suppress all frequencies above a certain pitch and the latter to remove all below a certain critical frequency. Such networks are illustrated in figure 5.7 and are termed low–pass and high–pass filters in accordance with their attenuation properties. Applications of these to acoustics are diverse and range from automobile exhaust silencers to sound–absorbing plenum chambers that are installed in ventilating systems.

The physical behaviour of the constituent resonators of a low–pass filter is now well understood, having been looked at previously, but it must be mentioned that for the high–pass counterpart, the filtering action of an orifice

* Fig. 5·40 - Fig. 5·47

does not result from the transmission of energy out of the pipe, but rather from the reflection of energy back toward the source.

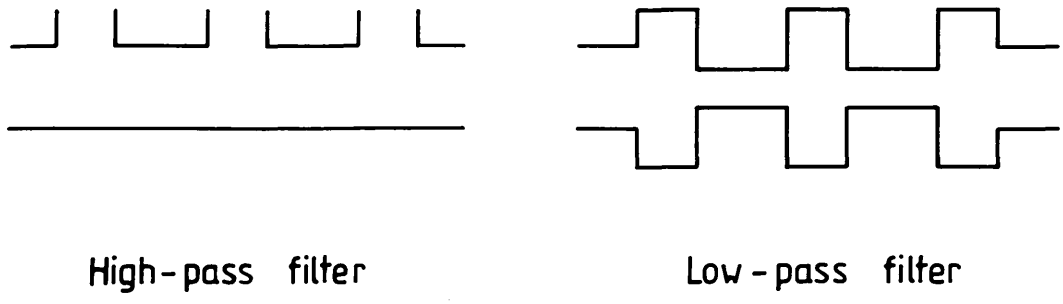

Figure 5.7 Acoustic filter networks

In the present context, the interactions of water waves with structures analagous to the low–pass filter have been investigated at each of three gap widths, given by:

$2b/\lambda$ = 1.0, 1.5 and 2.0

It was decided not to include smaller gaps here as the impedance of the single resonators proved to be more than adequate for such geometries. Within the first part of this study, the cumulative effects of *two* and *three* adjacent resonators are examined and assessed in relation to the cases of a single resonator and no resonator at the entrance. In the second part, similar comparisons are made for a configuration of *two* non–adjacent resonators, separated by half a wavelength (0.5λ). This latter part was undertaken because the particular filter we are trying to model comprises not only resonators, but short connecting channels as well, which add to the total impedance of the system. The electrical analogue of this setup is then a combination of inductors placed in series, with capacitors shunted across the line. Only the intermediate resonators (2 and 3) were employed as these were found to be the most effective of the four. Their lengths correspond to the peaks of the resonance curves obtained earlier as listed in Table 5.1. The geometries of all the problems tackled are shown in figures 5.8a–b. Arrangements resembling high–pass filters were not studied as the costs that would be incurred in the construction of such works would be prohibitive. Also, it might be beneficial to allow certain long–wave movements to occur for the purposes of 'harbour flushing', which aids in circulating and replacing otherwise stagnant water.

On inspecting the results,* we notice that the use of three adjacent cells of resonator 2 always leads to unacceptably high amplitudes in the

* Fig. 5·23a - Fig. 5·28c

neighbourhood of the entrance, regardless of the gap width. In fact, improvements over other configurations are detectable only at distances of at least 3λ into the harbour, which makes for an unsatisfactory overall perfomance. With two cells of the same resonator, we find that there is little advantage to be gained over the single–cell geometry, implying that such designs would not be cost–effective. By employing the slightly wider resonator 3, the trends become more encouraging. For the wider gaps, the three–cell configurations are found to be the most efficient, surpassing in perfomance those of two cells and single cells. With two–cell arrangements, however, excessive amplifications are observed in the vicinity of the mouth, with amplitudes reaching values as high as $2.2A_i$, A_i being the amplitude of the incident wave. When the gap width is reduced to $2b/\lambda=1.0$, we notice that the efficiency of two consecutive cells exceeds that of three, but the former again leads to the usual augmented amplitudes which now extend into the lees of the breakwaters.

The results pertaining to batteries of two non–adjacent resonators indicate that a quite remarkable impedance is afforded by such geometries. For the case of $2b/\lambda=1.0$, an almost 80% reduction in energy transmission is achieved when the elements of the filter are based on resonator 2. With resonator 3, the perfomance is equally impressive, with a reduction of approximately 50%. Even for the larger gaps, substantial improvements throughout the harbour are observed. The efficiencies of filters comprising cells of resonator 2 were generally seen to be better than those comprised of resonator 3 because of the smaller dimensions of the former in relation to the chosen separation between the elements. Also, the amplifications near the entrance were not as severe or strongly varying as had been encountered previously and in some cases, these were altogether absent. It is believed that if a larger number of resonators are utilised in this fashion and if the distance between them is increased ($>0.5\lambda$), the wave penetration into the harbour would reduce drastically, with no adverse effects on navigation. However, due to financial and topographical constraints, realistic limits must be imposed so as to keep such designs practical.

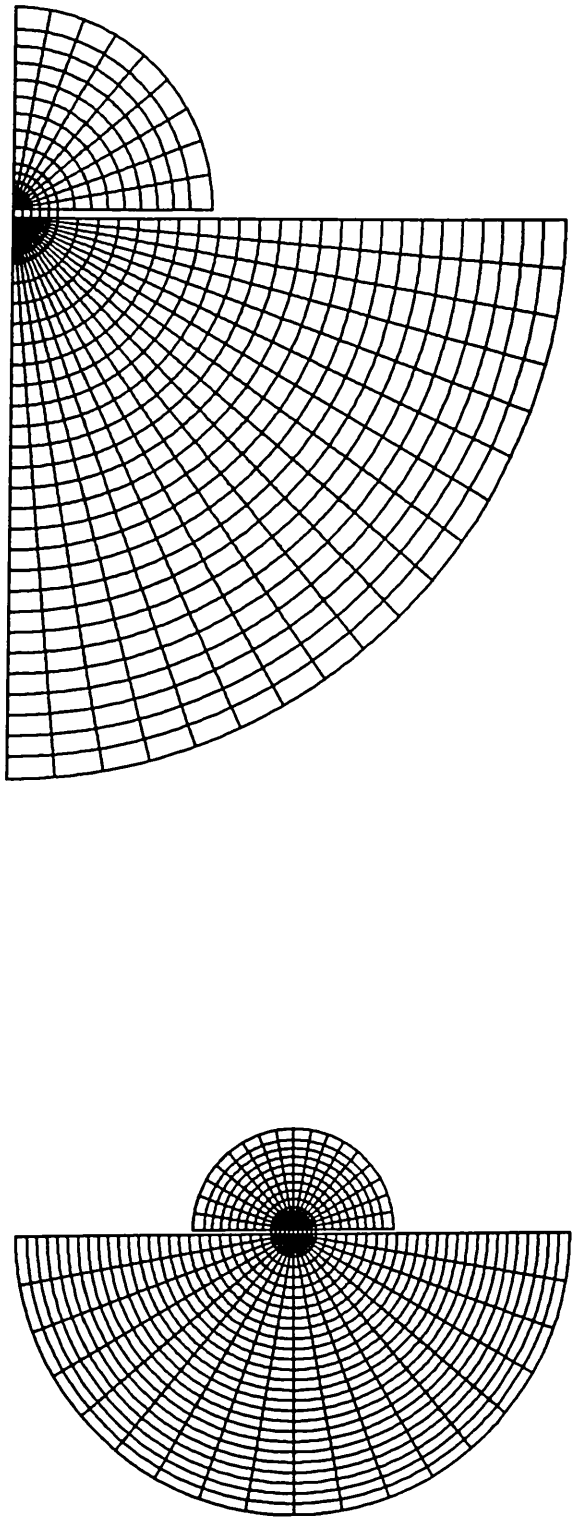

Figure 5.2 Finite element meshes

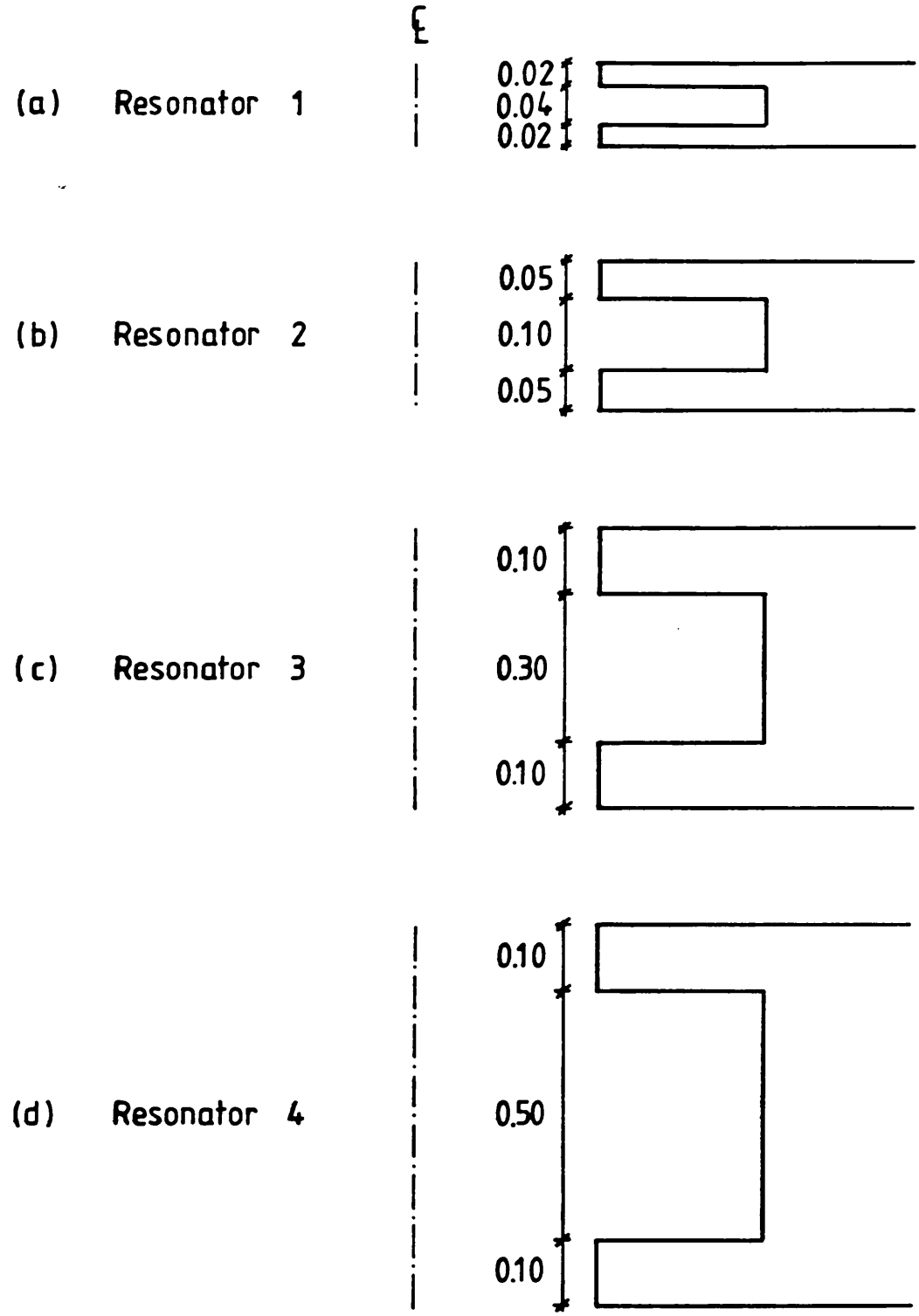

Figure 5.3 Resonator geometries

(Dimensions in units of wavelength)

Resonator no. / Gap width	1	2	3	4
0.5	0.23	0.21	0.22	0.26
1.0	0.22	0.18	0.12	0.12
1.5	0.23	0.20	0.18	0.23
2.0	0.22	0.18	0.11	0.10

Table 5.1 Optimum resonator lengths

(Dimensions in units of wavelength)

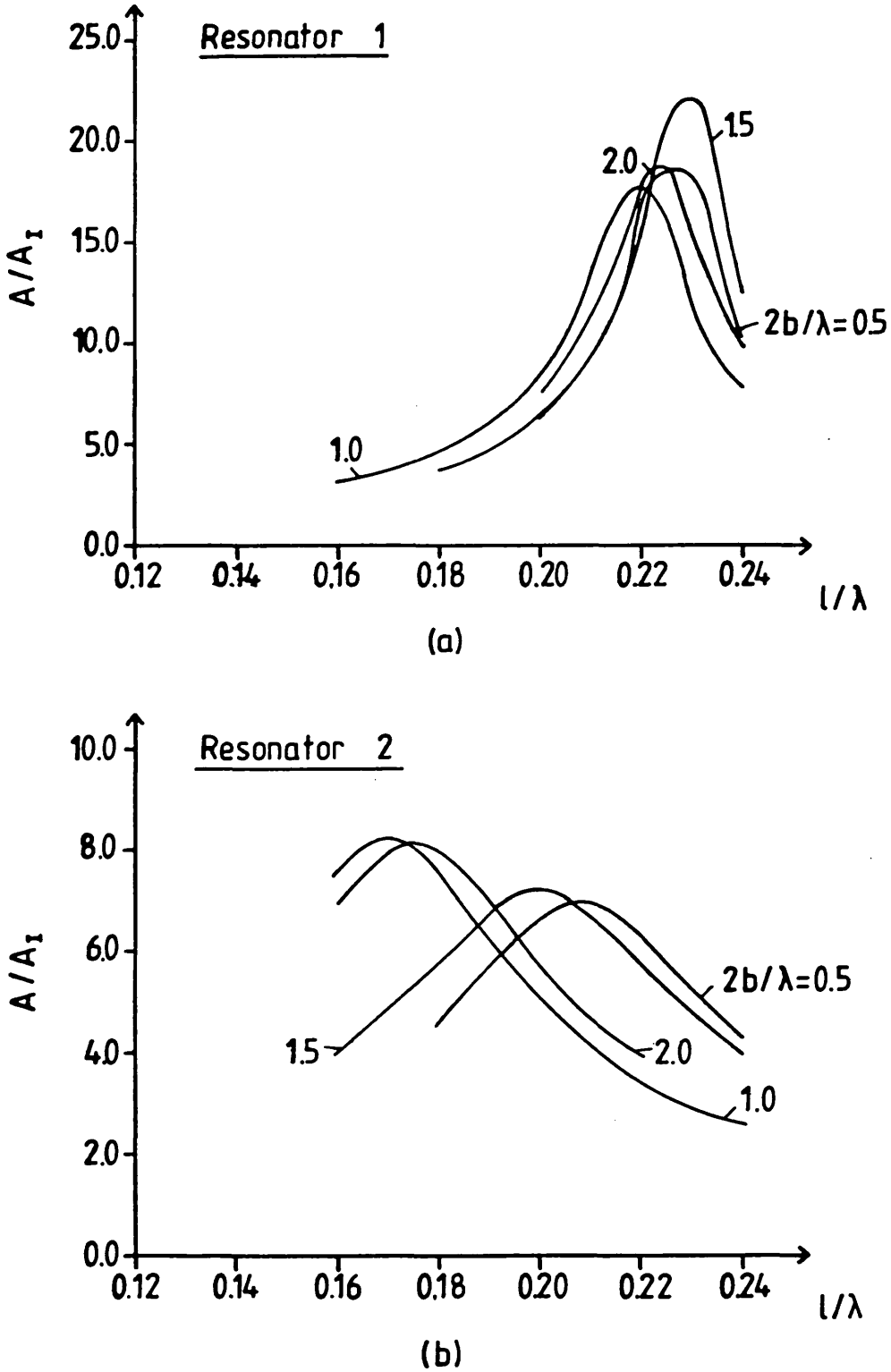

Figure 5.5 Amplification factors inside resonators

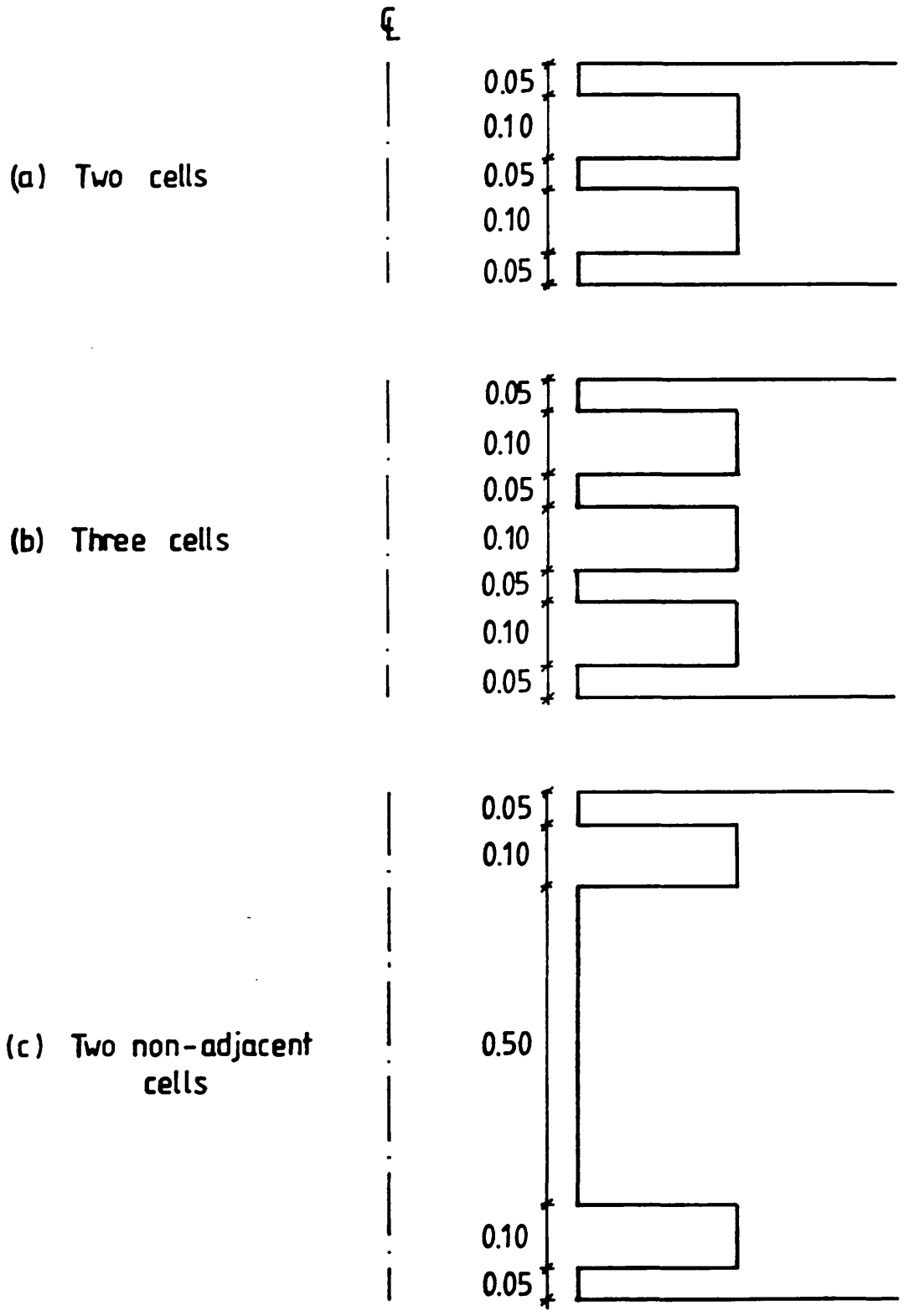

Figure 5.8a Filter geometries : Resonator 2

(Dimensions in units of wavelength)

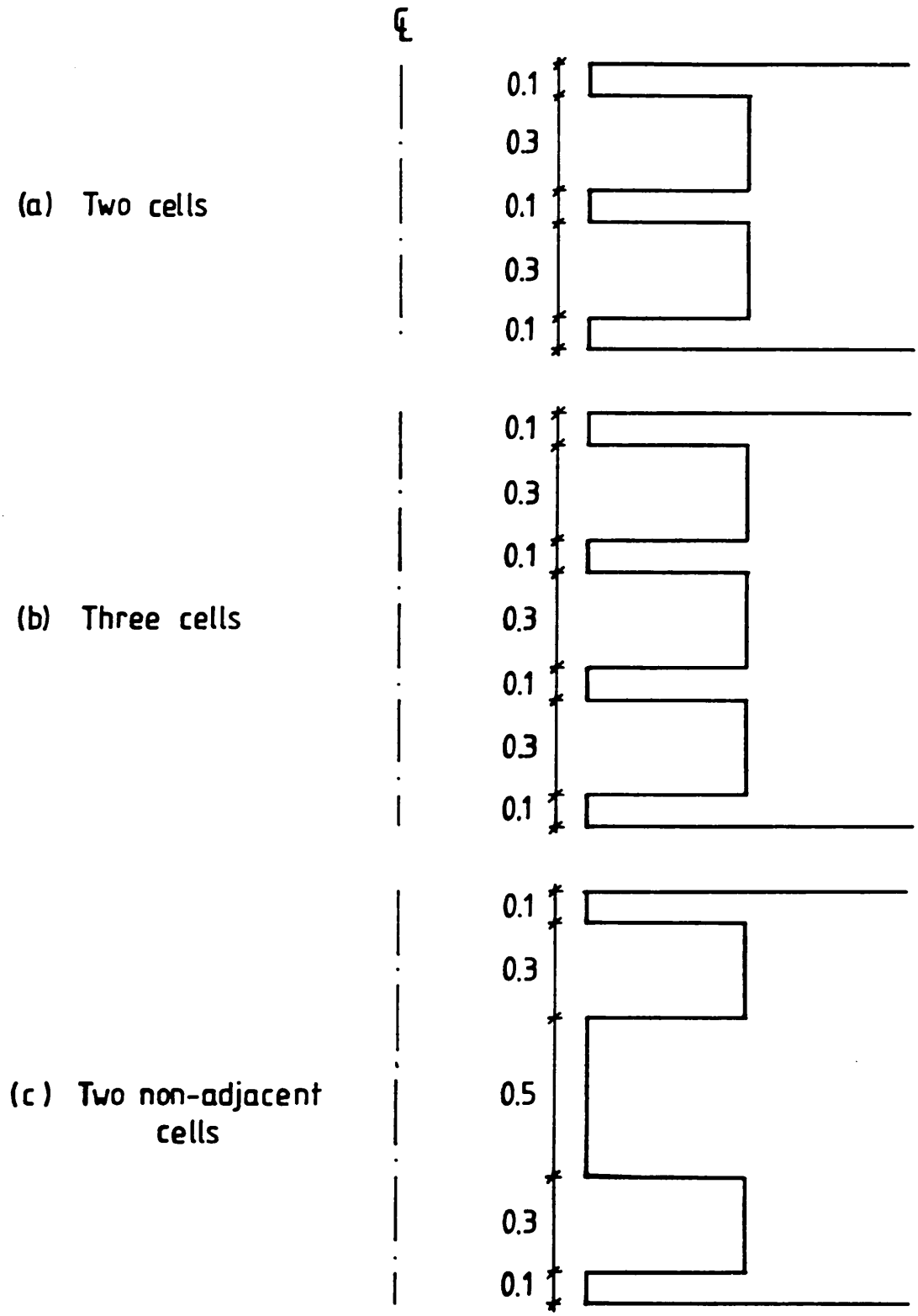

Figure 5.8b Filter geometries: Resonator 3

(Dimensions in units of wavelength)

CHANNELS

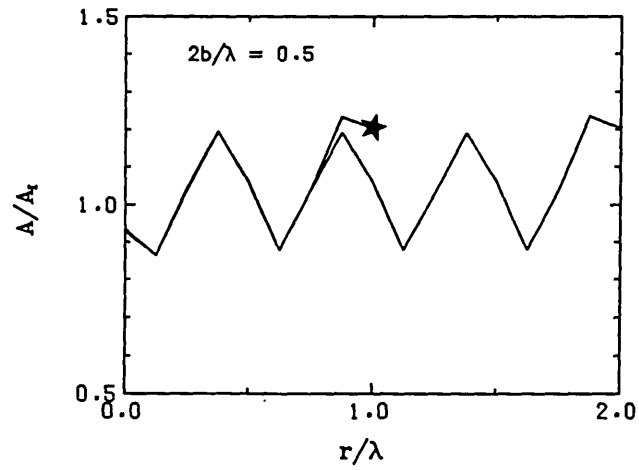

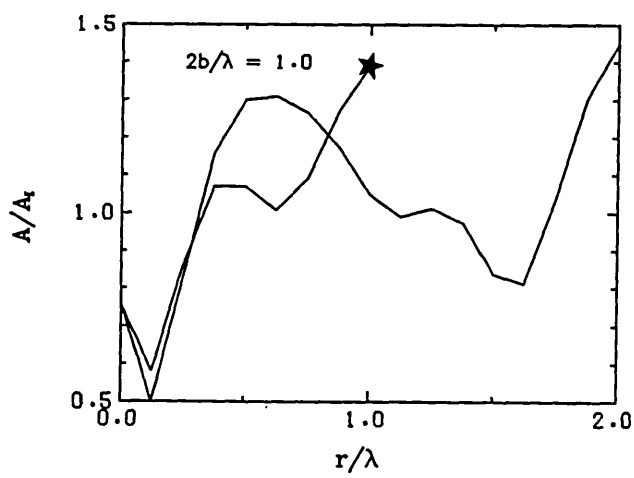

Figure 5.9 Amplitude profiles in channels

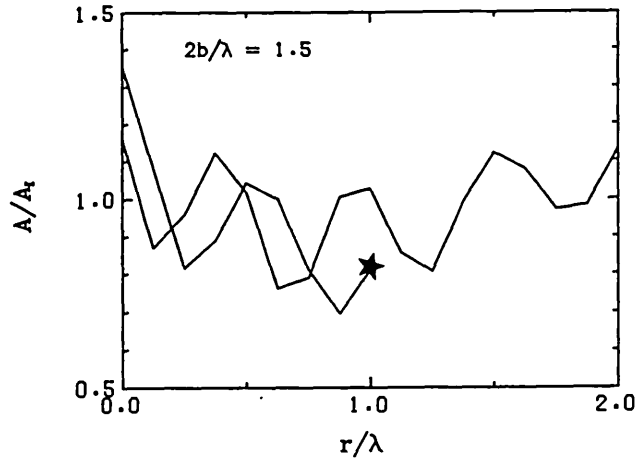

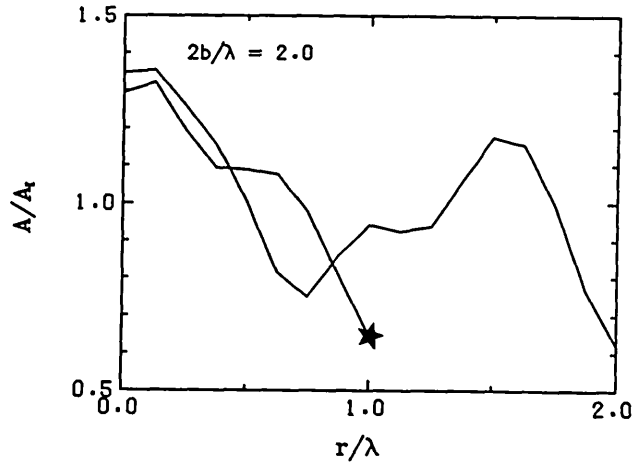

Figure 5.10 Amplitude profiles in channels

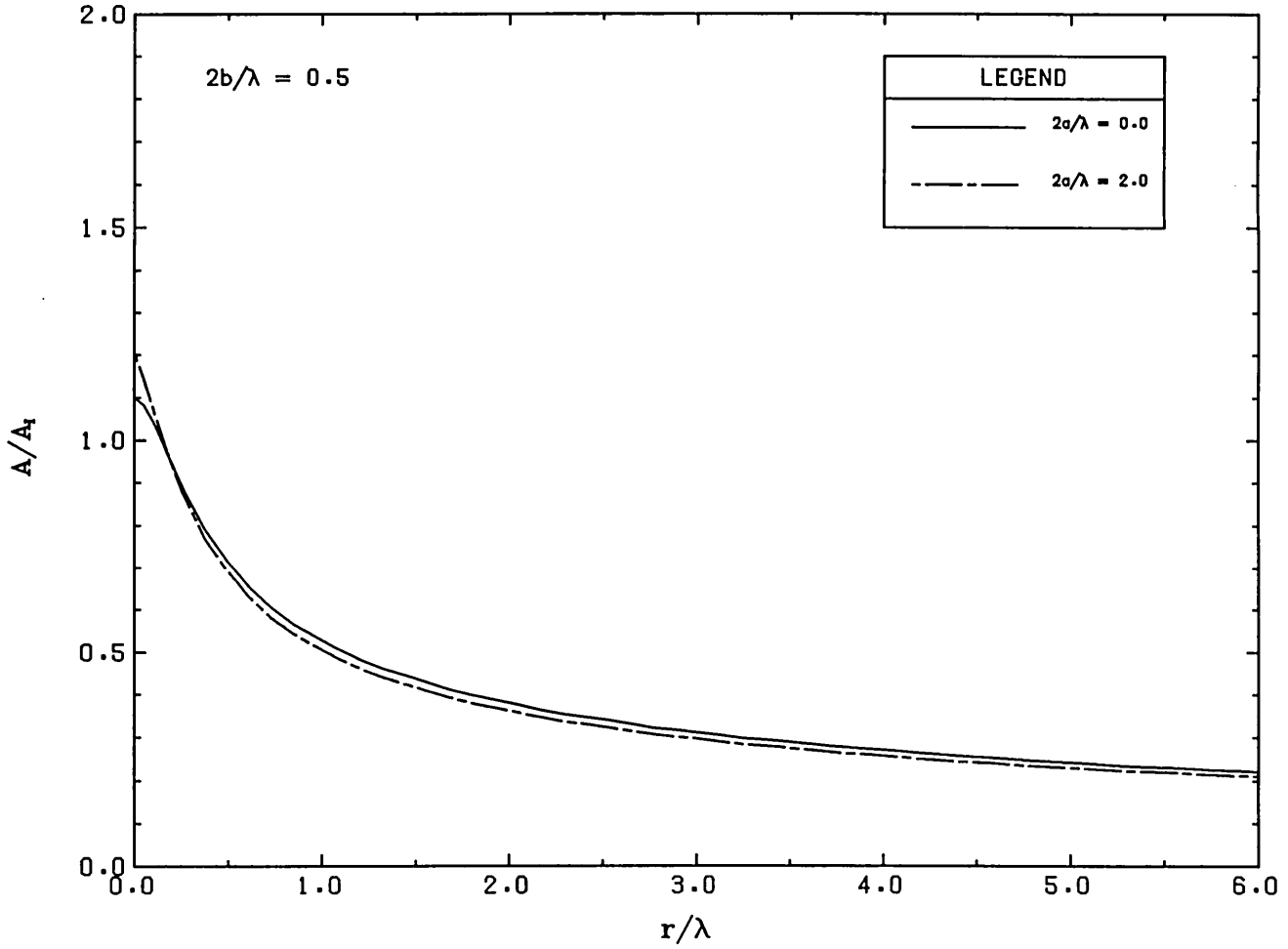

Fig. 5.11a PROFILES ALONG INCIDENT WAVE DIRECTION

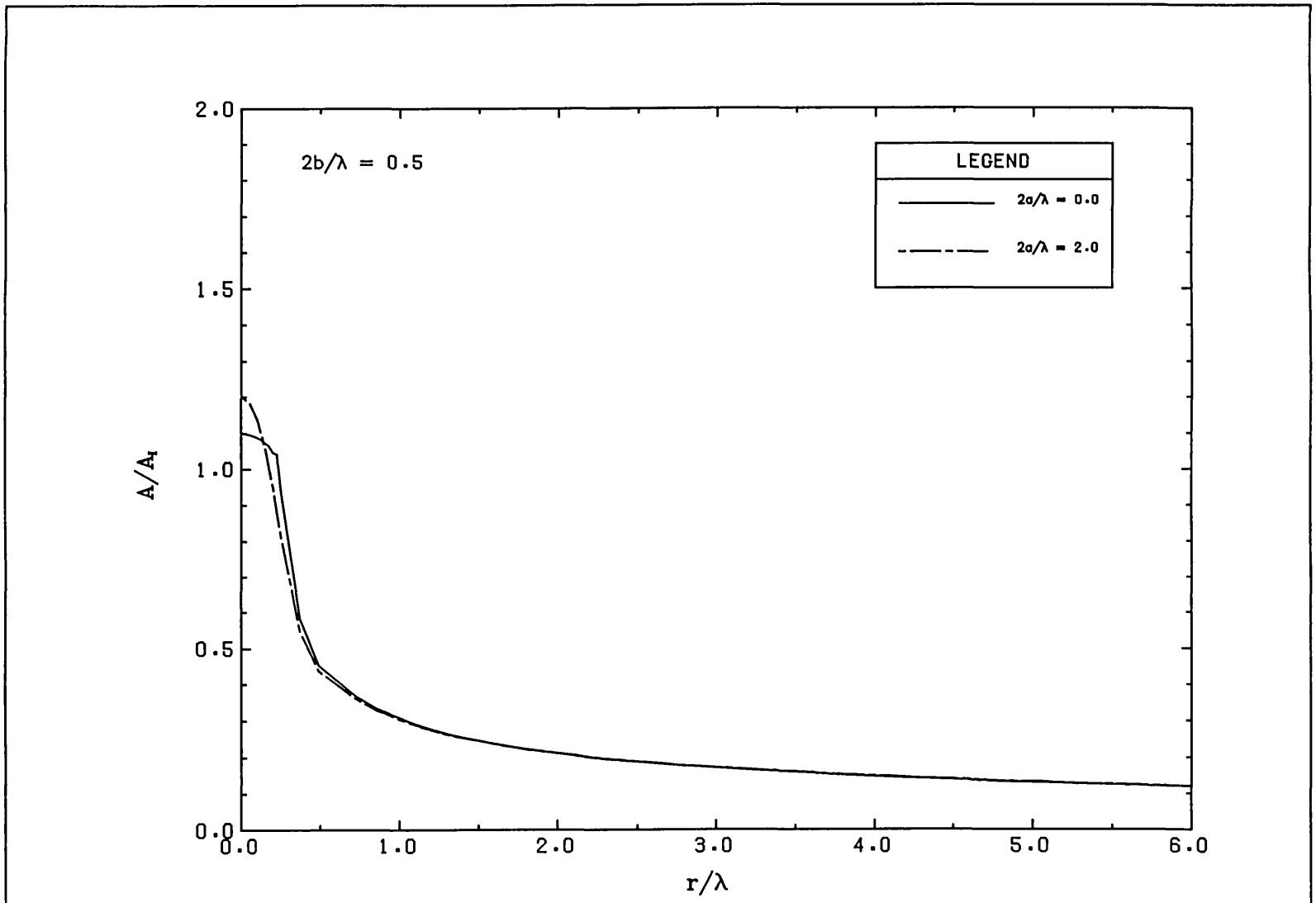

Fig. 5.11b PROFILES ALONG BREAKWATER

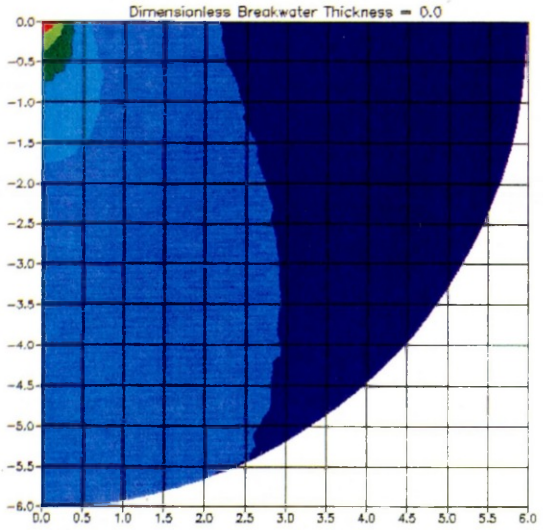

$2b/\lambda = 0.5$

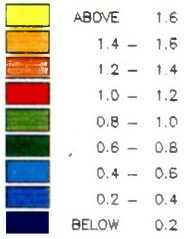

Fig. 5.11c

Amplitude contours

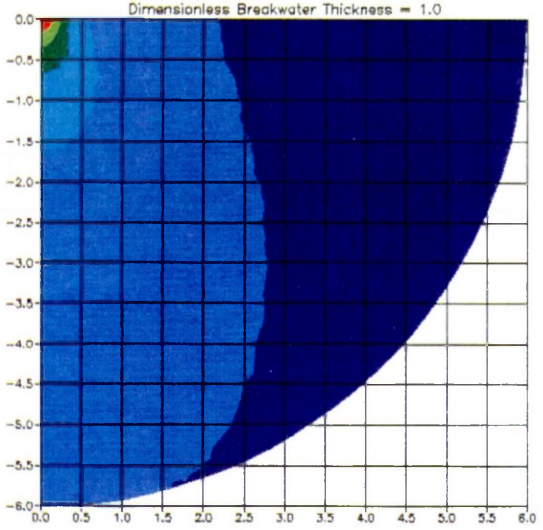

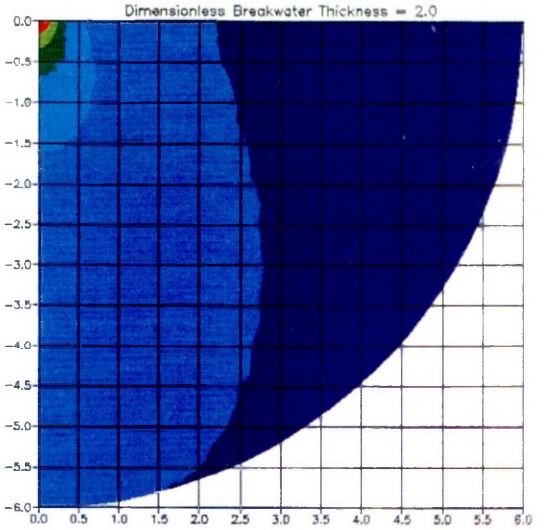

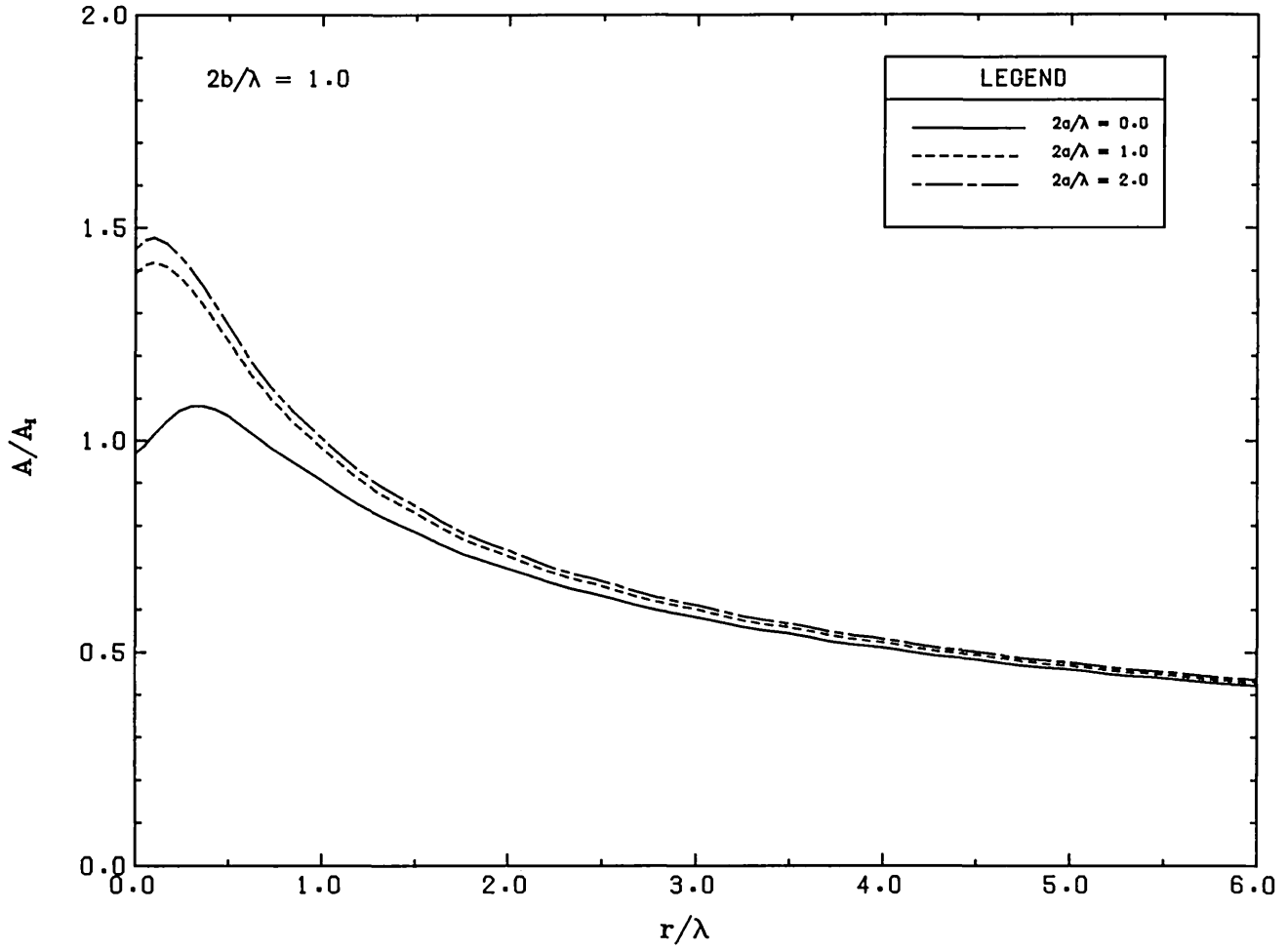

Fig. 5.12a PROFILES ALONG INCIDENT WAVE DIRECTION

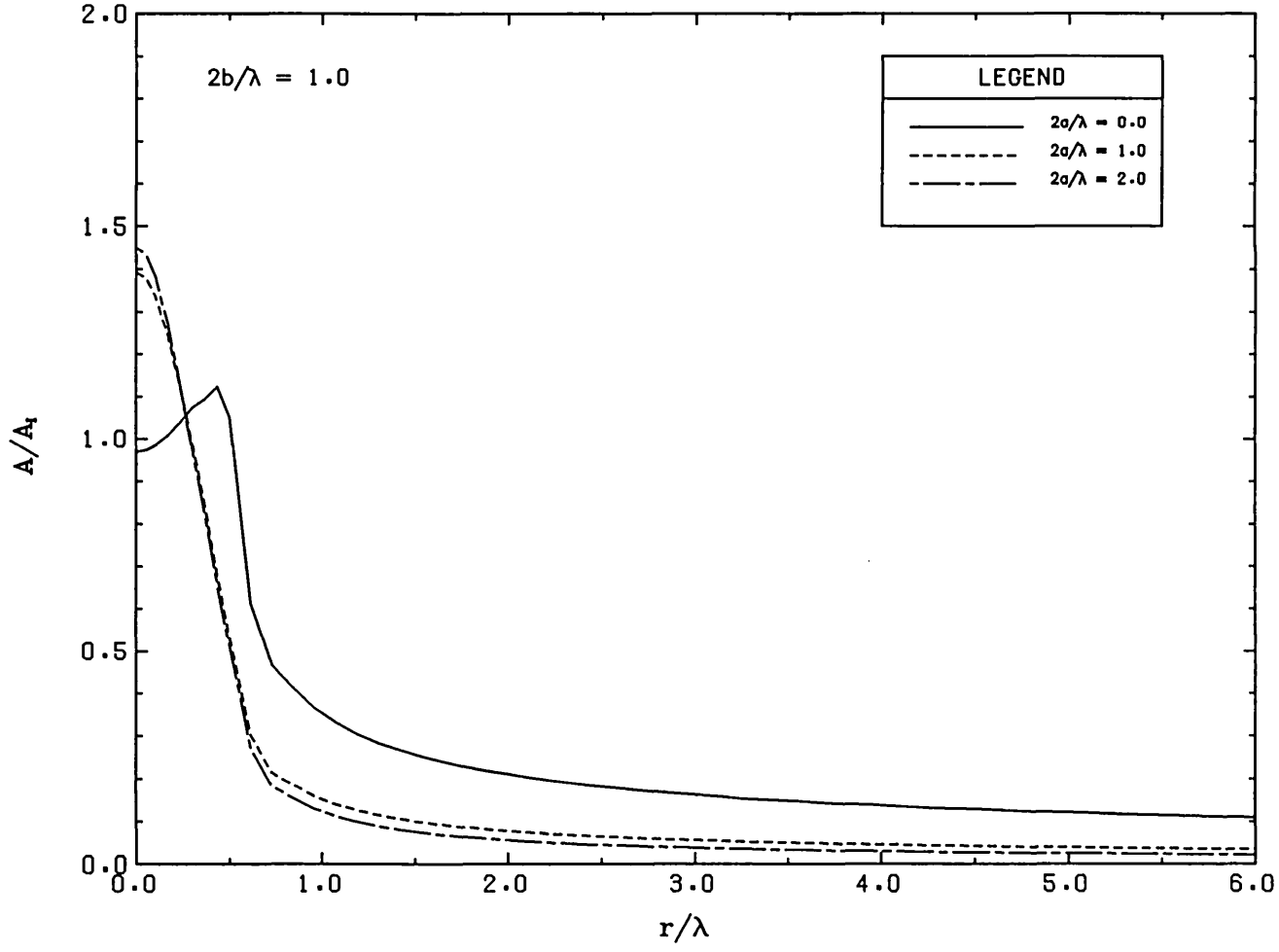

Fig. 5.12b PROFILES ALONG BREAKWATER

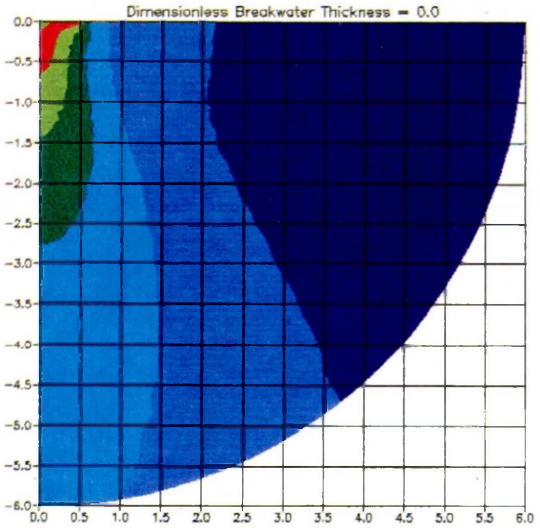

$2b/\lambda = 1.0$

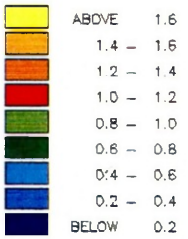

Fig. 5.12 c

Amplitude contours

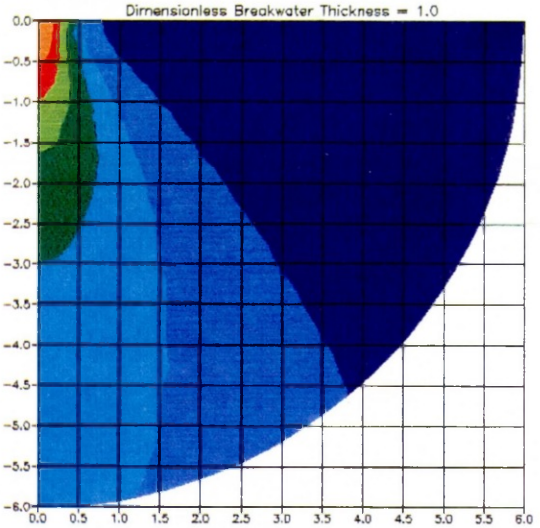

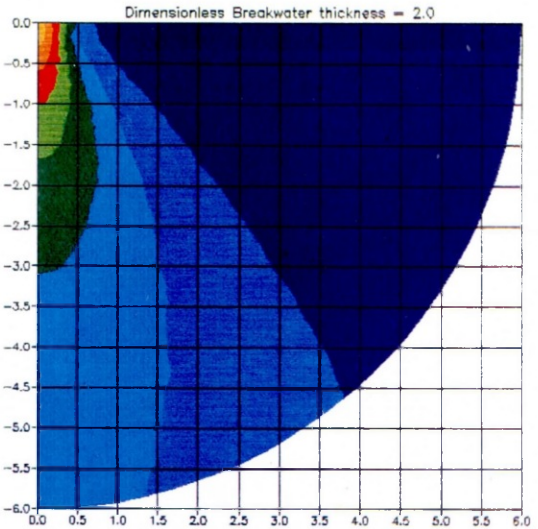

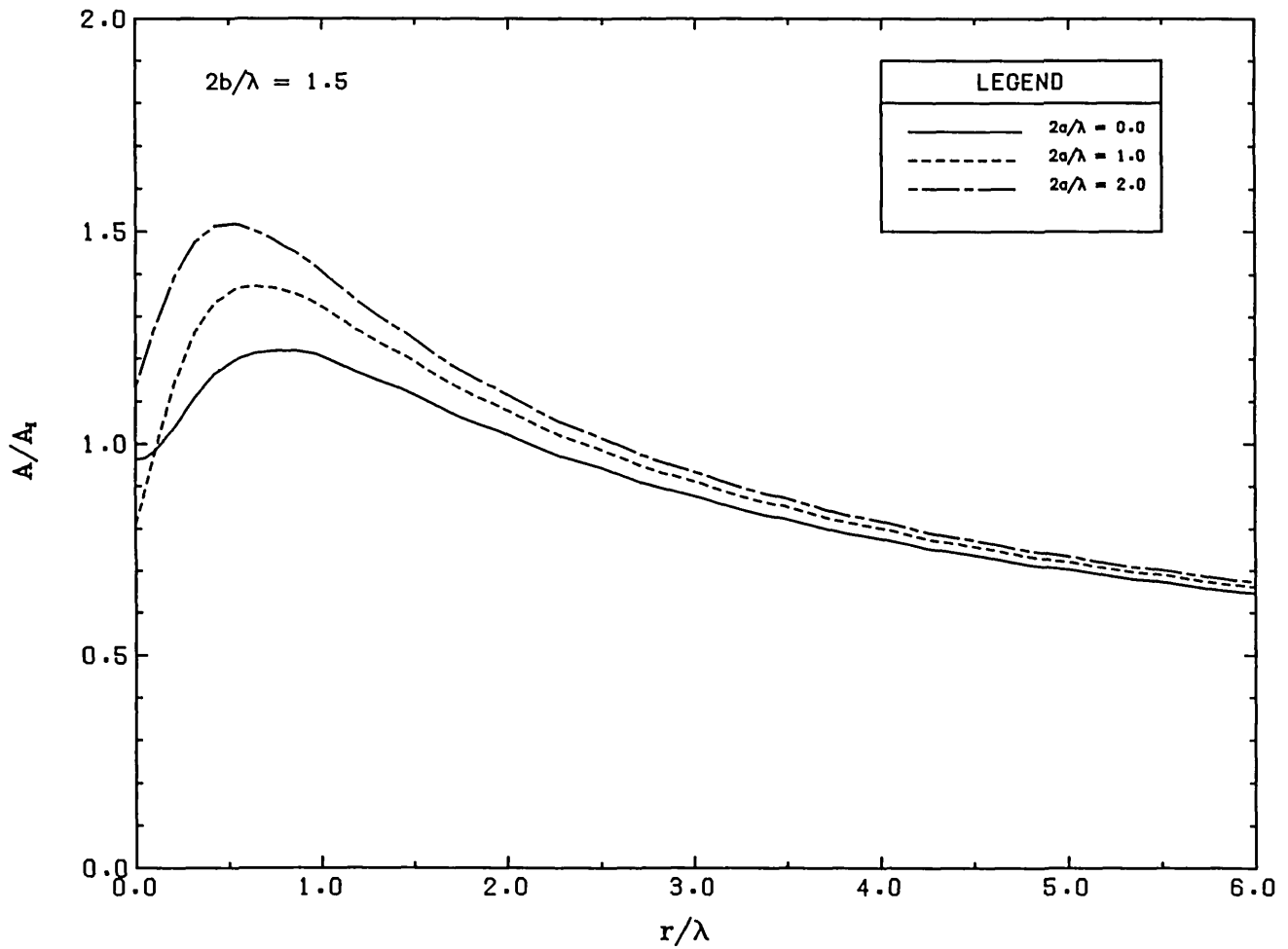

Fig. 5.13a PROFILES ALONG INCIDENT WAVE DIRECTION

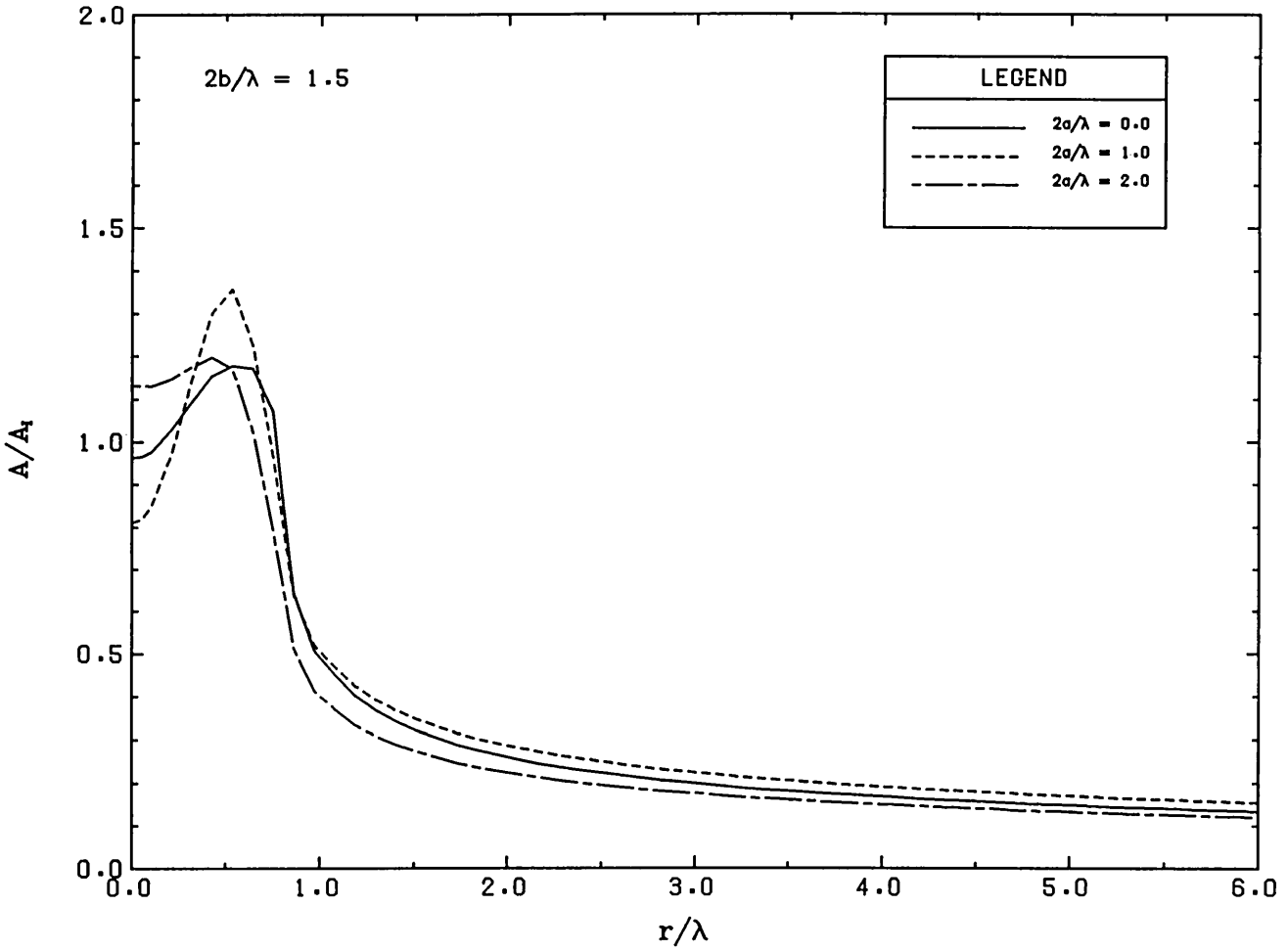

Fig. 5.13b PROFILES ALONG BREAKWATER

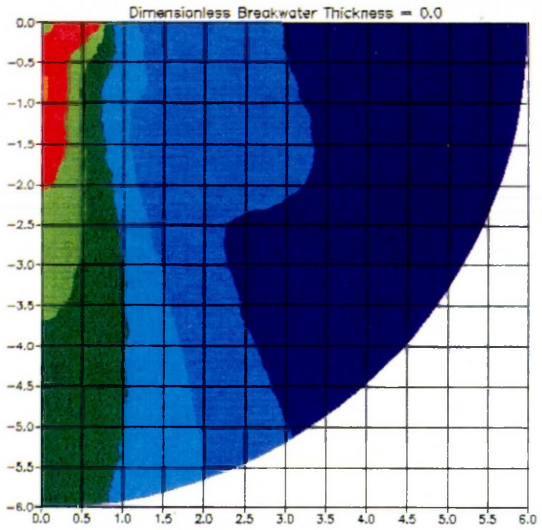

$2b/\lambda = 1.5$

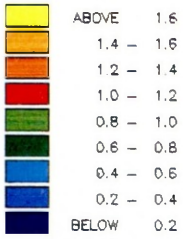

Fig. 5.13 c

Amplitude contours

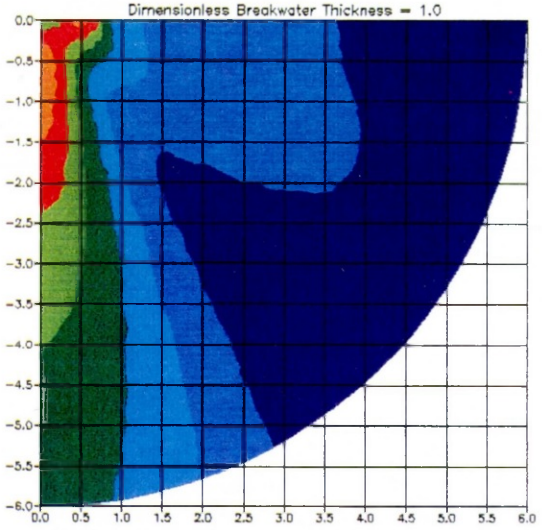

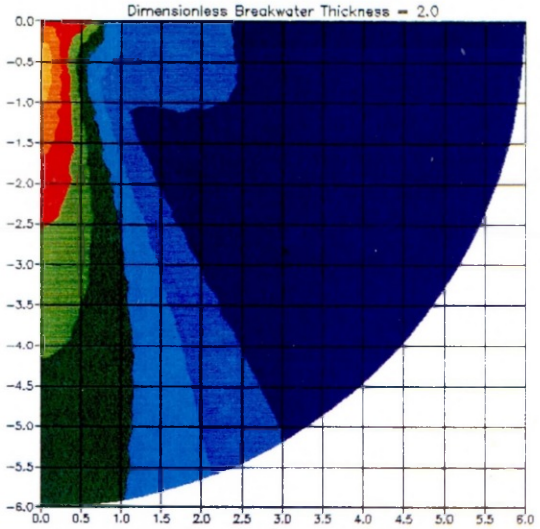

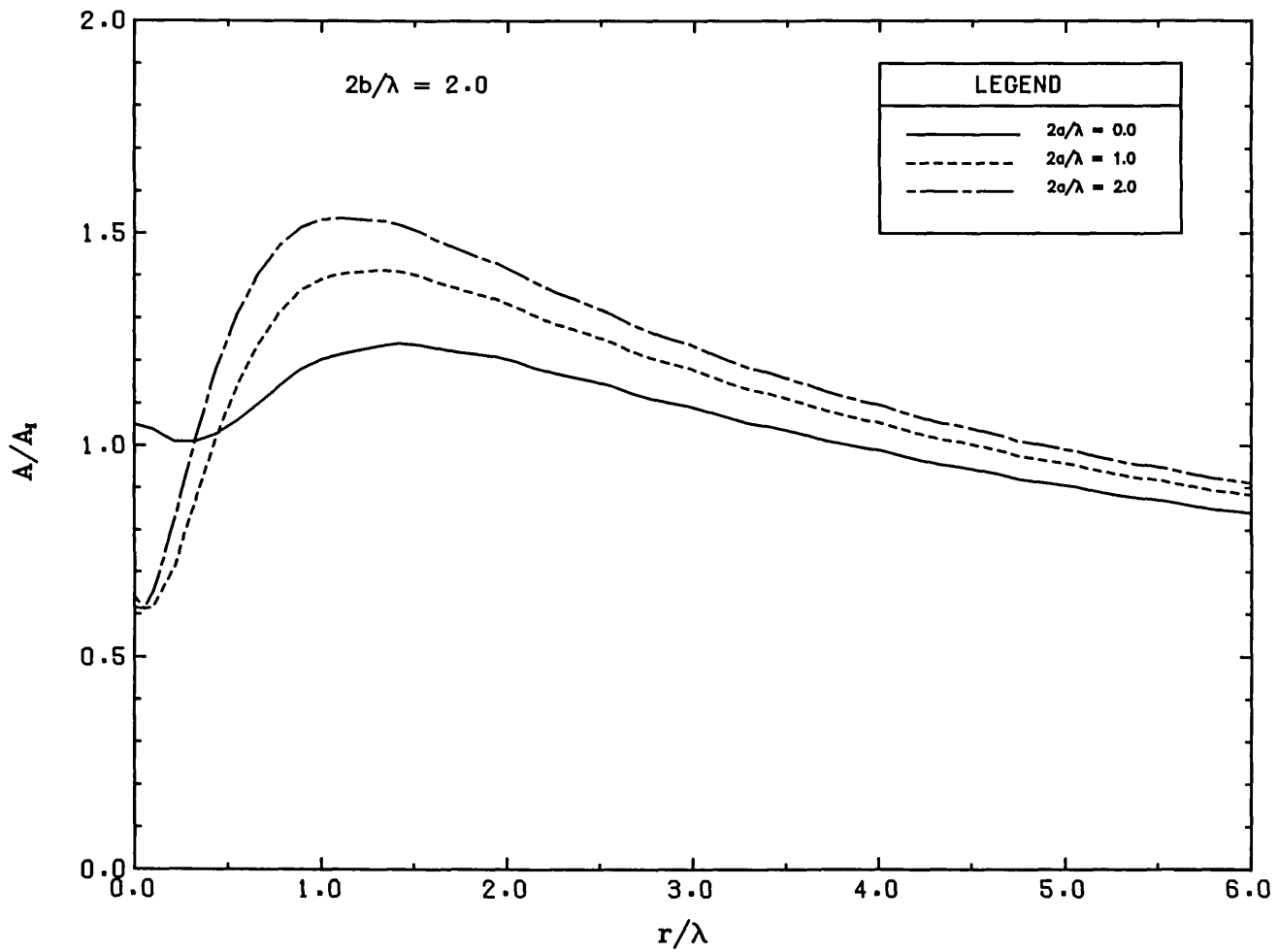

Fig. 5.14a PROFILES ALONG INCIDENT WAVE DIRECTION

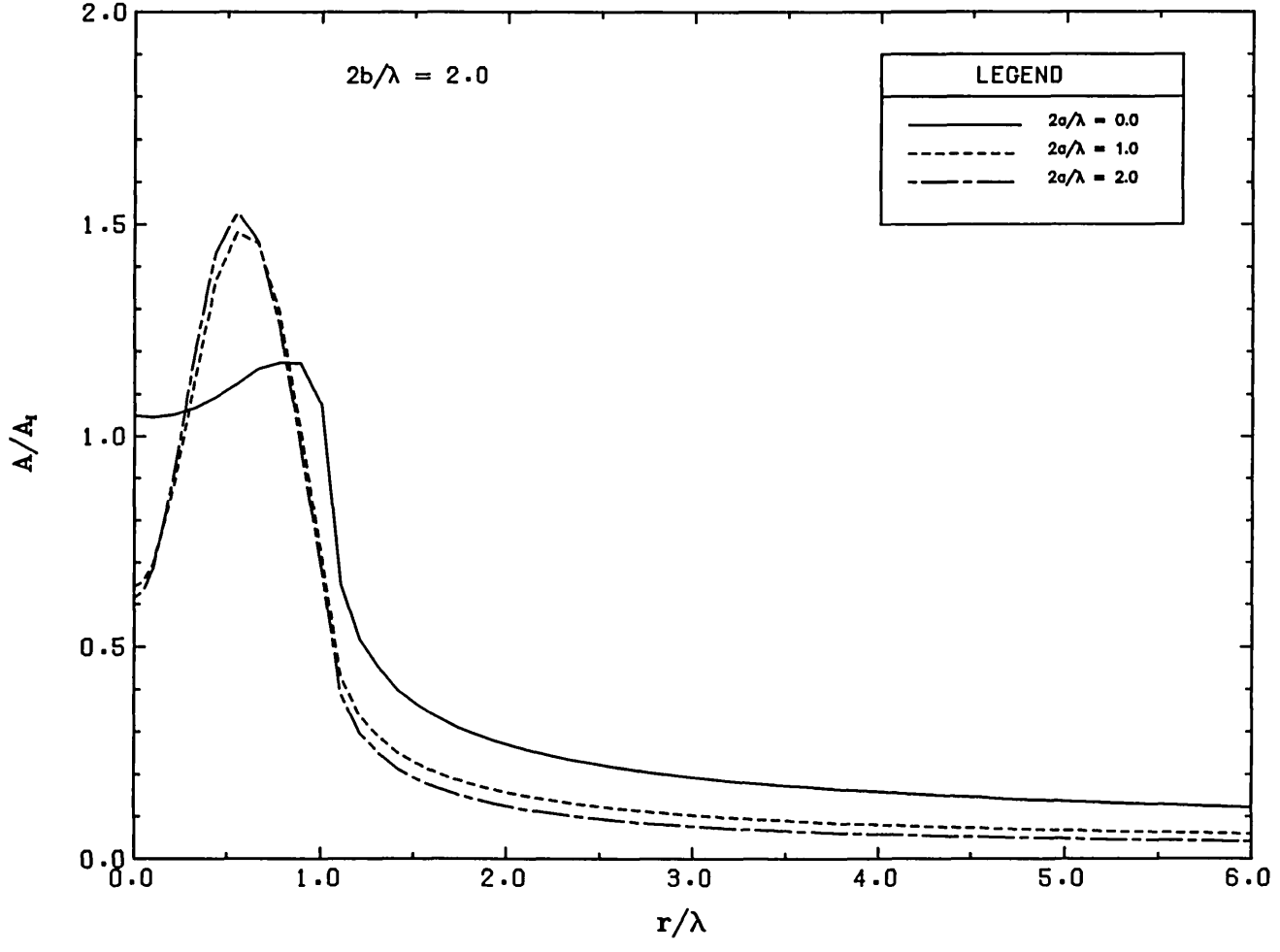

Fig. 5.14b PROFILES ALONG BREAKWATER

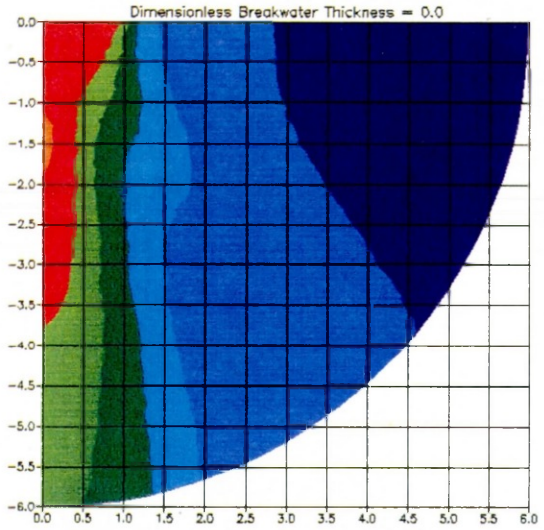

$2b/\lambda = 2.0$

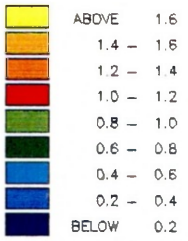

Fig. 5.14 c

Amplitude contours

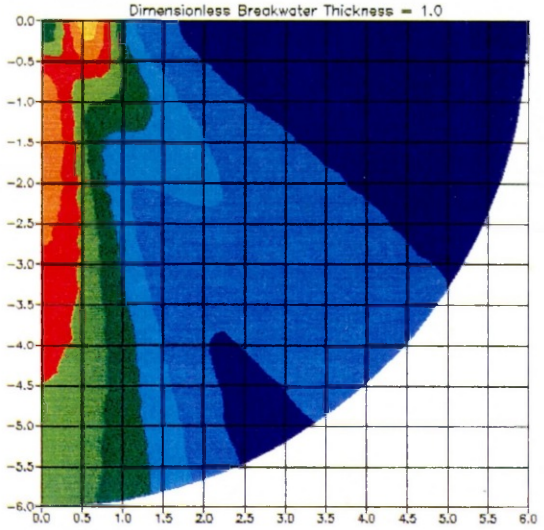

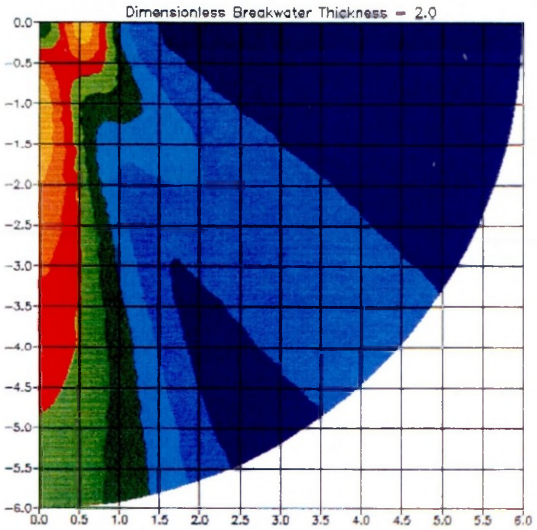

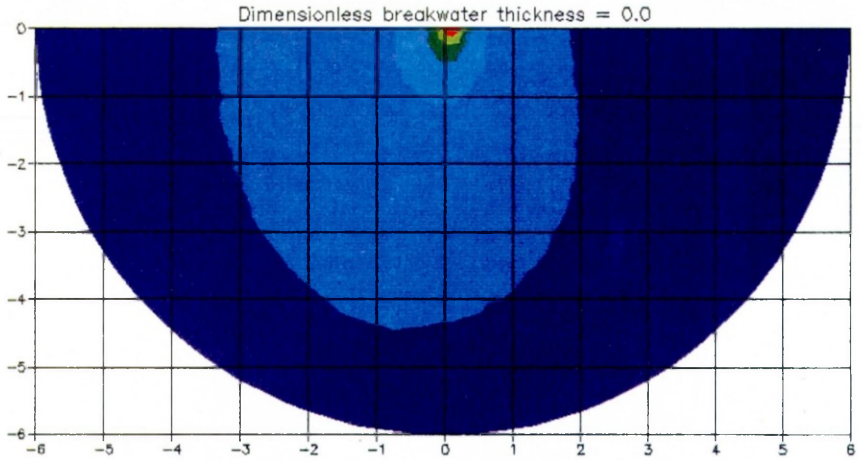

$2b/\lambda = 0.5$, $\theta = 30°$

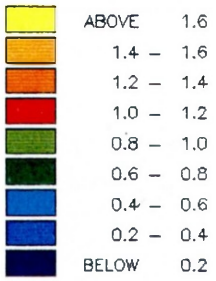

Fig. 5.32

Amplitude contours

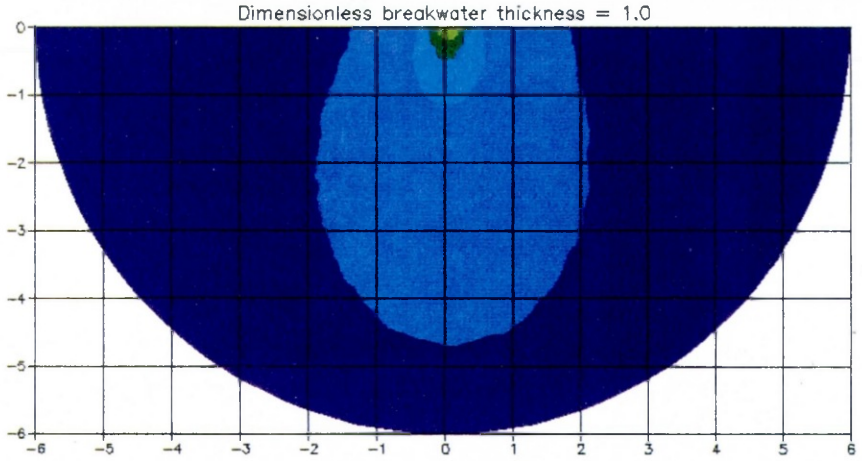

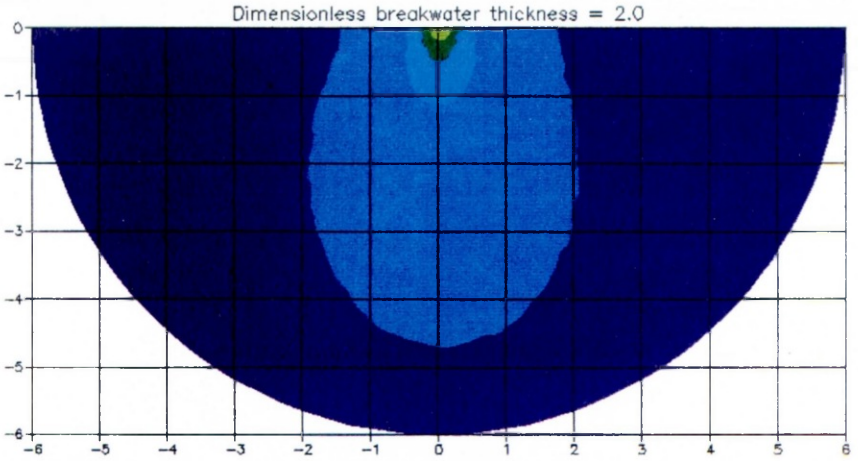

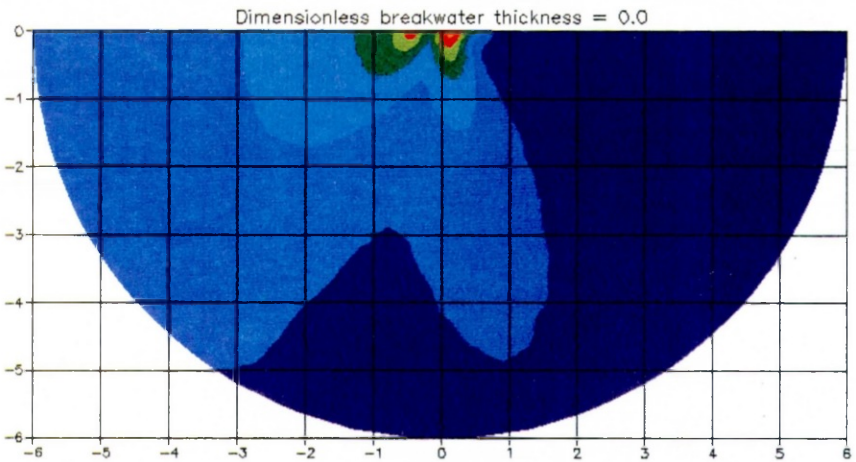

$2b/\lambda = 1.0$, $\theta = 30°$

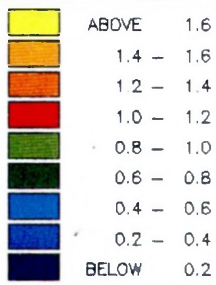

Fig. 5.33

Amplitude contours

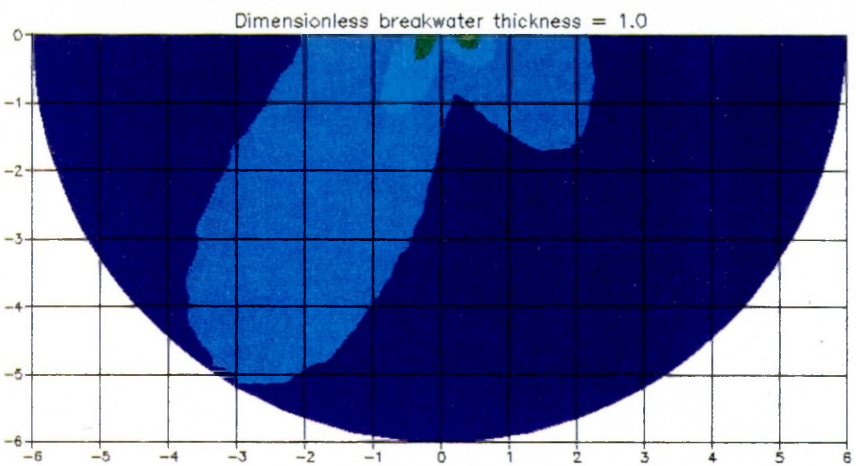

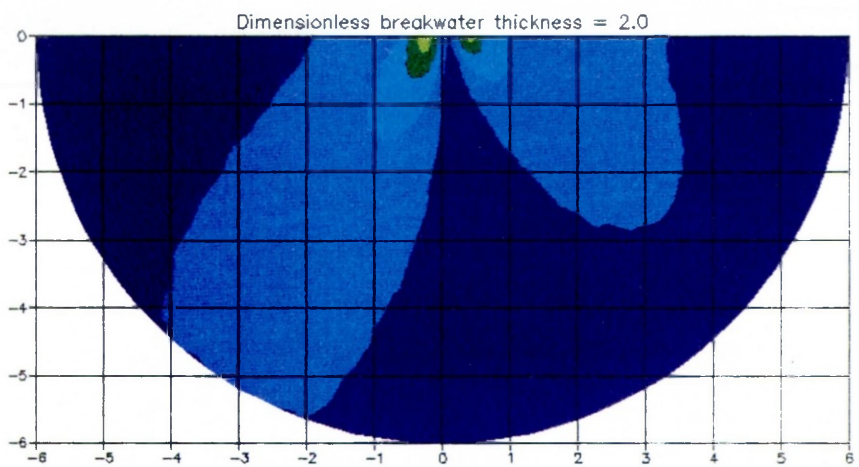

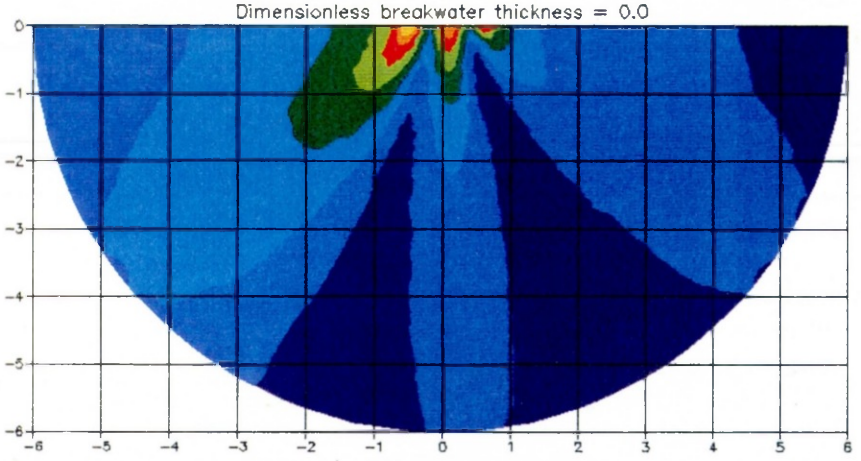

$2b/\lambda = 1.5$, $\theta = 30°$

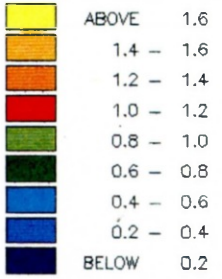

Fig. 5.34

Amplitude contours

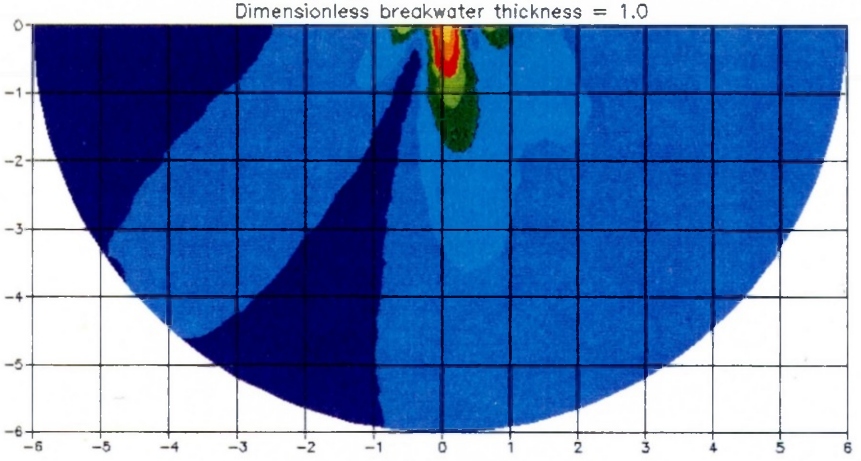

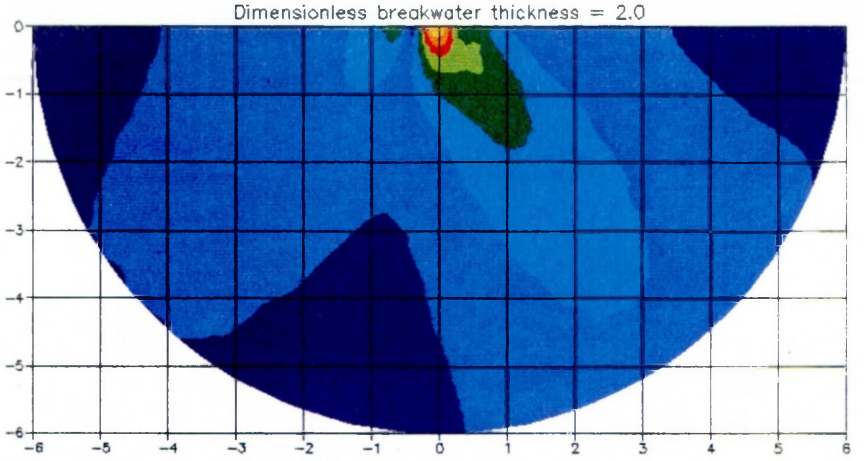

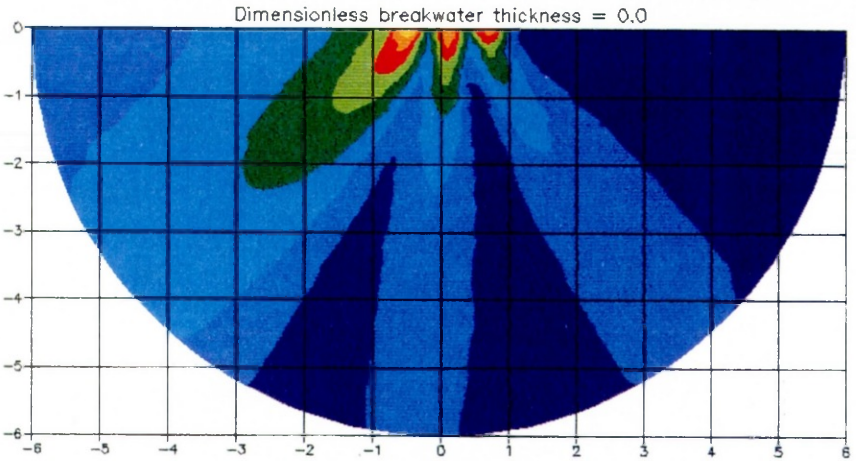

$2b/\lambda = 2.0$, $\theta = 30°$

ABOVE	1.6
1.4 –	1.6
1.2 –	1.4
1.0 –	1.2
0.8 –	1.0
0.6 –	0.8
0.4 –	0.6
0.2 –	0.4
BELOW	0.2

Fig. 5.35

Amplitude contours

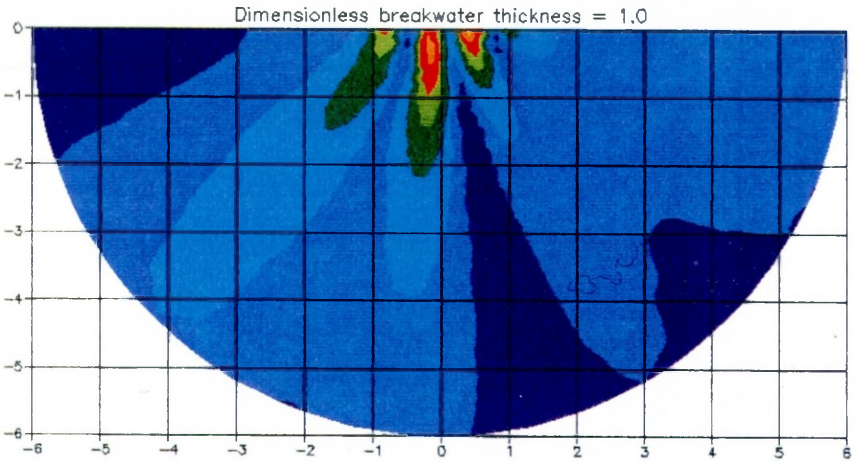

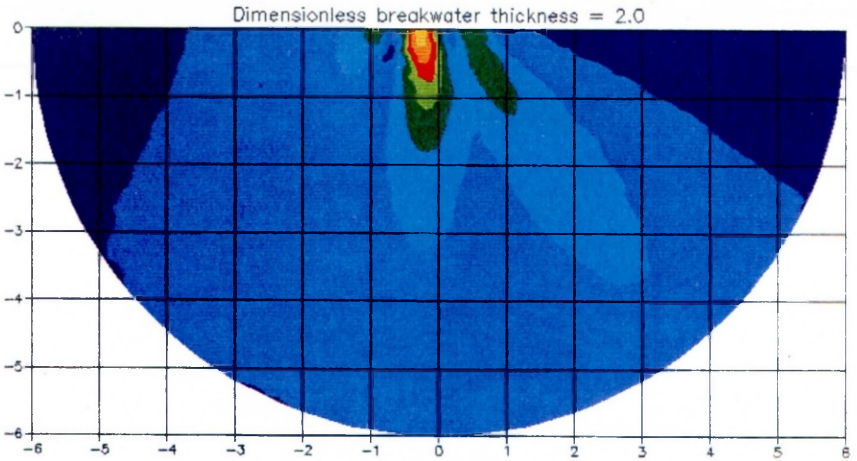

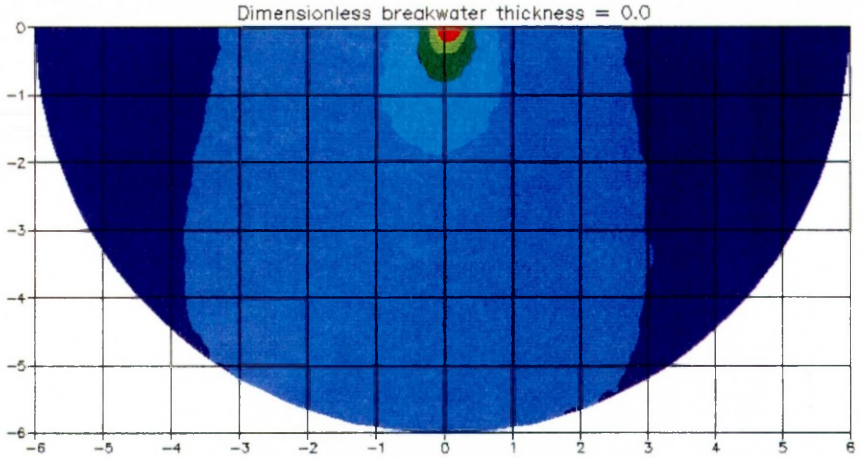

$2b/\lambda = 0.5$, $\theta = 60°$

ABOVE	1.6
1.4 –	1.6
1.2 –	1.4
1.0 –	1.2
0.8 –	1.0
0.6 –	0.8
0.4 –	0.6
0.2 –	0.4
BELOW	0.2

Fig. 5.36

Amplitude contours

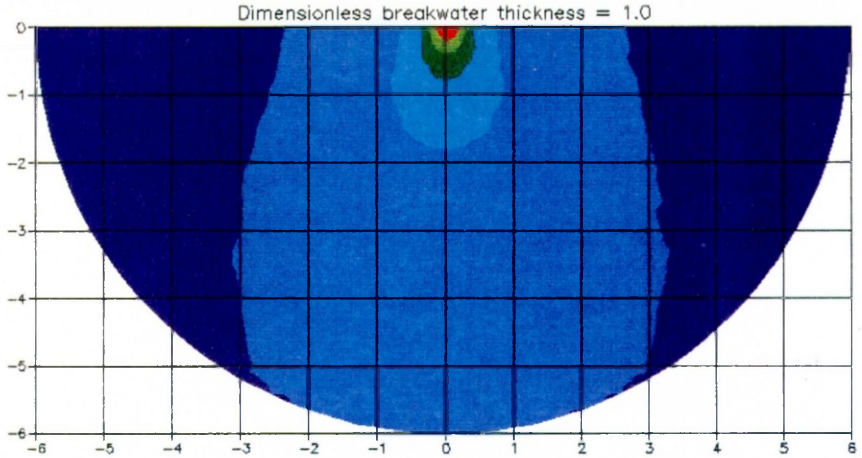

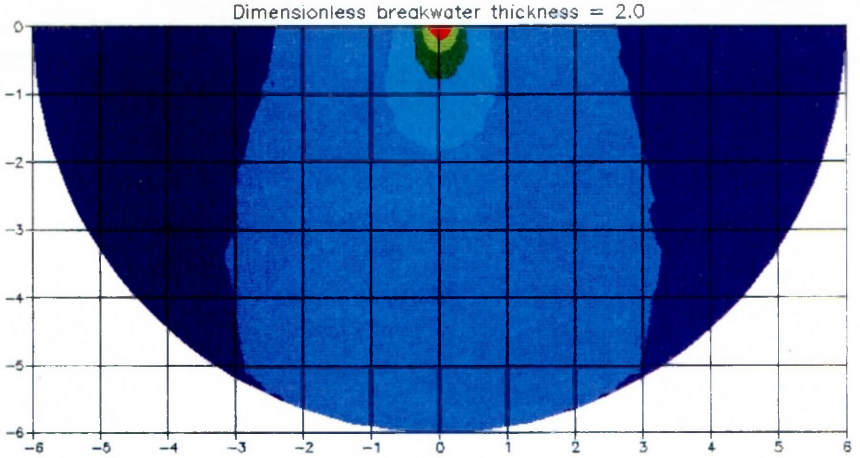

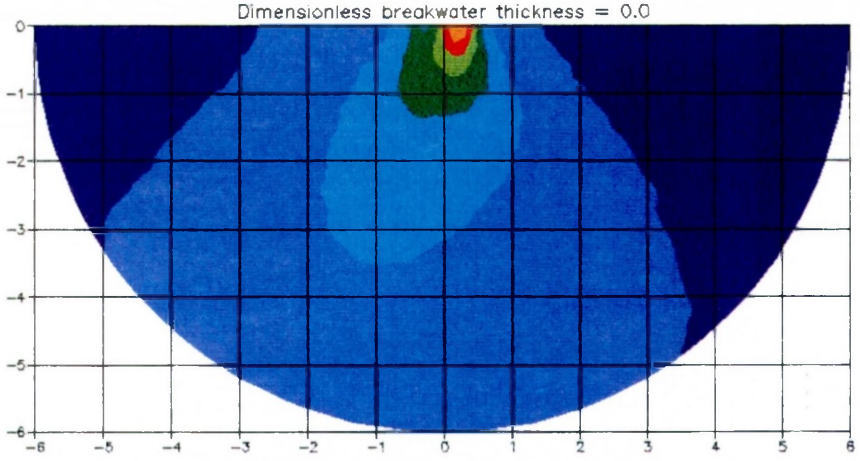

$2b/\lambda = 1.0$, $\theta = 60°$

ABOVE 1.6
1.4 – 1.6
1.2 – 1.4
1.0 – 1.2
0.8 – 1.0
0.6 – 0.8
0.4 – 0.6
0.2 – 0.4
BELOW 0.2

Fig. 5.37

Amplitude contours

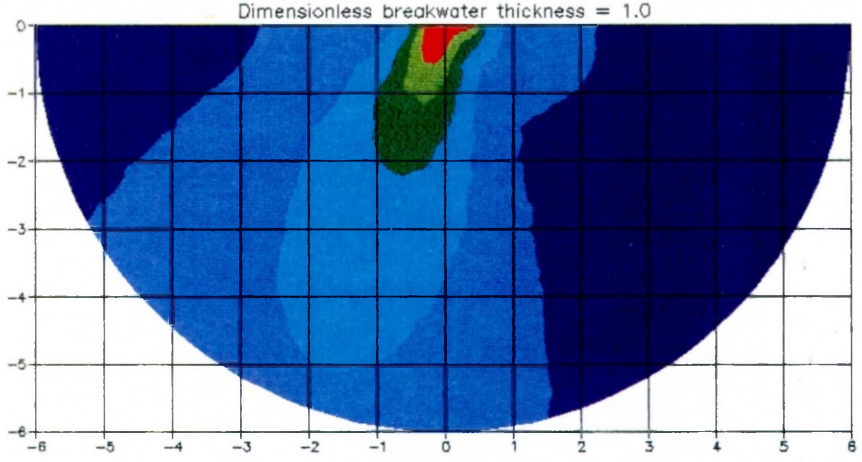

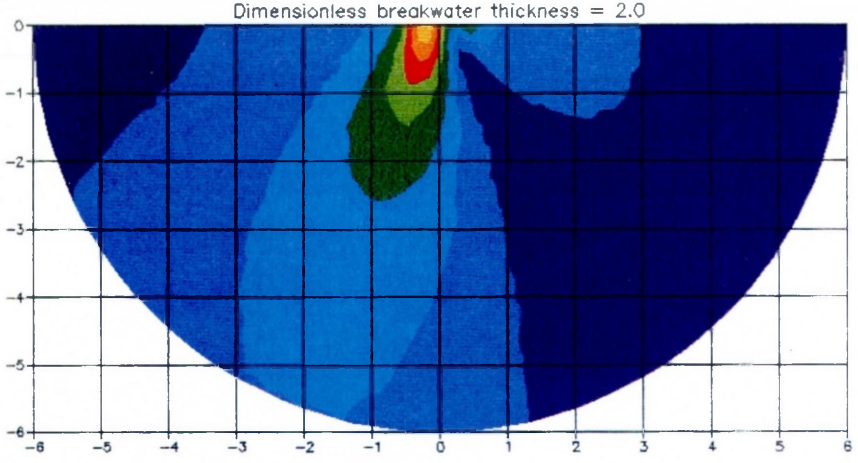

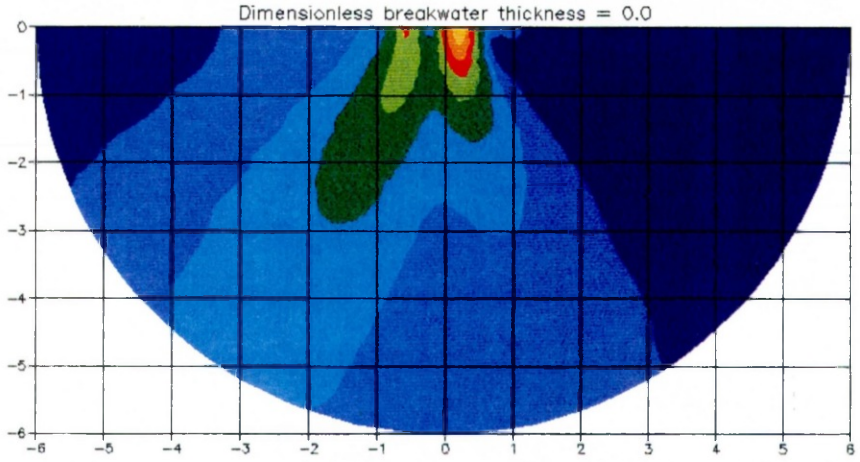

$2b/\lambda = 1.5$, $\theta = 60°$

ABOVE	1.6
1.4 –	1.6
1.2 –	1.4
1.0 –	1.2
0.8 –	1.0
0.6 –	0.8
0.4 –	0.6
0.2 –	0.4
BELOW	0.2

Fig . 5.38

Amplitude contours

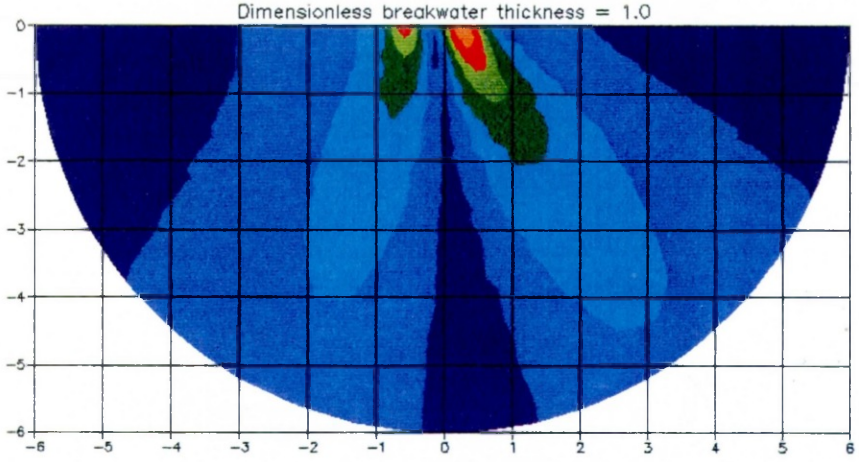

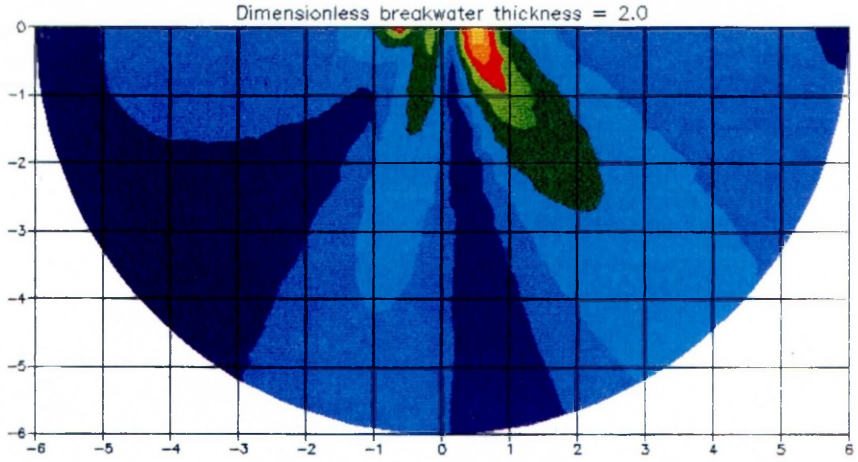

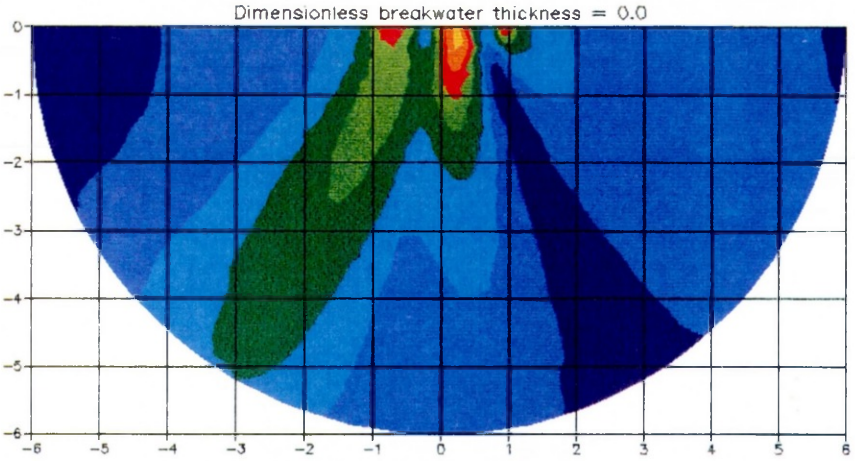

$2b/\lambda = 2.0$, $\theta = 60°$

ABOVE	1.6
1.4 –	1.6
1.2 –	1.4
1.0 –	1.2
0.8 –	1.0
0.6 –	0.8
0.4 –	0.6
0.2 –	0.4
BELOW	0.2

Fig. 5.39

Amplitude contours

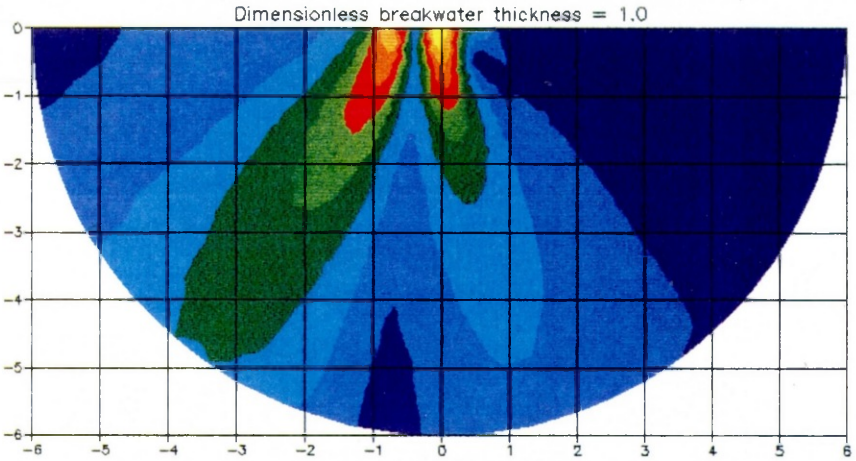

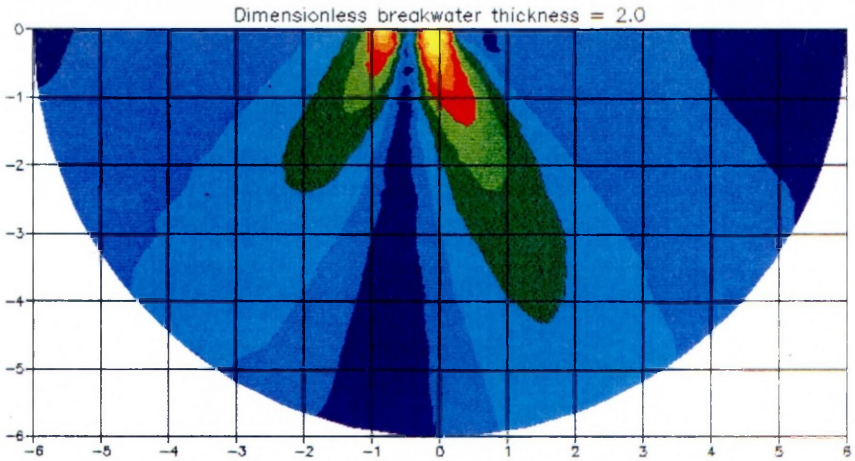

RESONATORS

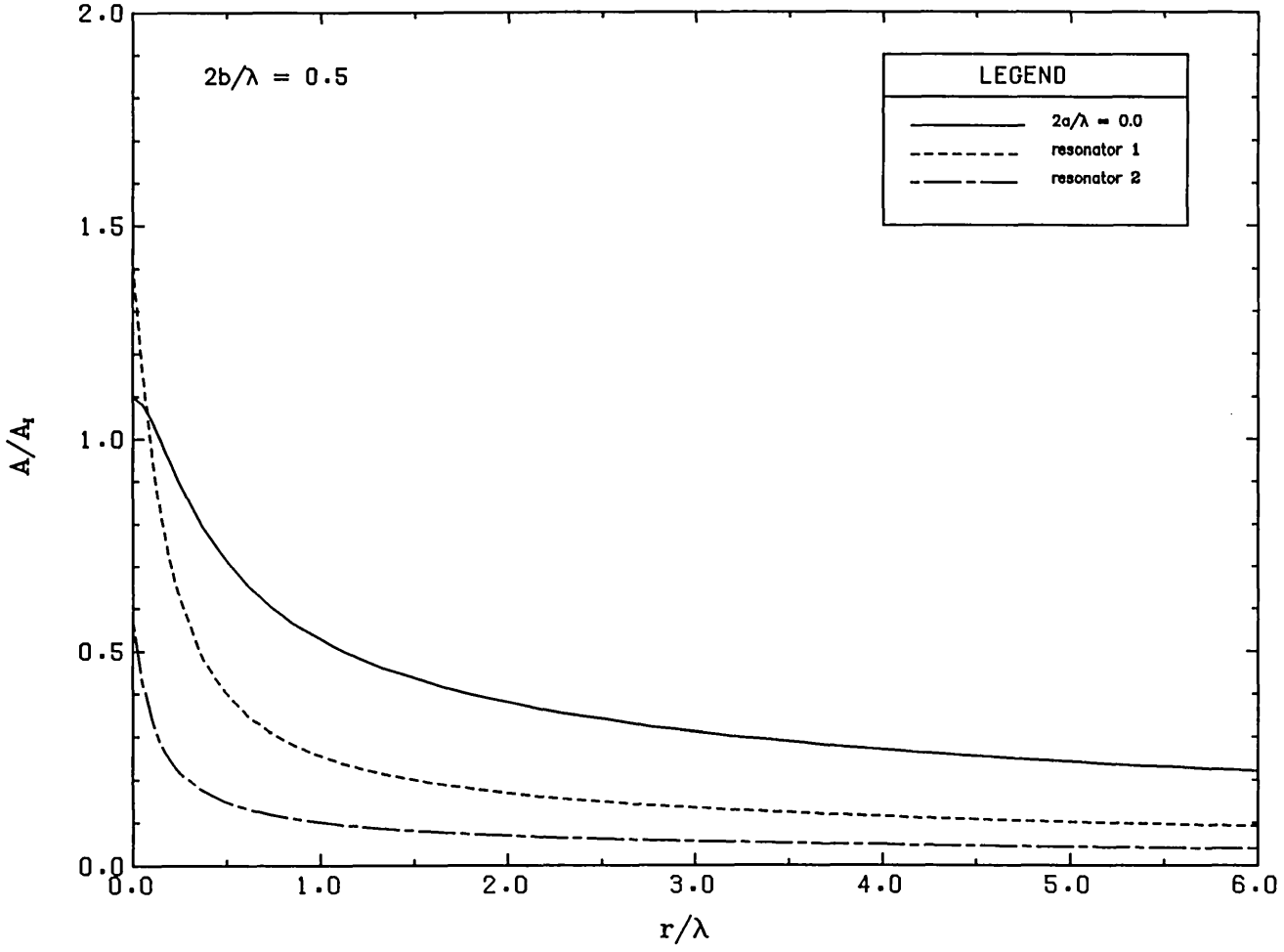

Fig. 5.15a PROFILES ALONG INCIDENT WAVE DIRECTION

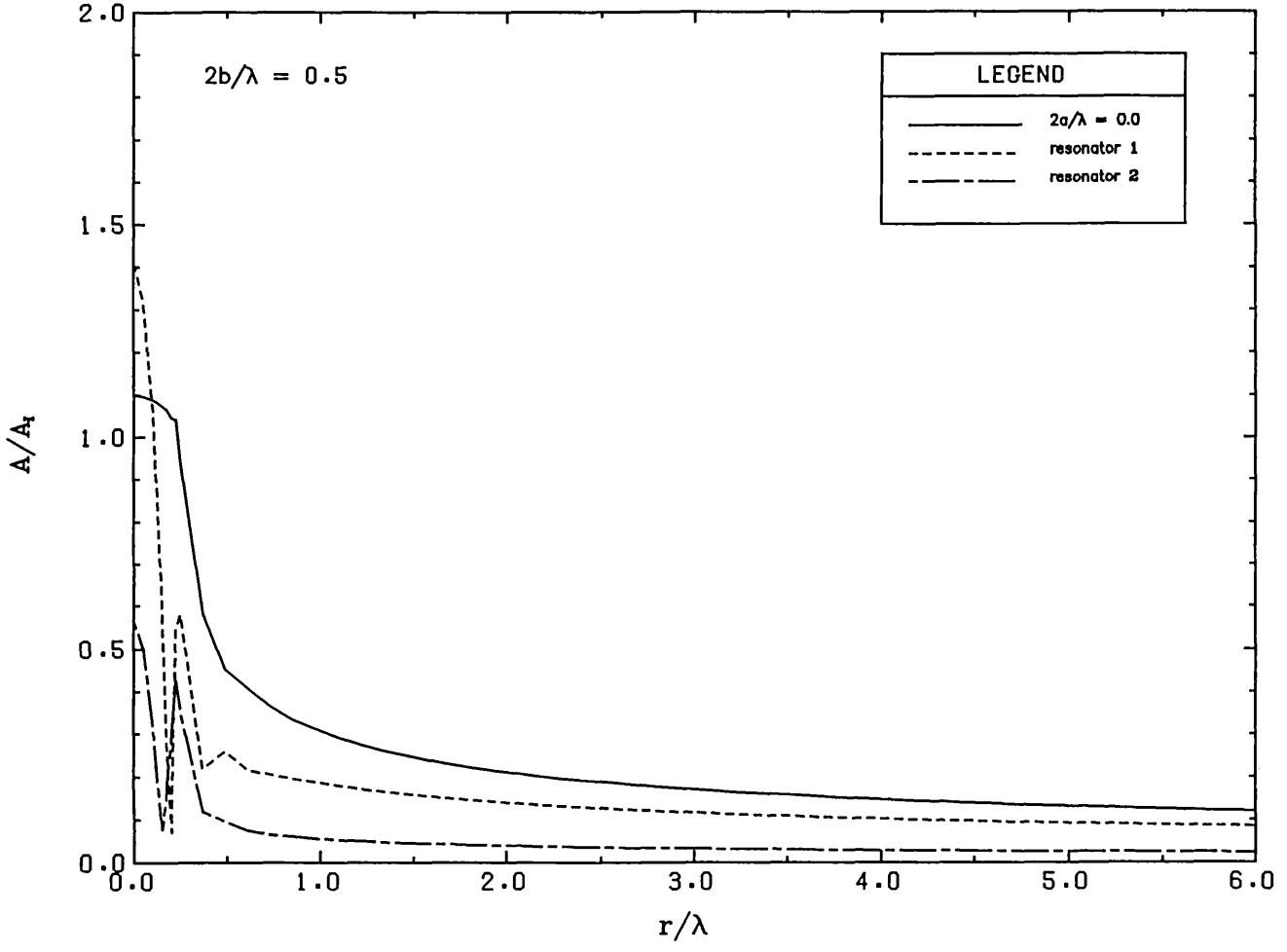

Fig. 5.15b PROFILES ALONG BREAKWATER

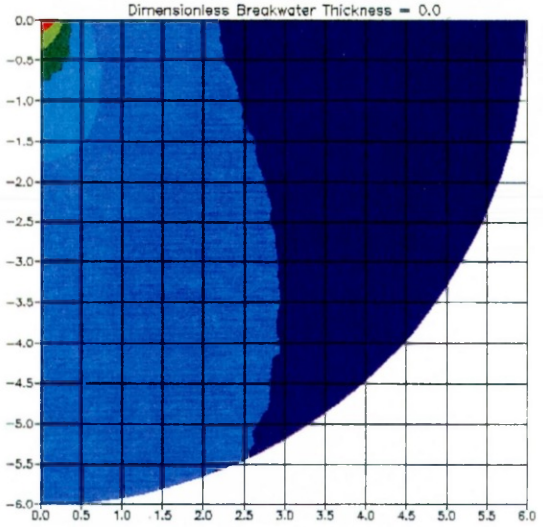

$2b/\lambda = 0.5$

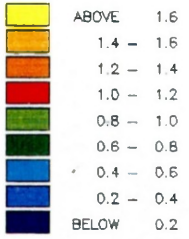

Fig. 5.15 c

Amplitude contours

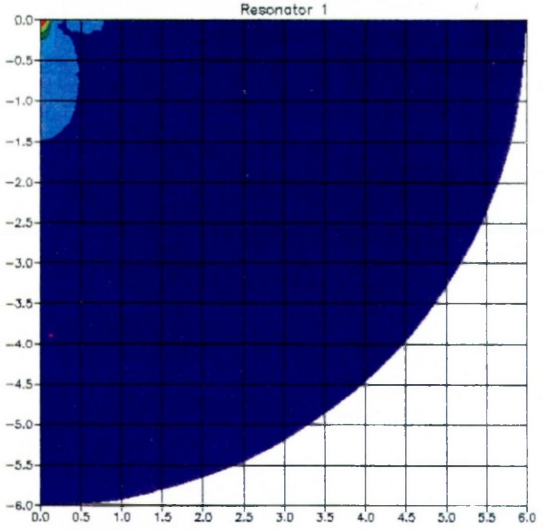

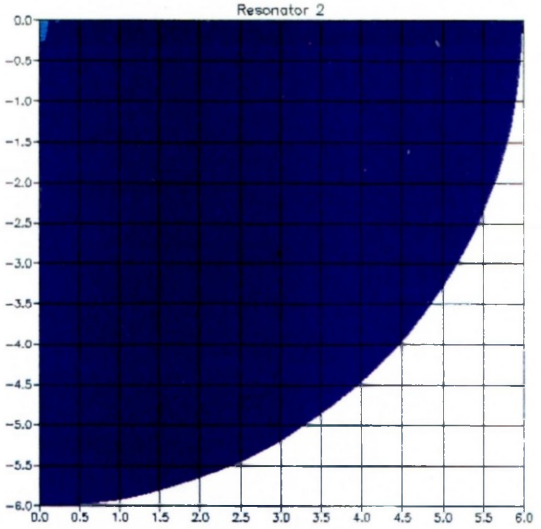

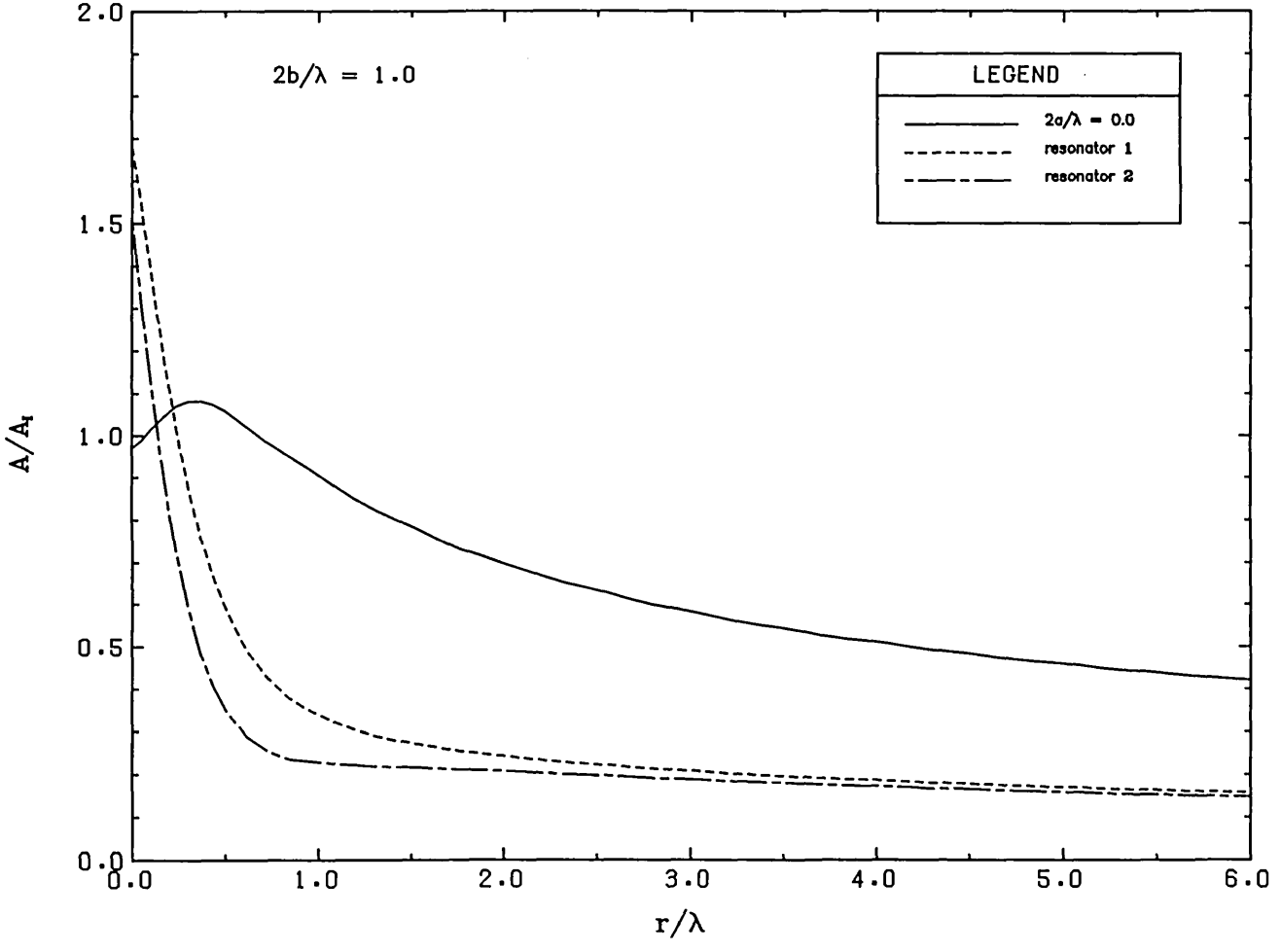

Fig. 5.16a PROFILES ALONG INCIDENT WAVE DIRECTION

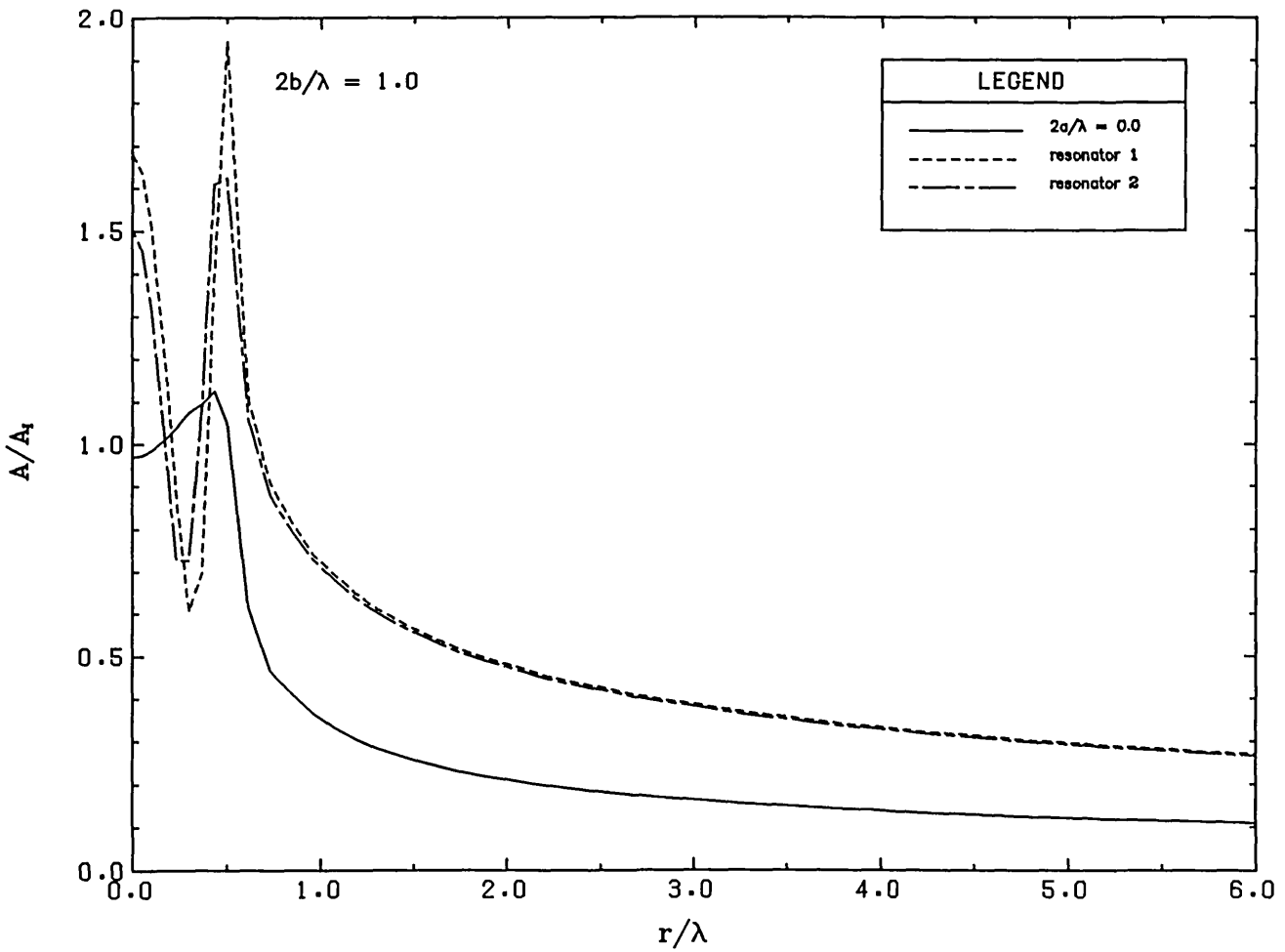

Fig. 5.16b PROFILES ALONG BREAKWATER

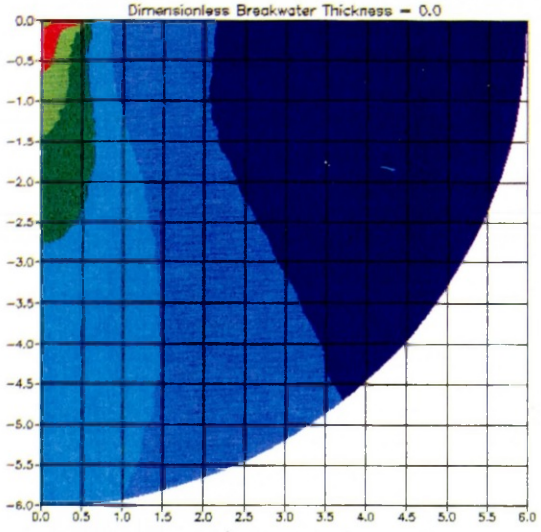

$2b/\lambda = 1.0$

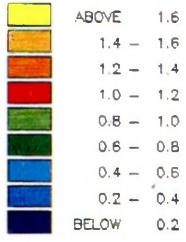

Fig. 5.16c

Amplitude contours

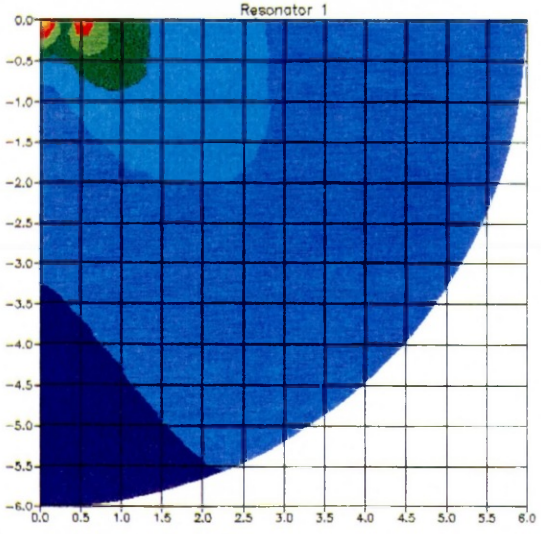

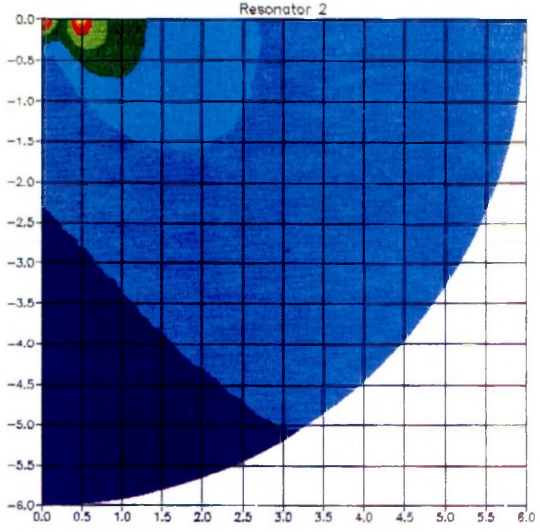

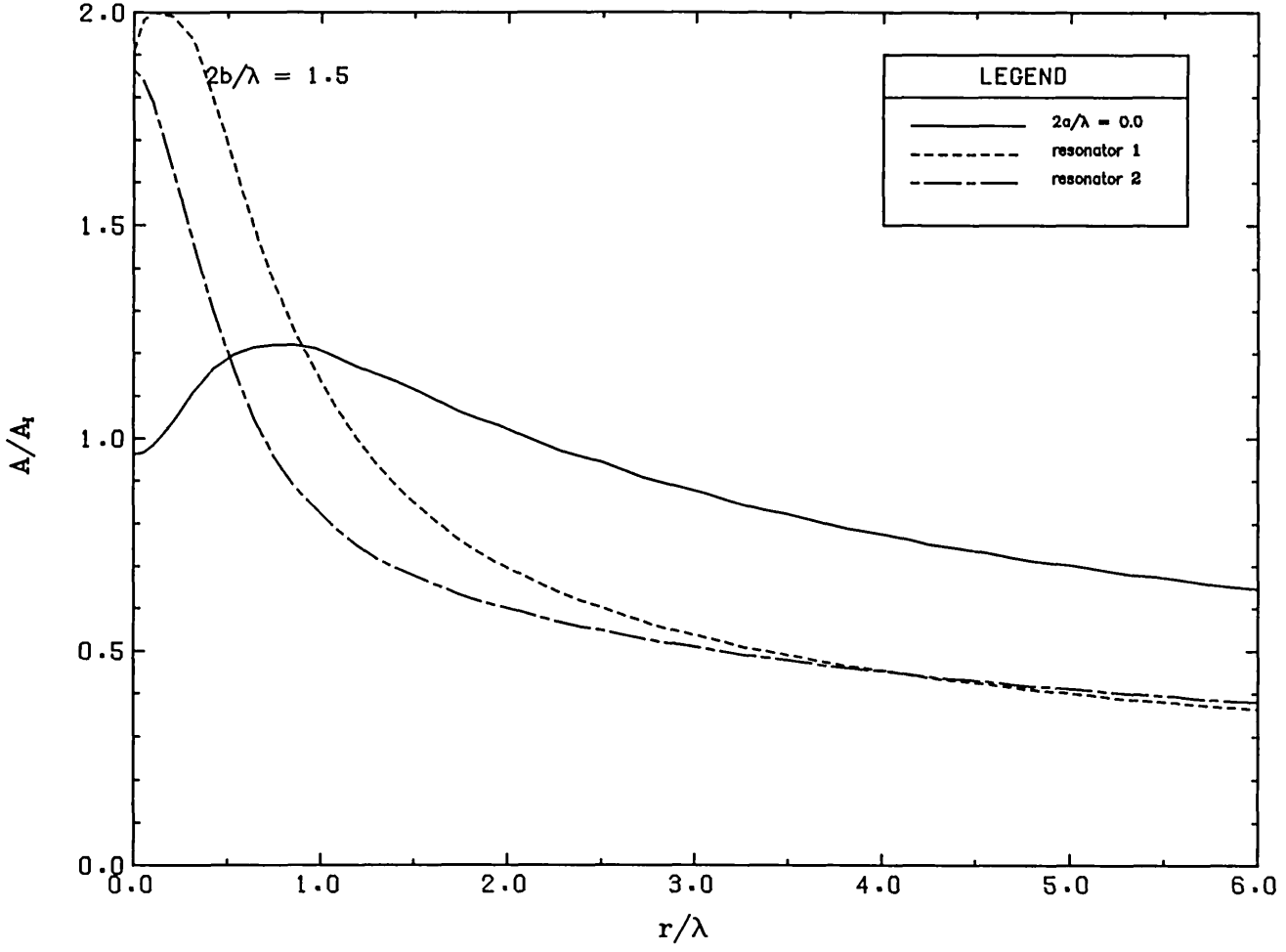

Fig. 5.17a PROFILES ALONG INCIDENT WAVE DIRECTION

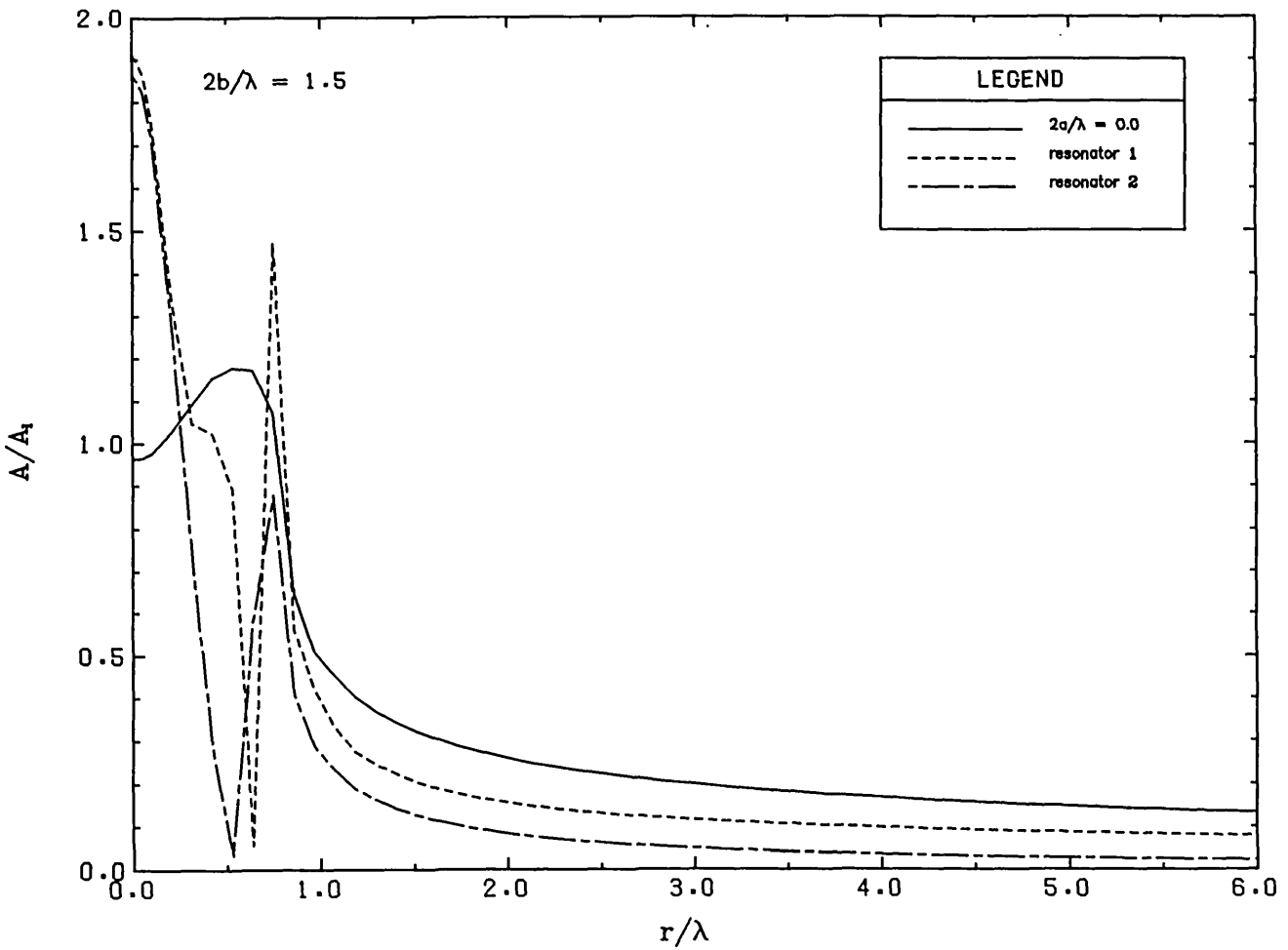

Fig. 5.17b PROFILES ALONG BREAKWATER

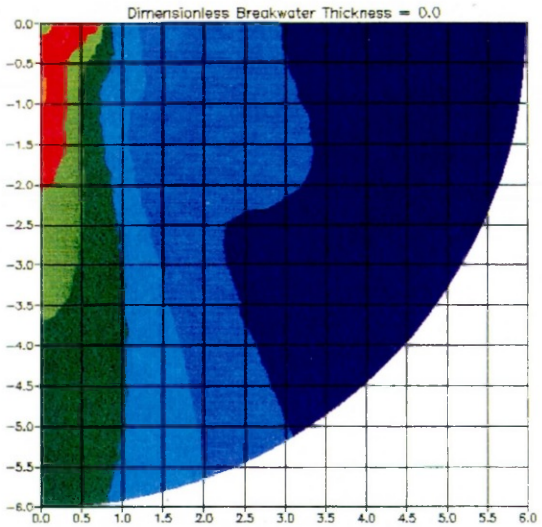

$2b/\lambda = 1.5$

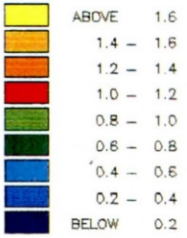

Fig. 5.17 c

Amplitude contours

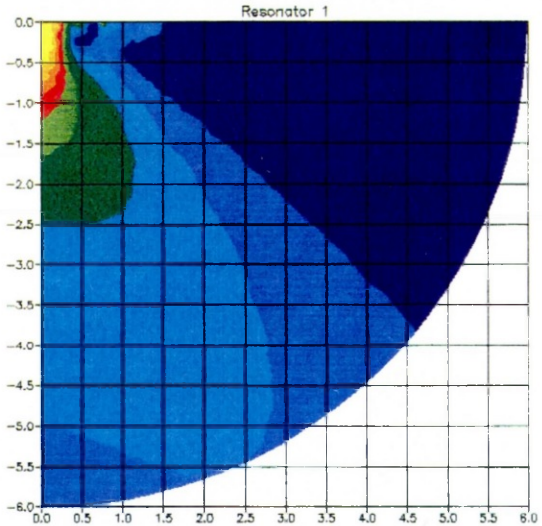

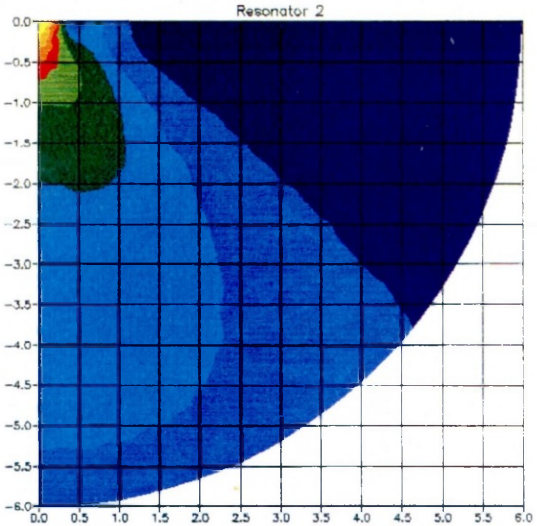

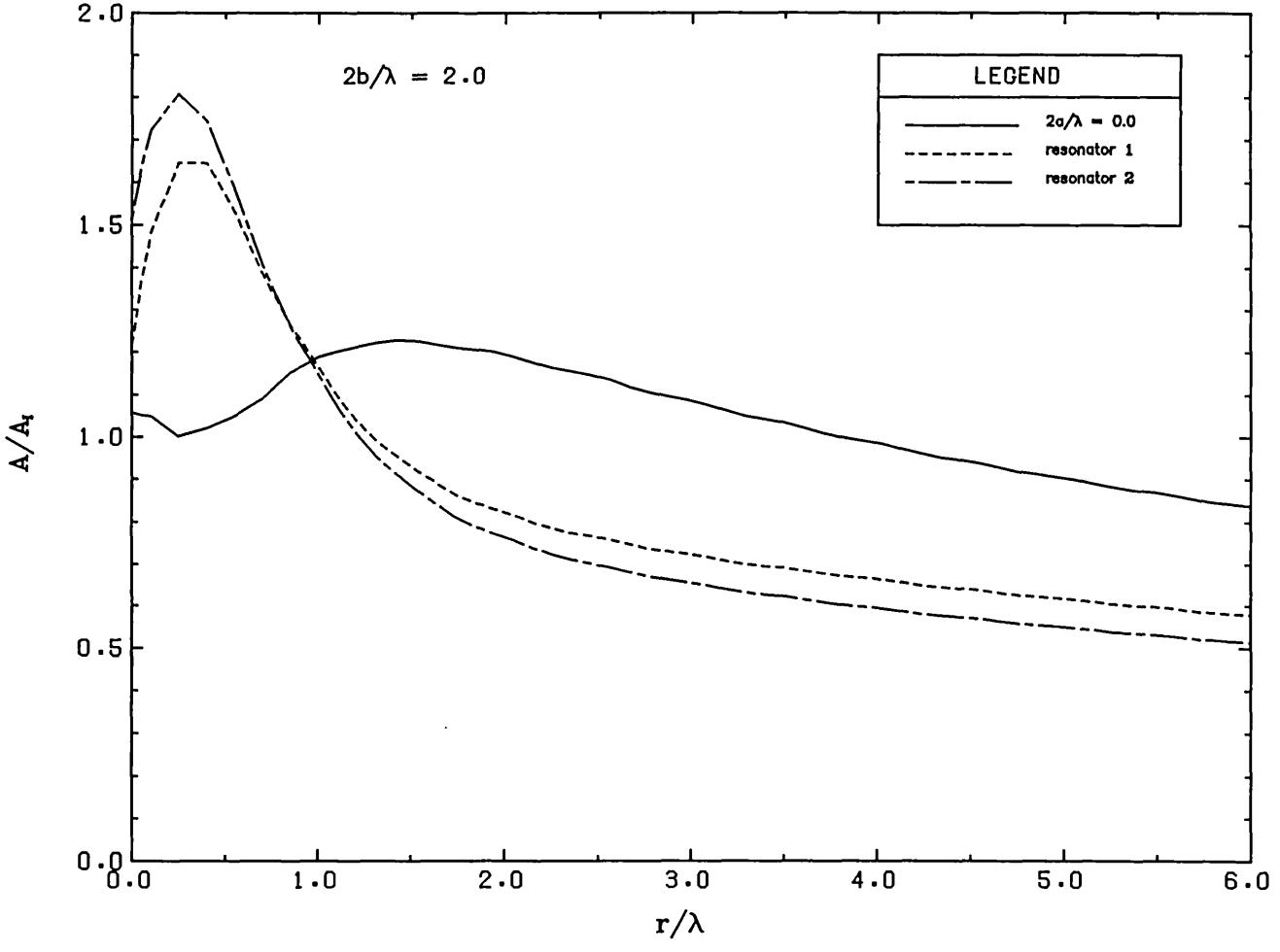

Fig. 5.18a PROFILES ALONG INCIDENT WAVE DIRECTION

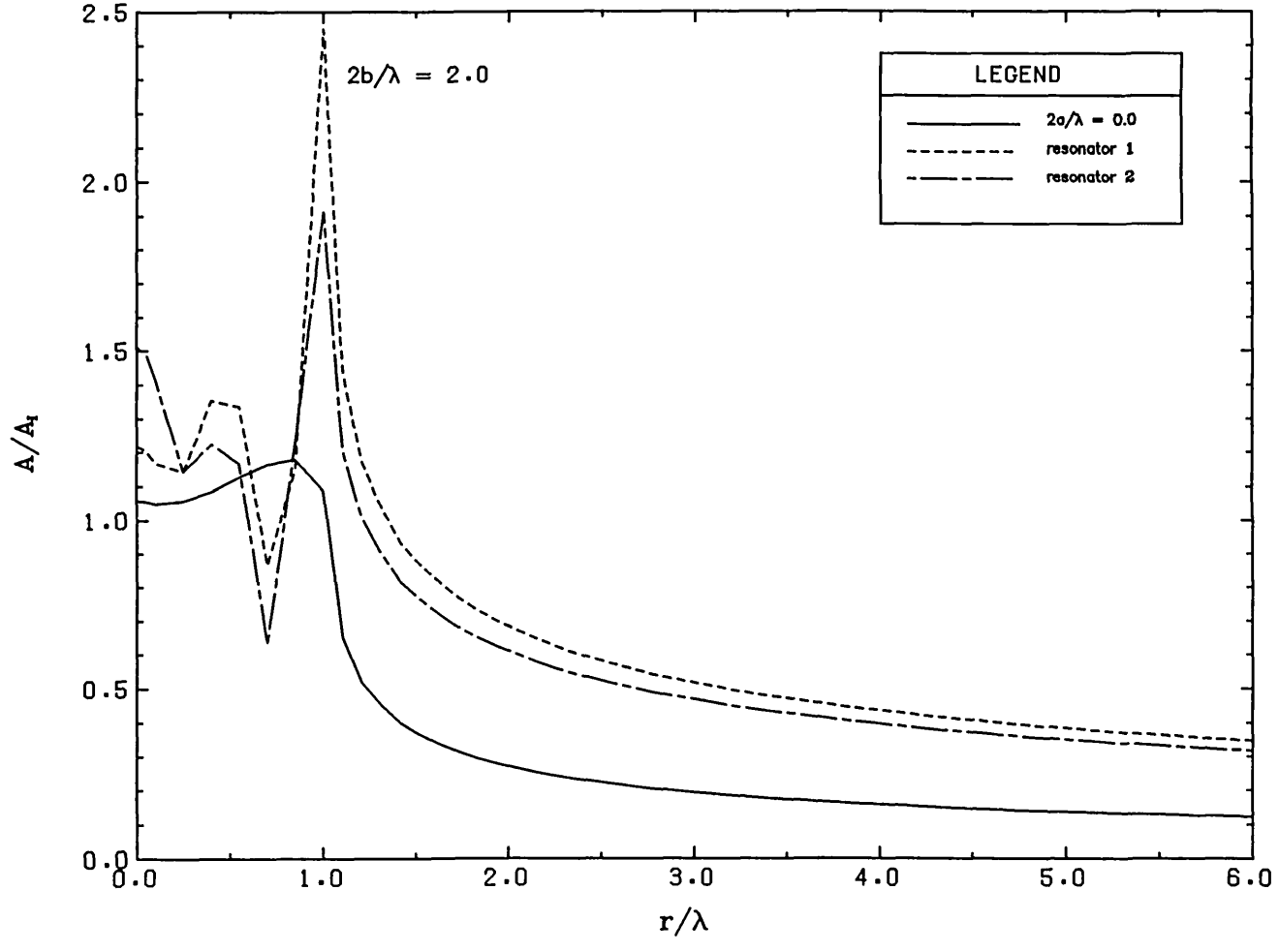

Fig. 5.18b PROFILES ALONG BREAKWATER

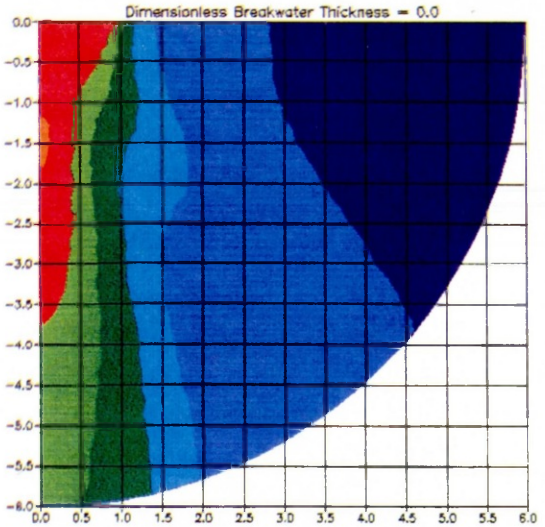

$2b/\lambda = 2.0$

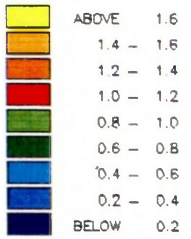

Fig. 5.18c

Amplitude contours

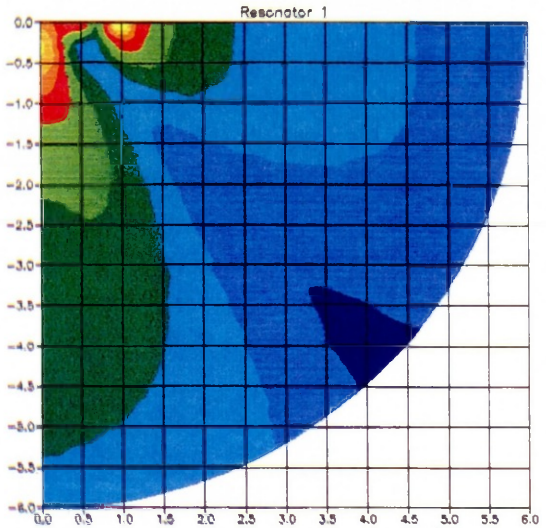

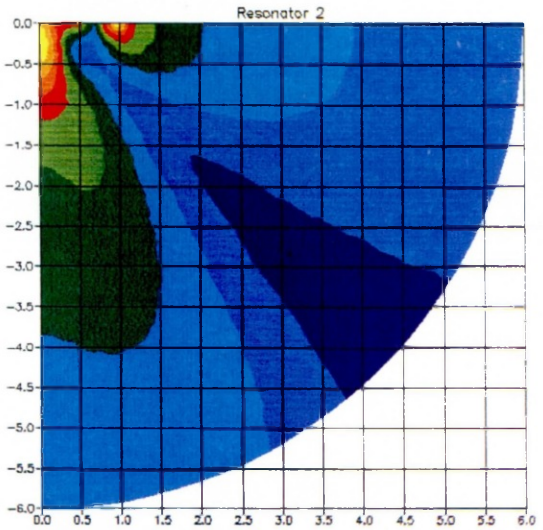

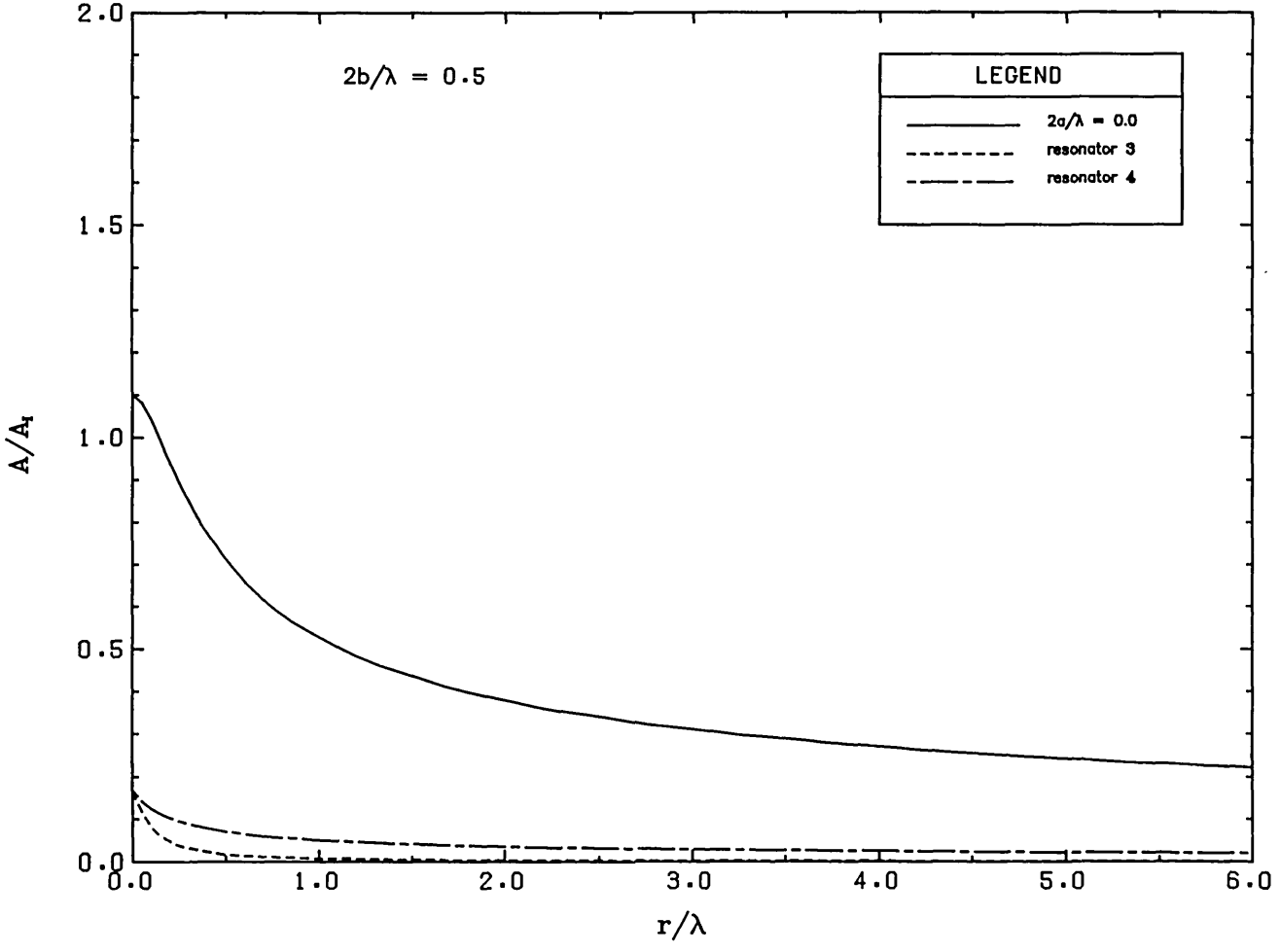

Fig. 5.19a PROFILES ALONG INCIDENT WAVE DIRECTION

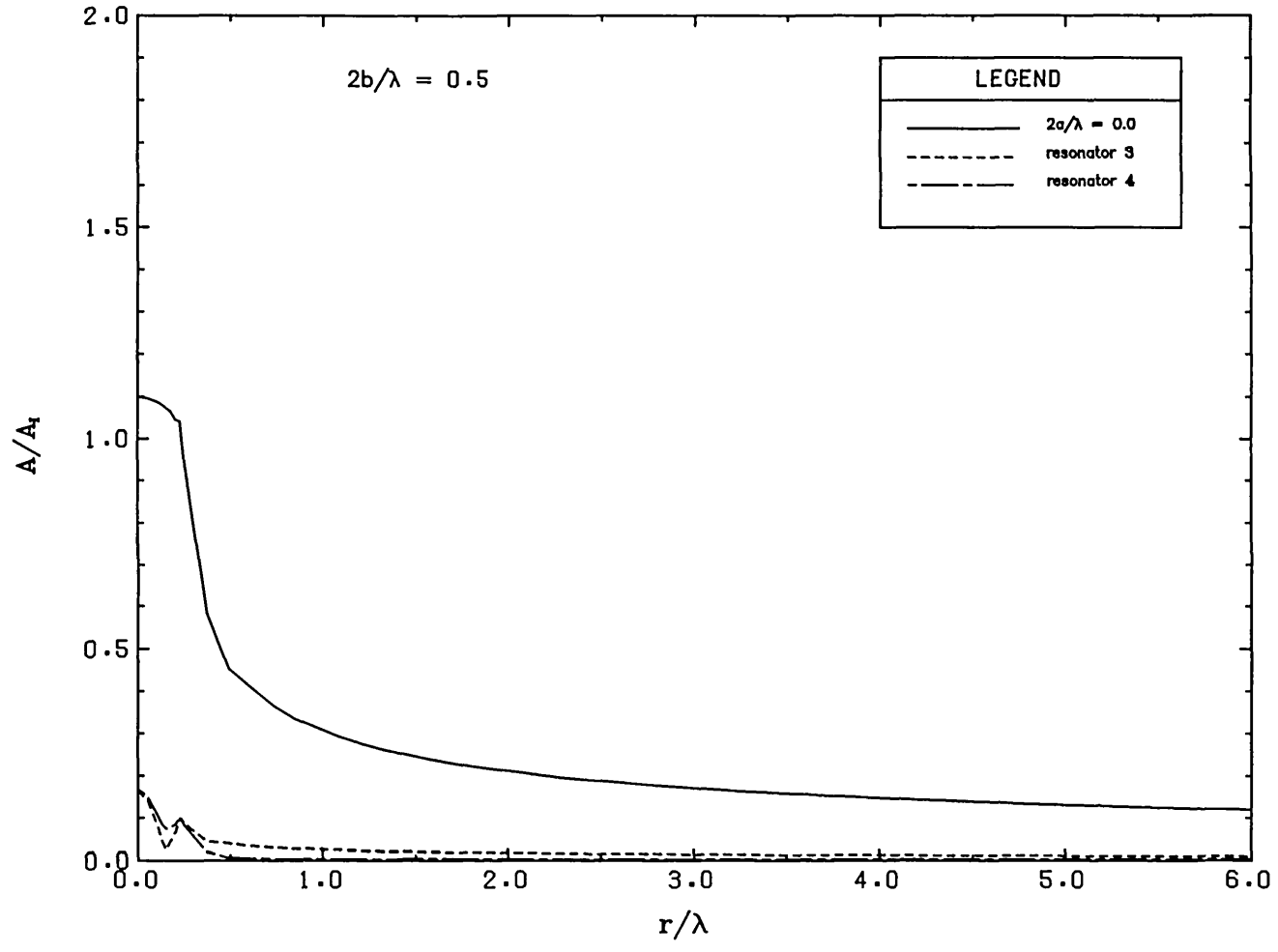

Fig. 5.19b PROFILES ALONG BREAKWATER

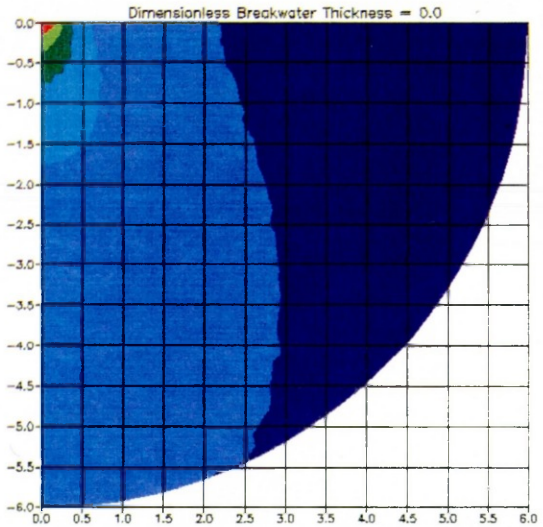

$2b/\lambda = 0.5$

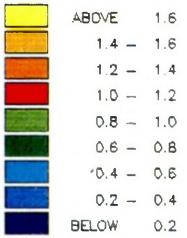

Fig. 5.19 c

Amplitude contours

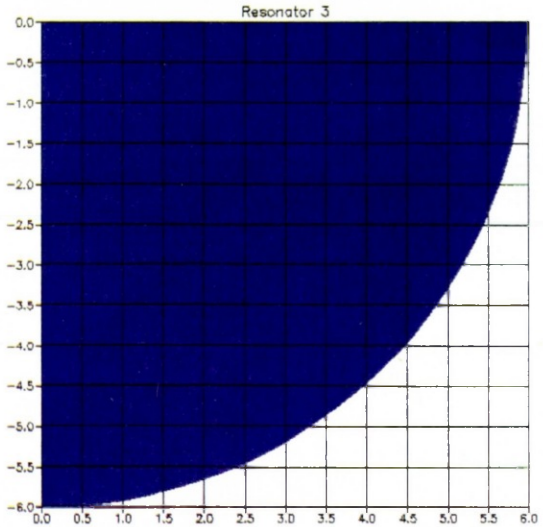

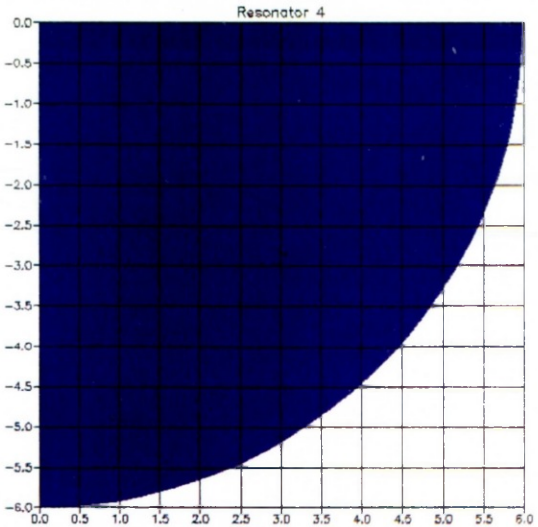

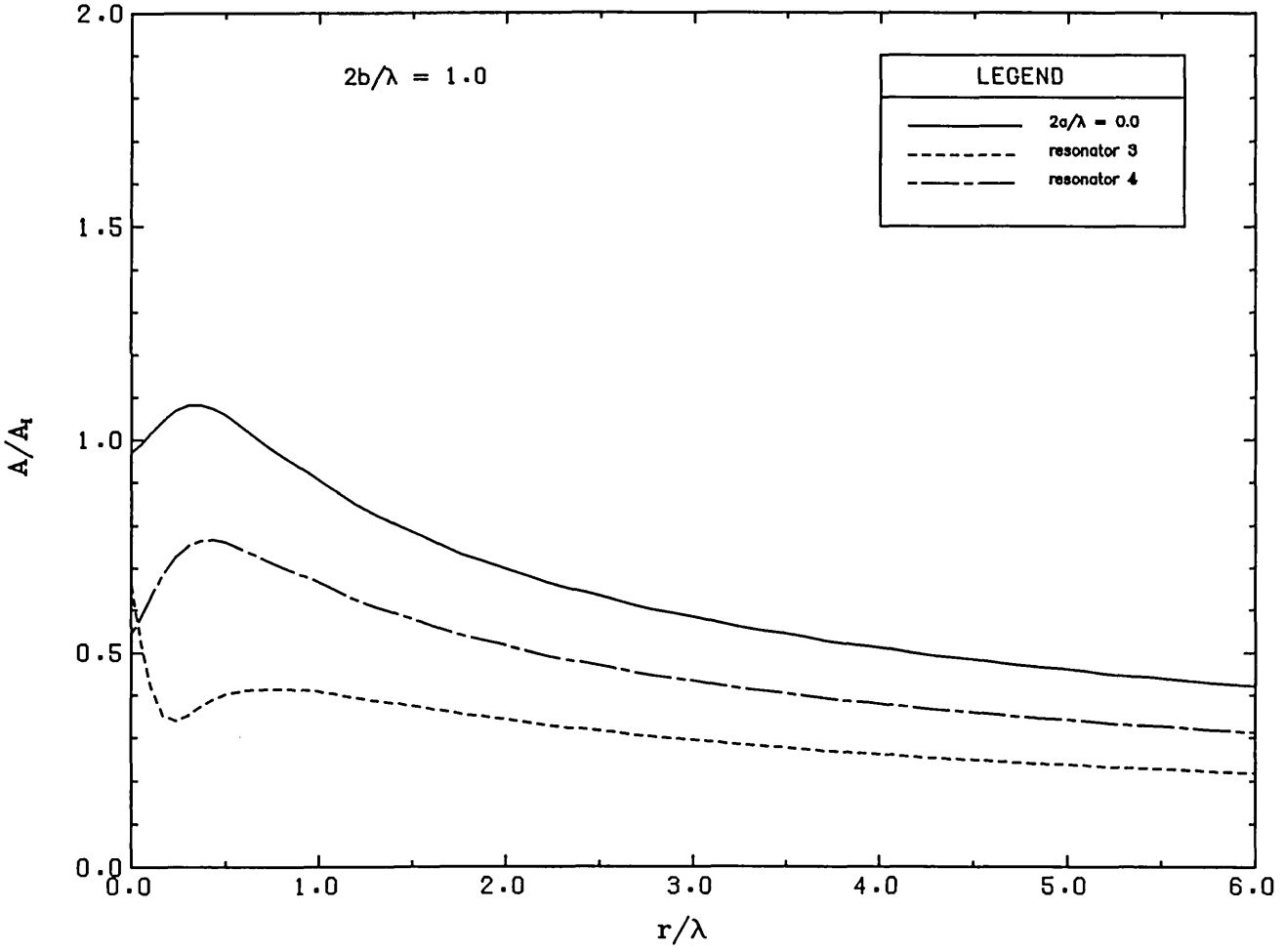

Fig. 5.20a PROFILES ALONG INCIDENT WAVE DIRECTION

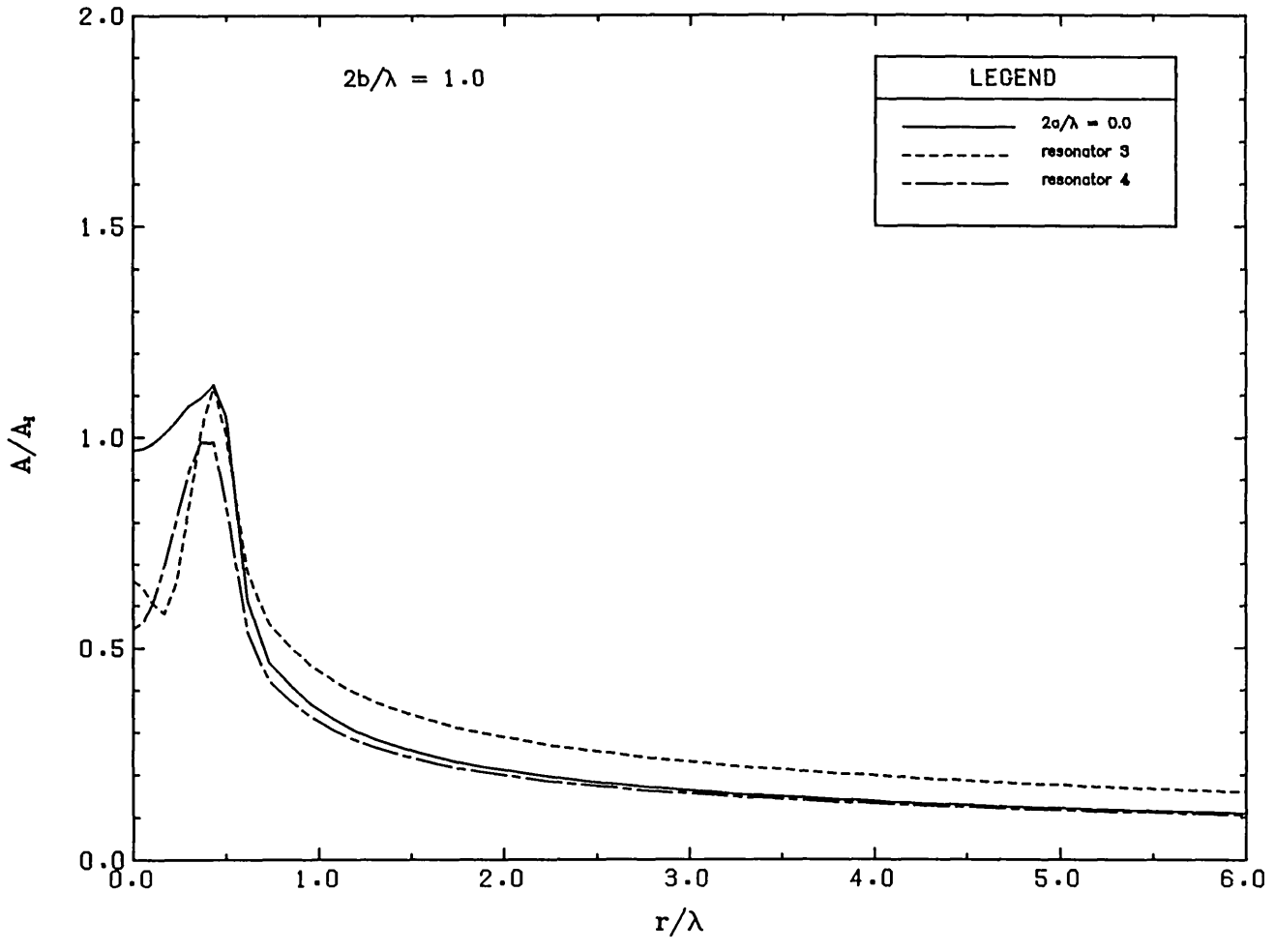

Fig. 5.20b PROFILES ALONG BREAKWATER

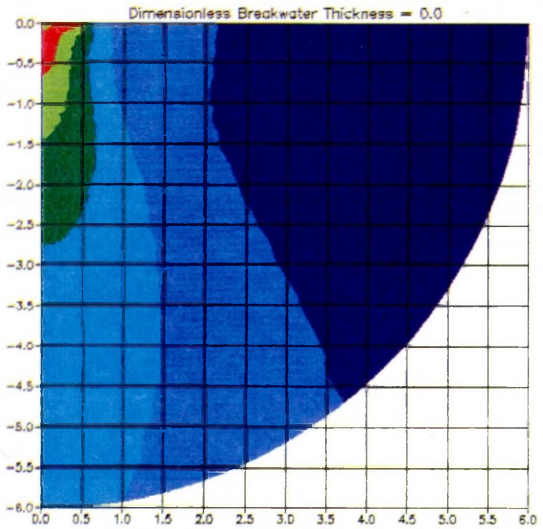

$2b/\lambda = 1.0$

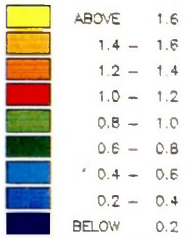

Fig. 5.20 c

Amplitude contours

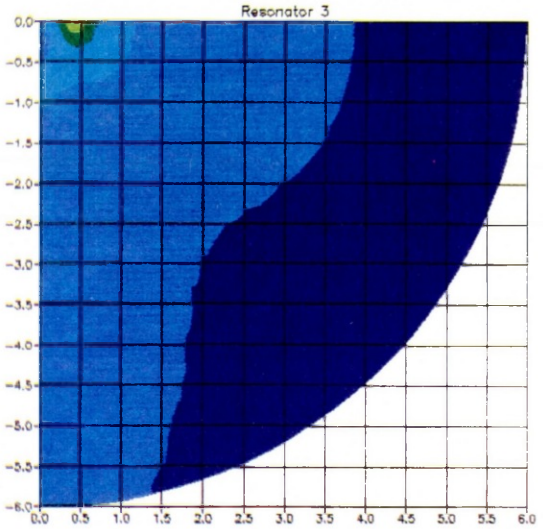

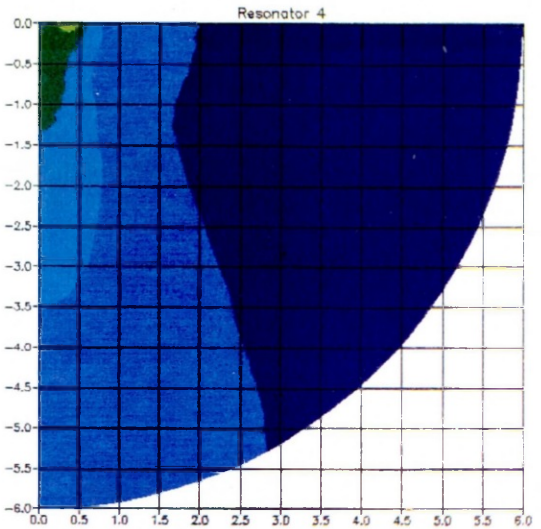

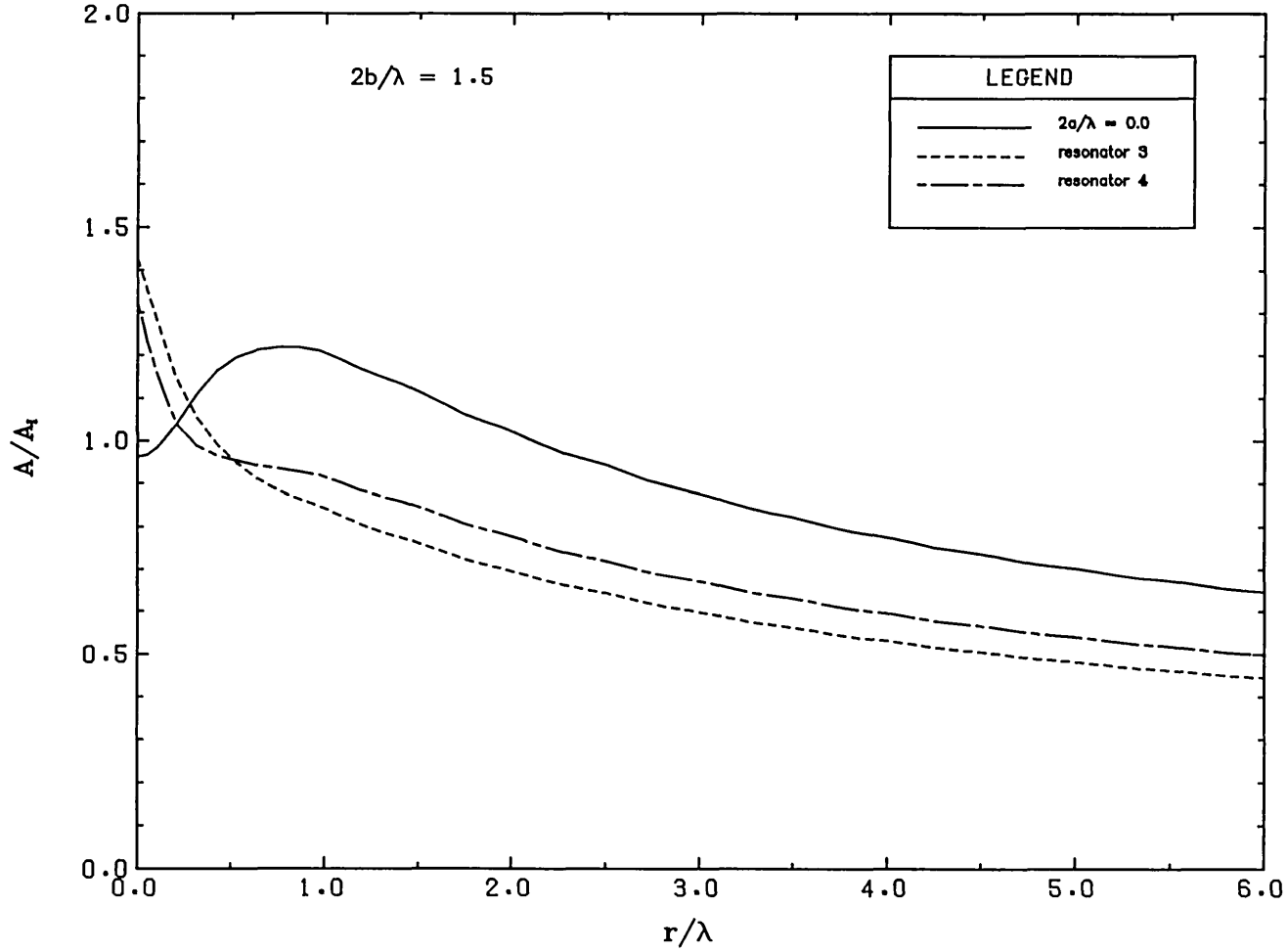

Fig. 5.21a PROFILES ALONG INCIDENT WAVE DIRECTION

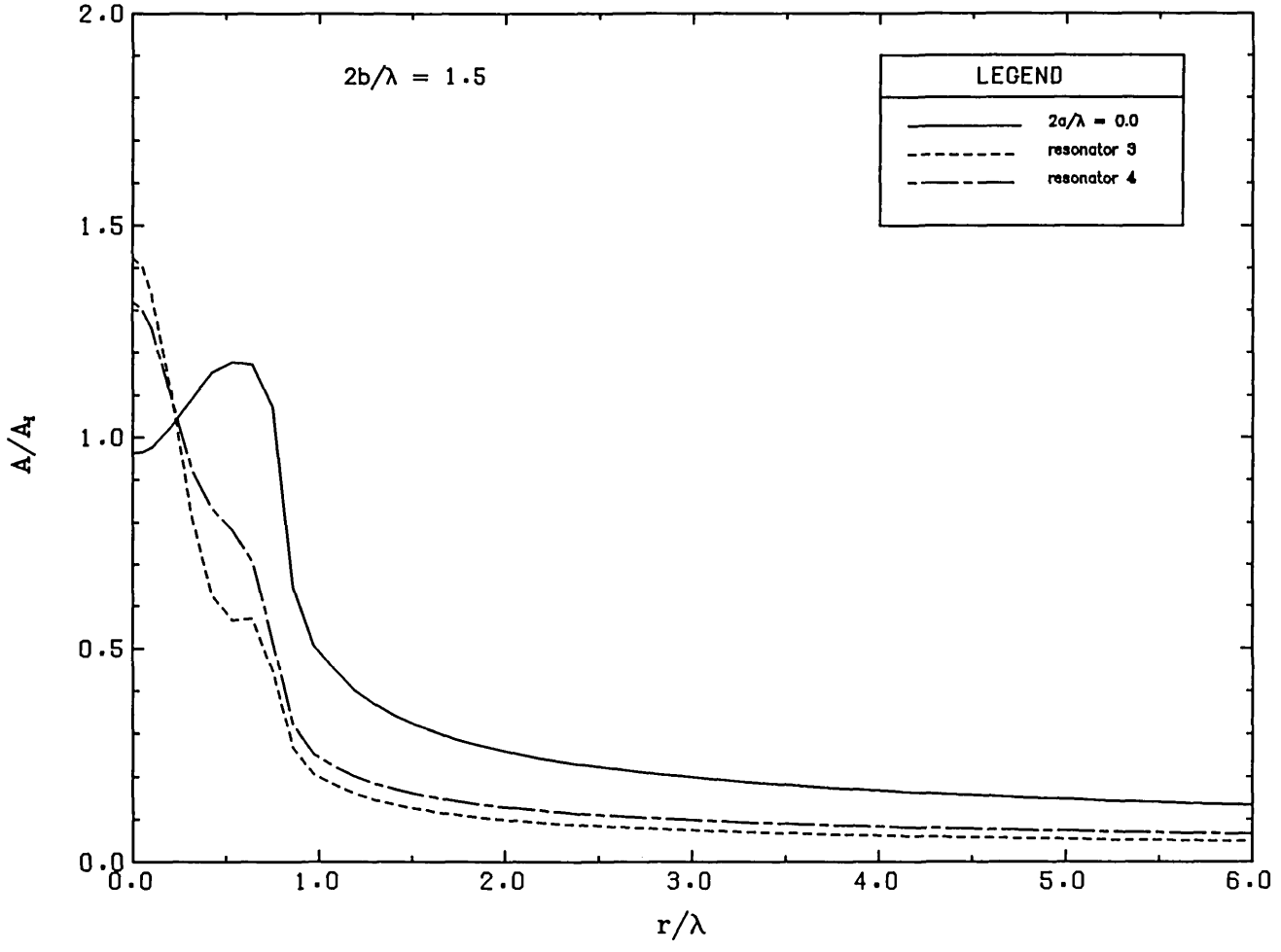

Fig. 5.21b PROFILES ALONG BREAKWATER

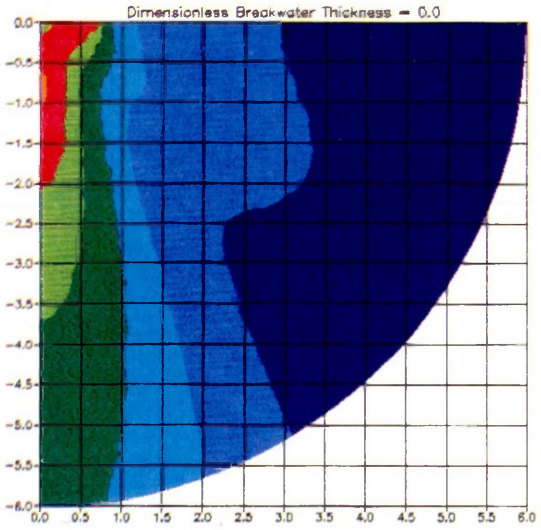

$2b/\lambda = 1.5$

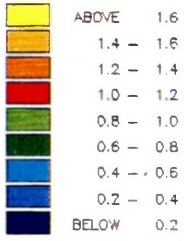

Fig. 5.21c

Amplitude contours

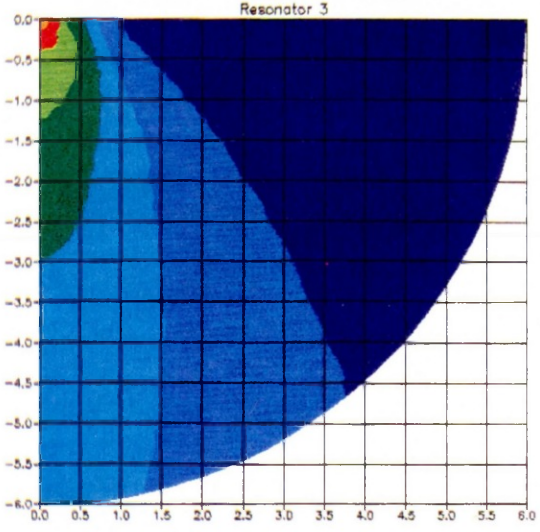

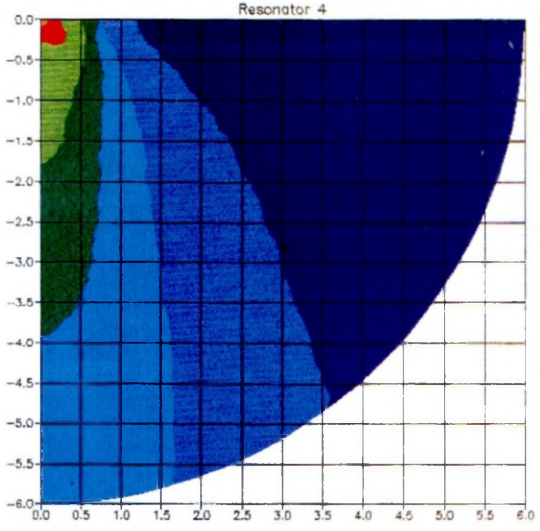

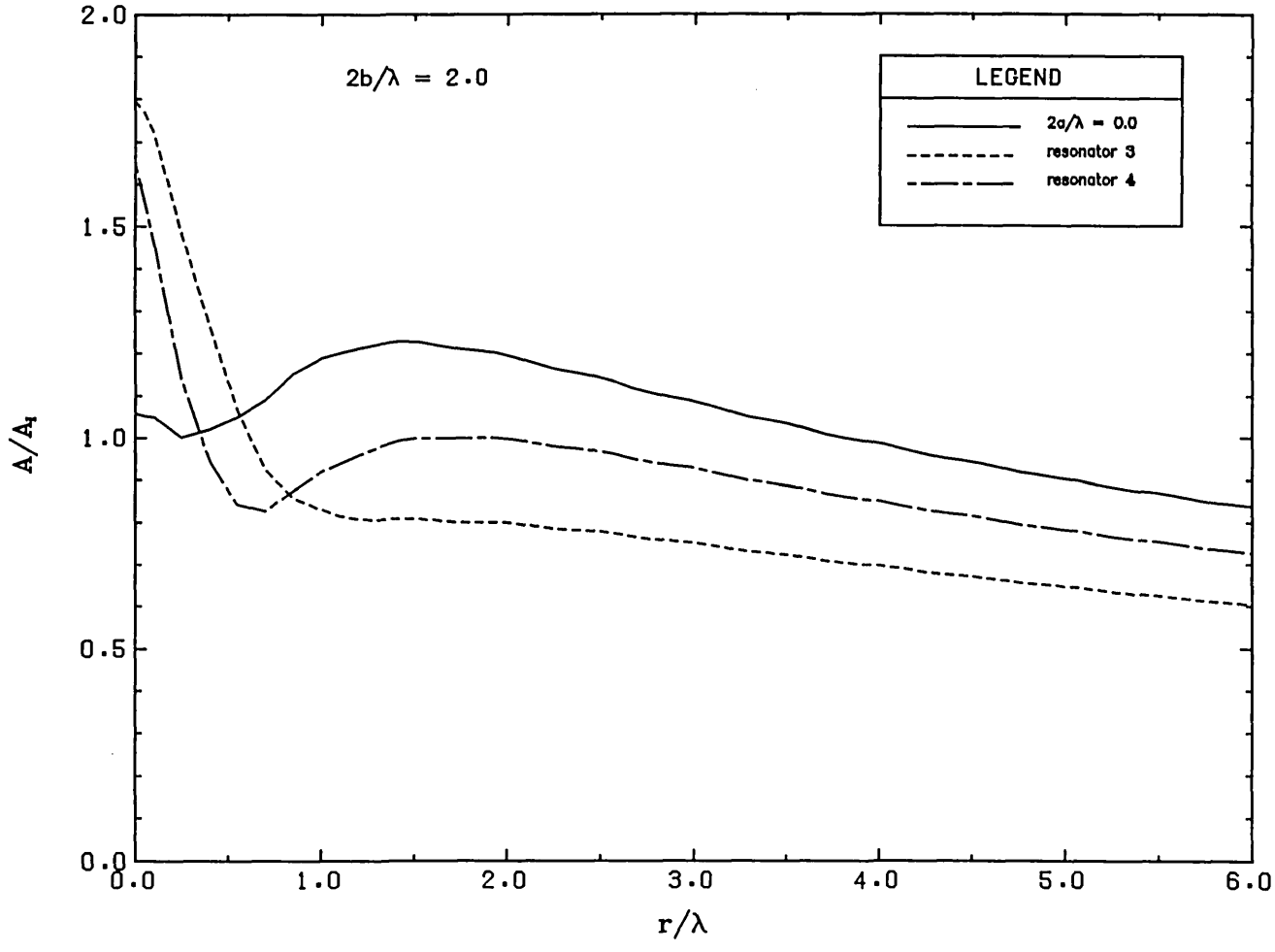

Fig. 5.22a PROFILES ALONG INCIDENT WAVE DIRECTION

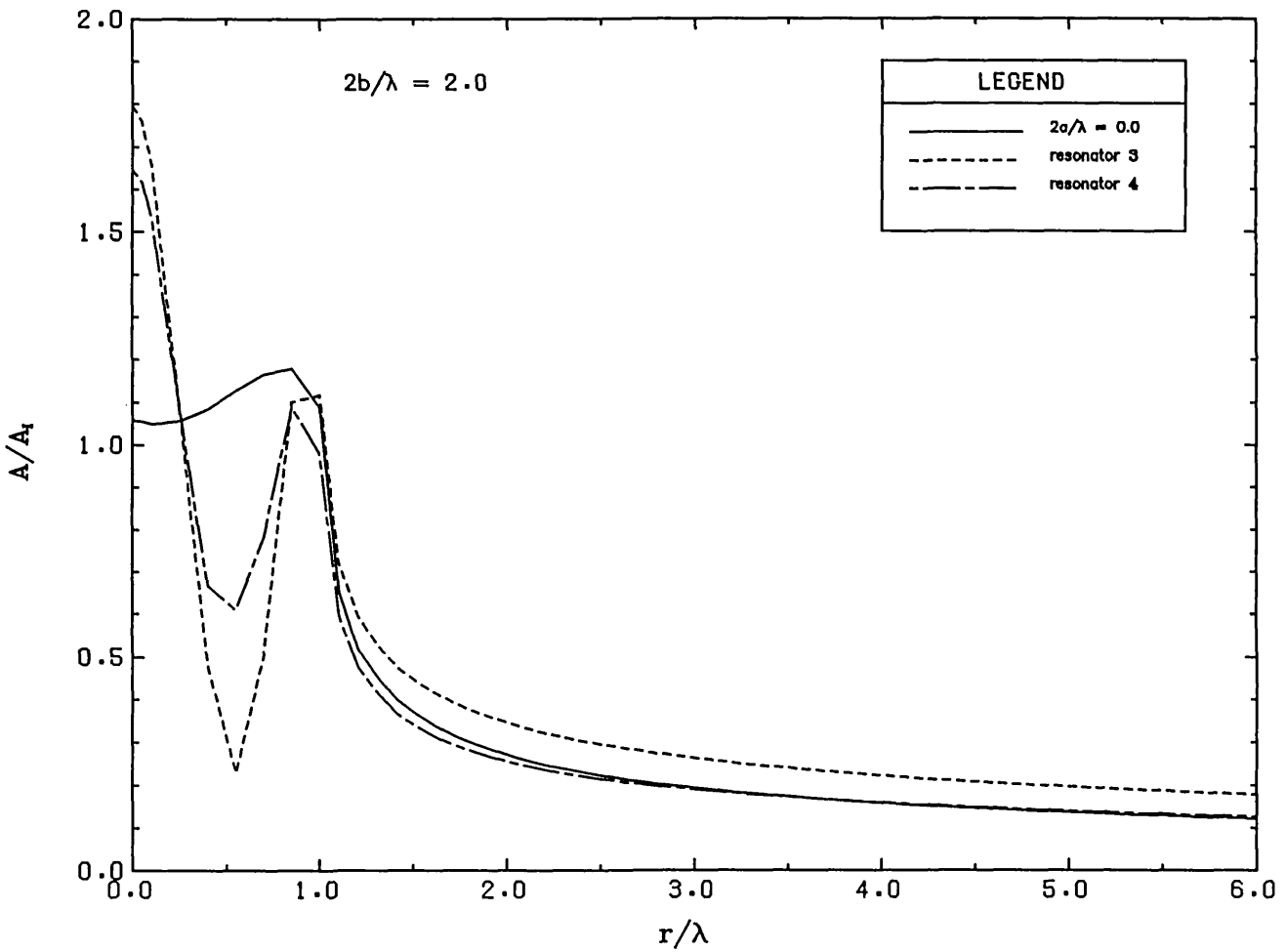

Fig. 5.22b PROFILES ALONG BREAKWATER

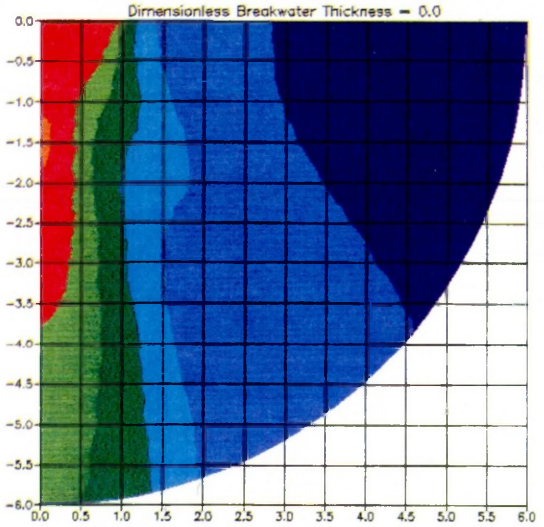

$2b/\lambda = 2.0$

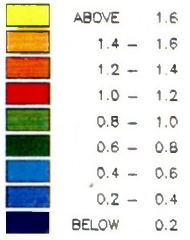

Fig. 5.22 c

Amplitude contours

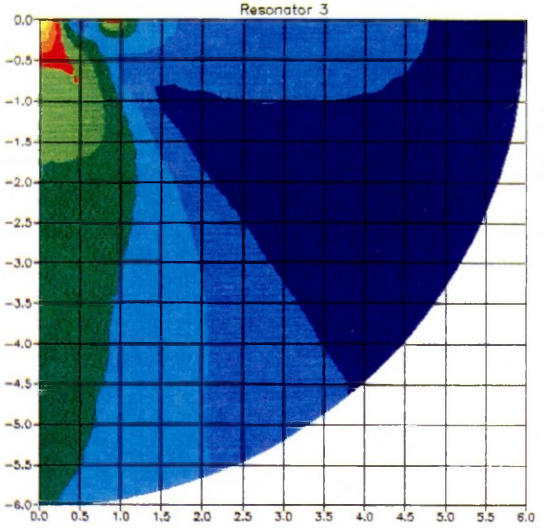

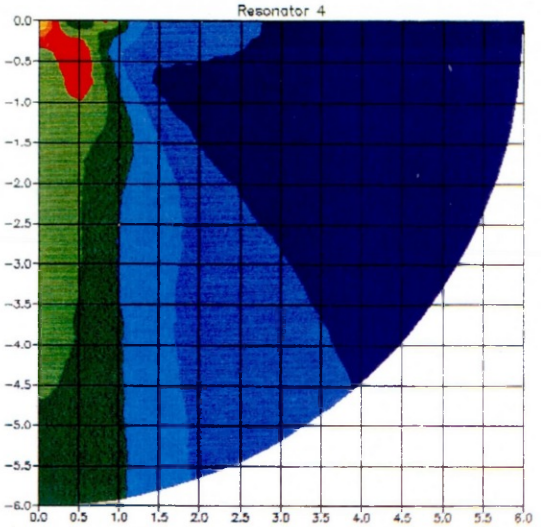

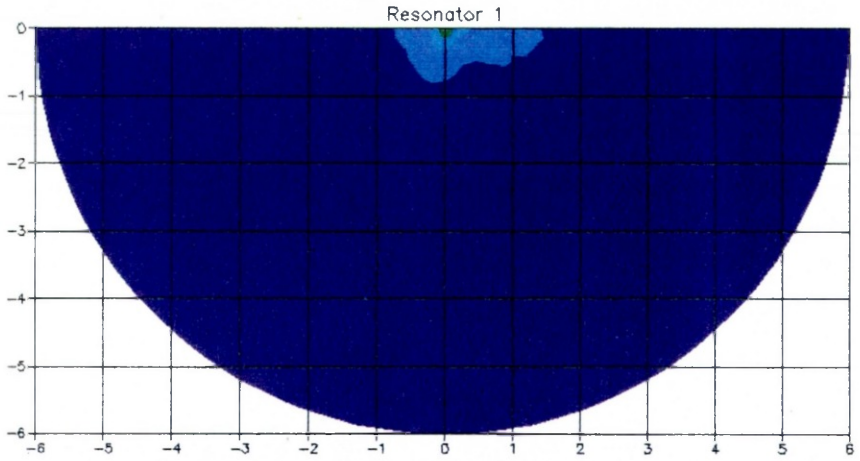

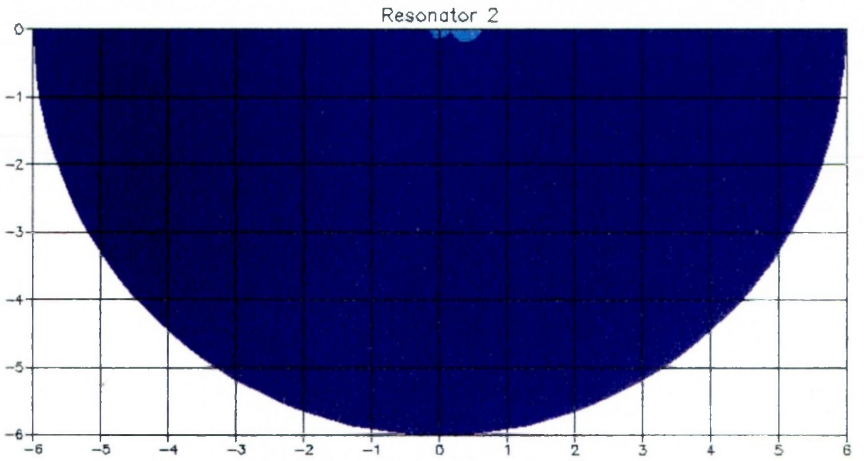

$2b/\lambda = 0.5$, $\theta = 30°$

Fig. 5.40 Amplitude contours

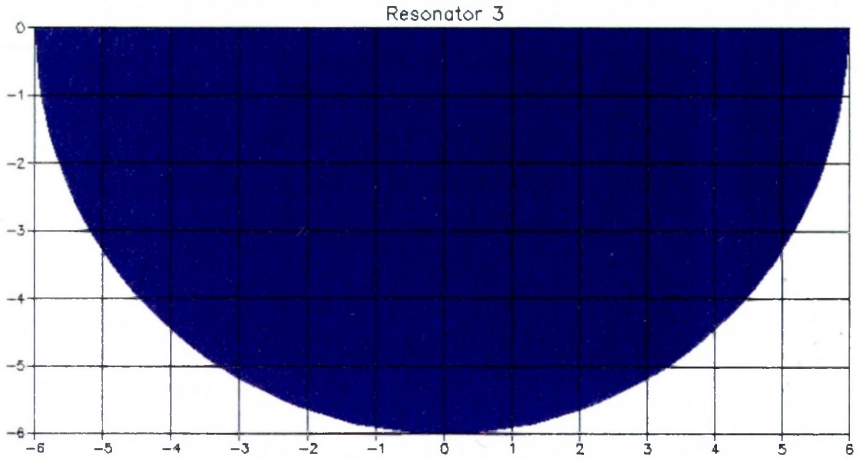

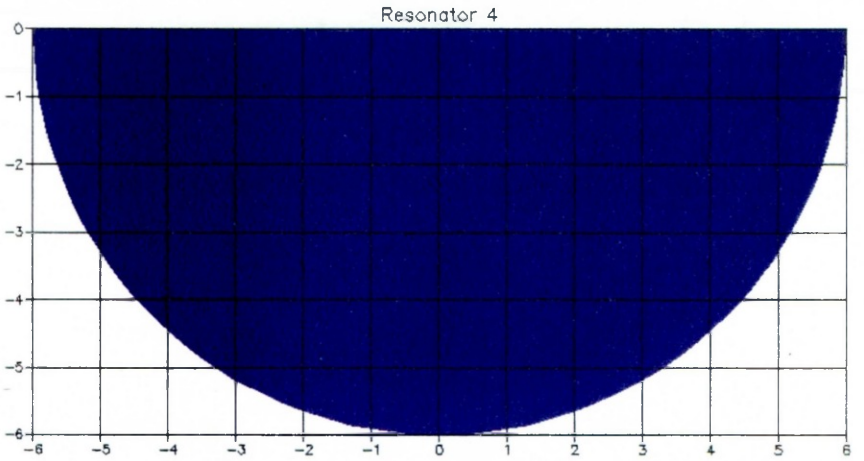

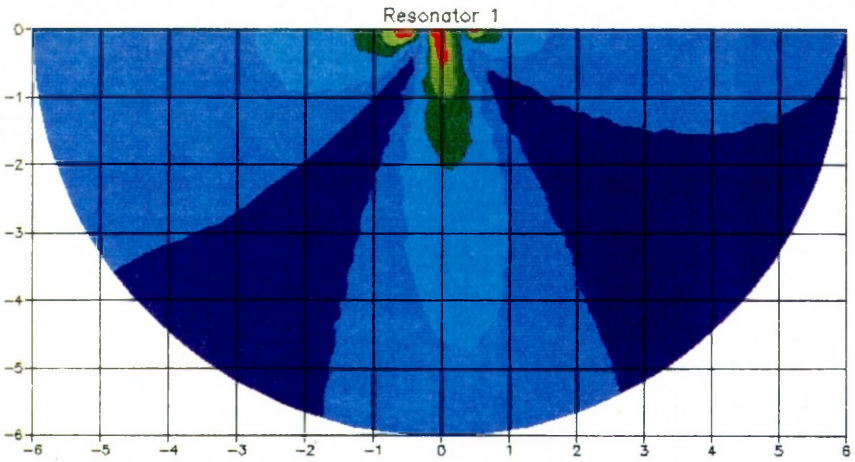

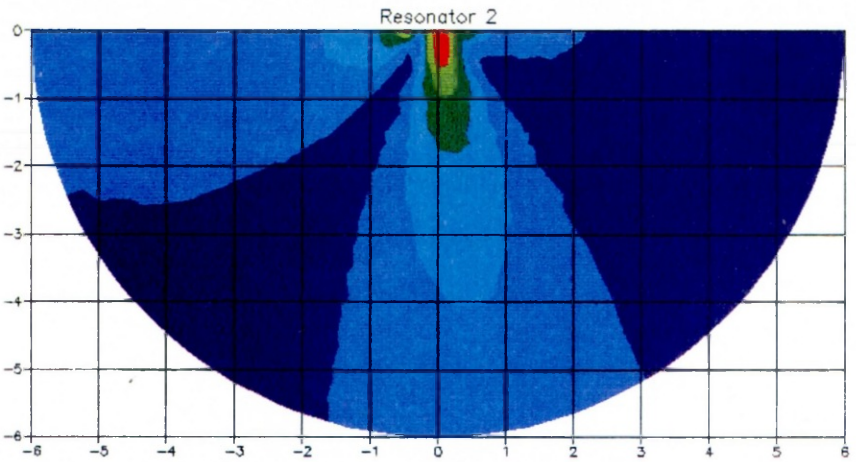

$2b/\lambda = 1.0$, $\theta = 30°$

Fig.5.41 Amplitude contours

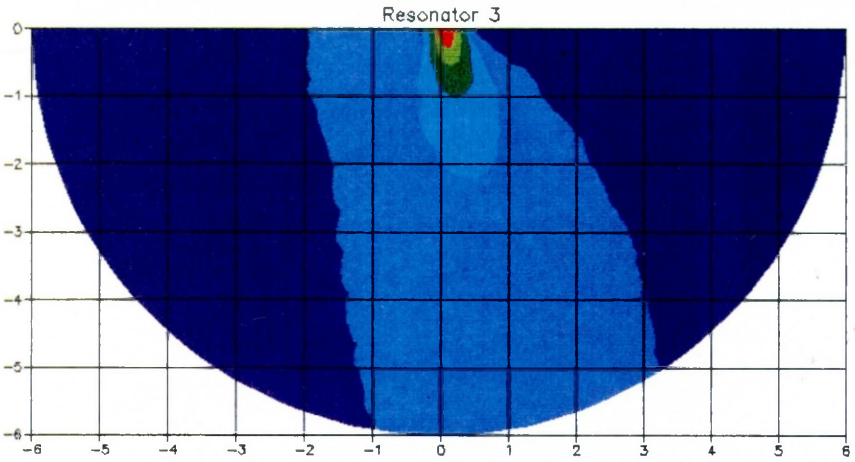

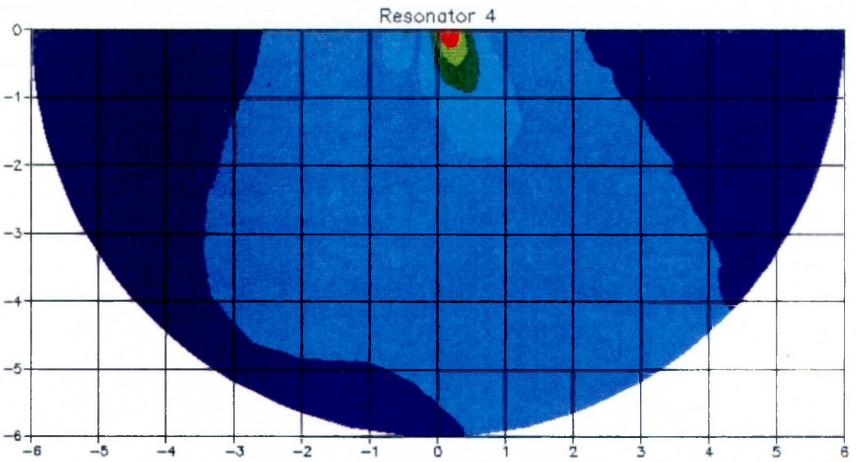

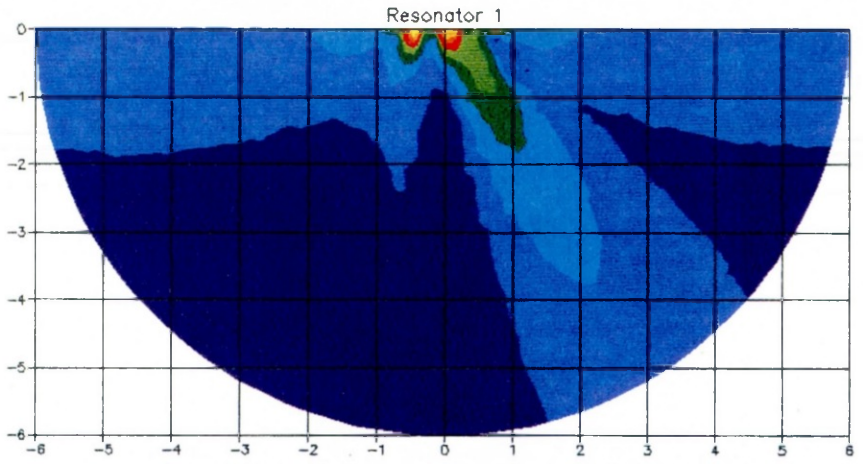

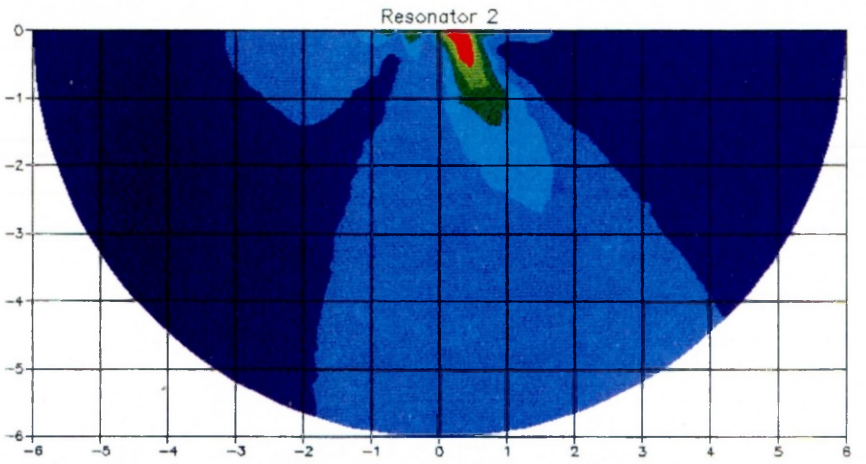

$2b/\lambda = 1.5$, $\theta = 30°$

Fig. 5.42 Amplitude contours

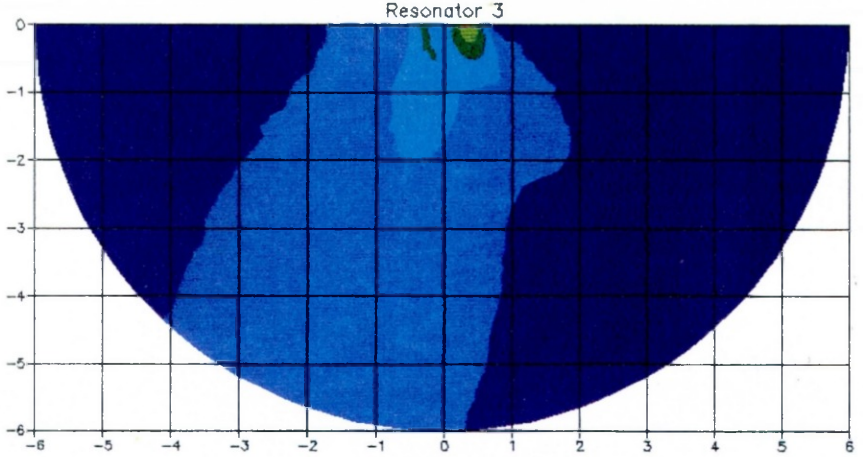

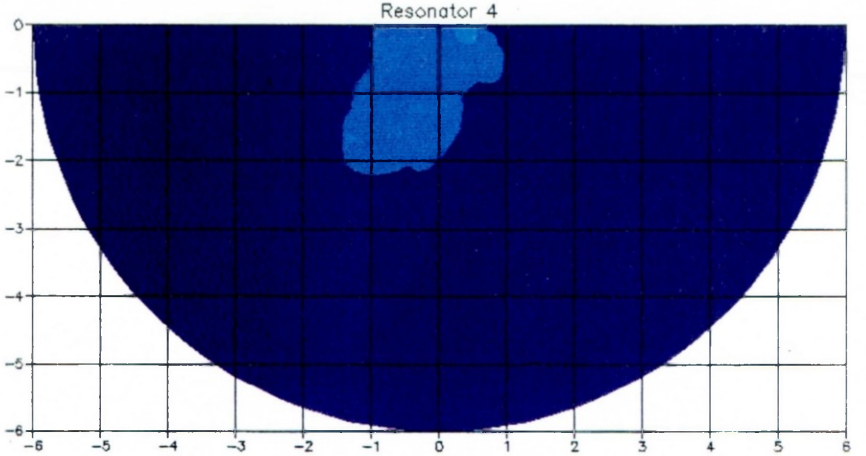

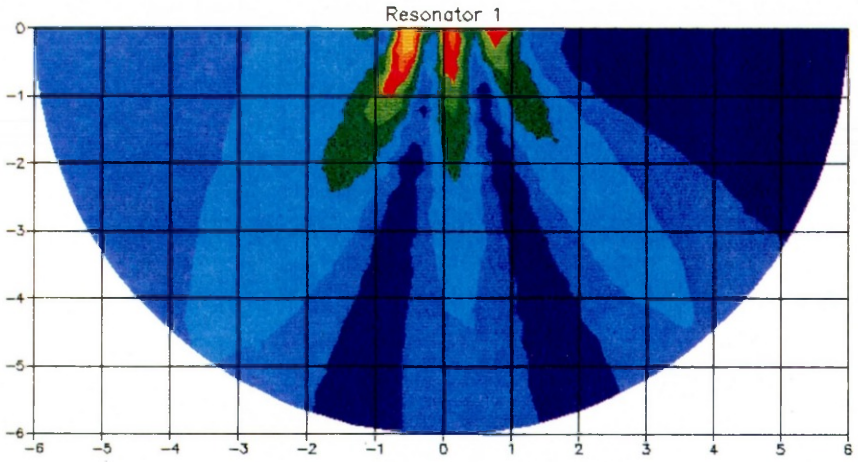

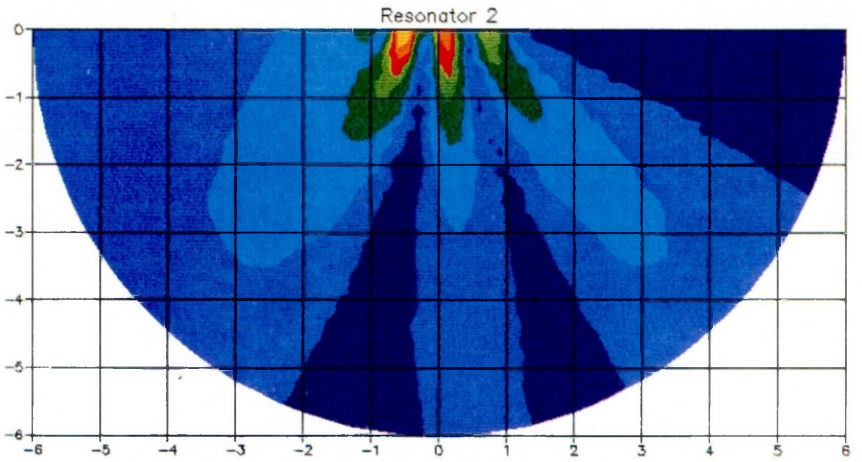

$2b/\lambda = 2.0$, $\theta = 30°$

Fig. 5.43 Amplitude contours

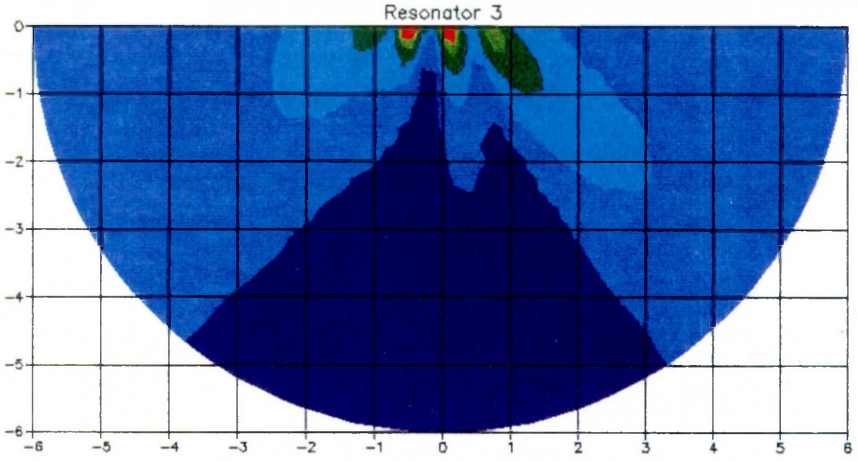

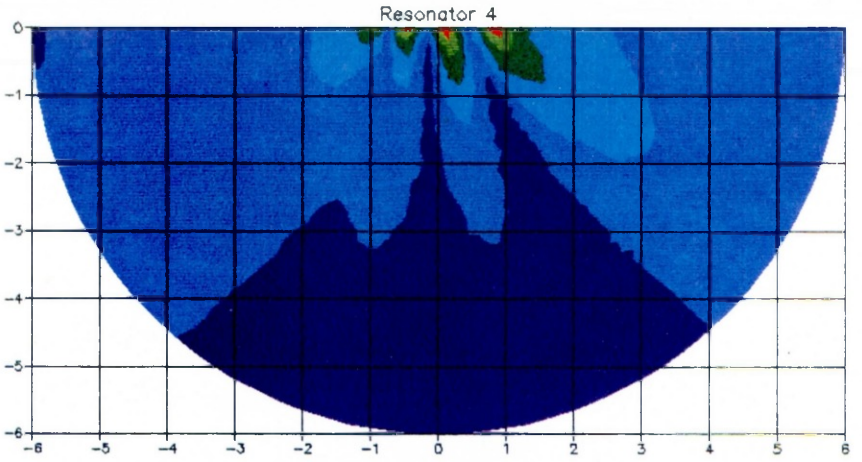

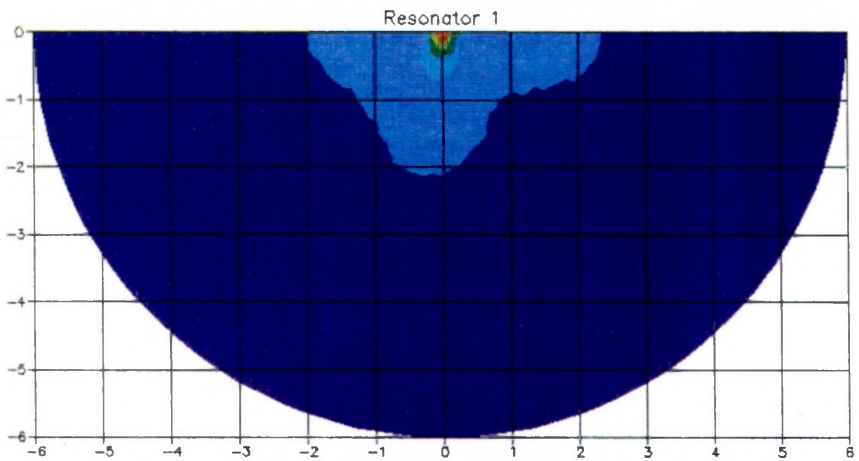

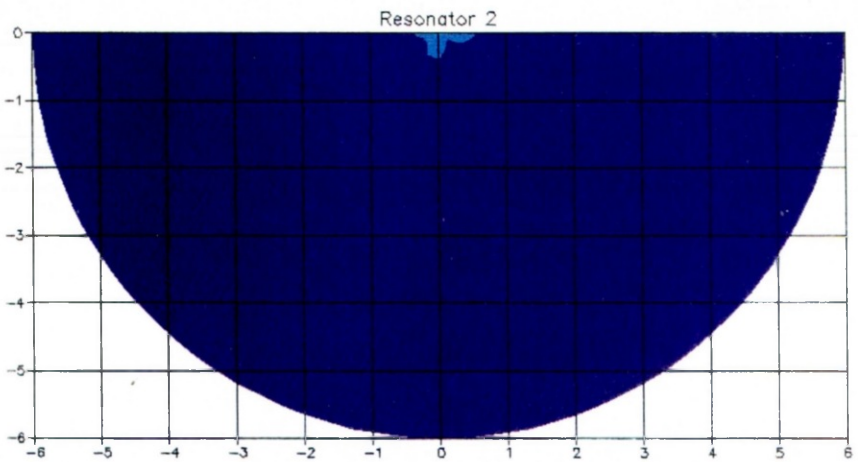

$2b/\lambda = 0.5$, $\theta = 60°$

Fig. 5.44 Amplitude contours

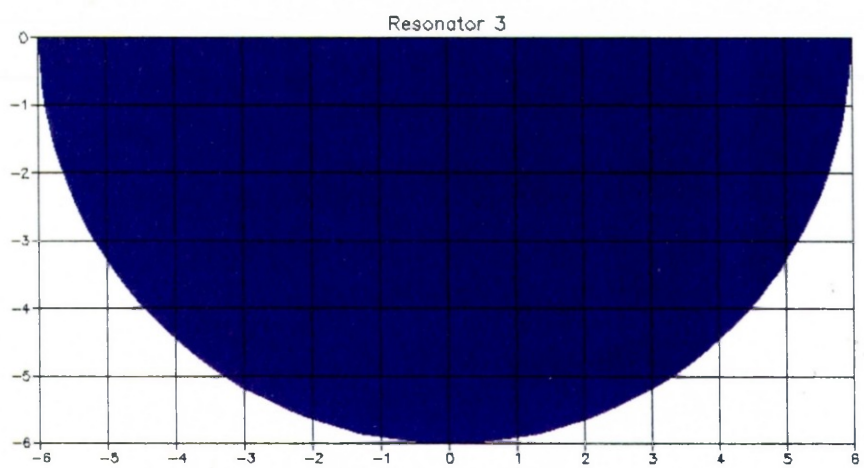

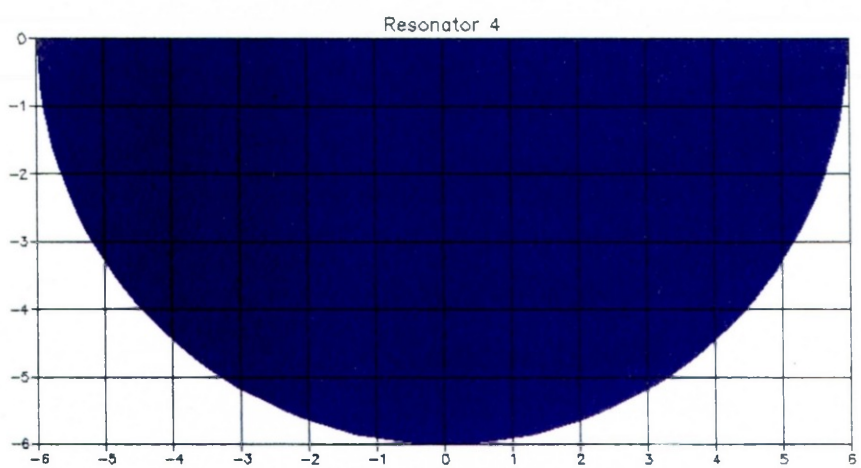

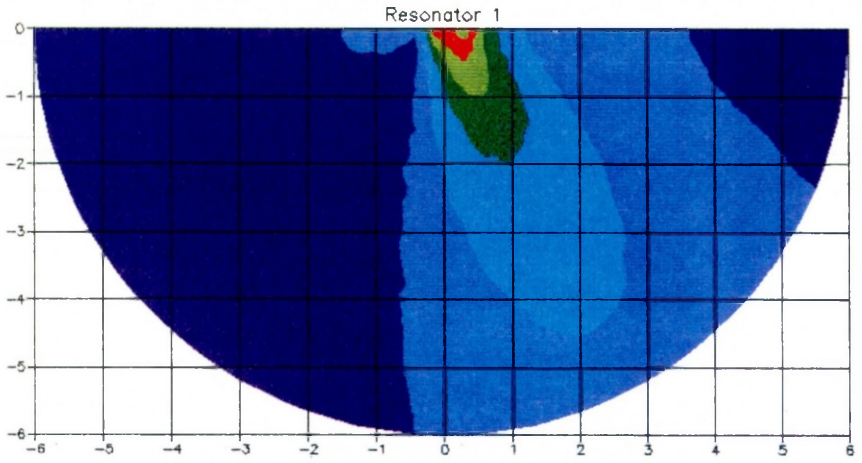

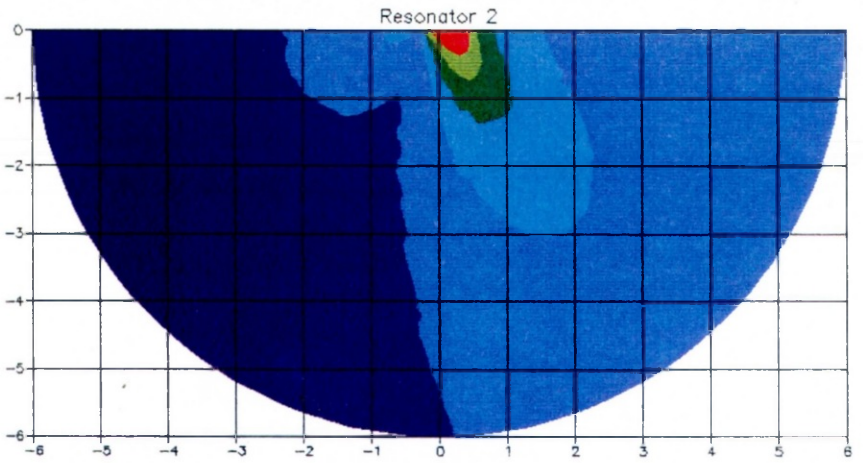

$2b/\lambda = 1.0$, $\theta = 60°$

Fig . 5.45 Amplitude contours

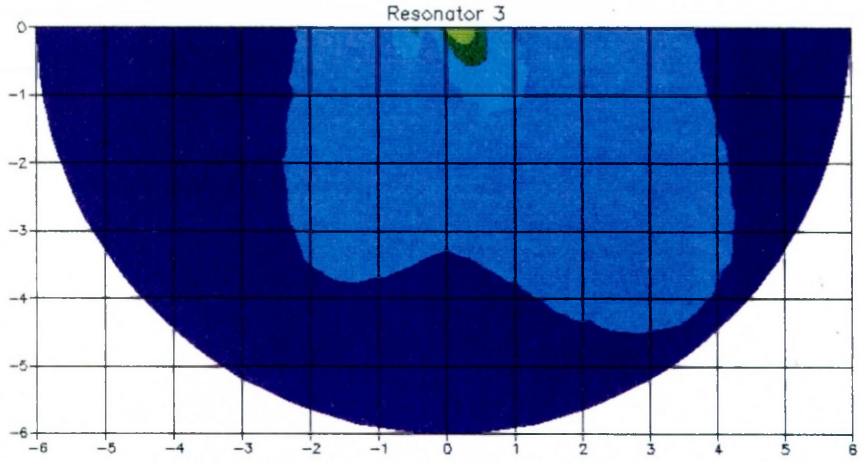

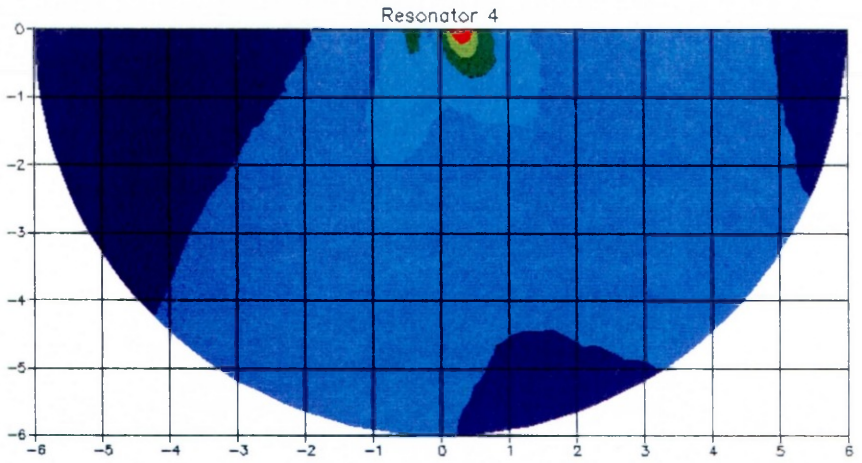

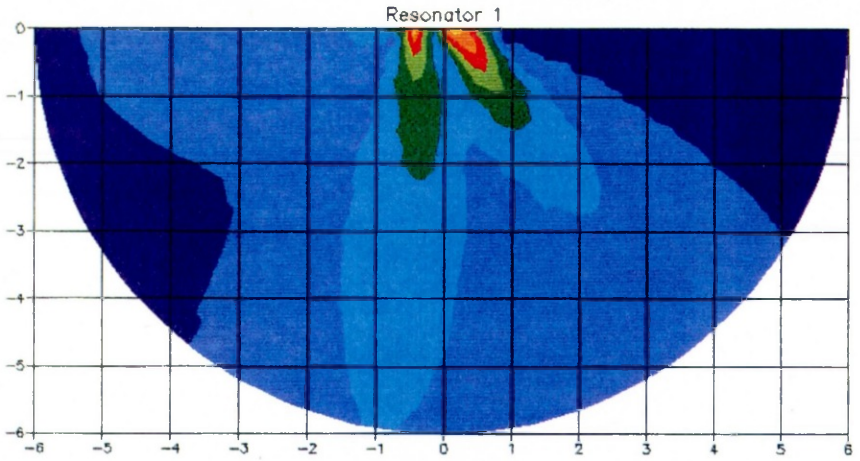

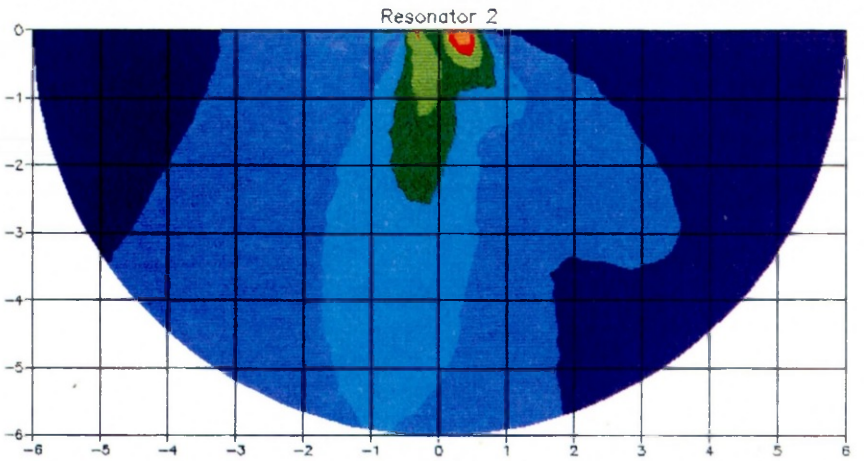

$2b/\lambda = 1.5$, $\theta = 60°$

Fig. 5.46 Amplitude contours

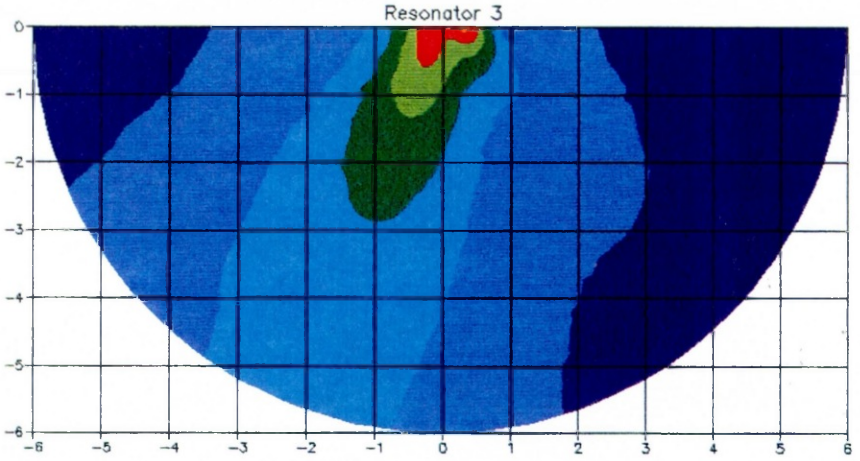

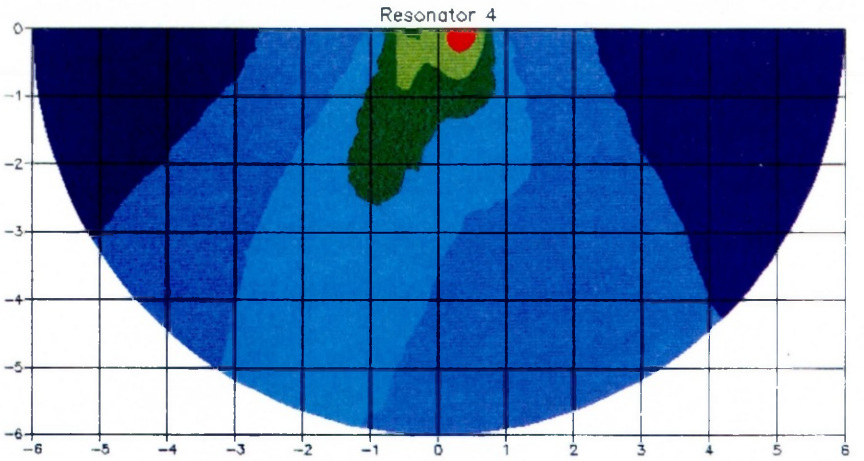

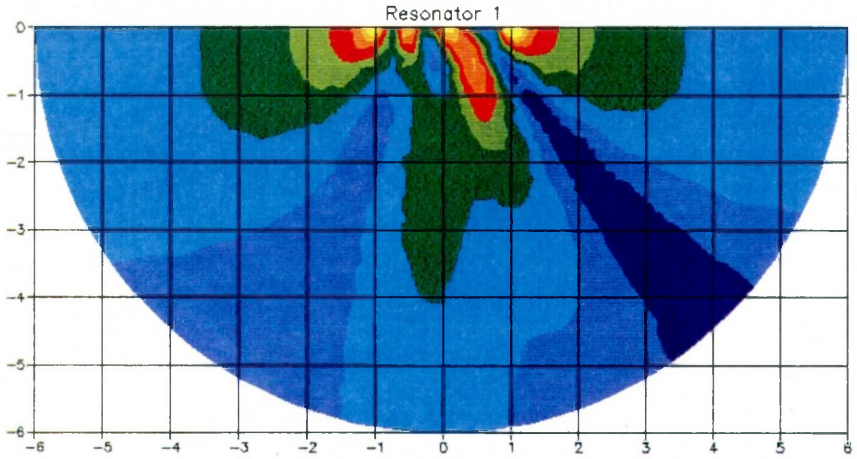

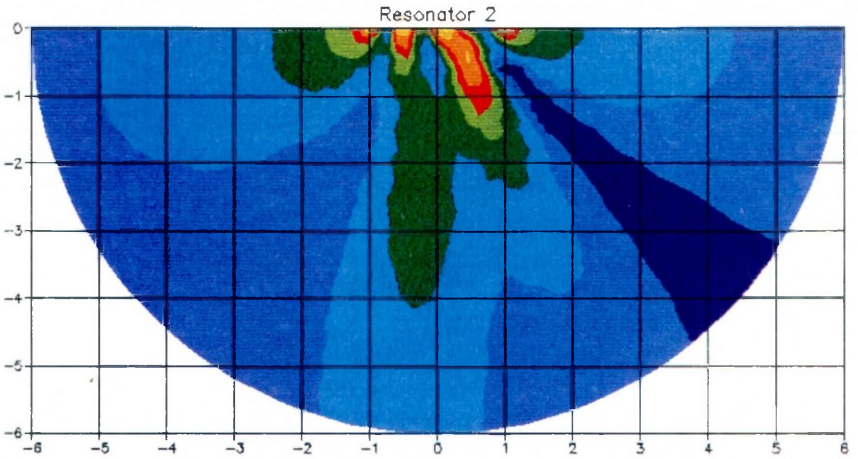

$2b/\lambda = 2.0$, $\theta = 60°$

Fig. 5.47 Amplitude contours

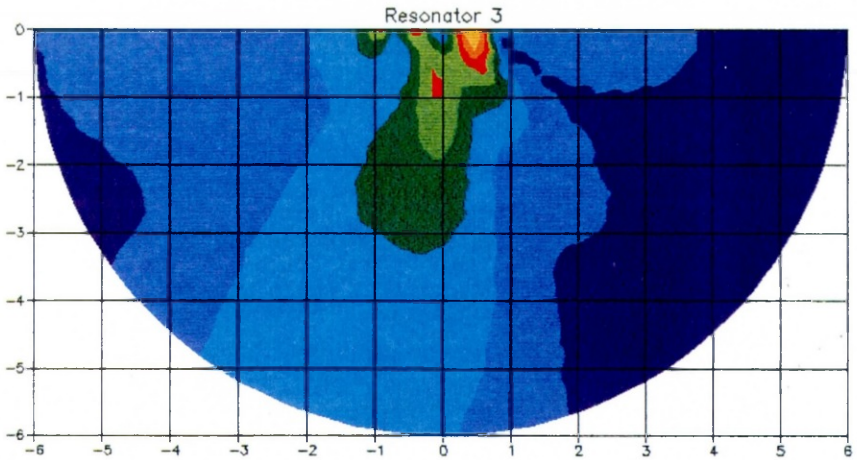

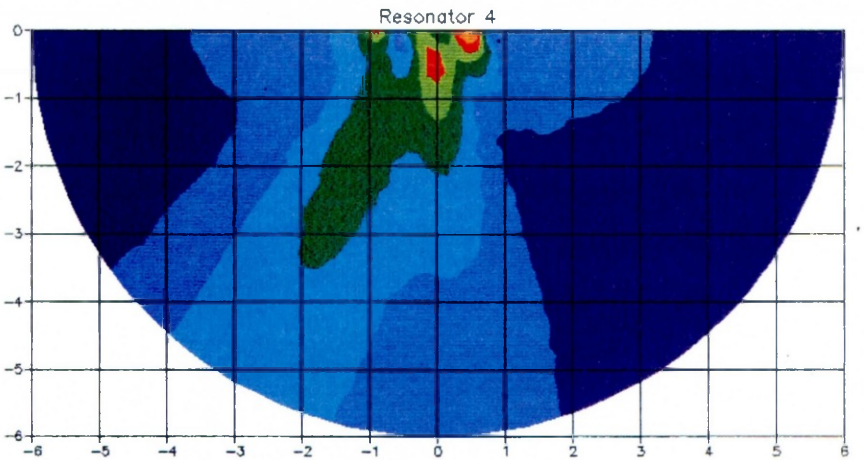

FILTERS

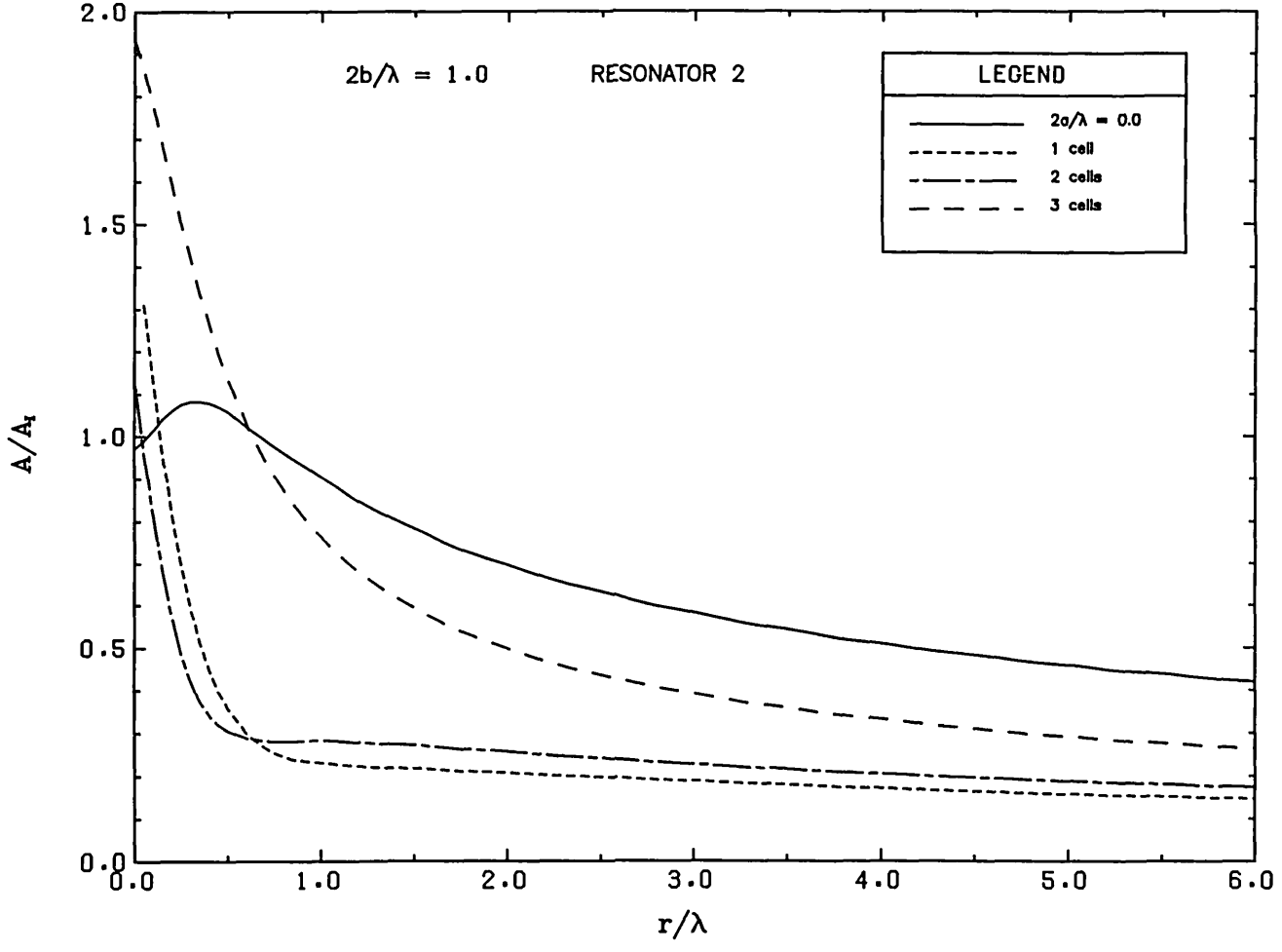

Fig. 5.23a PROFILES ALONG INCIDENT WAVE DIRECTION

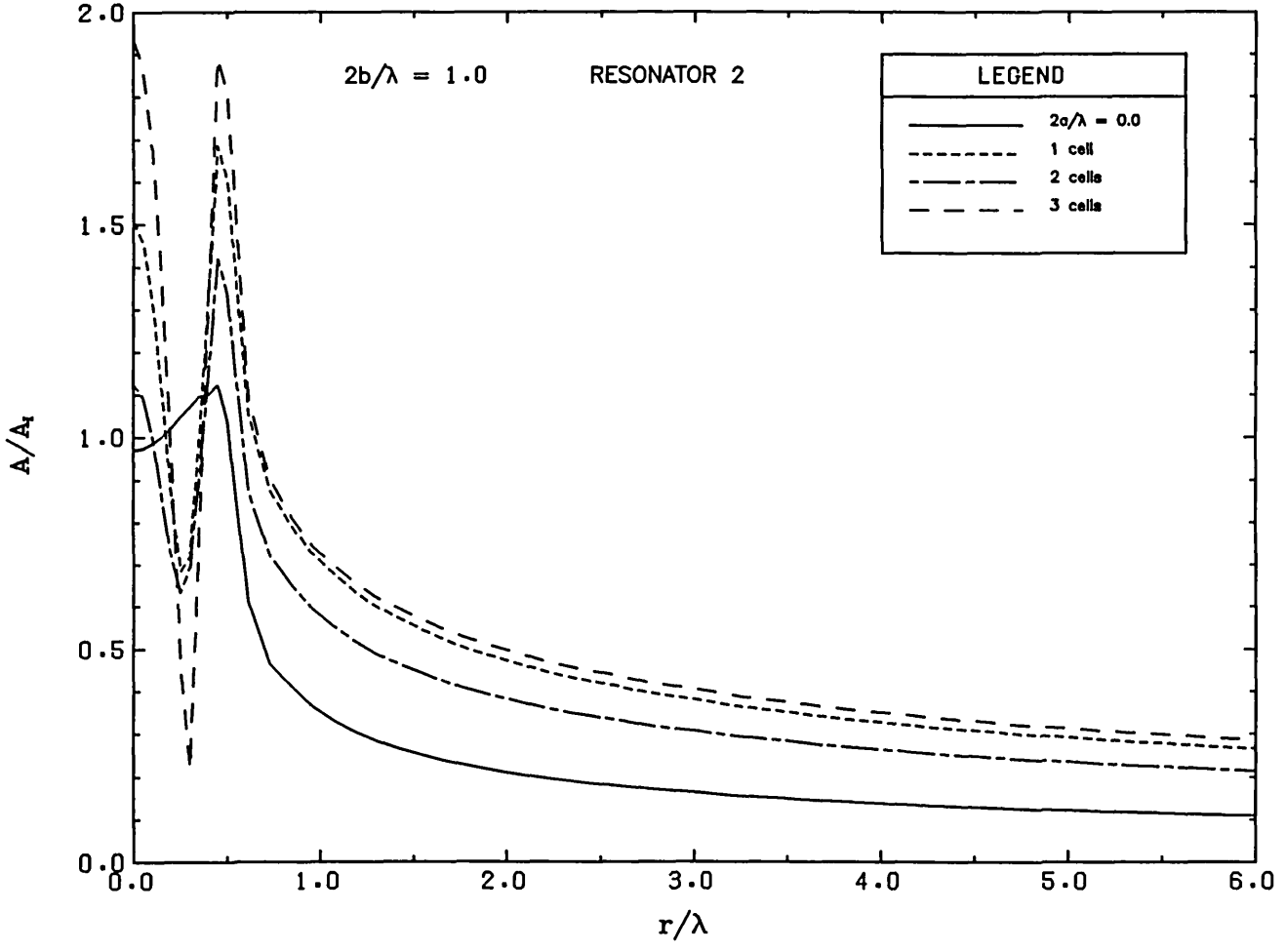

Fig. 5.23b PROFILES ALONG BREAKWATER

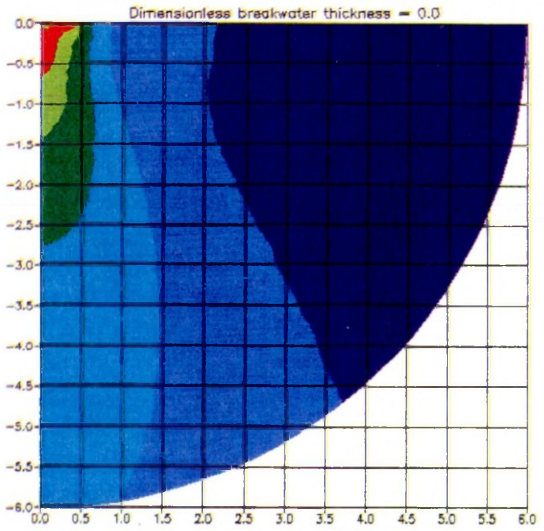

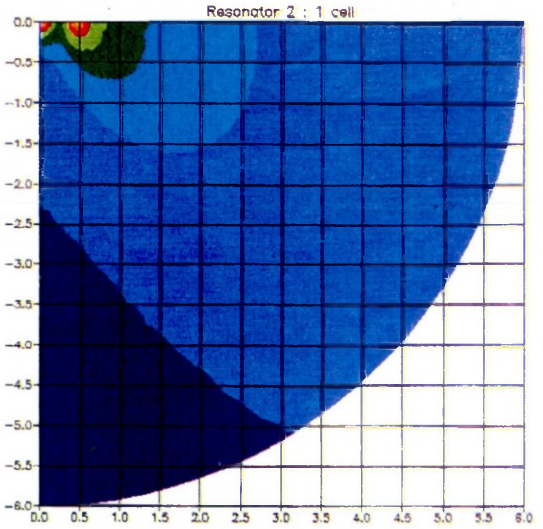

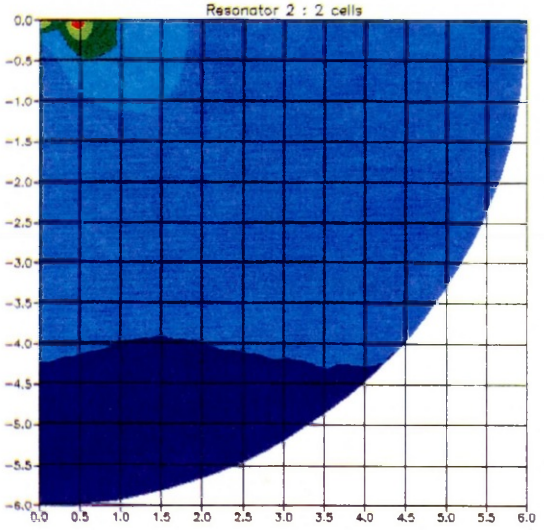

$2b/\lambda = 1.0$

Fig. 5.23c
Amplitude
contours

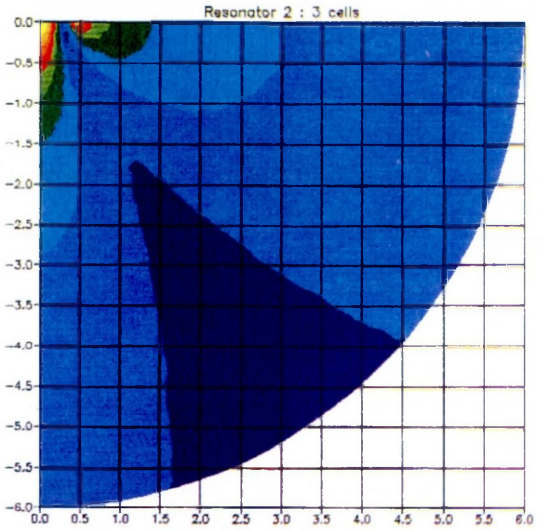

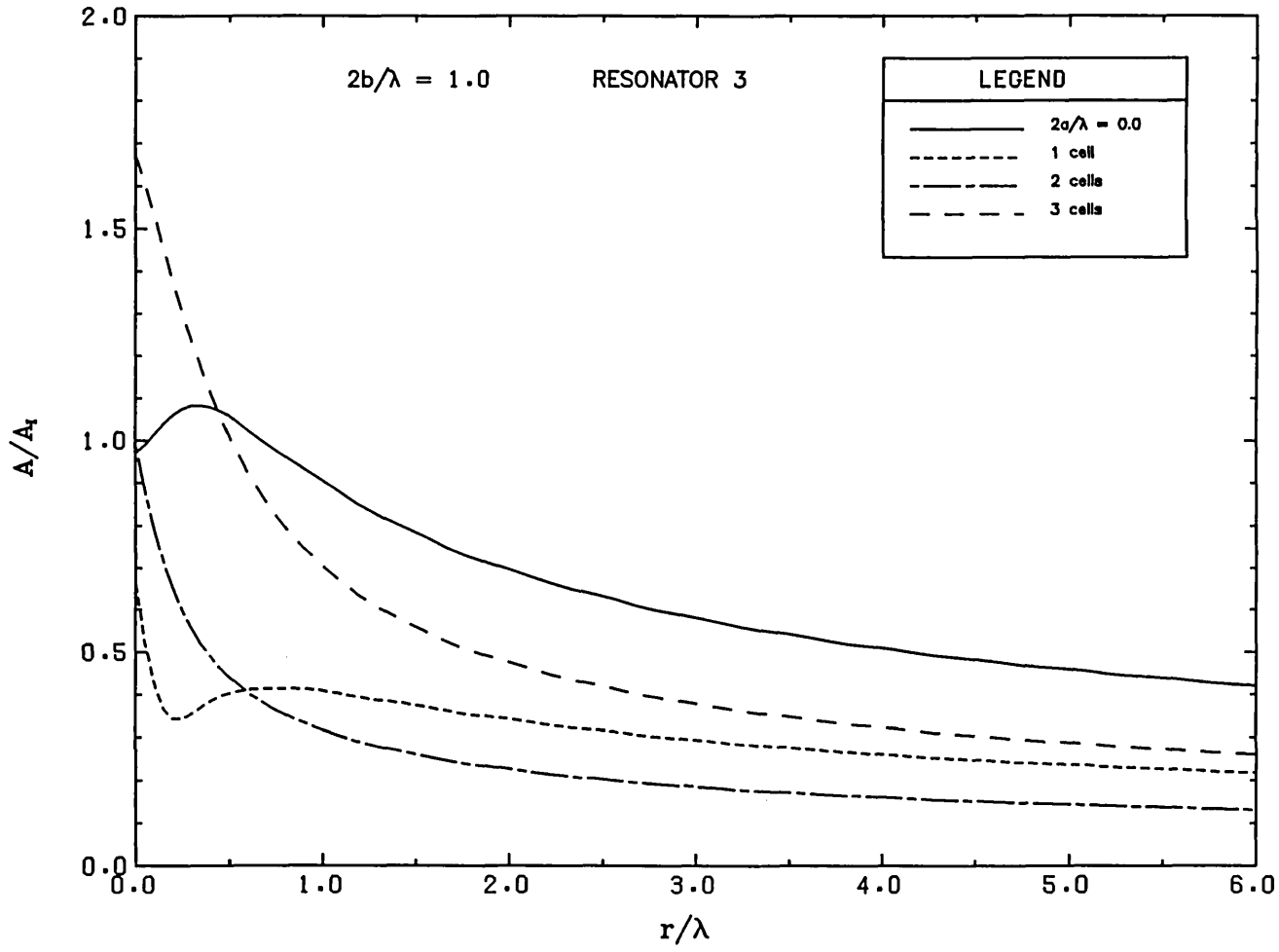

Fig. 5.24a PROFILES ALONG INCIDENT WAVE DIRECTION

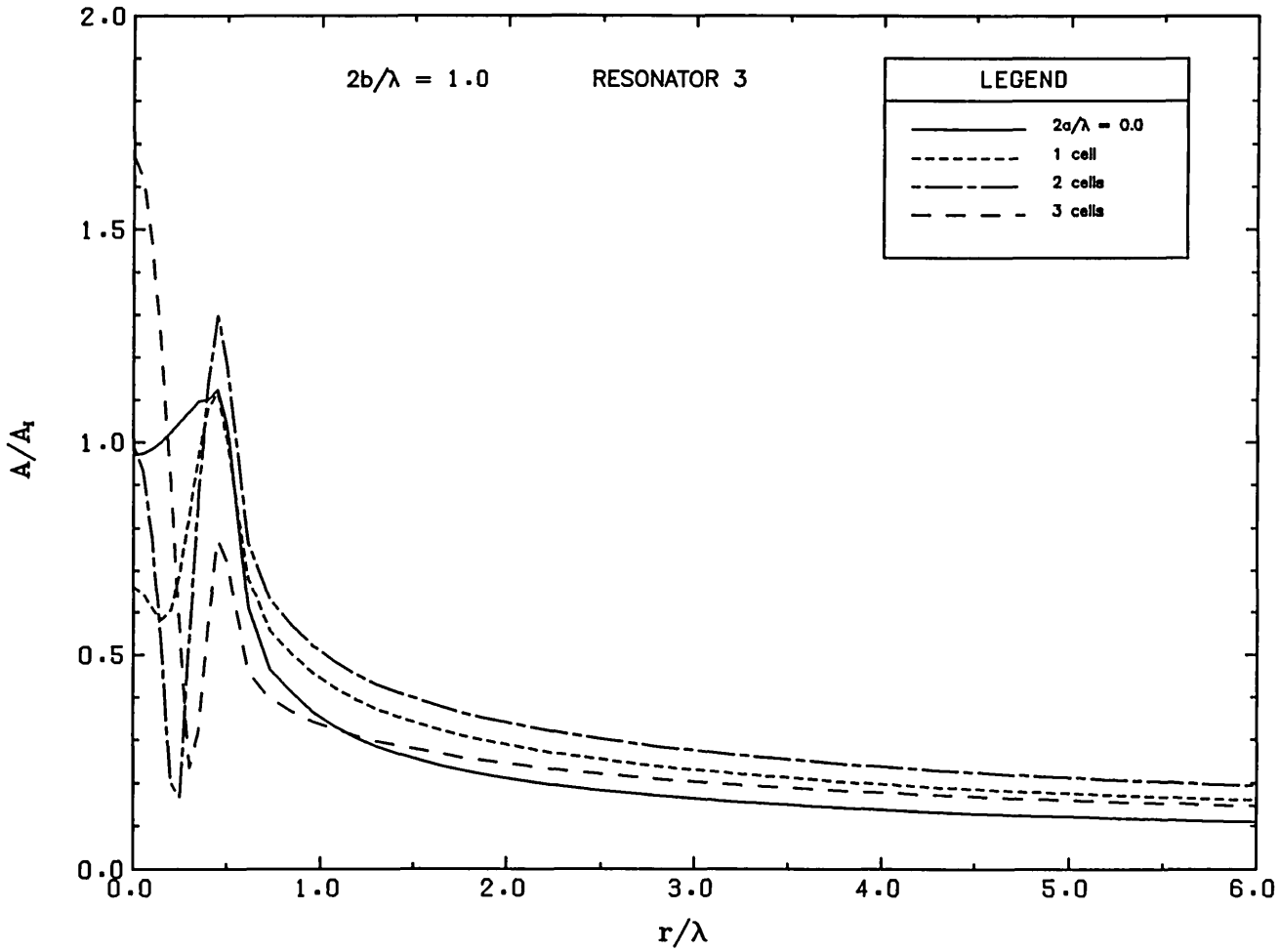

Fig. 5.24b PROFILES ALONG BREAKWATER

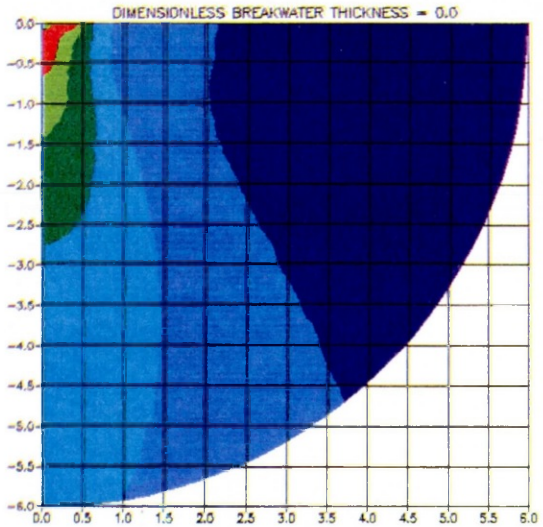

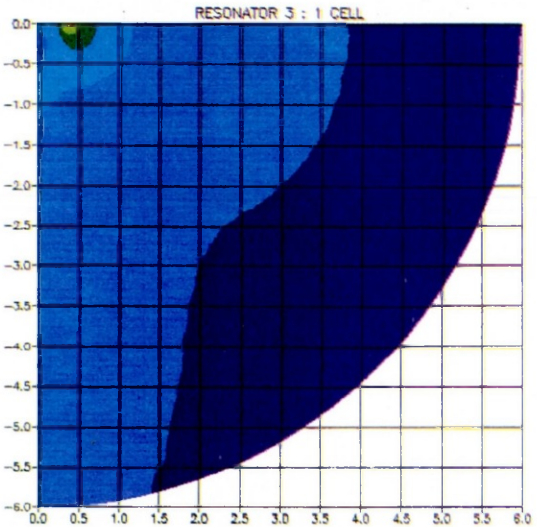

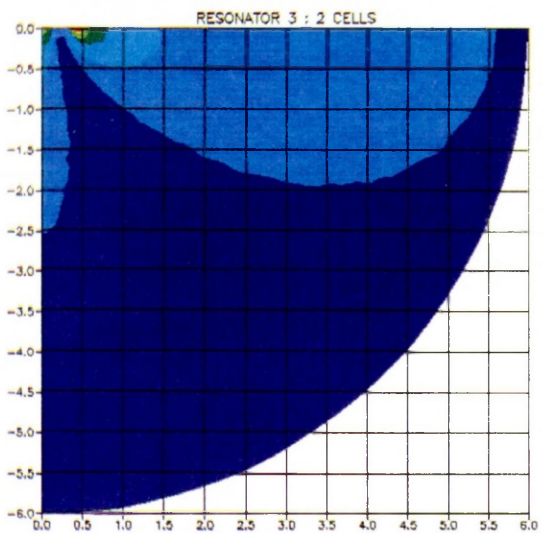

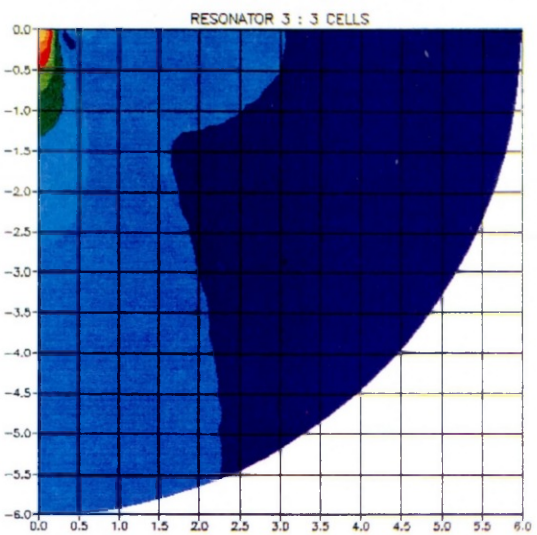

$2b/\lambda = 1.0$

Fig. 5.24 c
Amplitude
contours

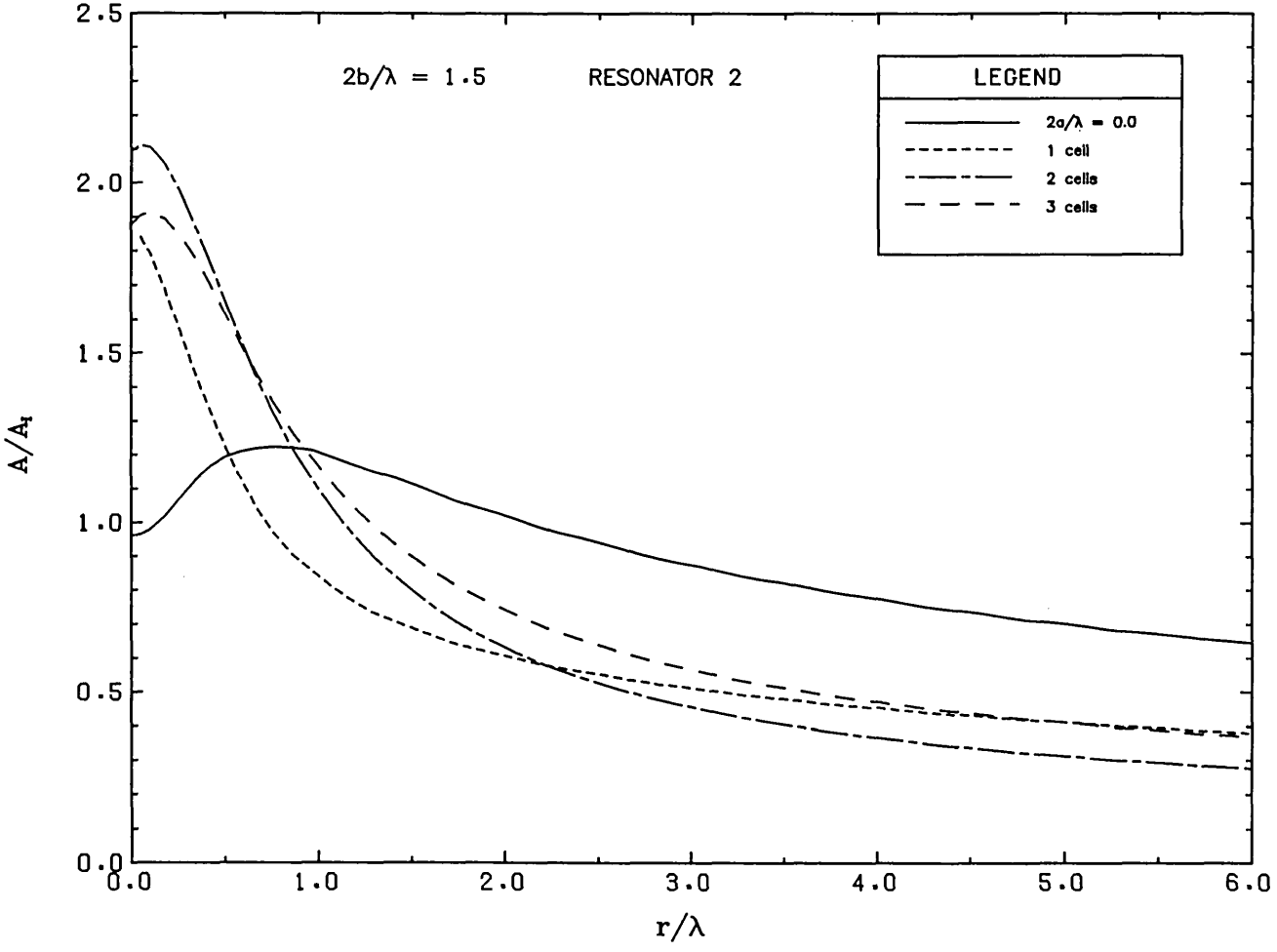

Fig. 5.25a PROFILES ALONG INCIDENT WAVE DIRECTION

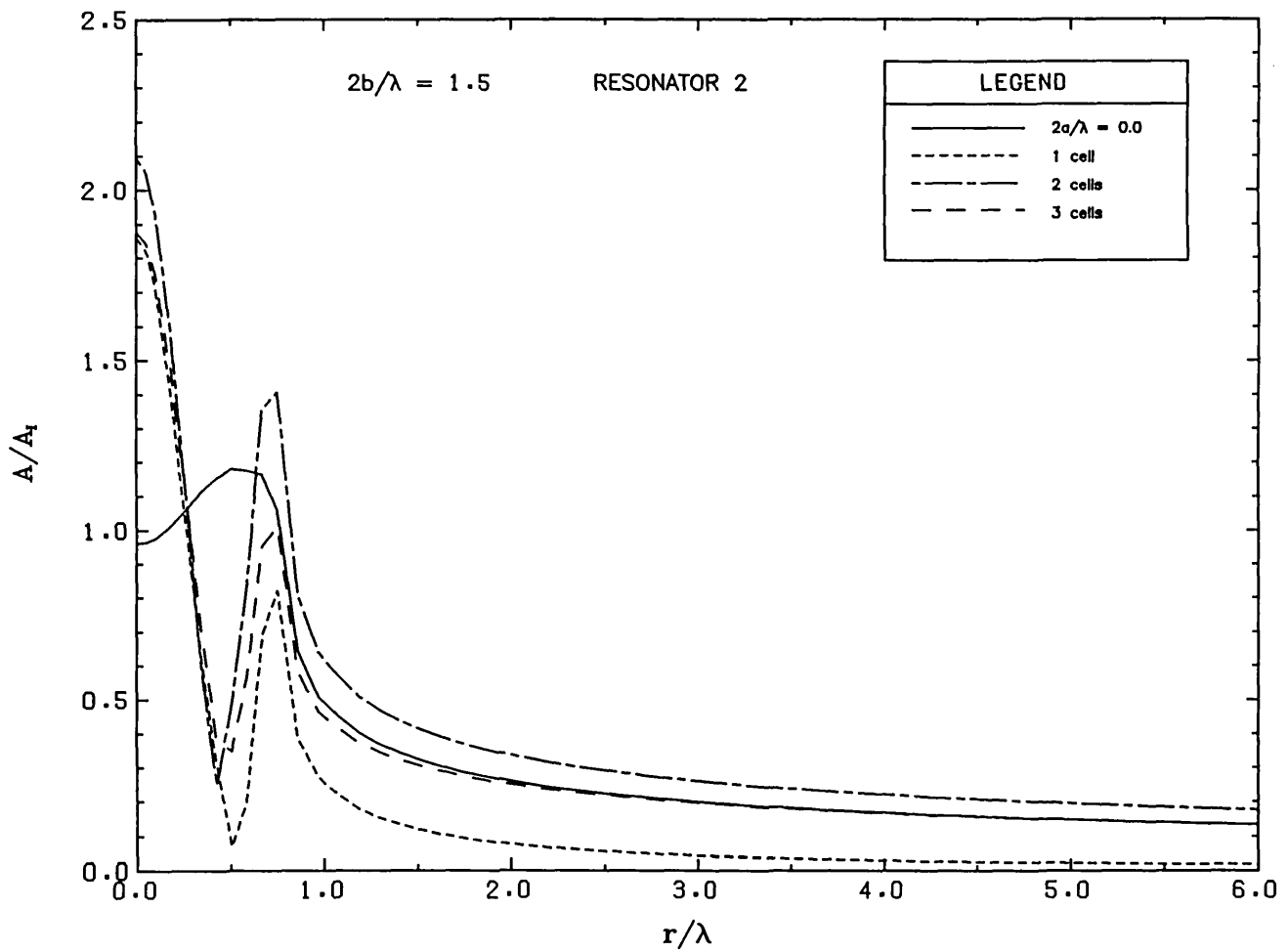

Fig. 5.25b PROFILES ALONG BREAKWATER

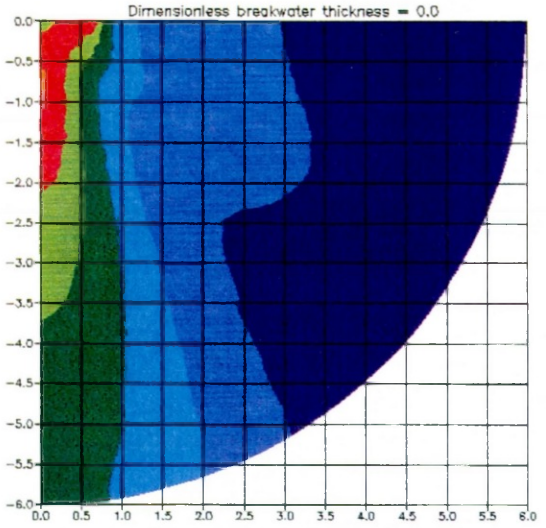

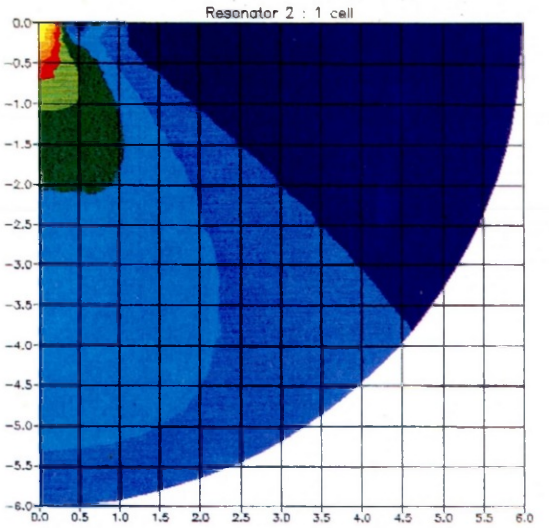

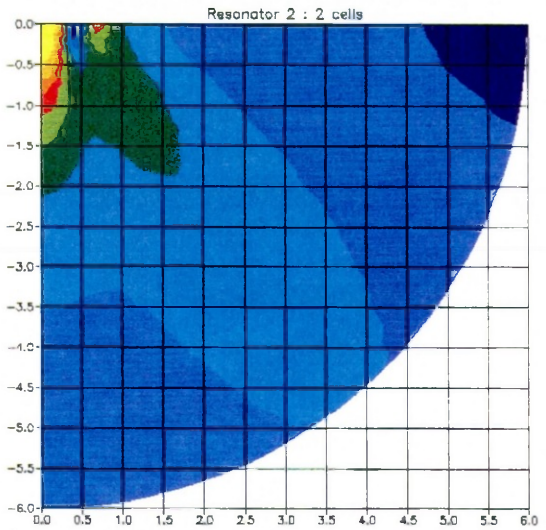

$2b/\lambda = 1.5$

Fig. 5.25 c
Amplitude
contours

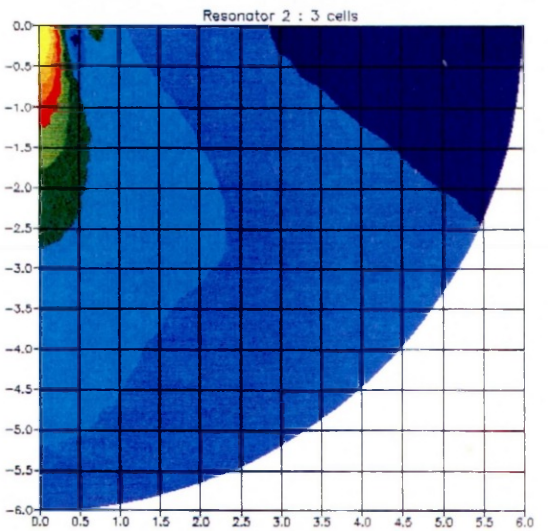

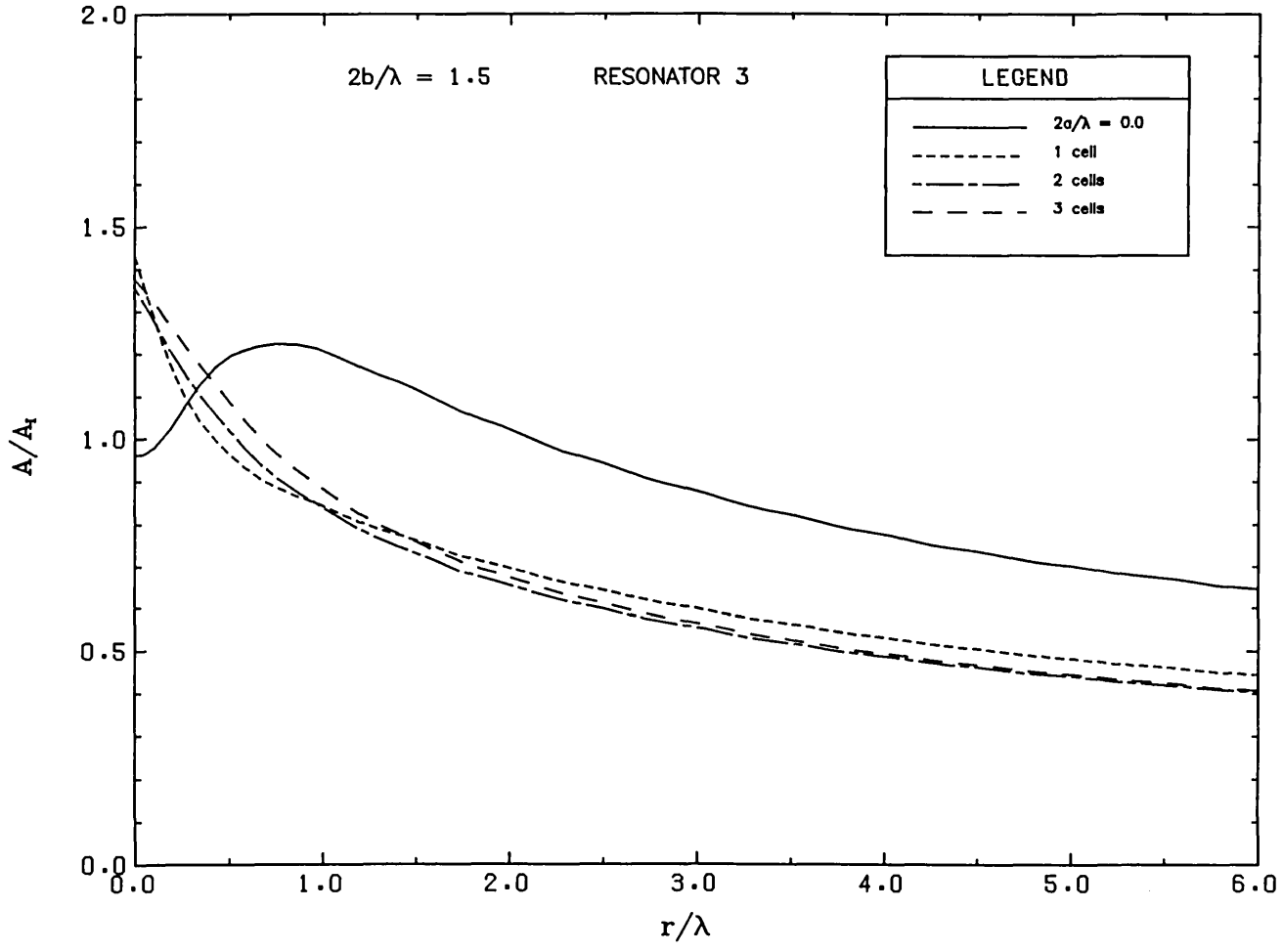

Fig. 5.26a PROFILES ALONG INCIDENT WAVE DIRECTION

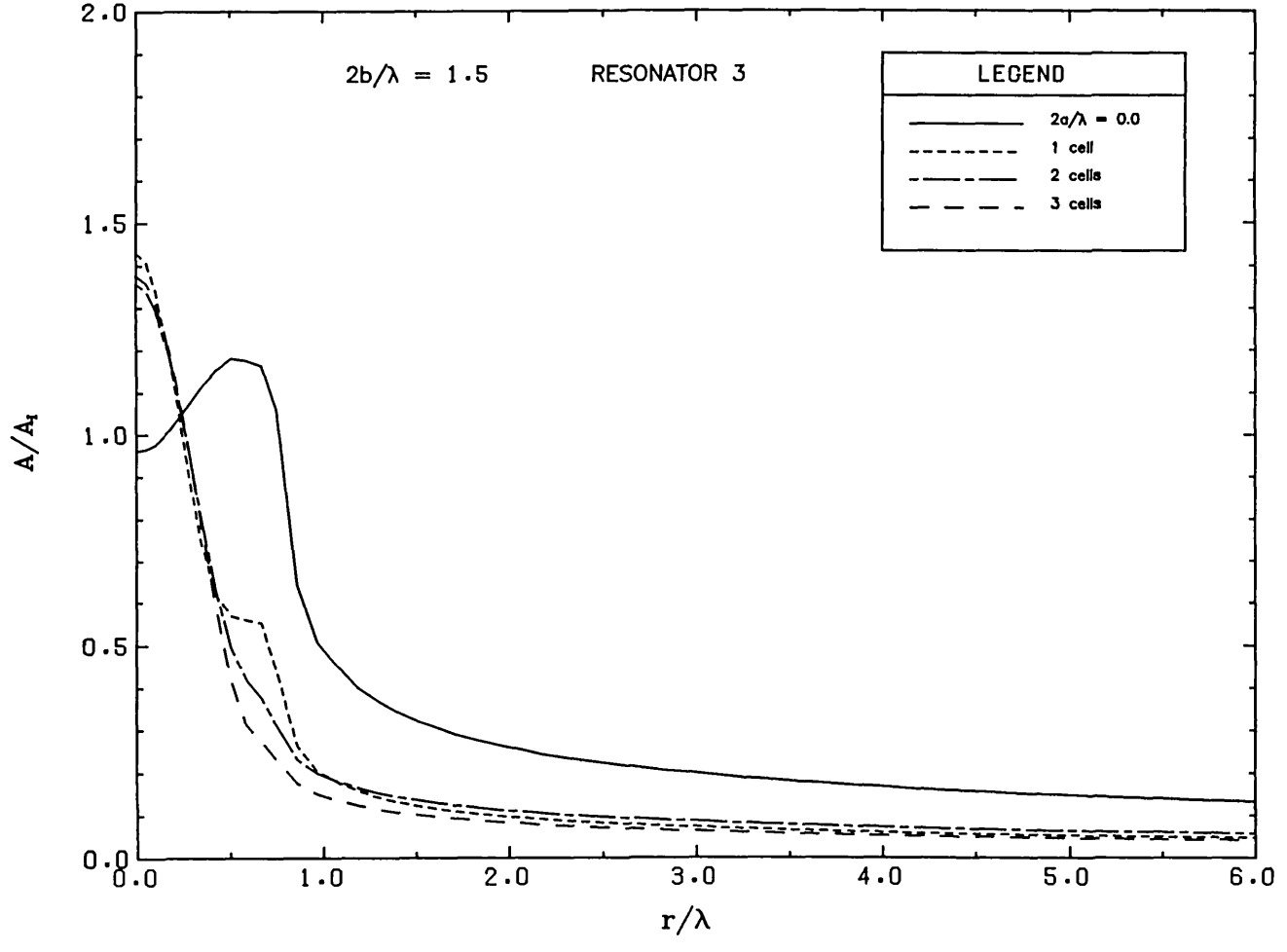

Fig. 5.26b PROFILES ALONG BREAKWATER

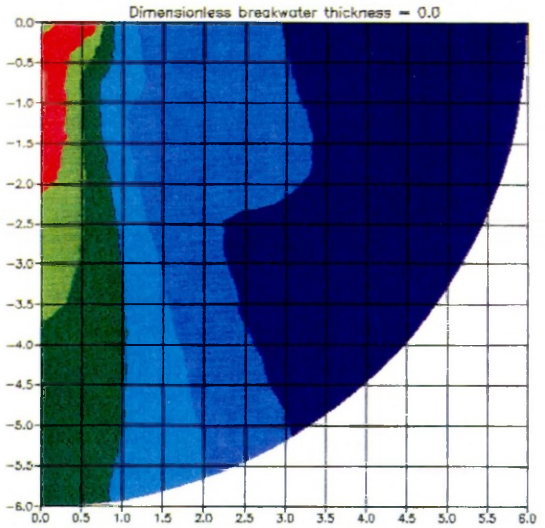

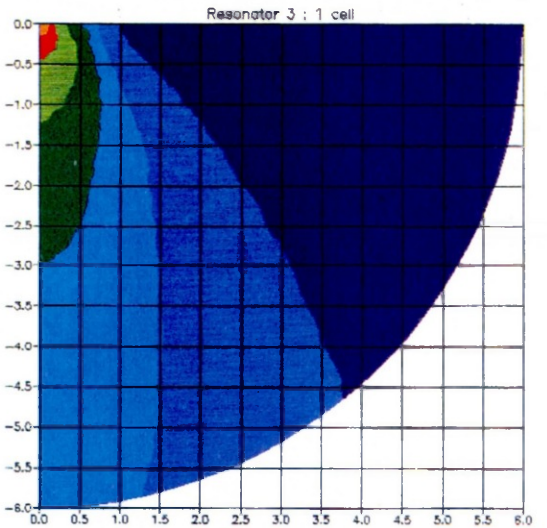

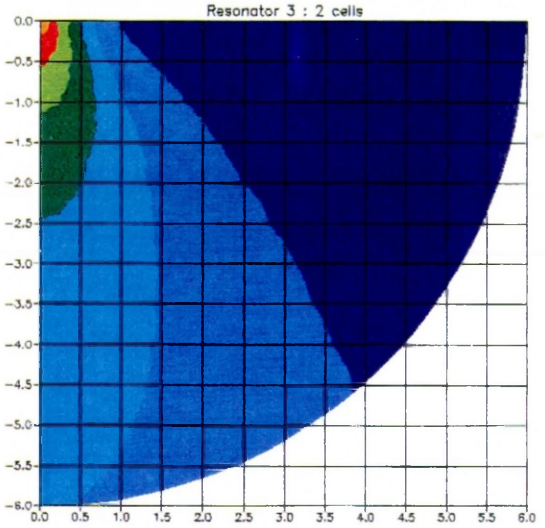

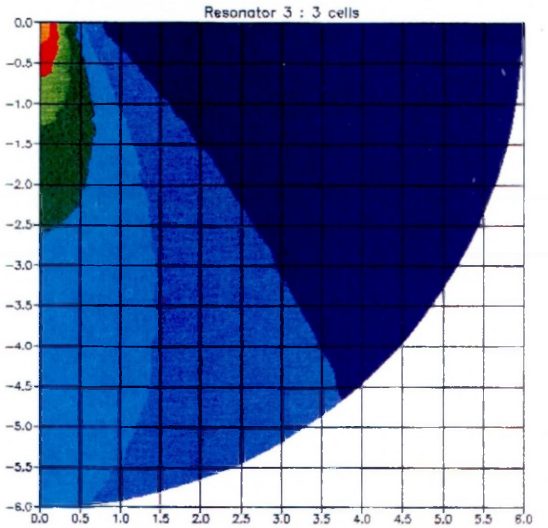

$2b/\lambda = 1.5$

Fig. 5.26 c

Amplitude contours

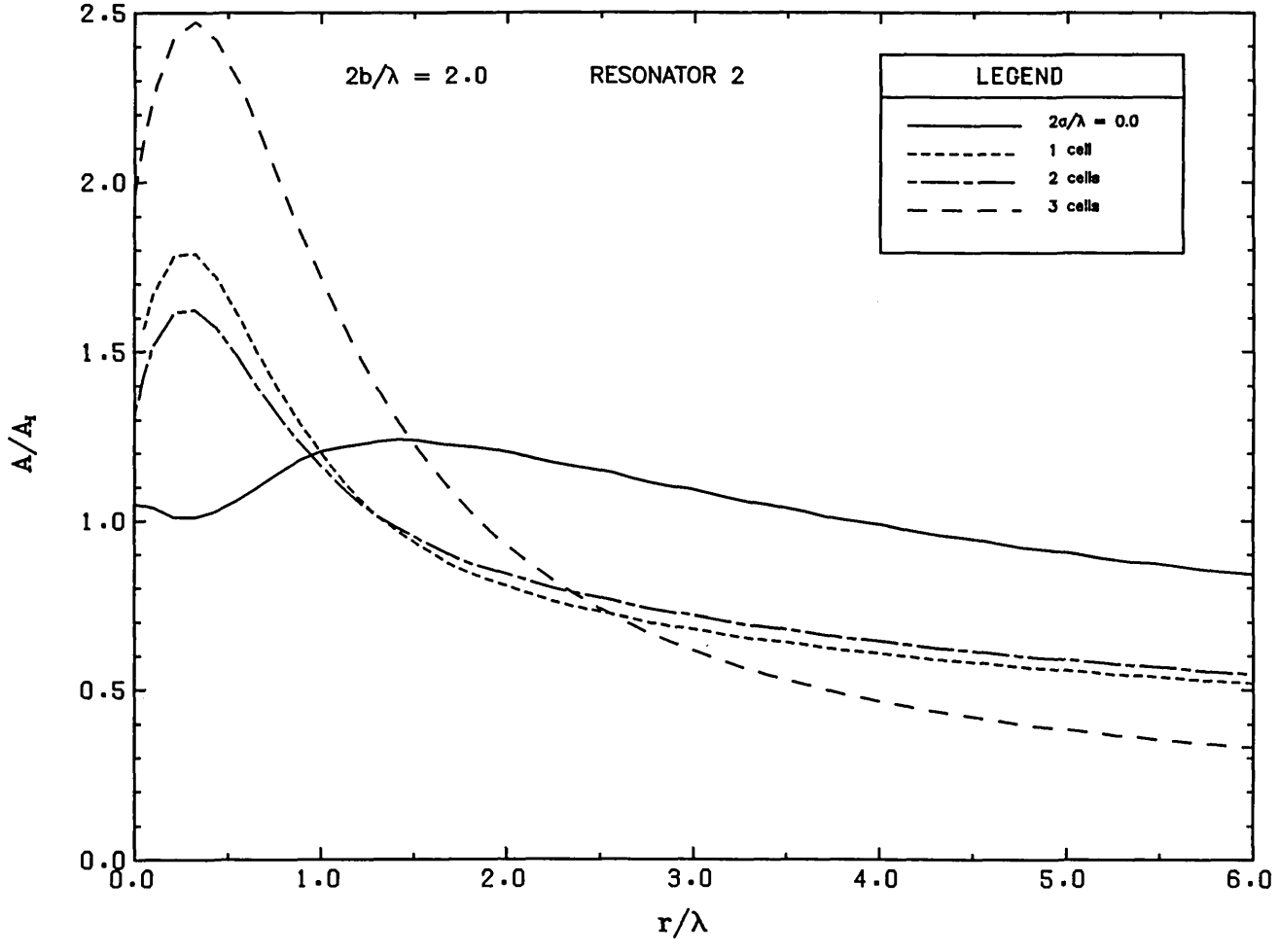

Fig. 5.27a PROFILES ALONG THE INCIDENT WAVE DIRECTION

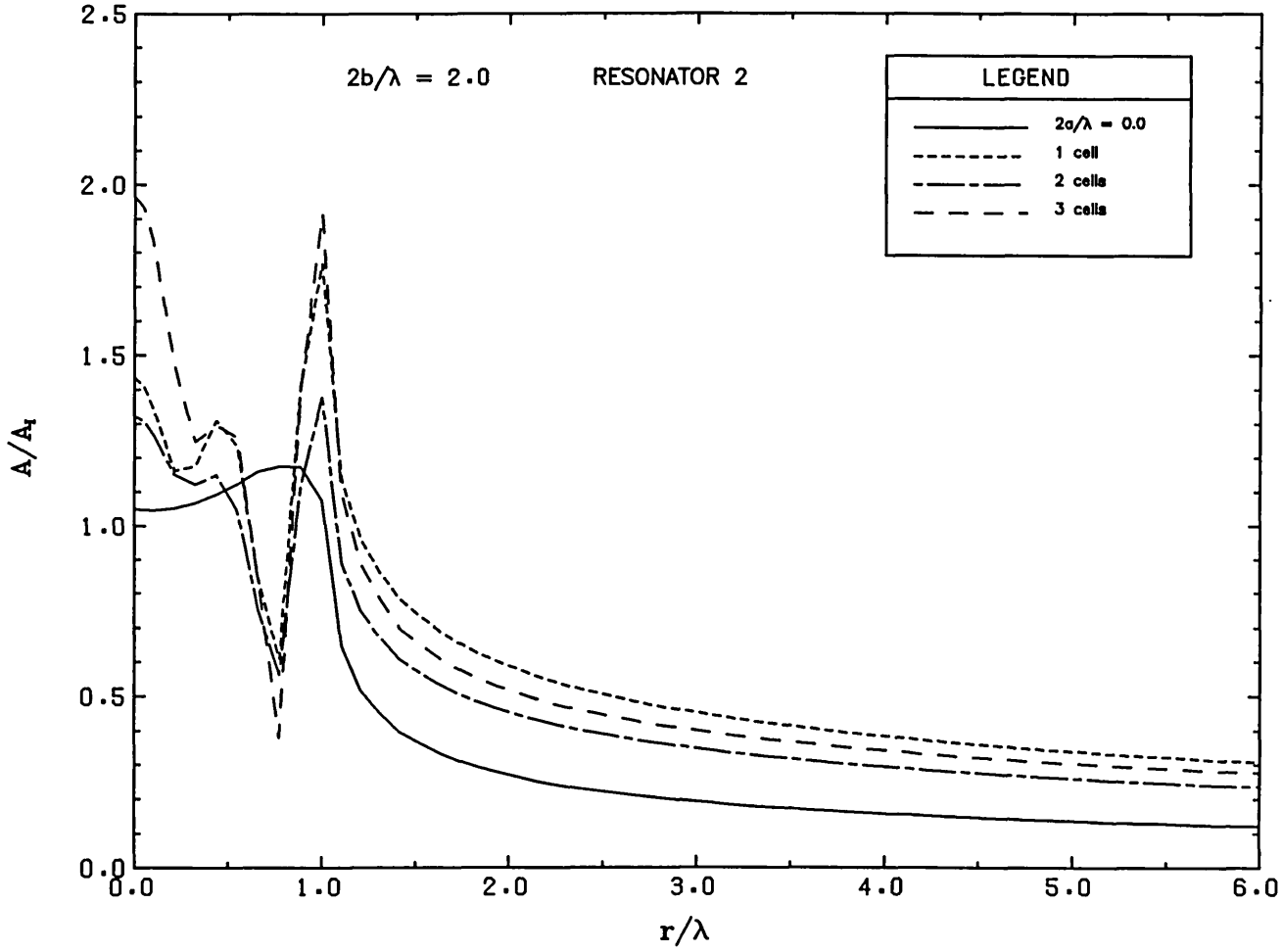

Fig. 5.27b PROFILES ALONG THE BREAKWATER

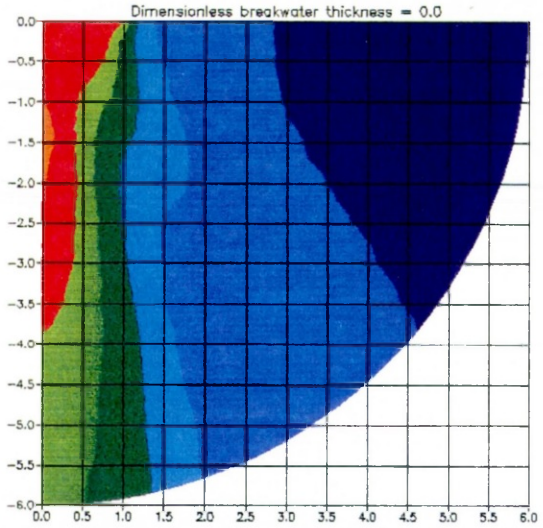

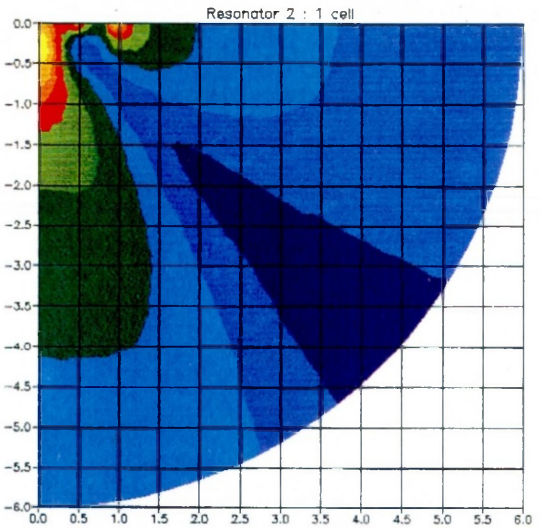

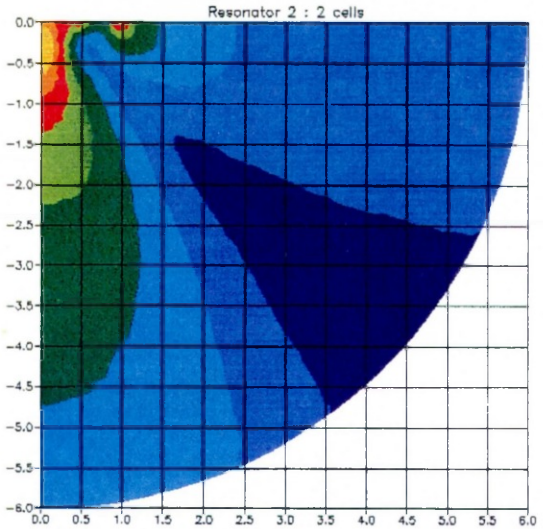

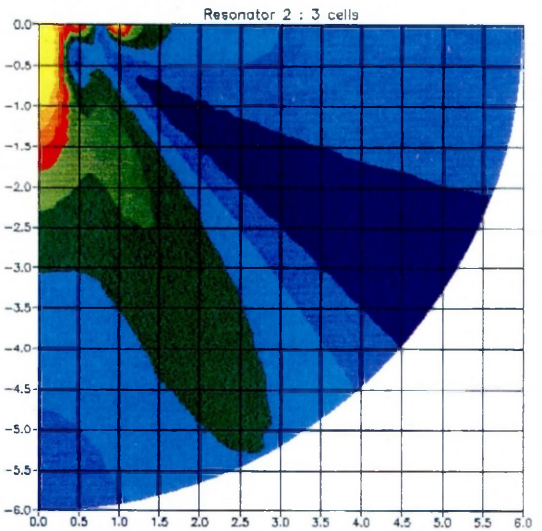

$2\,b/\lambda = 2.0$

Fig. 5.27c

Amplitude contours

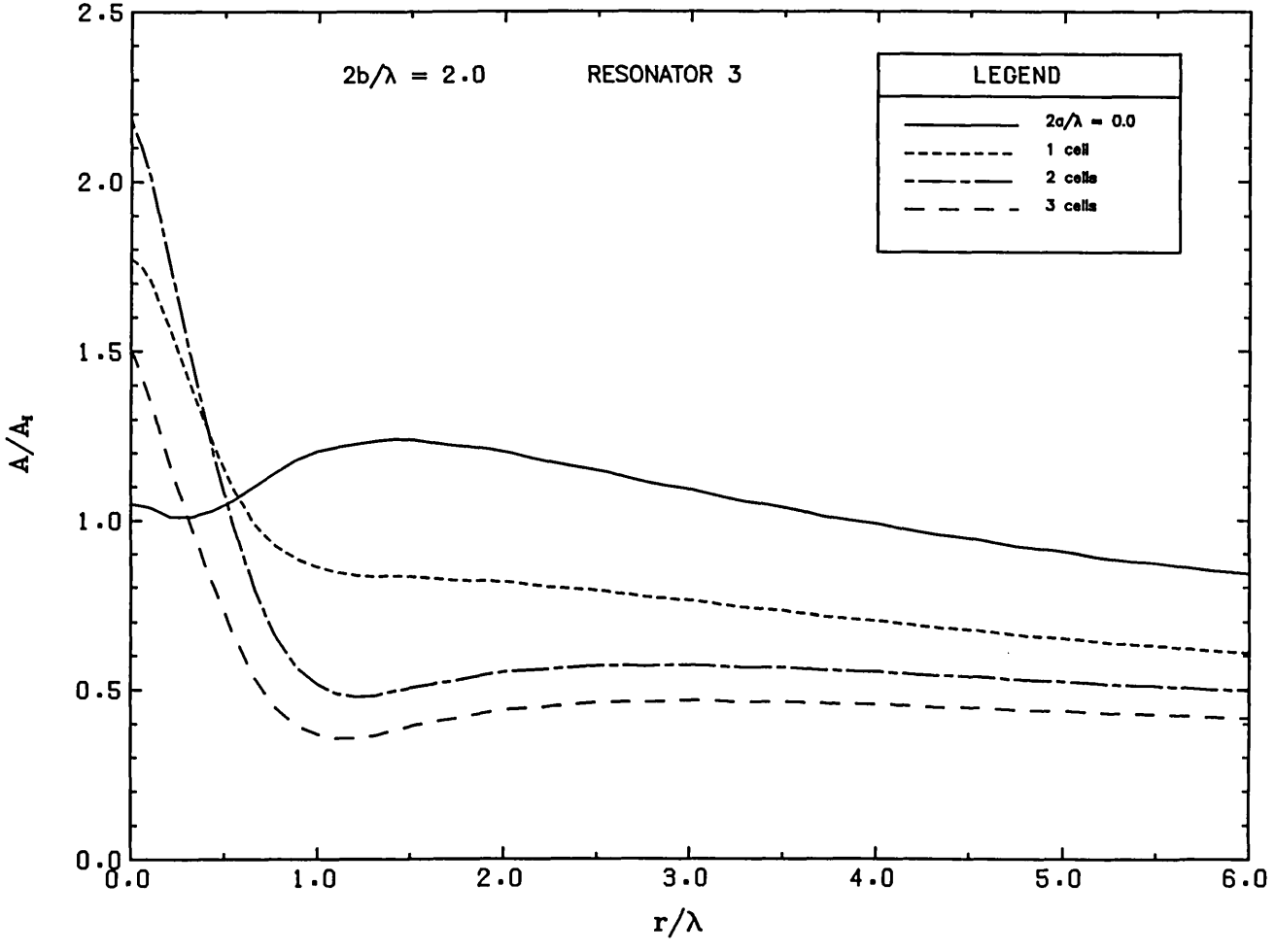

Fig. 5.28a PROFILES ALONG INCIDENT WAVE DIRECTION

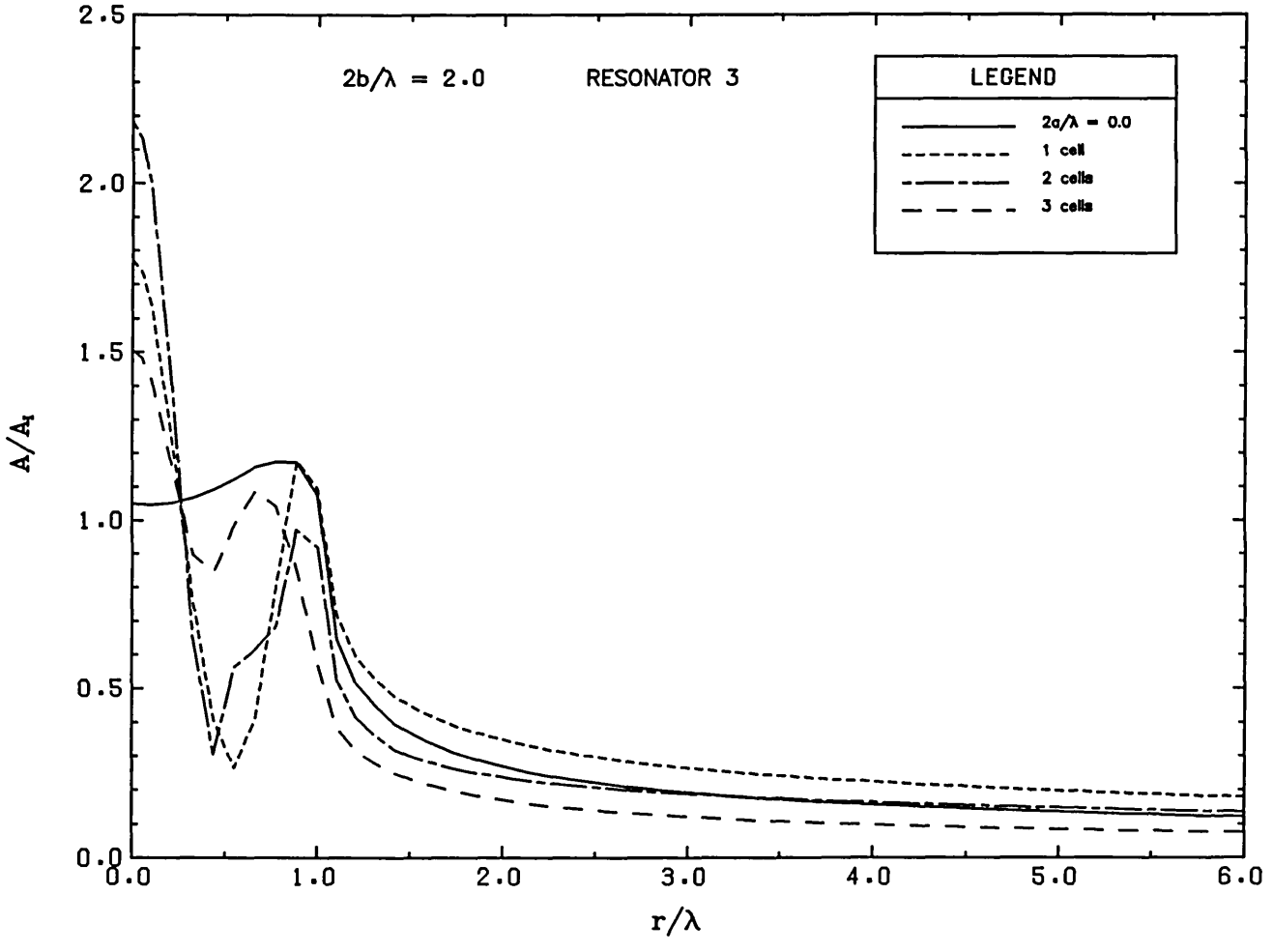

Fig. 5.28b PROFILES ALONG BREAKWATER

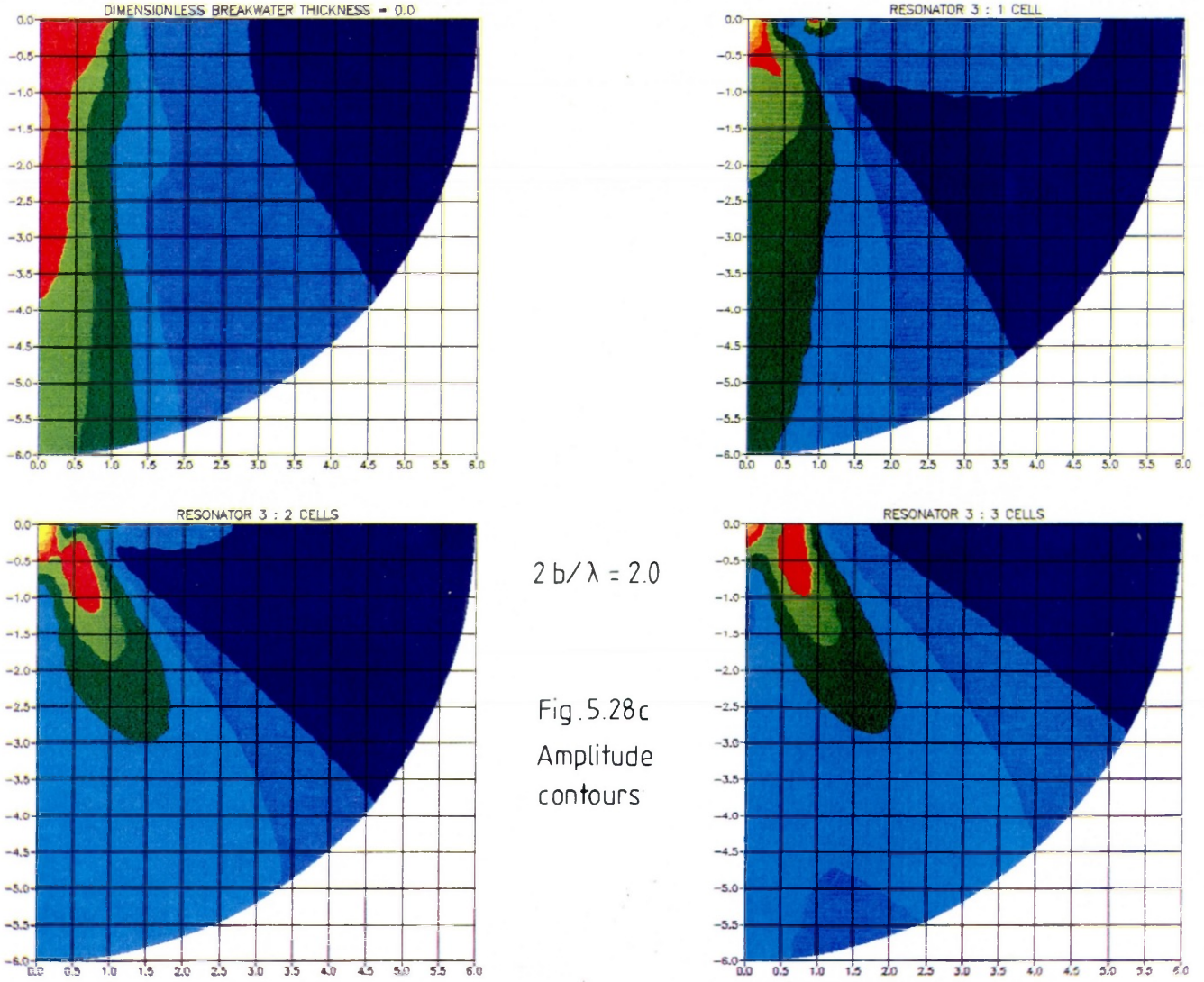

$2b/\lambda = 2.0$

Fig. 5.28c
Amplitude
contours

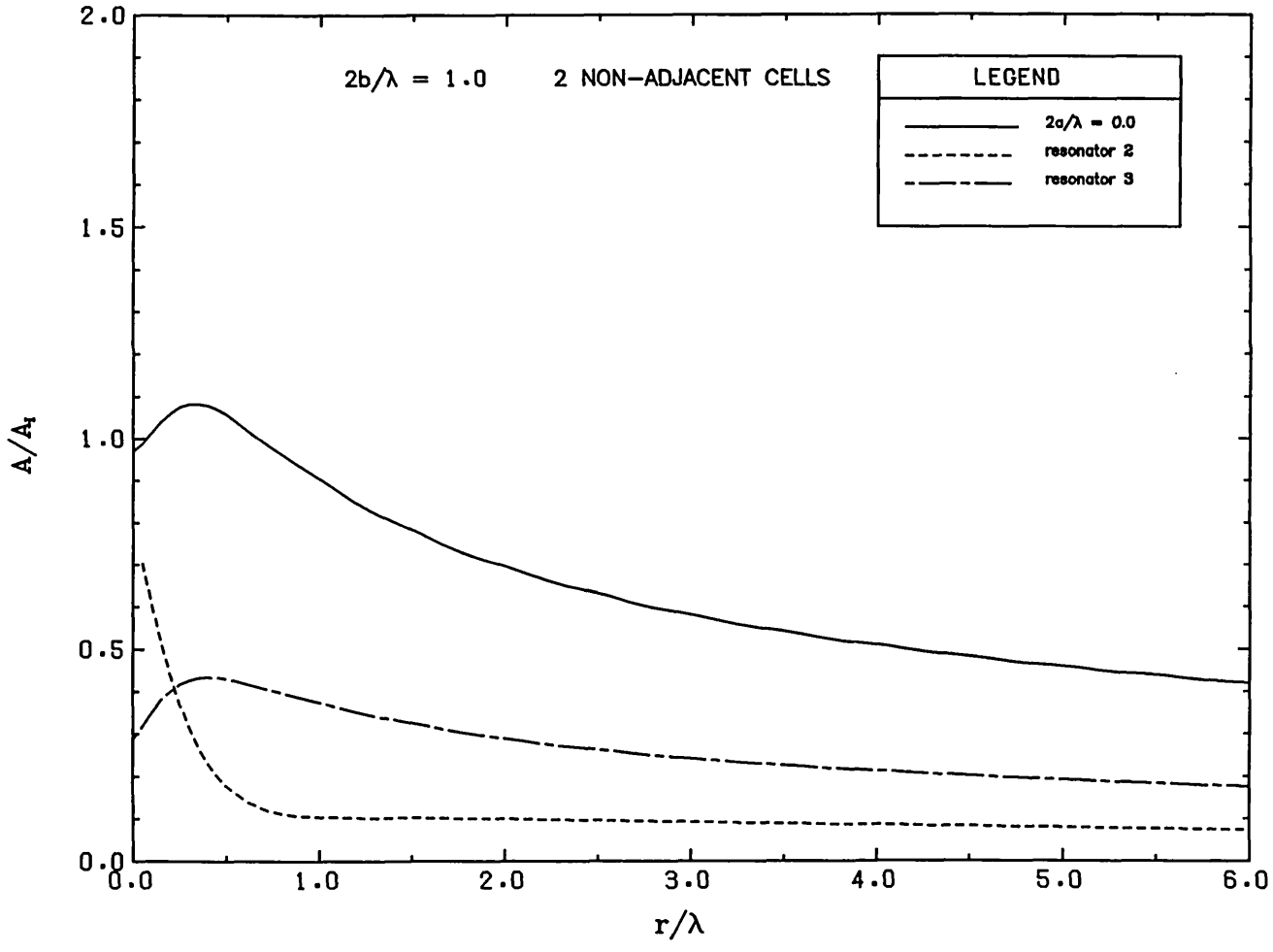

Fig. 5.29a PROFILES ALONG INCIDENT WAVE DIRECTION

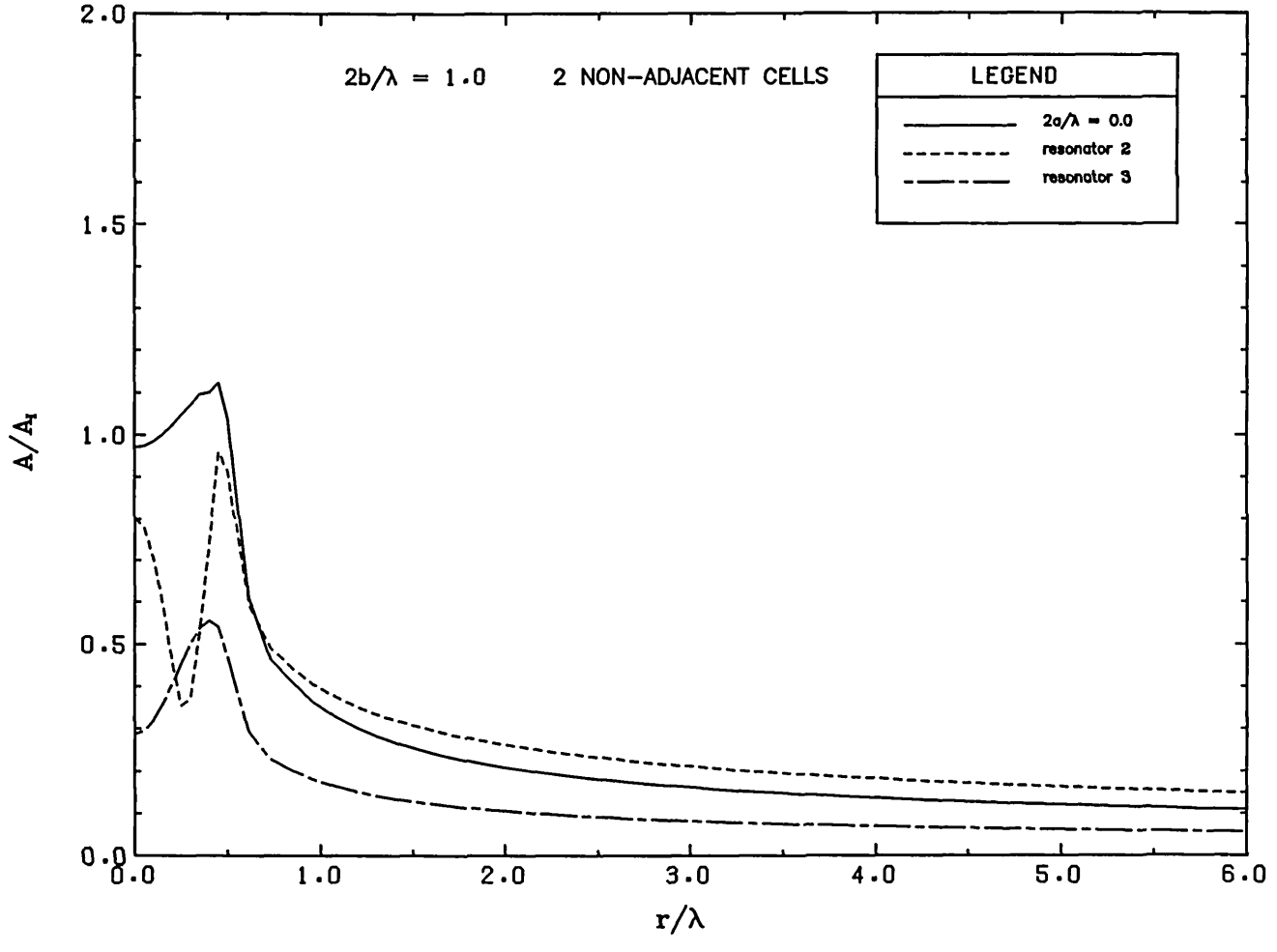

Fig. 5.29b PROFILES ALONG BREAKWATER

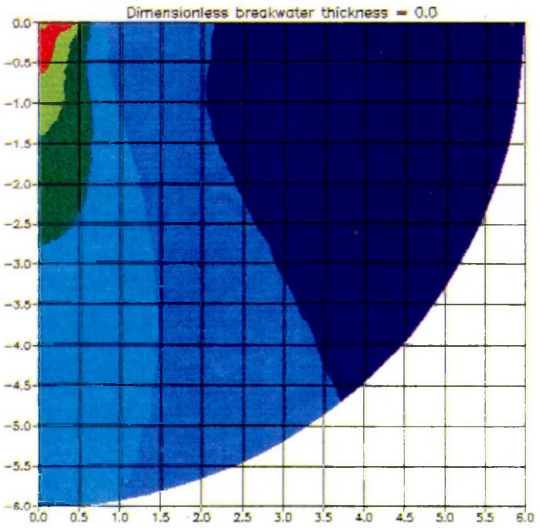

$2b/\lambda = 1.0$

Fig. 5.29c

Amplitude contours

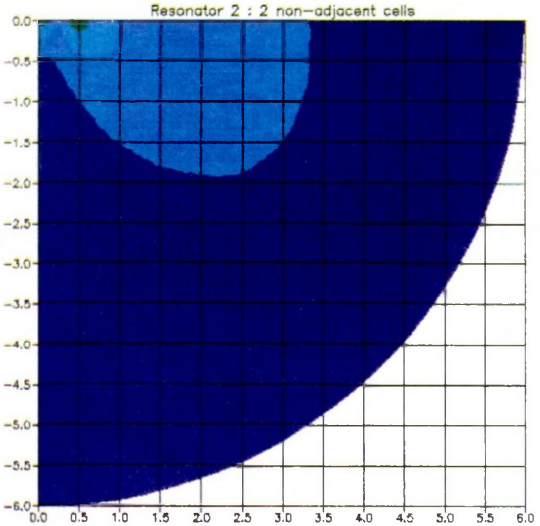

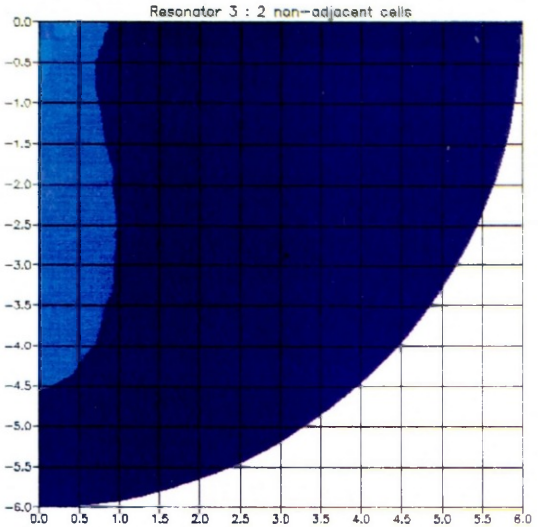

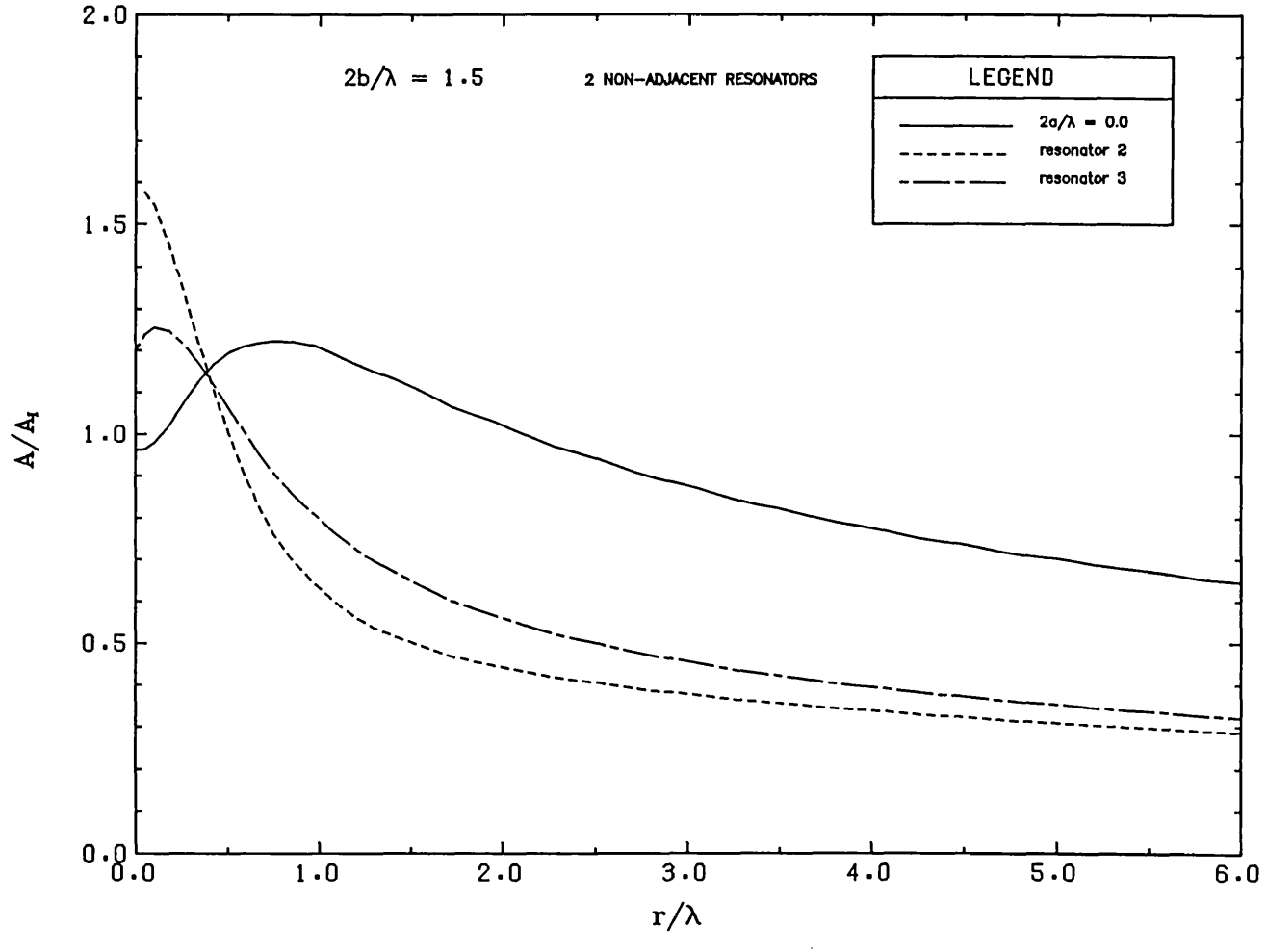

Fig. 5.30a PROFILES ALONG INCIDENT WAVE DIRECTION

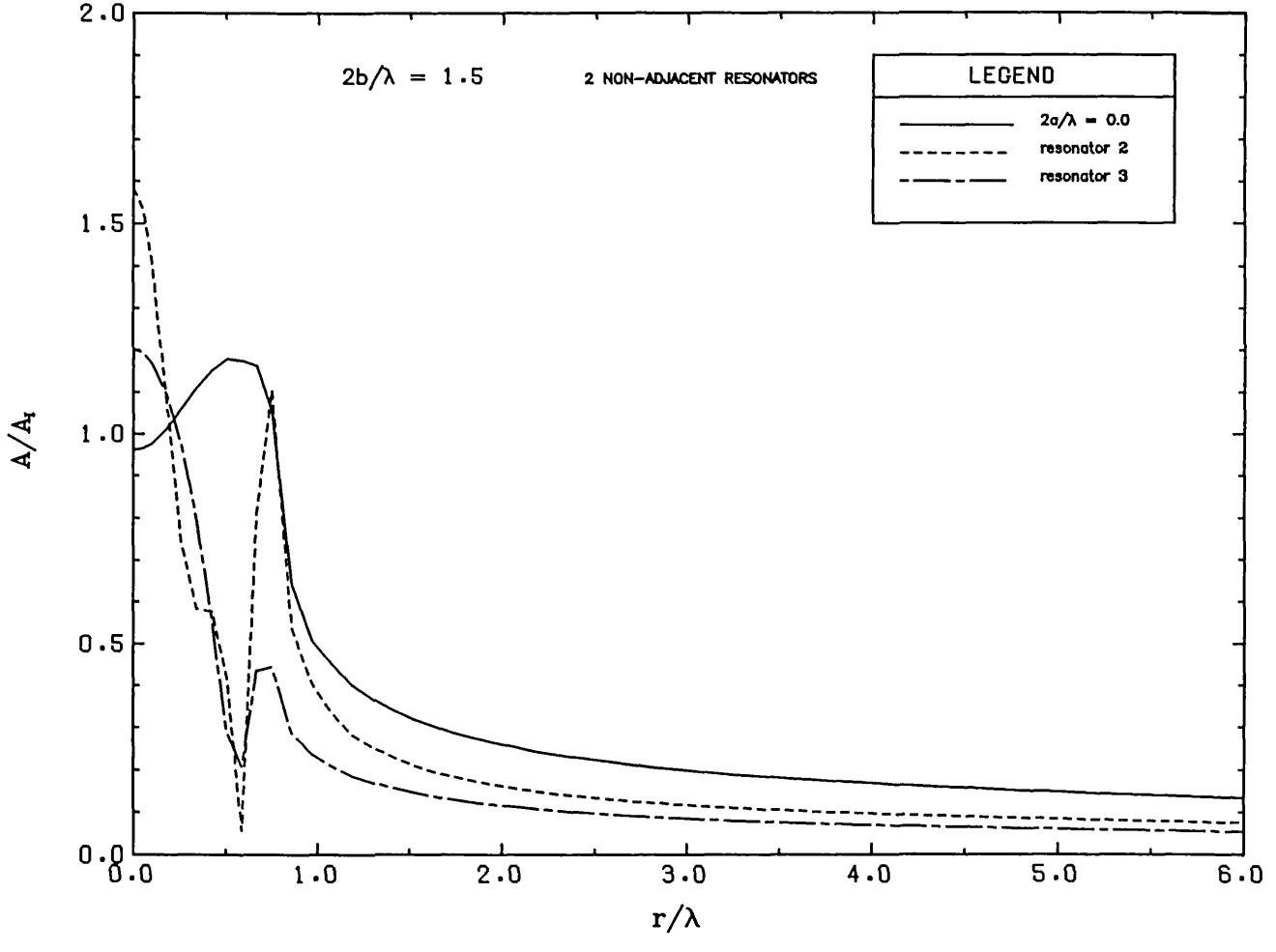

Fig. 5.30b PROFILES ALONG BREAKWATER

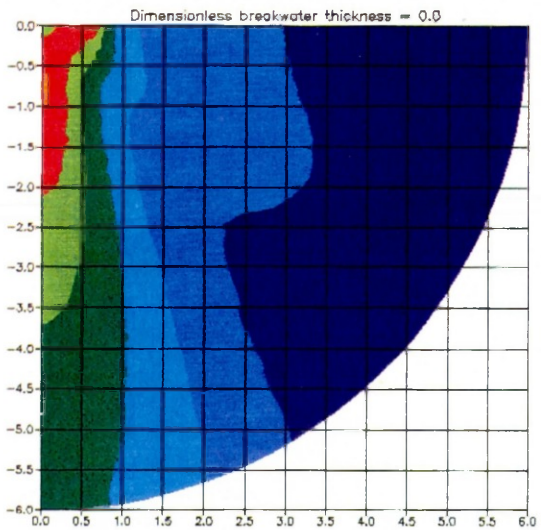

$2b/\lambda = 1.5$

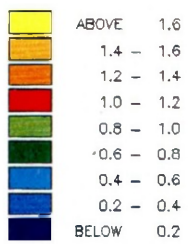

Fig. 5.30 c

Amplitude contours

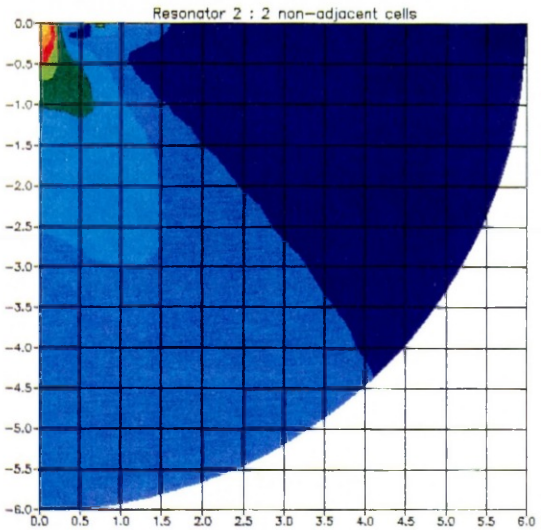

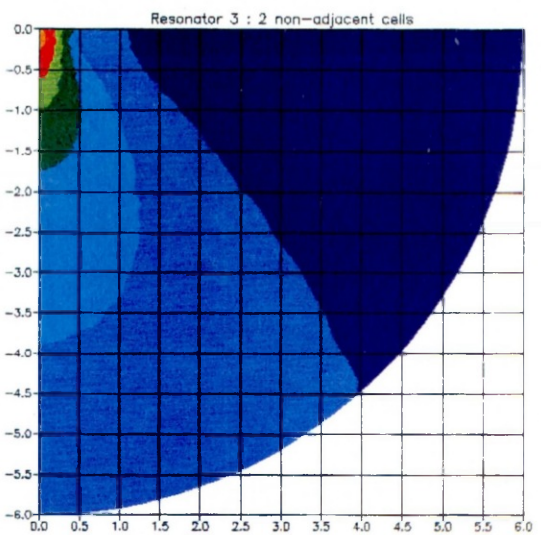

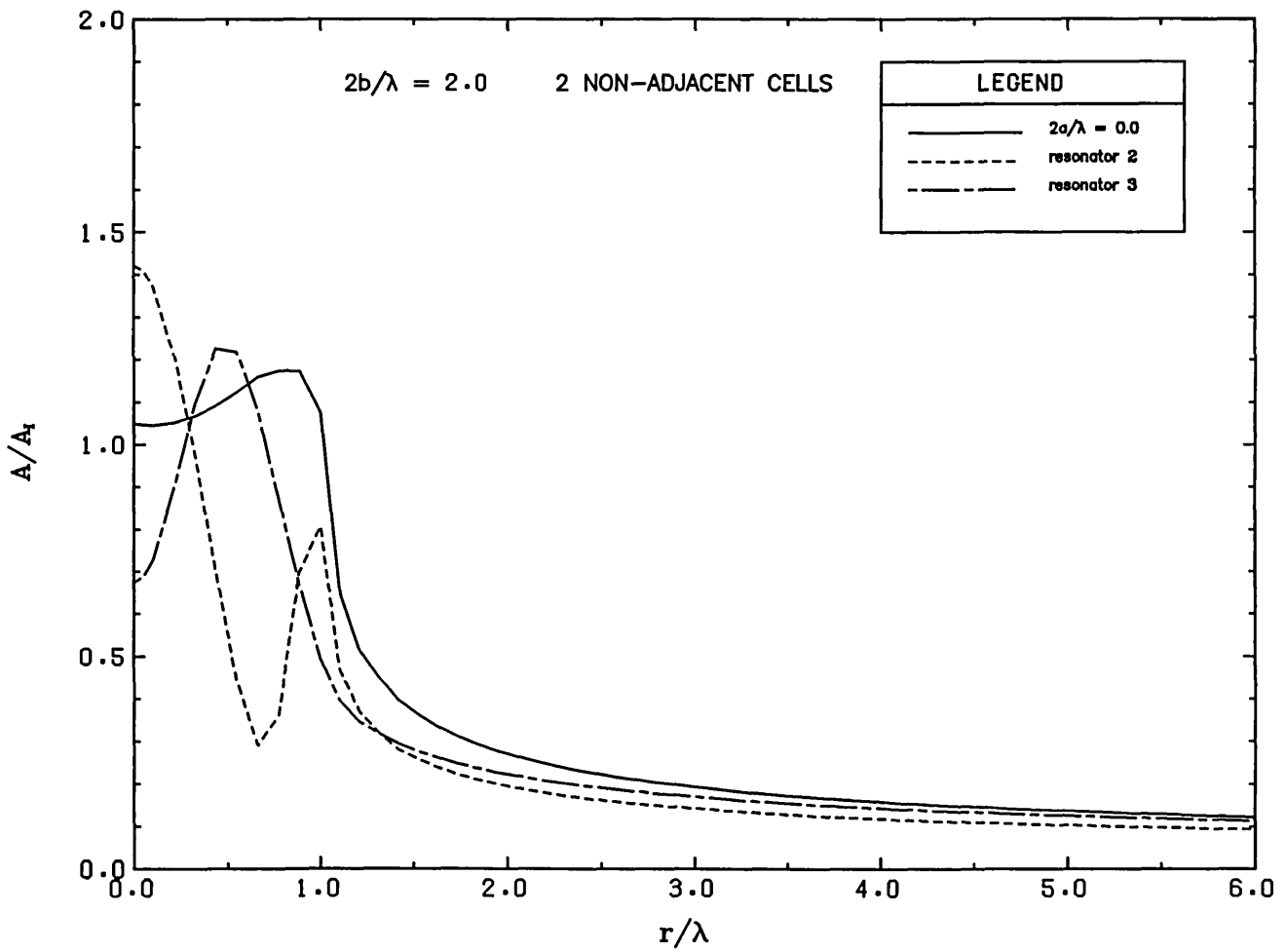

Fig. 5.31b PROFILES ALONG BREAKWATER

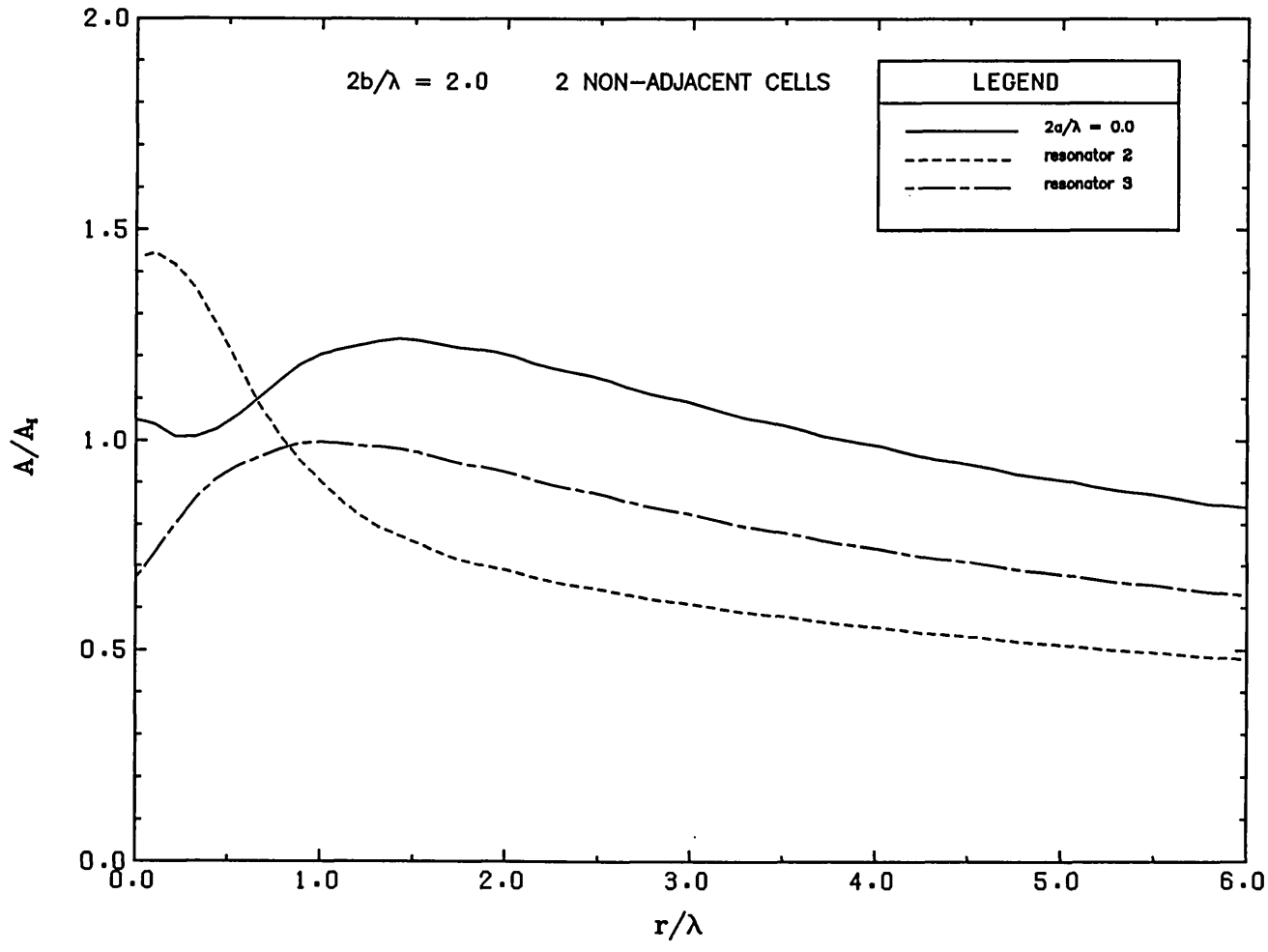

Fig. 5.31a PROFILES ALONG INCIDENT WAVE DIRECTION

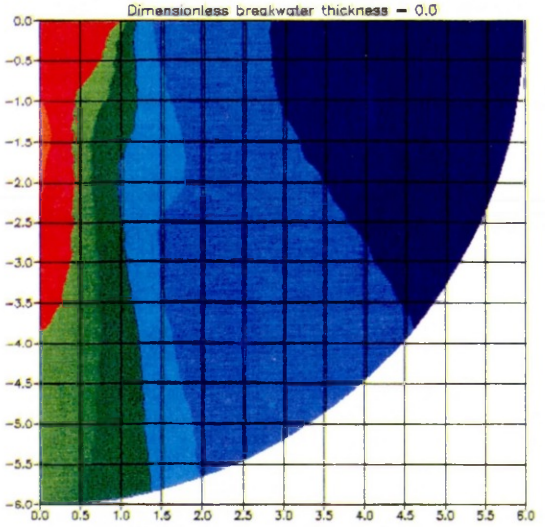

$2b/\lambda = 2.0$

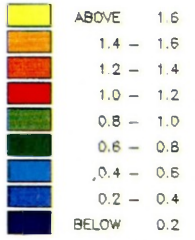

Fig. 5.31c

Amplitude contours

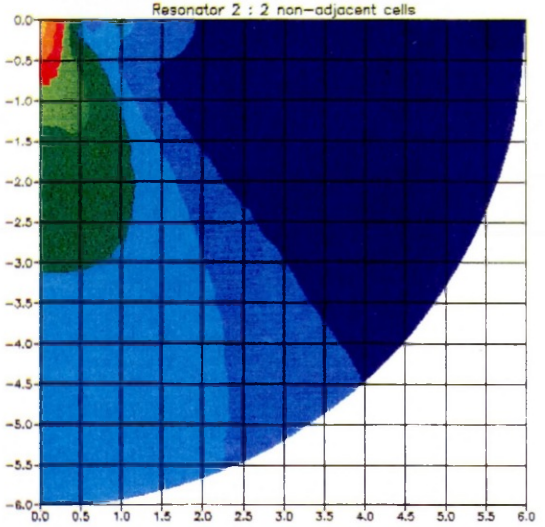

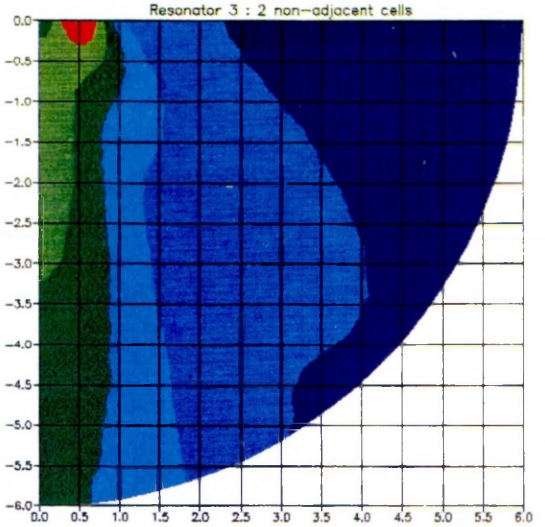

CHAPTER SIX
A model harbour

Our investigations of surface disturbances in harbours have so far been confined to models that are not bounded by coasts, where waves diffracting through the gap can propagate freely to infinity and diverge in the usual manner. This physical idealisation cannot be taken up when dealing with fully bounded harbours as their behaviour is strongly influenced by internal reflections, which have hitherto been absent. These are undesirable as they can lead to a massive accumulation of energy, especially when the frequency of excitation is close to one of the natural frequencies of the enclosed body of water. Such reflections can nevertheless be minimised by employing gently sloping inner boundaries so as to promote the breaking of the shorter waves; with incidence of longer period, the embankments would effectively act as vertical barriers, resulting in very little energy dissipation. Therefore, in order to extend the usefulness of our previous work and make it more applicable to real problems, the resonant oscillation characteristics of a finite–size harbour are examined in the following pages. In keeping with the general aim of this thesis, emphasis is placed on the design of efficient entrances which limit the adverse effects produced by the resonance phenomenon. In this connection, two different configurations (shown in figures 6.2a–b) have been studied: a channel and a resonator. The harbour geometry adopted is that proposed by Behrendt(1985), shown in figure 6.1, which is simple but fairly realistic.

Behrendt developed a finite element model based on linear shape functions for the combined diffraction–refraction problem, and modified it to include the effects of boundary absorption and bottom friction. This was then applied to calculating the response of the harbour for a single incident wave of period 9 seconds, whereupon it was deduced that such dissipative forces serve to substantially inhibit the build–up of high amplitudes. However, as the bottom friction was calculated for a very rough bed and for rather high waves, the damping was exaggerated in comparison with what one might find in nature. The same harbour was also utilised by Dong and Al–Mashouk(1989) to assess the perfomance of a transient numerical wave model in relation to the steady–state representation developed in this work. The former was a hyperbolic formulation of the mild slope equation, similar in form to a system of shallow water wave equations. It was found that at resonance the transient model required an exceedingly long numerical run time to attain steady–state conditions and even then, entire convergence could not be achieved.

In the first part of the present study, we derive the response of the harbour for a discrete set of wavelengths, ranging from 100m to 10,000m. These correspond to periods of between 9.33 seconds and 13.74 minutes if the uniform depth is taken to be 15m, as was done by Behrendt. Such a range is quite comprehensive as it covers a wide spectrum, from the wind–generated gravity and infragravity waves to tsunamis. According to Wilson(1965), critical surging of ships tends to occur as a result of excitation at periods of 25 seconds to 2 minutes. This work would therefore also provide adequate data for the dynamic analyses of moored vessels. In following previous work, all solid boundaries are assumed to be fully reflecting and all energy losses are neglected other than radiation damping. Only cases of normal incidence have been considered and consequently, due to symmetry, half the domain was discretised as shown by the finite element mesh of figure 6.1.

Following Lee(1971), the response of a harbour is defined as the variation of the amplification factor with the wavenumber parameter, kB; k being the wavenumber and B is a characteristic planform dimension of the harbour which in our case is taken to be the width, B=390m. The amplification factor inside the harbour is defined as the water level variation caused by a wave of amplitude, A_i, impressing on the entrance. This is a function of position and was calculated for a point at the centre of the backwall (point A), as this was thought to be a position of maximum agitation. The response curve, plotted in figure 6.3, displays several interesting features. Looking first at the low frequency end, we notice that the lowest mode of resonance leads to a severe amplification which reaches a value of A/A_i=9.0. This is known as the Helmholtz or pumping mode of oscillation which is characterised by a simultaneous rise or fall of the water level in the basin, high velocities in the entrance and the absence of any nodes or antinodes. As the wave frequency increases, the behaviour is seen to become more irregular. At a wavelength of about 129m, a quite severe and sharp resonance peak, of amplitude A/A_i=12.0, is observed. The reason for the occurence of this is due to the fact that at that particular frequency, the dimensions of the harbour basin are such that an integral number of half wavelengths exist both longitudinally and transversely. The phase interactions between the two standing waves lead to substantial reinforcements with obvious consequences. However, as the bandwidth of this resonance peak is very narrow, it may not be so important to moored ship response since the incident energy would also have to have a very sharp spectral peak at this frequency in order to excite such a mode of oscillation. On the other hand, a very broad bandwidth in the response curve indicates that energy almost anywhere within this frequency range can excite that form of motion. Such peaks are seen to occur in the graph

of figure 6.3. As these are potentially easily realised, it is the responsibility of the harbour engineer to undertake the necessary steps at the design stage to eliminate them.

Although energy dissipation has been neglected in the present study, we may nevertheless make a few brief deductions regarding its effect by reference to the work of other researchers. According to Kotense et al(1988), bottom friction may be of considerable influence on the harbour response at resonance, both for laminar and turbulent flow regimes. Also, a small reduction of reflection coefficients, such as might occur in the case of rubble mound breakwaters, may result in a drastic decrease of the harbour response at resonance. Dissipation due to flow separation at the harbour entrance has been examined by Gerber(1986) and found to be more critical for the lower modes of oscillation which are characterised by large horizontal velocities. We may therefore expect our response curve of figure 6.3 to be a theoretical 'upper limit' of the actual behaviour.

6.1 Channel

The impedance characteristics of an entrance channel are assessed in this section to determine whether any improvements in wave conditions can be achieved by the utilisation of such structures. A length of 100m was chosen, which might seem somewhat exaggerated in absolute terms, but in comparison with the range of wavelengths considered, the channel would range widely in classification from being insignificantly short, at the low frequency end, to being appreciably long for the higher frequency waves. A harbour response curve has been derived as before for this new geometry and is plotted along with that of the previous case in figure 6.4. A comparison between the two reveals that the effects of the channel are to a large extent governed by the relative width of the gap.

With the shorter waves, the two curves are almost identical which implies that the channel serves no useful purpose. With reference to our work on semi–infinite harbours, we may attribute this to the very weak reflections which would then occur at the open ends. Obviously, if the waves were made very short, a beaming effect might start to dominate which would radically alter the wave field. However, in order for this to happen and be noticeable, wavelengths of the order of 40m or less would be required. Although these are outside our range, such short waves would correspond to periods of less than 5 seconds and as such would not be of any practical consequence as they are rapidly attenuated.

With the longer waves, we encounter what has been previously termed the channel paradox: at resonance, the amplification factors are seen to increase,

while at non–resonant frequencies the response is diminished, as the channel is introduced. The former is especially apparent for the Helmholtz mode of oscillation where a near doubling of amplitudes occurs. In our analytical work on the transmission of long waves through short channels, it was deduced that significant impedance properties were afforded by such configurations, provided the harbour was of an unbounded nature. In the present context, the channel plays the dual role of impeding both the inflow and outflow of energy. At resonance, the radiation damping is critical in order to maintain finite amplitudes throughout the harbour. If this is impaired, by placing a channel at the mouth for example, very high amplitudes ensue. Although the penetration of waves is also impaired, this is more than offset by the diminution in re–radiation back through the entrance. On the other hand, if resonance does not occur, the radiation damping would be much reduced and the channel would then act to curtail the response. This is then in accordance with the observed trends.

To illustrate the above effects further, amplitude contours have been plotted for four wavelengths that were deemed representative of the behaviour. These are λ = 500.00m, 377.00m, 163.36m and 100.00m. The variations in only half the harbour have been displayed due to the symmetrical conditions. Considering first the longest wavelength, λ=500.00m, which corresponds to a minimum on the response curve, we notice that the amplitudes everywhere are diminished as a result of the channel. For λ=377.00m, the reverse trends are observed as this is a point of resonance, or a maximum, on the curve. The channel is then seen to augment the amplitudes by as much as 50% in some areas. The plots for the two other wavelengths show that the two cases of the harbour having and not having an entrance channel, have indistinguishable patterns which demonstrates the afore–mentioned short–wavelength trends.

6.2 Resonator

With the objective of limiting the adverse amplifications that occur inside the basin at resonance, quarter–wavelength resonators placed at the harbour mouth are now investigated. When their lengths are fixed, these structures would be 'tuned' to reflect waves of single frequency and accordingly, it is important that these should correspond to troublesome modes of basin oscillation. Obviously, this type of resonator would be highly impractical for impeding long waves because of the necessary length. We are therefore confined, in our present problem, to studying the behaviour of the shorter waves. Six wavelengths were chosen for this purpose: λ= 213.00m, 129.00m, 125.66m, 122.52m, 108.91m and 100.00m. On inspecting the harbour response curve of figure 6.3, we see that all

of these correspond to points of severe resonance which was the basis of our selection criterion. The width of the resonator was taken to be 30m, making it intermediate to wide in classification over the range of wavelengths considered. The complete geometry is shown in figure 6.2b.

The first step in the analysis involved determining the lengths (l_{opt}) of the resonators subject to the usual condition of maximum induced resonance inside them. For each wavelength, a graph was therefore plotted for the variation, with length, of the amplitude at the backwall of the harbour (point A). An example for the case of λ=108.91m is shown in figure 6.5. The optimum lengths are then those that correspond to the minima of these curves, which were found to be as follows:

λ=213.00m	l_{opt}=47.00m
129.00m	26.00m
125.66m	22.60m
122.52m	24.50m
108.91m	17.42m
100.00m	16.00m

In deriving the above–mentioned graphs, an increment in length of 0.02λ was used as this was thought to be adequate for practical purposes. If this is made smaller, the values of l_{opt} could be further refined, but there is no point in carrying this out as one must always allow for minimum tolerances during construction. A trend was detected in that if the length of the resonator was made less than the optimum, an augmented response resulted. This is believed to be due to the hindrance of the radiation damping by virtue of reverse phase interactions.

The original harbour response curve has been plotted again in figure 6.6, incorporating the points corresponding to the six wavelengths where the resonators have been employed. For a better comparison, amplitude contours have also been plotted for half the basin. The results demonstrate the quite remarkable efficiencies achieved with such resonators. Substantial overall reductions in amplitudes are observed for all the cases treated and furthermore, there are no adverse amplifications near the entrance. This latter effect was absent because of the relatively wide resonator geometry. The most severe case of resonance which occurs at λ=129.00m, is seen to be greatly ameliorated by the resonator as the maximum amplitudes are lowered from A/A_i=12.0 to A/A_i<3.0. This represents a 75% reduction which is also attained in the other cases considered. Part of the reason why the resonator was found to be so efficient is because of the relatively small gap width of the harbour. This is 78m which, even by comparison with the smallest wavelength, λ=100m, is deemed to be small (with reference to previous

work).

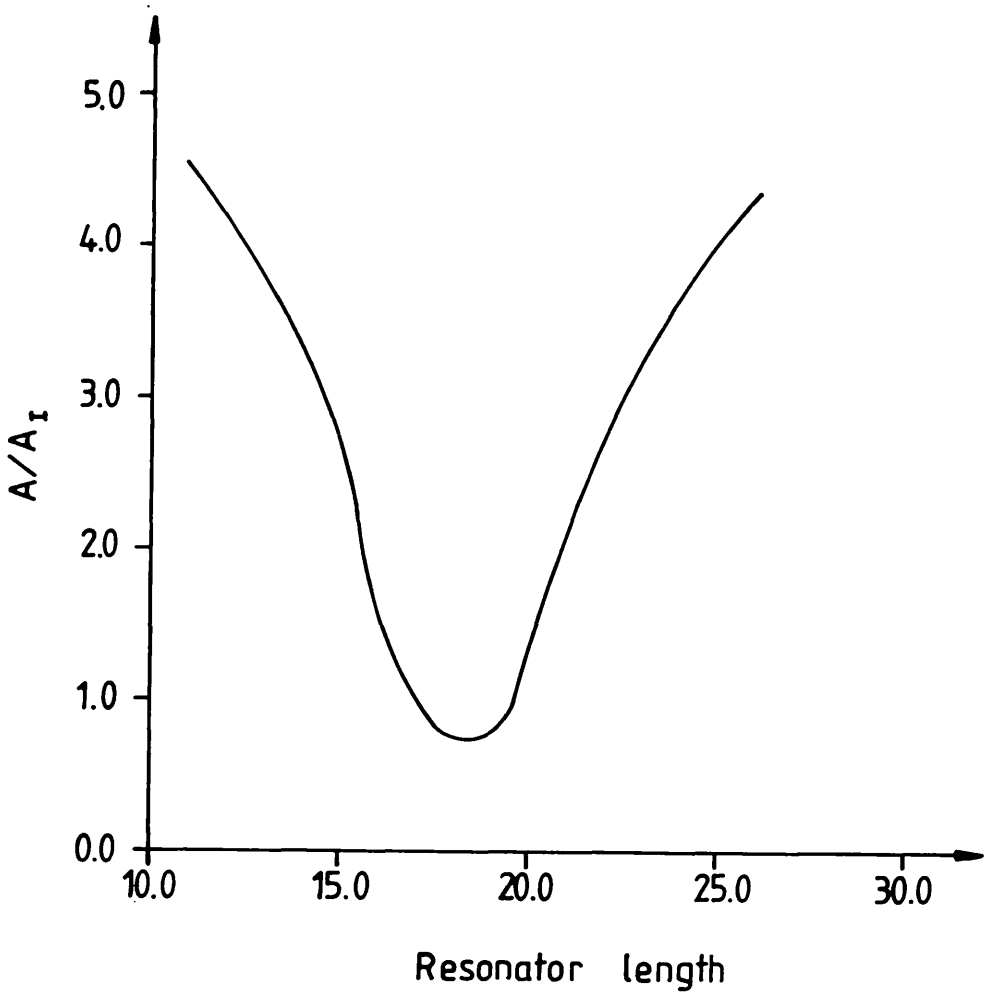

Figure 6.5 Variation of amplitude at point A with resonator length (λ=108.91m)

It is of practical interest to note that certain structures in harbours, like rectangular berths, might act as resonators if suitable conditions prevail. In these adventitious circumstances their effects could be quite adverse, not only to navigation, but to cargo handling operations as well and accordingly, great care must be excercised in their design. One example where this problem might be particularly acute is the harbour at Zeebrugge which is shown in figure 6.7 (diagram taken from the work of Van Damme(1982)). The two berths near the entrance are amenable to excitation because of their shapes and unsheltered layout. Waves amplified by them would not be returned seawards immediately, but would be reflected back into the harbour by virtue of the outer breakwaters. This

process might then lead to severe wave agitation in the vicinity of the mouth and might well have contributed to the capsizing of a cross channel ferry in that location. On the other hand, a form of protection by internal jetties might prove useful were analysis and model studies used to achieve a suitable configuration.

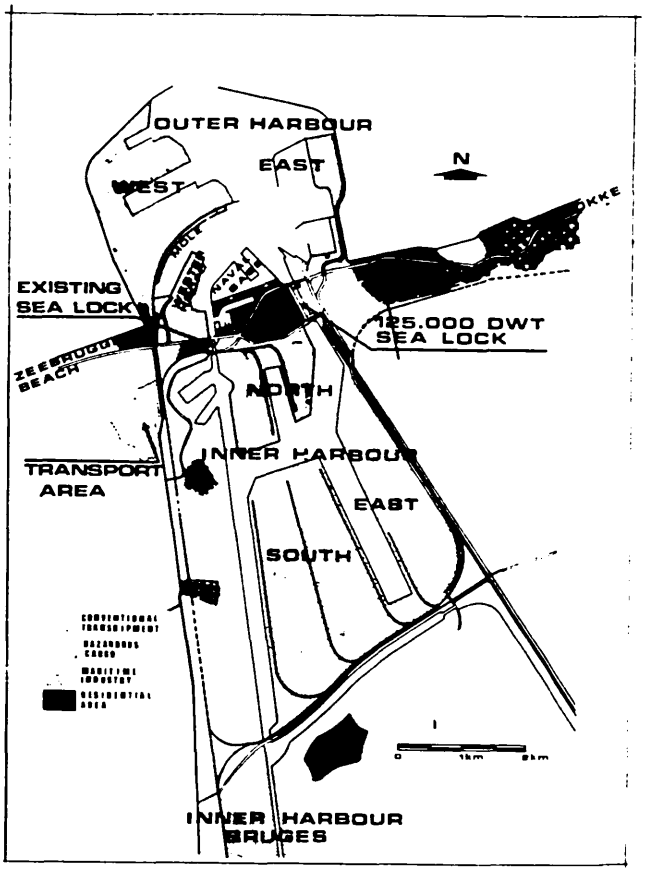

Figure 6.7 General layout of Zeebrugge harbour

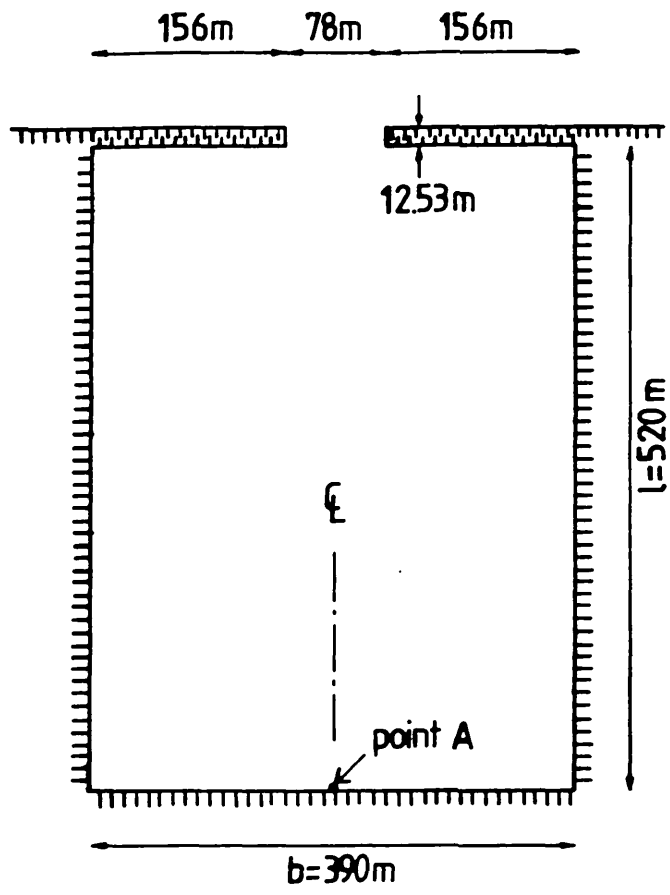

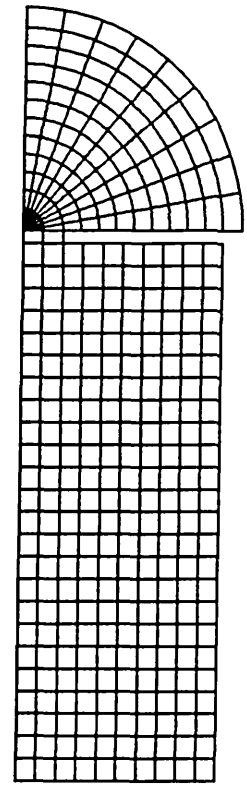

Figure 6.1 Model harbour geometry and finite element mesh

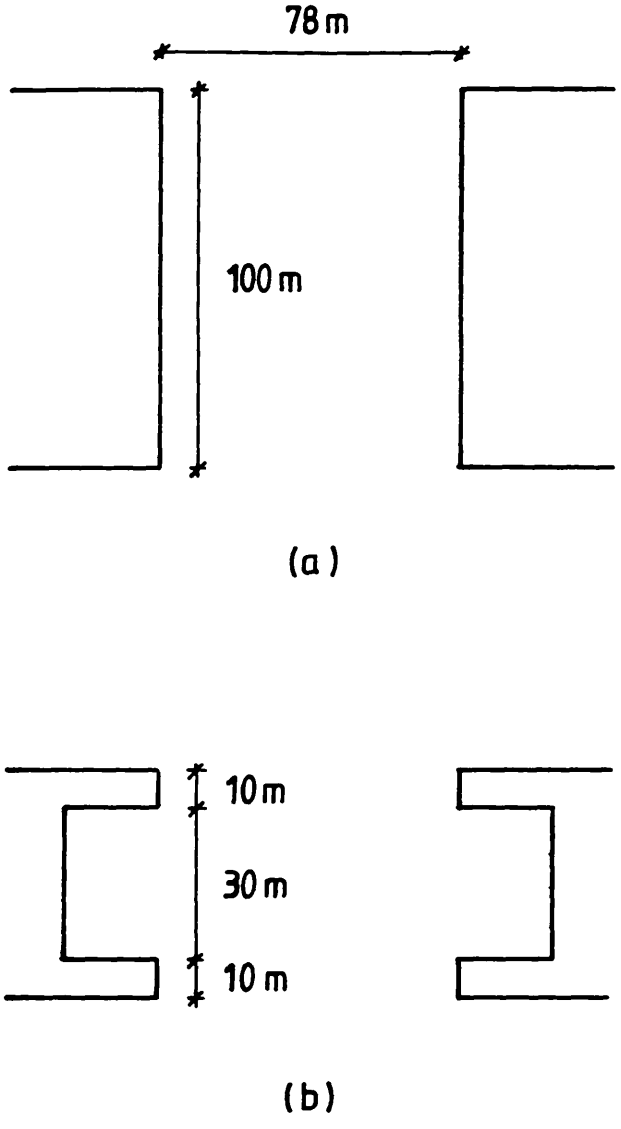

Figure 6.2 Entrance configurations studied

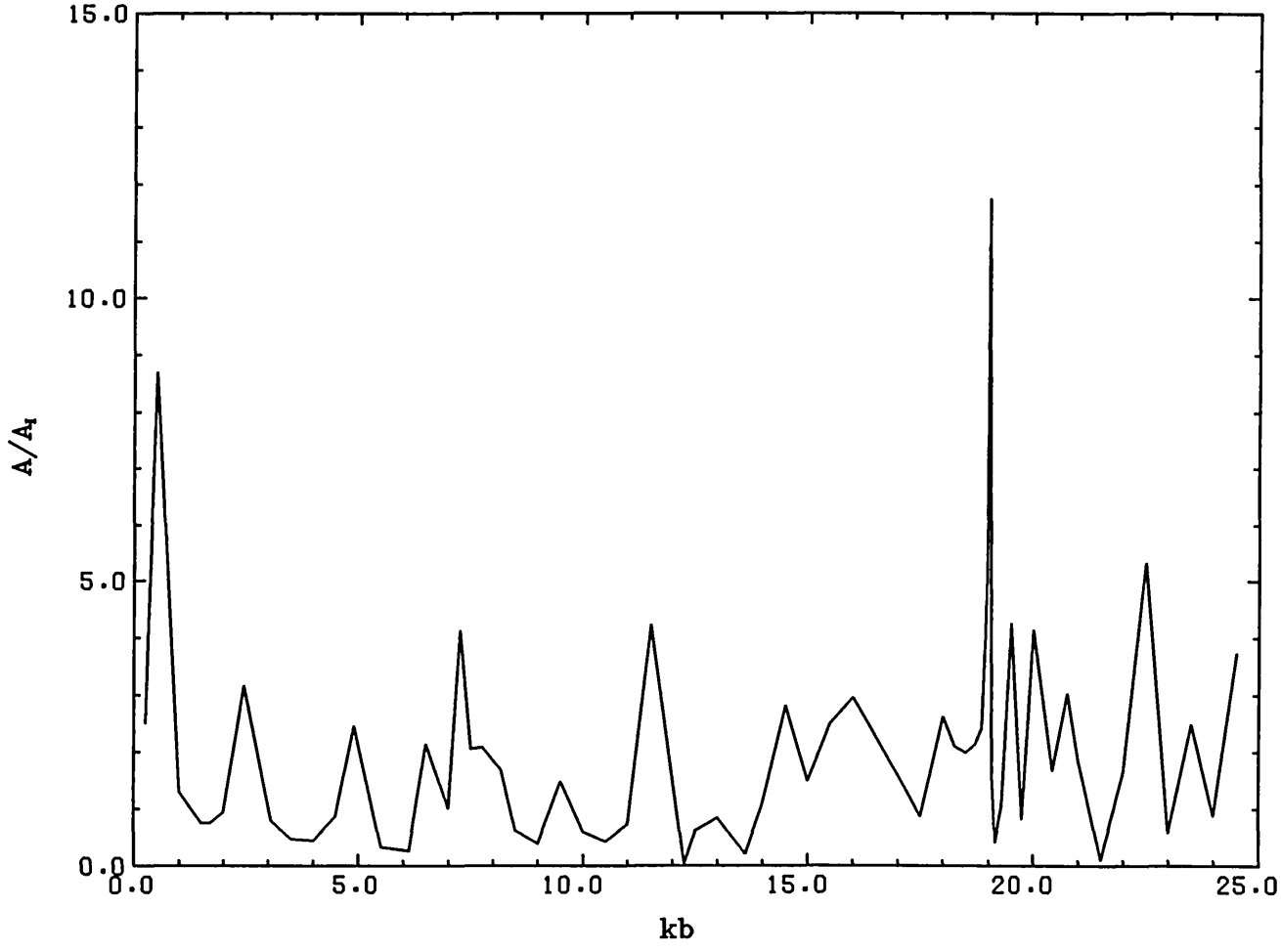

Fig. 6.3 RESPONSE CURVE FOR MODEL HARBOUR

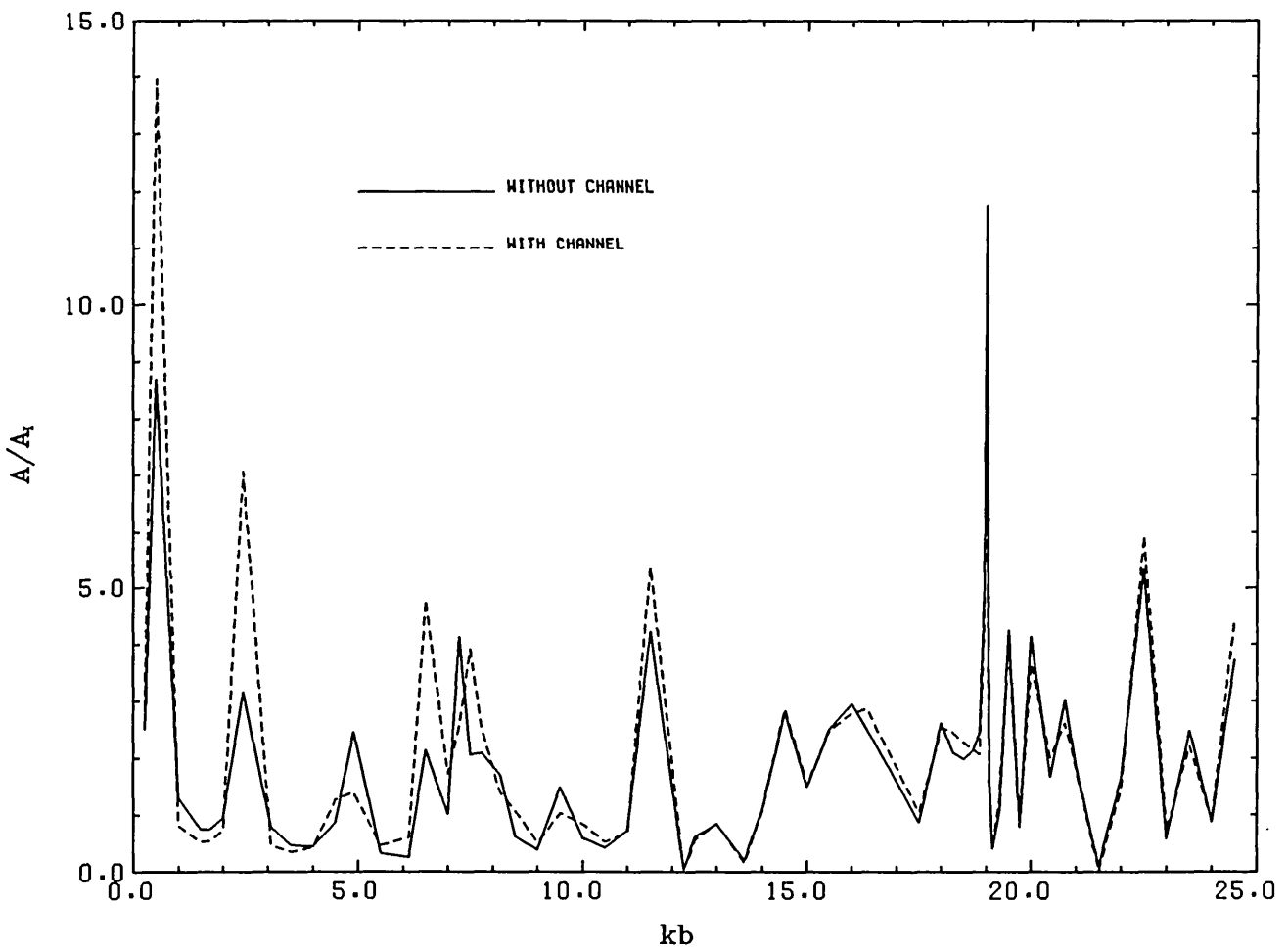

Fig. 6.4 HARBOUR RESPONSE CURVES

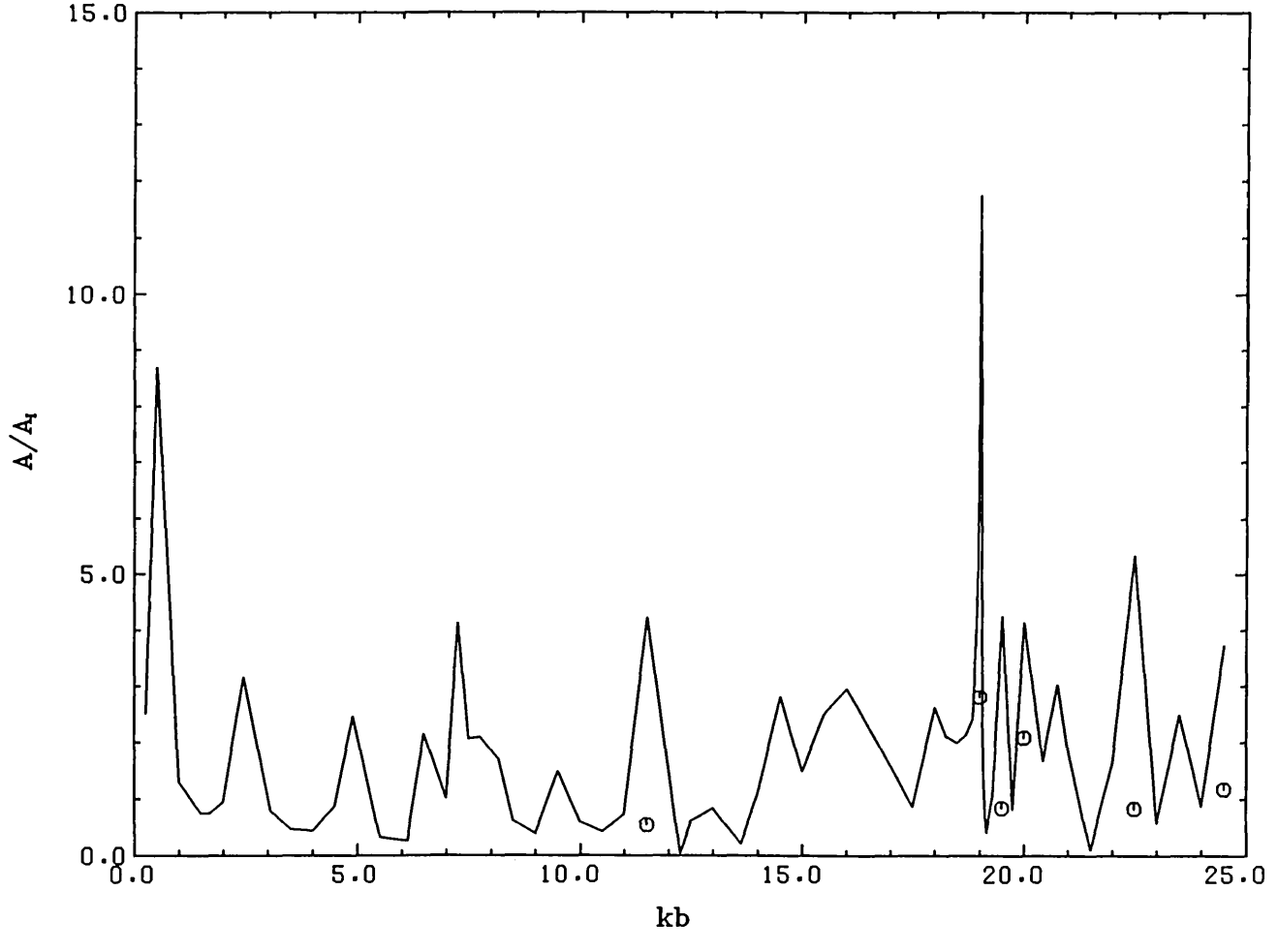

Fig. 6.6 HARBOUR RESPONSE CURVE SHOWING EFFECTS OF RESONATORS

CHANNEL

Fig. 6.8

Amplitude contours

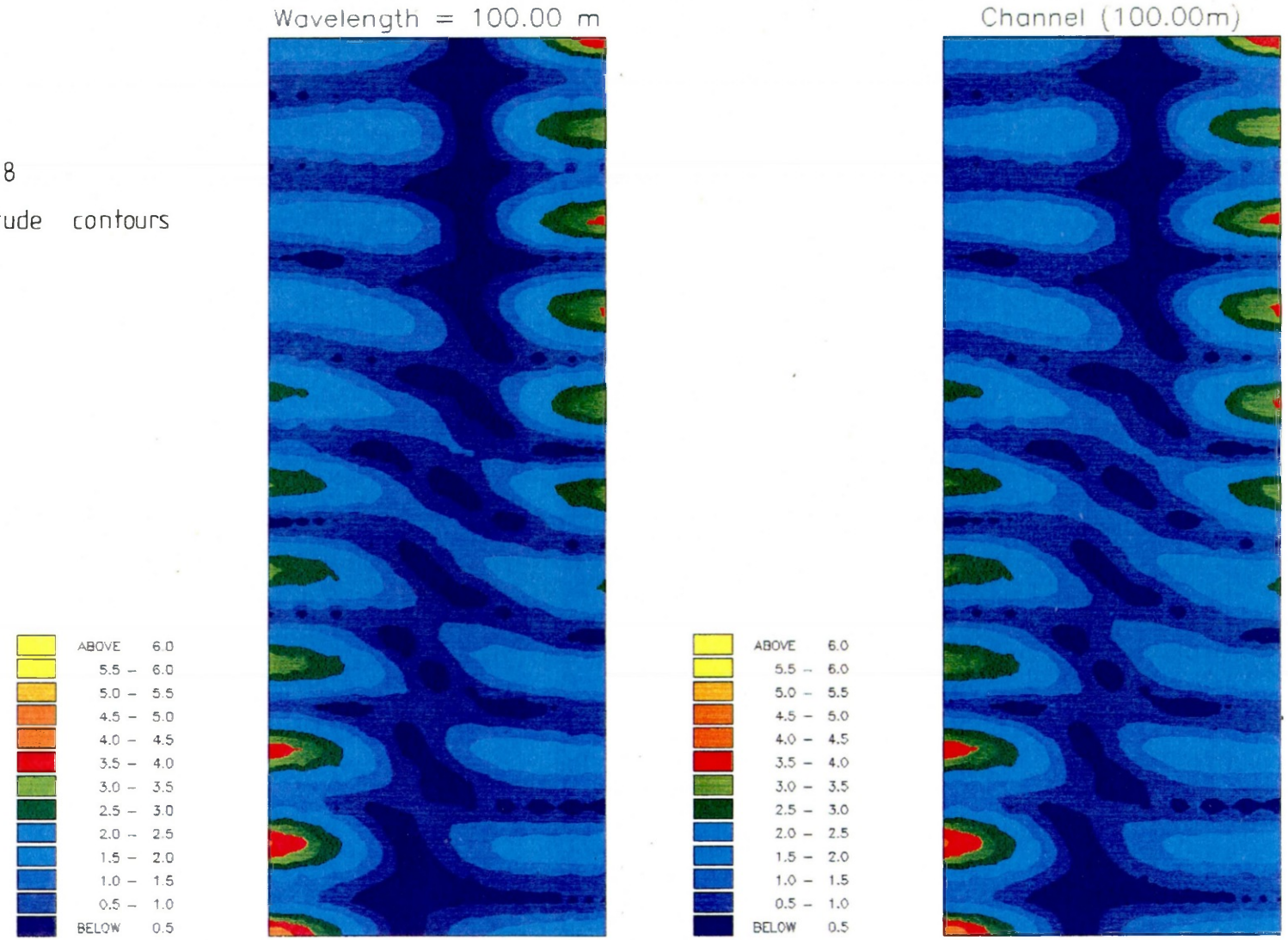

Fig. 6.9

Amplitude contours

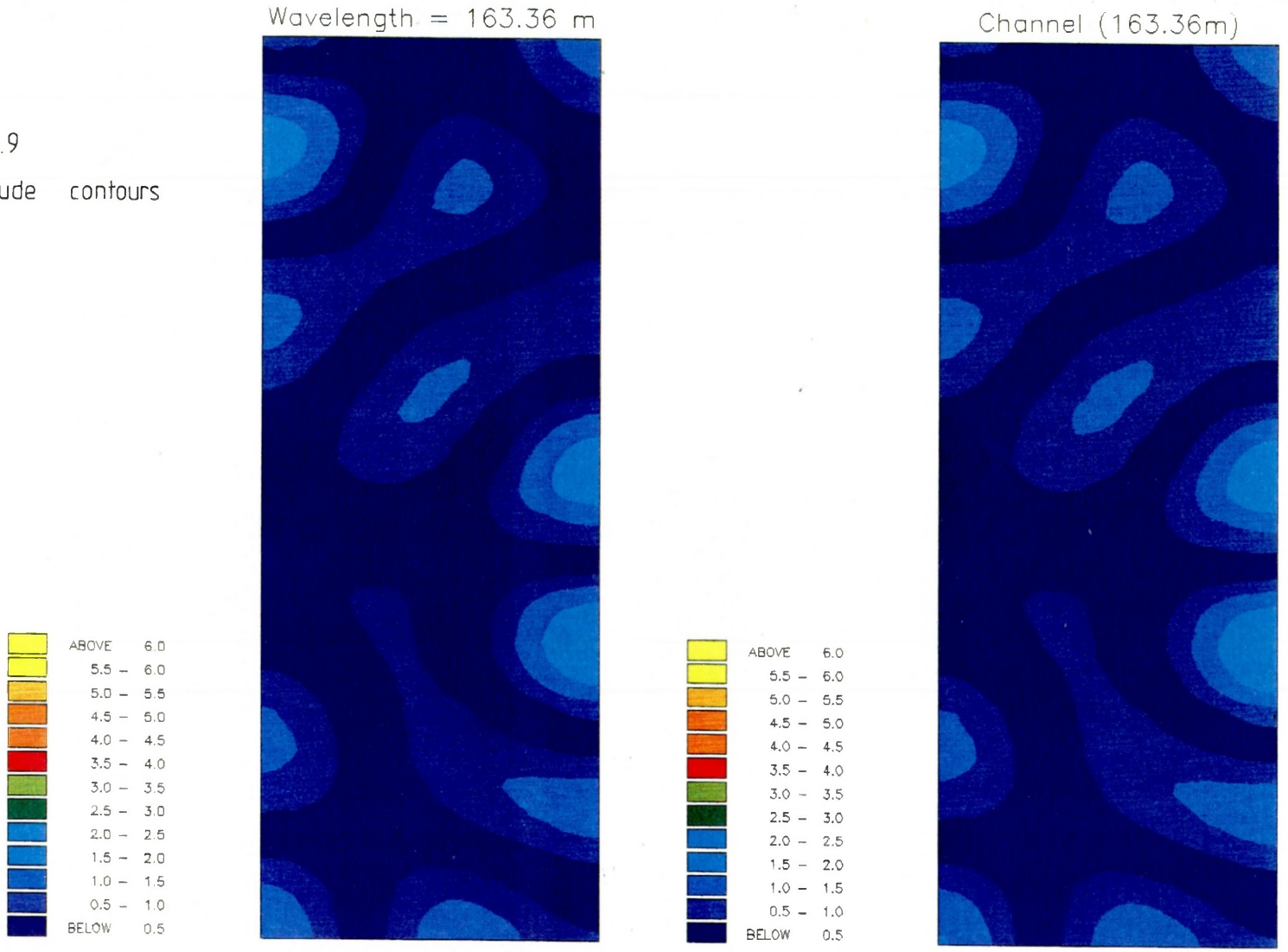

Fig. 6.10

Amplitude contours

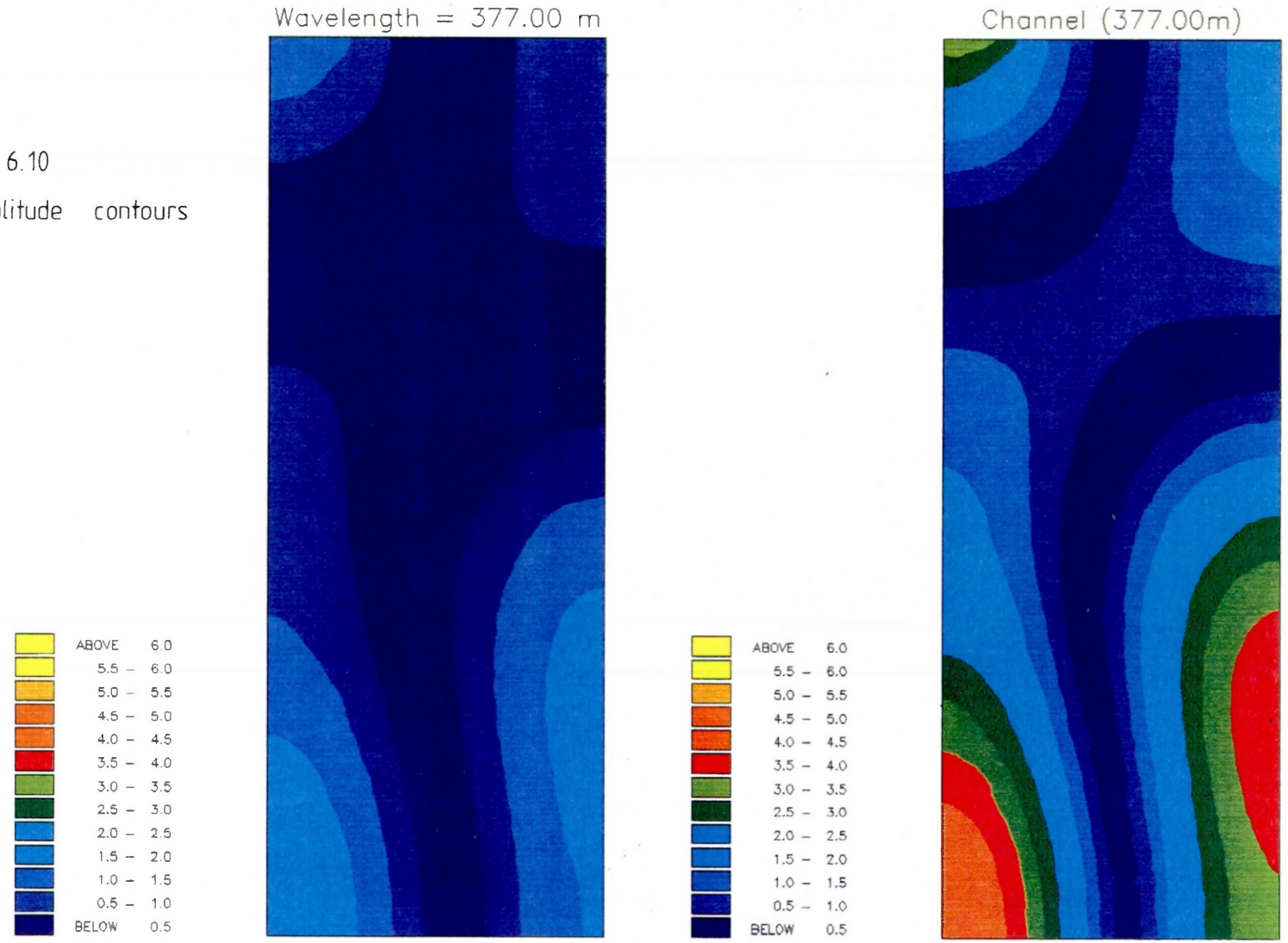

Fig. 6.11

Amplitude contours

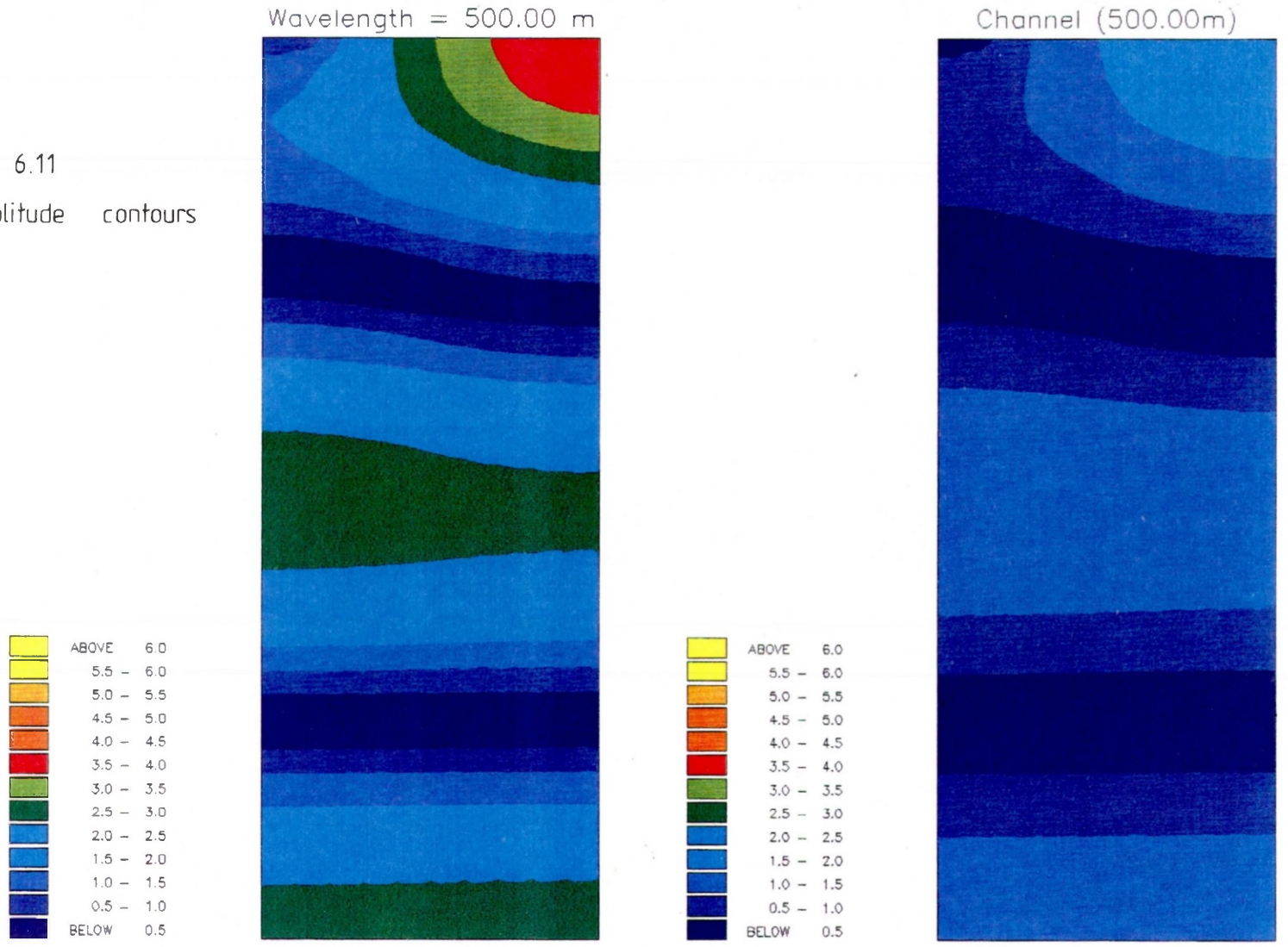

RESONATOR

Fig. 6.12

Amplitude contours

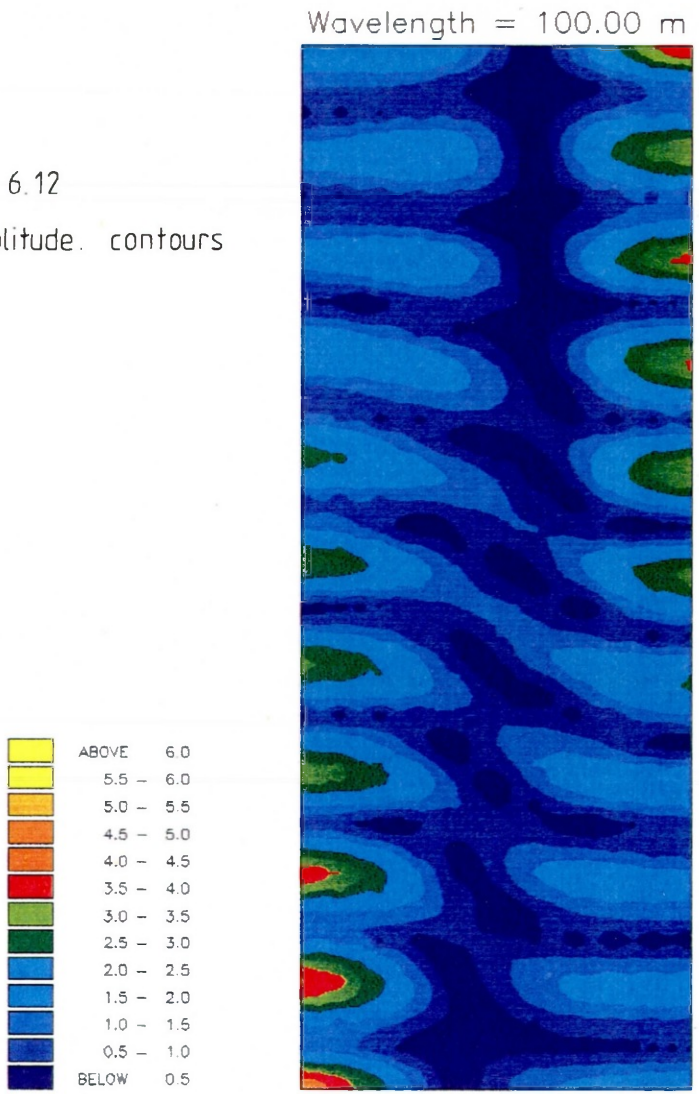

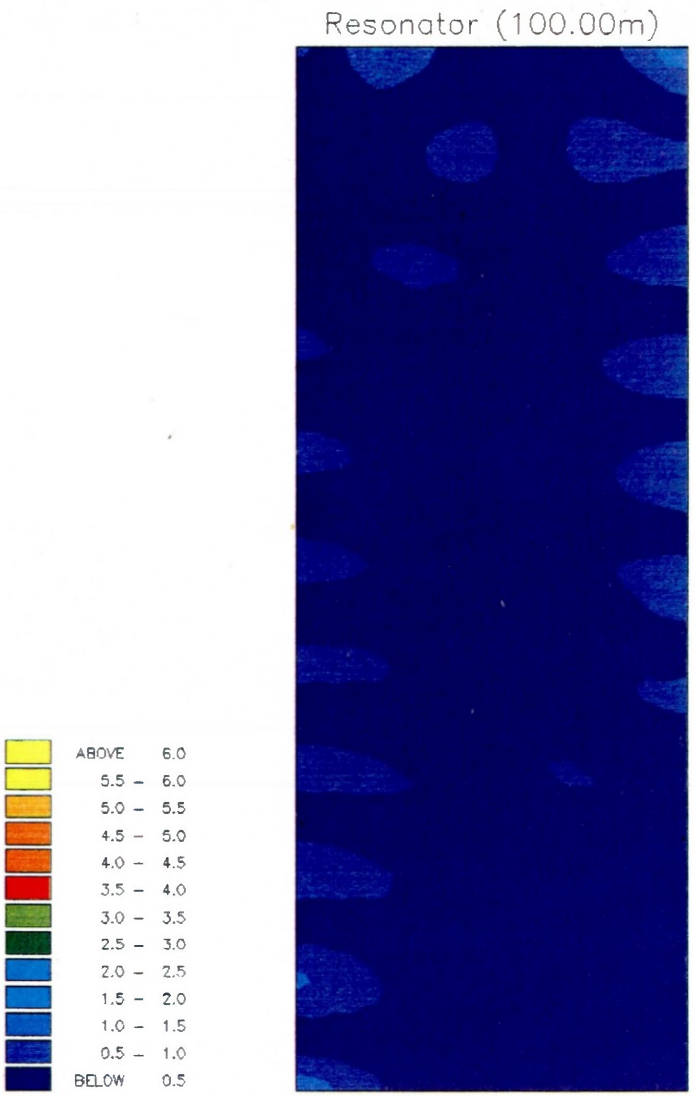

Fig. 6.13

Amplitude contours

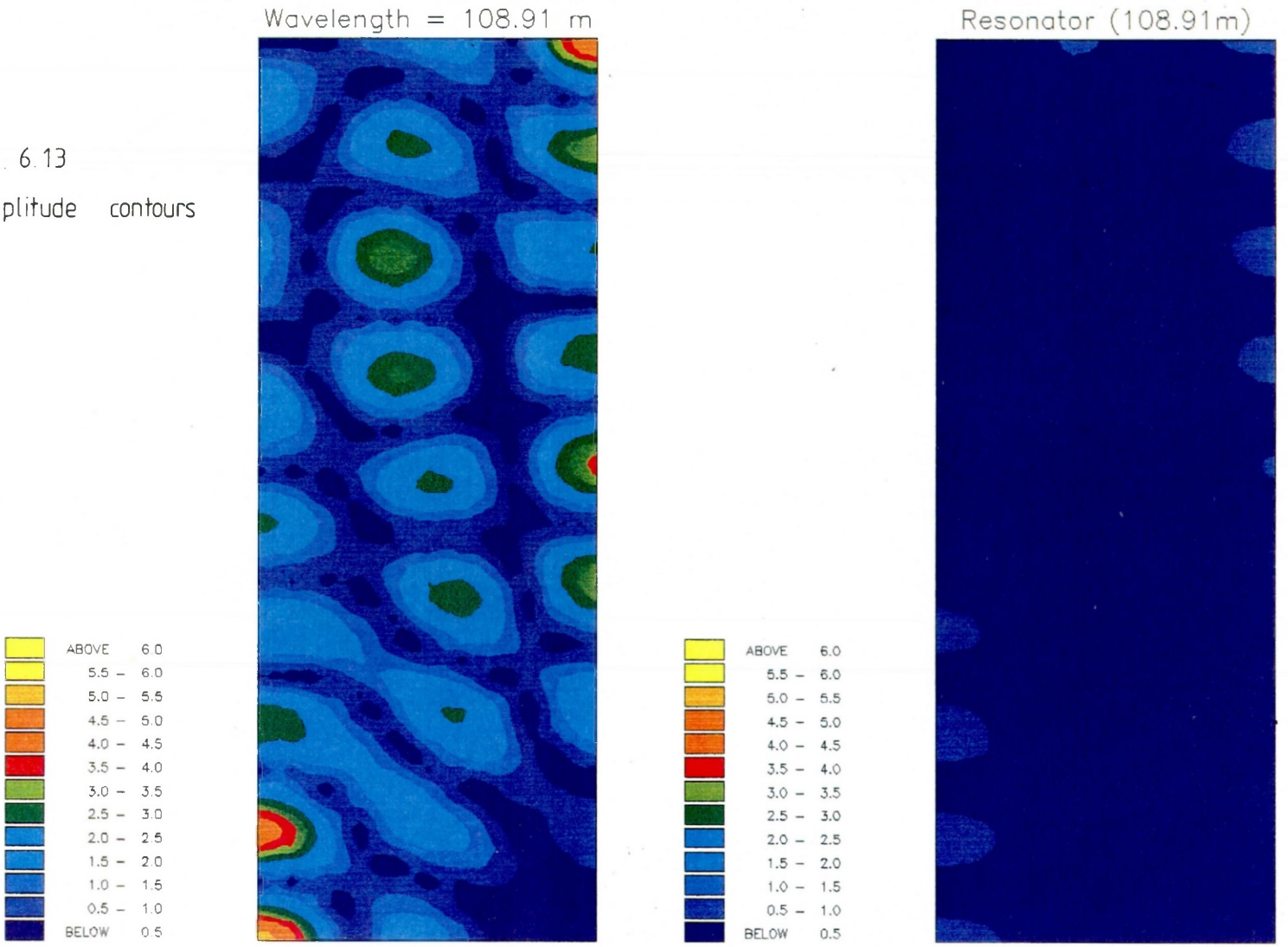

Fig. 6.14

Amplitude contours

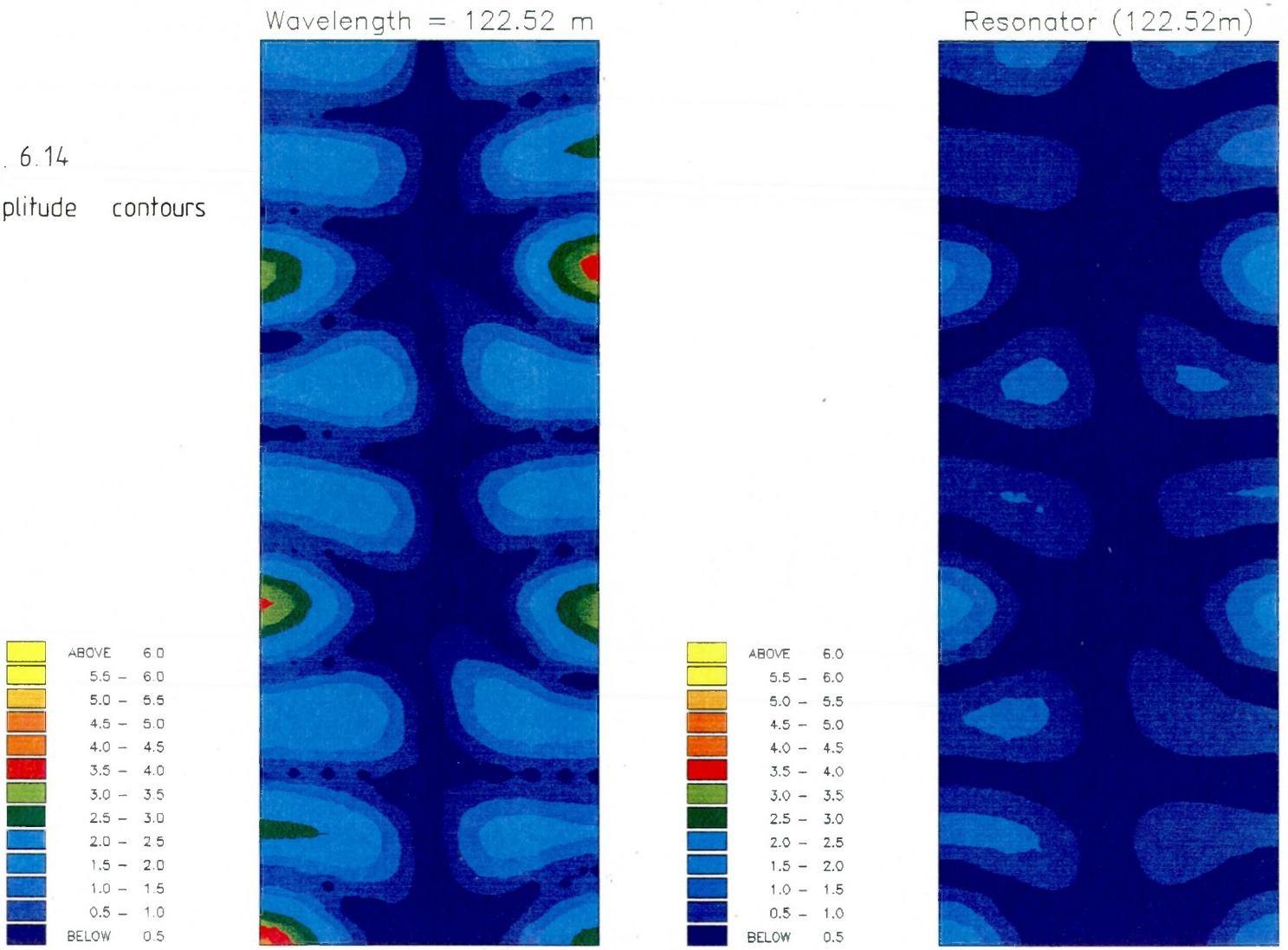

Fig . 6.15

Amplitude contours

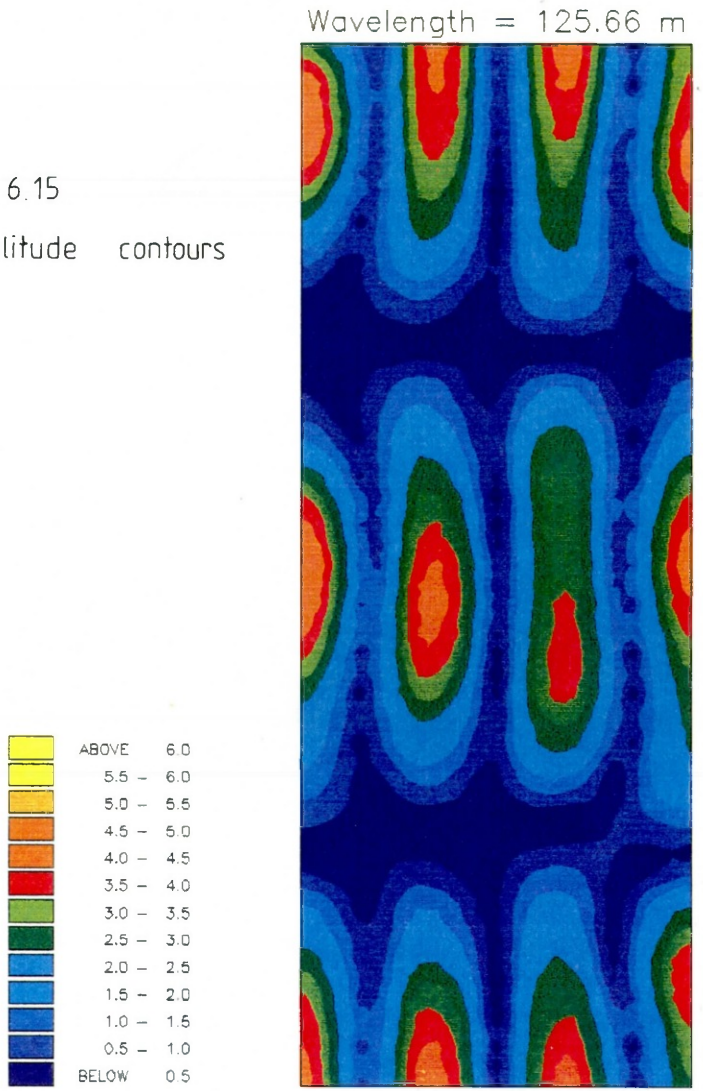

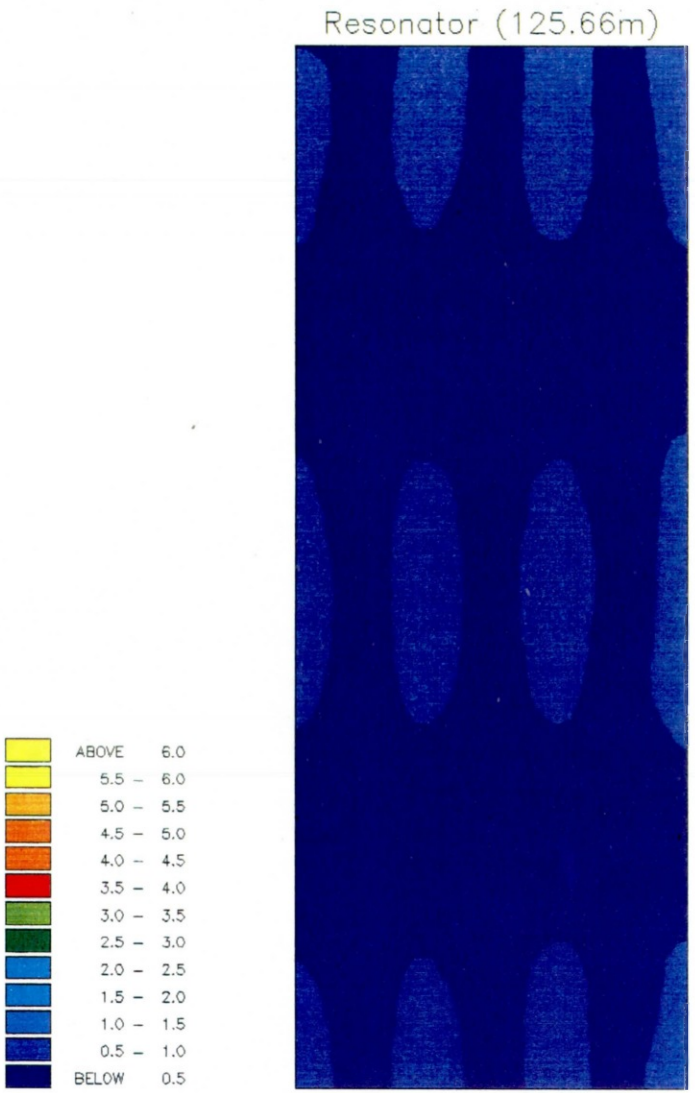

Fig. 6.16

Amplitude contours

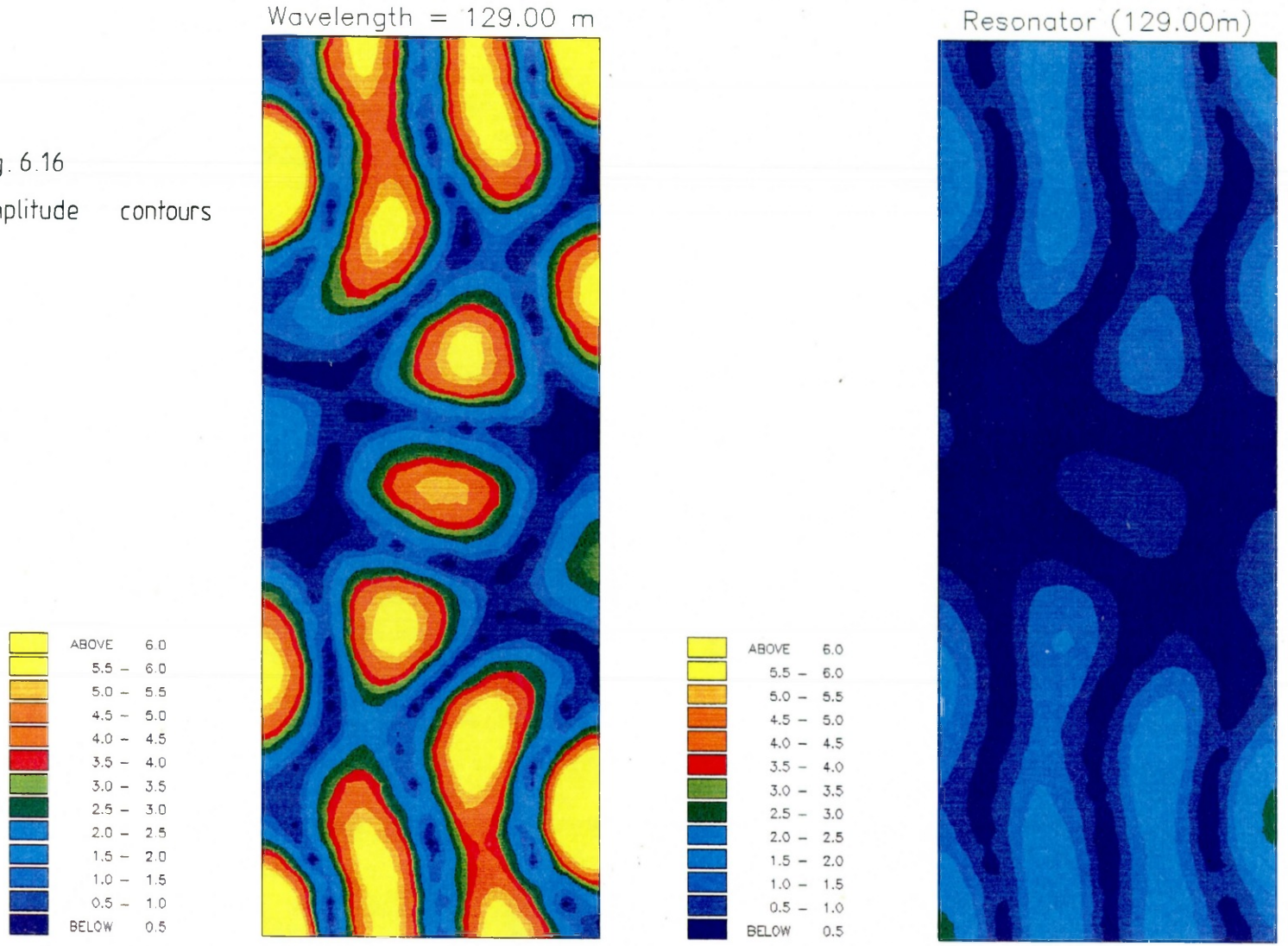

Fig. 6.17

Amplitude contours

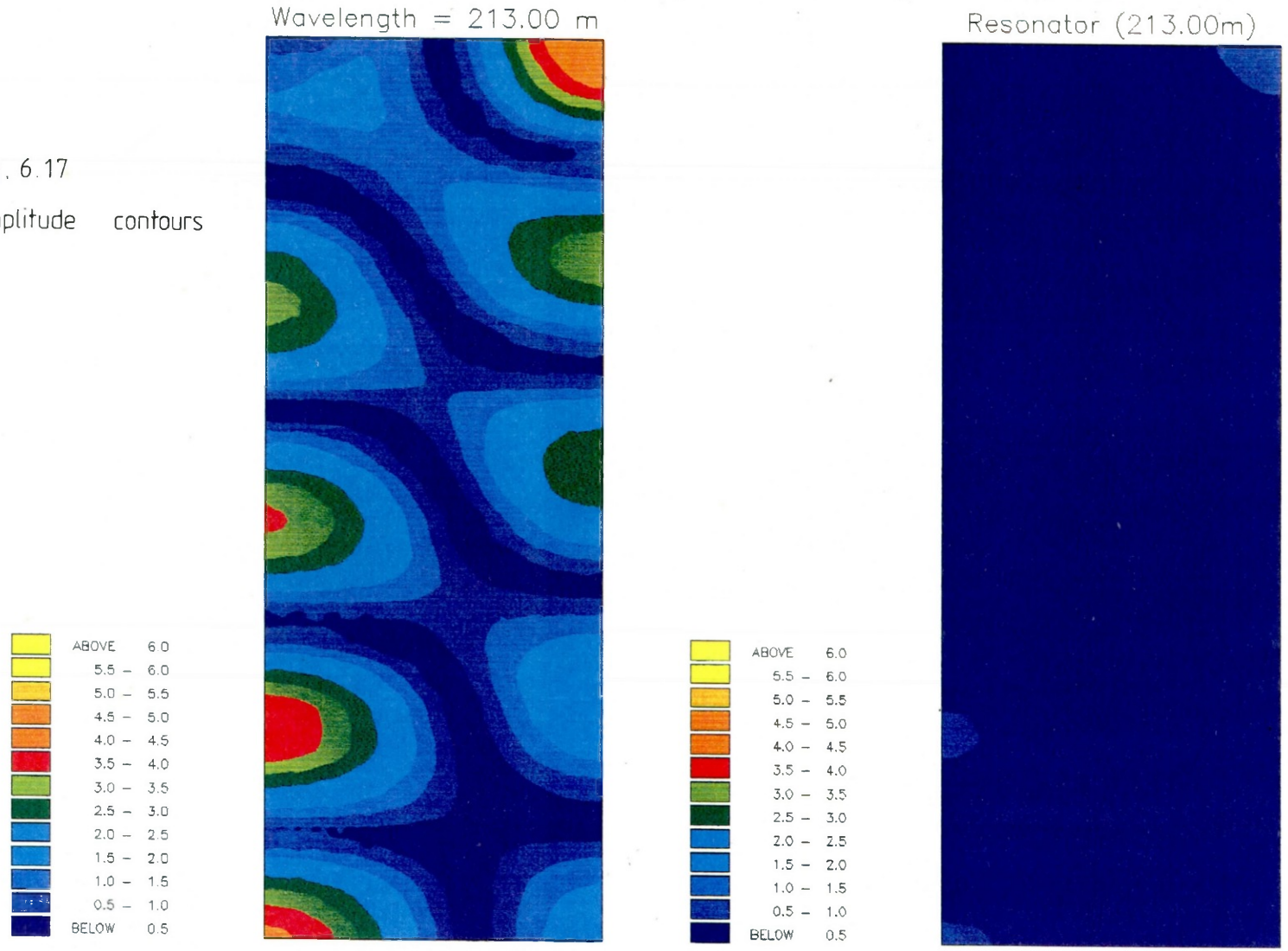

CHAPTER SEVEN
Concluding remarks

7.1 General conclusions

The deductions arrived at in the three major previous chapters are summarised here for convenience. Chapters three, five and six deal with analytical investigations, the semi–infinite harbour and the model harbour respectively.

7.1.1 Analytical investigations

(1) *Scattering at the outlet of a semi–infinite channel*

(a) The energy transmission coefficient is rapidly diminished as the separation between the channel walls is decreased. This is associated with the high amount of reflection at the open end.

(b) When the channel is terminated in an infinite flange, there is considerably higher energy transmission into the harbour as compared with the case when it is unflanged.

(2) *Diffraction by a thick breakwater*

(a) Short entrance channels or the small thickness of a breakwater can reduce the energy transmission into the harbour by a significant amount.

(b) The impedance of such configurations is directly proportional to the effective size of the gap which is given by the ratio, a/b, where 2a is the thickness of the breakwater and 2b is the gap width, provided $(2a,2b) \leqslant 0.2\lambda$.

(3) *Transmission through a long channel*

(a) The energy transmission coefficient and the amplitudes in the channel are periodically dependent on the channel length.

(b) The channel serves to impede the penetration of waves into the harbour over a wide range of wavelengths.

(c) When the length of the channel is roughly equal to an integral number of half–wavelengths, resonance will occur.

(d) Resonance in the channel leads not only to augmented amplitudes there, but also to increased energy transmission into the harbour.

(e) Resonant amplitudes are rapidly diminished as the width of the channel is increased.

7.1.2 Semi–infinite harbour

(1) *Channels*

(a) If the gap width is between 0.5λ and 1.0λ, the channel will not have any effect on the wave field inside the harbour, regardless of its length. This is because of the greatly reduced reflections at the open ends.

(b) When the gap width is greater than one wavelength, the channel would have the effect of increasing the amplitudes in the centre of the harbour while diminishing them in the lee of the breakwaters. This is attributed to the beaming of the shorter waves by the wide entrance.

(c) Inside the channel, the transverse and longitudinal standing waves might present a problem to navigation.

(2) *Resonators*

(a) The impedance of quarter–wavelength resonators is a consequence of the 180° phase difference which exists between the incident wave passing down the gap and the 'delayed' wave which has been amplified in its passage through the resonator.

(b) The optimum lengths of narrow resonators are to a large extent independent of the harbour gap width.

(c) When the gap width is small, typically less than 0.5λ, both narrow and wide resonators are very efficient at impeding the energy of incoming waves. With the wide resonators, an almost 100% reduction in energy transmission may be chieved.

(d) When the gap width is greater than one wavelength, the narrow resonators can lead to adverse amplifications near the entrance and to areas of higher amplitudes behind the breakwaters. Accordingly, the wider resonators should then be employed as these lead to overall improvements.

(e) If the resonators are made too wide, their efficiency will be reduced. Therefore, resonators of intermediate widths should generally be employed.

(f) With oblique incidence (angles from the normal greater than about 30°), the widest resonators are the most efficient for all gap widths.

(3) *Filters*

(a) Arrangements comprising two and three adjacent cells of resonators should be avoided as these can cause unacceptably high amplitudes in the neighbourhood of the entrance for the wider gaps.

(b) Batteries consisting of two non–adjacent cells of resonators separated by 0.5λ lead to significant overall improvements in conditions inside the harbour. It is advisable to make the distance between the two cells as large as possible within, of course, practical limitations.

7.1.3 Model harbour

(1) *Channel*

(a) At incoming wave frequencies which are giving rise to resonance in the basin, the channel will serve to amplify the response in the harbour. This is particularly severe for the lower modes of oscillation.

(b) At non–resonant frequencies, the channel will diminish the response.

(c) For the shorter waves, the channel will not have any noticeable effect on the wave field inside the harbour. This is because with wider gaps, the reflection at the open ends will be greatly reduced. If the waves are made very short, however, beaming will occur.

(2) *Resonator*

(a) Quarter–wavelength resonators may be advantageously used to limit the adverse effects of harbour resonance. Reductions in amplitude of up to 80% can be achieved by proper design.

(b) If the lengths of such resonators are made less than the optimum, higher amplitudes might be induced in the harbour basin as a result of the impaired radiation damping.

7.2 Suggestions for further work

It would be beneficial if a thorough experimental investigation could be carried out to verify the wealth of results obtained in this work. The present author did attempt such a task, but it was felt that the particular wave basin available was not adequate enough. This is because the reflections on the seaward

side of the breakwaters could not be prevented from being re–reflected off the generator paddle. Such behaviour severely distorts the conditions and accordingly leads to unrepresentative results. It would therefore be ideal to use a wave generator which is capable of absorbing the reflected wave.

In reality, ocean waves are wind generated and so they are not of simple sinusoidal form of constant height and direction of propagation. Wind generated waves in the ocean propagate in two dimensions and display a wide range of frequencies and amplitudes. It would be desirable to apply our work to a realistic wave spectrum to assess the perfomance of the various entrance configurations studied. This should be theoretically straightforward because of the linear nature of our problem.

7.3 Closure

The work described in this thesis provides a more rational basis for the design of harbour entrances in relation to the control of wave penetration at the mouth. It must, however, be noted that in a design context there will be restrictions of space and cost which impose limitations on the extent to which the optimum solutions discussed previously can be implemented.

The results from our mathematical models may be utilised to obtain a suitable configuration for a physical model, thus reducing the laborious task of varying the many geometrical parameters.

REFERENCES

Abramowitz, M. and Stegun, I.A. (1965) Handbook of mathematical functions. Dover.

Astley, R.J. (1983) Wave envelope and infinite elements for acoustical radiation. Int. J. Num. Meth. Fl., **3**, pp. 507–526.

Becker, E.B., Carey, G.F. and Oden, J.T. (1981) Finite Elements An Introduction, Prentice Hall.

Behrendt, L. (1985) A finite element model for water wave diffraction including boundary absorption and bottom friction. Inst. of Hydrodynamics and Hydraulic Eng., Tech. Univ. of Denmark, Series Paper no. 37.

Berkhoff, J.C.W. (1972) Computation of combined refraction–diffraction. Proc. 13th Int. Conf. Coast. Eng., pp. 471–490.

Berkhoff, J.C.W. (1975) Linear wave propagation problems and the finite element method. Finite Elements in Fluids, eds. Callagher, R.H., Oden, J.T., Taylor, C. and Zienkiewicz, O.C., **1**, pp. 251–264.

Berkhoff, J.C.W. (1976) Mathematical models for simple harmonic linear water wave diffraction and refraction. Delft Hydraulics Lab., publication no. 163.

Bettess, P. (1977) Infinite elements. Int. J. Num. Meth. Eng., **11**, pp. 53–64.

Bettess, P. and Zienkiewicz, O.C. (1977) Diffraction and refraction of surface waves using finite and infinite elements. Int. J. Num. Meth. Eng., **11**, pp. 1271–1290.

Bettess, P., Liang, S.C. and Bettess, J.A. (1984) Diffraction of waves by semi–infinite breakwaters using finite and infinite elements. Int. J. Num. Meth. Fl., **4**, pp. 813–832.

Bettess, P. (1987) A simple wave envelope element example. Comm. Appl. Num. Meth., **3**, pp. 77–80.

Blue, F.L. and Johnson, J.W. (1949) Diffraction of water waves passing through a breakwater gap. Trans., Geophys. Un., **30**, pp. 705–718.

Bruun, P. (1973) Port Engineering. Gulf Publishing Company.

Carr, J.H. and Stelzriede, M.E. (1952) Diffraction of water waves by breakwaters. U.S. Nat. Bur. of Standards, Circ. 521, pp. 109–125.

Carrier, G.F., Shaw, R.P. and Miyata, M. (1971) The response of narrow–mouthed harbours in a straight coastline to periodic incident waves. J. Appl. Mech., A.S.M.E., **46**, pp. 335–344.

Chatterton, S.A. (1983) FINEL User Reference Manual.

Chatterton, S.A. (1983) FINEL Programmers Reference Manual.

Chen, H.S. and Mei, C.C. (1974) Oscillations and wave forces in an offshore harbour. Report no. 190, Parsons Lab., M.I.T.

Davy,N. (1944) The field between equal semi–infinite rectangular electrodes or magnetic pole pieces. Phil. Mag., **35**, pp. 819–840.

Defant, A. (1944) Physical Oceanography. Pergamon.

Dong, P. and Al–Mashouk, M. (1989) Comparison of transient and steady–state wave models for harbour resonance. Int. Conf. Hydraulic and Environmental Modelling of Coastal, Estuarine and River Waters, Univ. of Bradford.

Fraenkel, L.E. (1969) On the method of matched asymptotic expansions. Proc. Camb. Phil. Soc., **65**, pp. 209–284.

Gerber, M. (1986) Modelling dissipation in harbour resonance. Coast. Eng., **10**, pp. 211–252.

Gilbert, G. and Brampton, A.H. (1985) The solution of two wave diffraction problems using integral equations. Hydraulics Research, Report no. IT 299.

Guiney, D.C., Noye, B.J. and Tuck, E.O. (1972) Transmission of water waves through small apertures. J. Fl. Mech., **55**, pp. 149–161.

Havelock, T.H. (1940) The pressure of water waves on a fixed obstacle. Proc. Roy. Soc. of London, **A175**, pp. 409–421.

Henshell, R.D. and Shaw, K.G. (1975) Crack tip finite elements are unnecessary. Int. J. Num. Meth. Eng., **9**, pp. 495–507.

Houston, J.R. (1978) Interaction of tsunamis with the Hawaiian Islands calculated by a finite element numerical model. J. Phys. Oceanography, **8**, pp. 93–102.

Houston, J.R. (1981) Combined refraction and diffraction of short waves using the finite element method. Appl. Ocean Res., **3**, pp. 163–170.

Hwang, L. and Tuck, E.O. (1970) On the oscillations of harbours of arbitrary shape. J. Fl. Mech., **42**, pp. 447–464.

James, W. (1968) Rectangular resonators for harbour entrances. Proc. 11th Int. Conf. Coast. Eng., pp. 1512–1530.

James, W. (1970) An experimental study of end effects for rectangular resonators on narrow channels. J. Fl. Mech., **44**, pp. 615–621.

James, W. (1971) Two innovations for improving harbour resonators. Proc. A.S.C.E., **97**, pp. 115–122.

Kellog, O.D. (1929) Foundations of potential theory. Julius Springer.

Kinsler, L.E., Frey, A.R., Coppens, A.B. and Sanders, J.V. (1982) Fundamentals of Acoustics. John Wiley and Sons.

Kober, H. (1957) Dictionary of conformal transformations. Dover.

Kotense,J.K., Meijer, K.L., Dingemans, M.W., Mynett, A.E. and van den Bosch, P. (1988) Wave energy dissipation in arbitrarily shaped harbours of variable depth. Delft Hydraulics Lab., publication no. 387.

Kubo, M., Aoki, S. and Segura, J.J. (1985) Attenuation of wave induced oscillation in ports by improving the conditions at the harbour entrance. Proc. 19th Int. Conf. Coast. Eng., pp. 2933–2951.

Lacombe, H. (1952) The diffraction of a swell. A practical approximate solution and its justification. U.S. Nat. Bur. of Standards, Circ. no. 521, pp. 129–140.

Lamb, H. (1925) The dynamical theory of sound. Dover.

Lamb, H. (1932) Hydrodynamics. Cambridge University Press.

Lee, J.J. (1971) Wave induced oscillations in harbours of arbitrary geometry. J. Fl. Mech., **45**, pp. 375–394.

Liu, P.L. (1975) Scattering of water waves by a pair of semi–infinite barriers. J. Appl. Mech., A.S.M.E., **42**, pp. 777–779.

Liu, P.L. and Wu, J. (1986) Transmission of oblique waves through submerged apertures. Appl. Ocean Res., **8**, pp. 144–150.

Liu, P.L. (1987) Resonant reflection of water waves in a long channel with corrugated boundaries. J. Fl. Mech., **179**, pp. 371–381.

Liu, P.L. and Wu, J. (1988) Wave transmission through submerged apertures. J. Waterway, Port, Coast. and Ocean Eng., A.S.C.E., **113**, pp. 660–671.

Longhurst, R.S. (1973) Geometrical and physical optics. Longman.

MacCamy, R.C. and Fuchs, R.A. (1952) Wave forces on piles: a diffraction theory. Inst. Eng. Res., Waves Investigation Lab., Series 3, Issue 334, Berkely, California.

McLachlan, N.W. (1947) Theory and application of Mathieu functions. Clarendon Press.

Mei, C.C. (1978) Numerical methods in water wave diffraction and radiation. Ann. Rev. Fl. Mech., **10**, pp. 393–416.

Memos, C.D. (1980) Energy transmission by surface waves through an opening. J. Fl. Mech., **97**, pp. 557–568.

Memos, C.D. (1980) An extended approach to wave scattering through a harbour entrance. Bull., P.I.A.N.C., **35**, pp. 20–26.

Miles, J.W. and Munk, W. (1961) Harbour Paradox. J. Waterways and Harbours Division, A.S.C.E., **87**, pp. 111–130.

Morse, P.M. and Rubenstein, P.J. (1938) The diffraction of waves by ribbons and slits. Phys. Rev., **54**, pp. 895–898.

Morse, P.M. (1948) Vibration and sound. McGraw–Hill.

Morse, P.M. and Ingard, K.U. (1968) Theoretical acoustics. McGraw–Hill.

Nayfeh, A.H. (1981) Introduction to perturbation techniques. Wiley.

Newman, J.N. (1974) Interaction of water waves with two closely spaced vertical obstacles. J. Fl. Mech., **66**, pp. 97–106.

Newman, J.N., Sortland, B. and Vinje, T. (1984) Added mass and damping of rectangular bodies close to the free surface. J. Ship Res., **28**, pp. 219–225.

Noble, B. (1958) Methods based on the Wiener–Hopf technique. Pergamon Press.

Penney, W.G. and Price, A.T. (1944) Diffraction of sea waves by breakwaters. Directorate, Misc. Weapons Development Technical History 26, Artificial Harbours, Sec. 3D.

Penney, W.G. and Price, A.T. (1952) The diffraction theory of sea waves and the shelter afforded by breakwaters. Phil. Trans. Roy. Soc., **A244**, pp. 236–253.

Pos, J.D. (1983) Wave diffraction using finite and infinite elements. Comp. Meth. Appl. Mech. Eng., **41**, pp. 219–235.

Pos, J.D. (1985) Asymmetrical breakwater gap wave diffraction using finite and infinite elements. Coast. Eng., **9**, pp. 101–123.

Putnam, J.A. and Arthur, R.S. (1948) Diffraction of water waves by breakwaters. Trans., Am. Geophys. Un., **29**, pp. 481–490.

Rayleigh, Lord (1894) The theory of sound. Macmillan.

Rayleigh, Lord (1897) On the passage of waves through small apertures in plane screens and allied problems, Phil. Mag., **43**, pp. 259–272.

Roy, N. (1962) Effect of entrance on seiche motion in ocean ports. Proc. 8th Int. Conf. Coast. Eng., pp. 93–113.

Schwarzchild, (1902) Die Beugung und polarisation des lichts durch einen spalt. Math. Ann., **55**, pp. 177–247.

Shore Protection Manual (1984). U.S. Army C.E.R.C.

Smallman, J.V. (1986) Diffraction by a gap between two breakwaters: solution for long waves by matched asymptotic expansions. J. Fl. Mech., **172**, pp. 143–155.

Sobey, R.J. and Johnson, T.L. (1986) Diffraction patterns near narrow breakwater gaps. J. Waterways, Harb. and Coast. Eng. Div., A.S.C.E., **112**, pp. 512–528.

Sommerfeld, A. (1896) Mathematische theorie der diffraktion. Math. Ann., **47**, pp. 317–374.

Tsay, T.K. and Liu, P.L. (1983) A finite element model for wave refraction and diffraction. Appl. Ocean Res., **5**, pp. 30–37.

Tuck, E.O. (1971) Transmission of water waves through small apertures. J. Fl. Mech., **49**, pp. 65–74.

Unluate, U. and Mei, C.C. (1973) Long wave excitation in harbours: an analytical study. Report no. 177, Ralph M. Parsons Lab., M.I.T.

Valembois, J. (1953) Etude de l'action d'ouvrages resonants sur la propagation de la houle. Proc. Minnesota Int. Hydr. Conv., pp. 193–200.

Van Damme, L.V. (1982) Zeebrugge's main breakwaters. Proc. 18th Int. Conf. Coast. Eng., pp. 1745–1764.

Van Dyke, M. (1964) Perturbation methods in fluid mechanics. Academic.

Wehausen, J.V. and Laitone, E. (1960) Surface waves. Handbuch der Physik, ed. S. Flugge, Springer.

Wilson, B.W. (1965) Full scale observation of the behaviour of moored ships. Proc., N.A.T.O. Advanced Study Inst. on Analytical Treatment of Problems of Berthing and Mooring.

Zienkiewicz, O.C. (1978) The finite element method in engineering science. McGraw–Hill.

Zienkiewicz, O.C., Bettess, P. and Kelly, D.W. (1978) The finite element method for determining fluid loading on rigid structures: two and three dimensional formulations. Chap. 4 of Numerical methods in offshore engineering.

Zienkiewicz, O.C., Emson, C. and Bettess, P. (1983) A novel boundary infinite element. Int. J. Num. Meth. Eng., **19**, pp. 393–404.

Zienkiewicz, O.C., Bando, K., Bettess, P., Emson, C. and Chiam, T.C. (1985) Mapped infinite elements for exterior wave problems. Int. J. Num. Meth. Eng., **21**, pp. 1229–1251.